The Institute of Paper Science and Technology

Atlanta, Georgia

Doctor's Dissertation

Spectroscopic Evaluation of the Gas Phase Above a Burning Black Liquor Char Bed

Patrick J. Medvecz

October, 1991

SPECTROSCOPIC EVALUATION OF THE GAS PHASE ABOVE A BURNING BLACK LIQUOR CHAR BED

A Thesis Submitted by

Patrick J. Medvecz

B.S. 1985, Purdue University Calumet

M.S. 1987, Lawrence University (Institute of Paper Chemistry)

in partial fulfillment of the requirements
of the Institute of Paper Science and Technology
for the degree of Doctor of Philosophy,
Atlanta, Georgia

October, 1991

TABLE OF CONTENTS

LIST OF FIGURES

LIST OF TABLES

ABSTRACT

Fourier transform infrared absorption spectroscopy has been used for the determination of gas temperatures and concentrations (CO and CO_2) above a burning, laboratory scale black liquor char bed. In order to establish temperature and concentration calculation methodologies, measurements were first made in a well controlled high temperature gas cell. Infrared absorption spectra of $CO/CO_2/N_2$ gas mixtures were recorded in the gas cell at temperatures between 295-1250 K. From the spectra, gas temperature measurements were made by mathematically describing the temperature dependent Boltzman distribution of the molecules responsible for the P branch of the fundamental CO absorption band. Gas concentration measurements were made by first determining the temperature dependent line strengths of 21 CO and 19 CO_2 absorption lines. The line strength data were then used to calculate the gas concentration by using the Bouguer-Lambert absorption law and assuming a Lorentzian line profile for the individual vibrational-rotational absorption lines. Prior to their use for gas temperature and concentration measurements, the absorption peaks were all mathematically corrected for photometric errors resulting from distortions caused by the finite resolution of the spectrometer.

In the gas cell, the accuracy of the temperature calculation methodology was established by comparing spectroscopically measured gas temperatures with those measured with a thermocouple. The average difference was between 2-4%. The gas cell was also used to evaluate the temperature dependence of line strengths. The accuracy of these values was established by comparisons with theoretical predictions and other experimentally reported values. In general the CO and CO_2 line strengths determined in this work were within 10% of both the alternative experimental values and the theoretical predictions. The line strengths were then used to calculate CO and CO_2 gas concentrations in the high temperature gas cell. On average, the spectroscopically determined concentrations of CO and CO_2

agreed with metered or NDIR (nondispersive infrared gas analyzer) measurements to within 3.6 and 4.9%, respectively.

A reactor has also been built to provide an environment in which infrared absorption spectra could be recorded during black liquor combustion. In this environment, gas temperatures have been measured with an accuracy of 2-3% at temperatures between 450-750 K. Gas concentrations have been measured with accuracies of better than 10% at concentrations between 0.3-1.3%.

INTRODUCTION

The economic feasibility of the kraft pulping process is a result of the success of the kraft recovery cycle. A principal component of this cycle is the recovery furnace. Combustion of black liquor within the furnace accomplishes four objectives; final evaporation of the black liquor, combustion of the organic fraction of the liquor, recovery of the spent pulping chemicals, and energy (heat) recovery. Although the recovery furnace has been used for more than 60 years, much of the combustion chemistry that occurs within it is not fully understood. With a modern day emphasis on optimizing the combustion of black liquor, in order to maximize solids throughput, a more complete understanding of furnace performance and operation is needed.

The development of a mathematical model which simulates the chemistry, fluid mechanics, and heat and mass transfer within a recovery boiler is potentially an excellent tool, capable of improving the current understanding of the operation and performance of a recovery furnace. A model of this type can be used to safely and inexpensively predict furnace performance given changes in operating variables, and can be used to suggest alternative burning strategies. The Institute of Paper Science and Technology (IPST) has in the past,[1-3] and is again currently, developing models of this type. Before these models can be accurately developed, however, a complete understanding of the chemical processes occurring within the furnace is required.

There have been significant efforts directed towards the development of a fundamental understanding of the chemical and physical processes occurring within a kraft recovery boiler. In part, these efforts have involved direct measurements within the furnace; these measurements, however, have been difficult to obtain. These difficulties arise first, because many chemical processes are occurring simultaneously within the furnace, including; drying, pyrolysis, char combustion, char gasification, inorganic reactions, and fuming, see Fig. 1.[4]

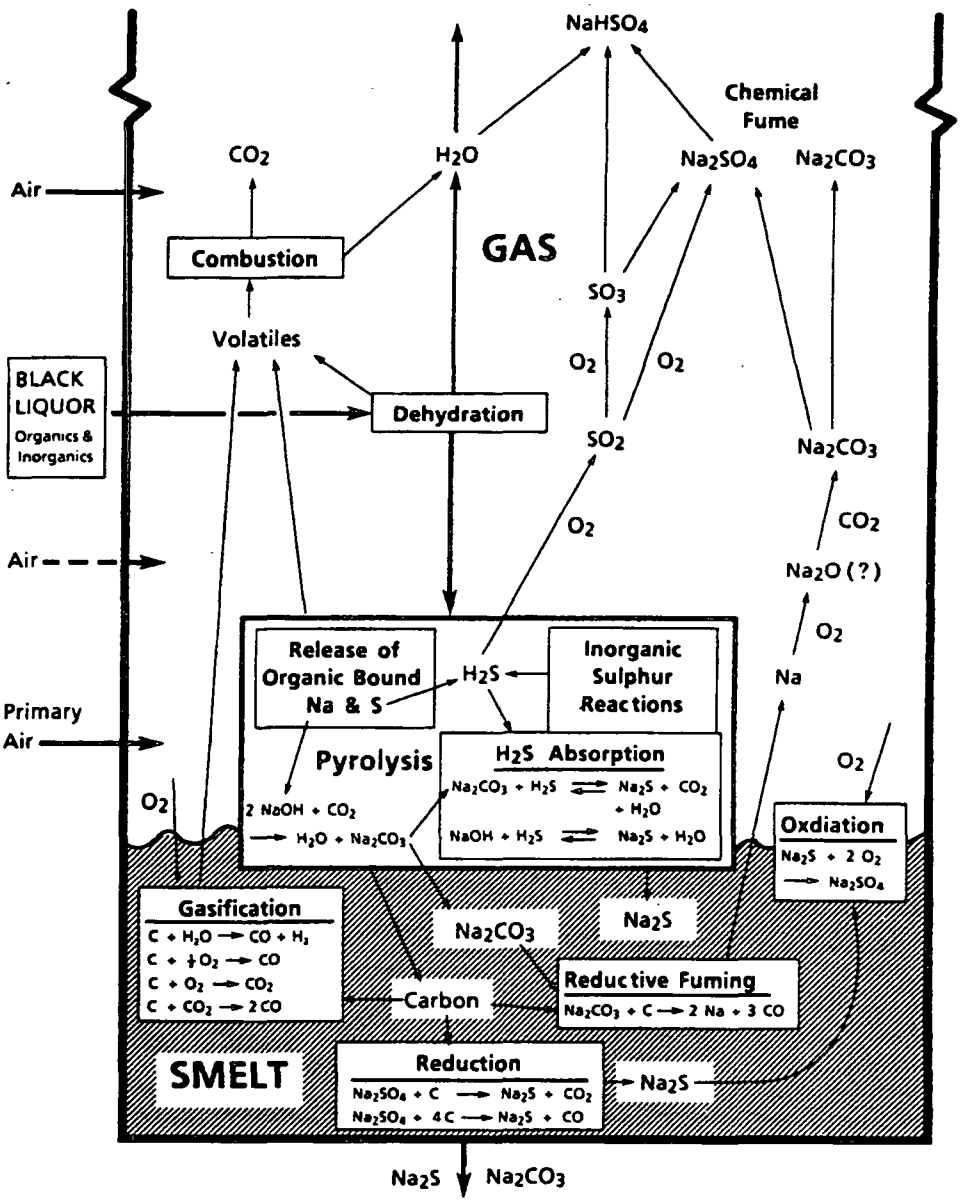

Figure 1. Chemical reactions occurring within a recovery furnace as described by Blackwell and King.[4] (Reprinted from reference 1 with permission from B. Blackwell, and Sandwell and Company Limited, Vancouver, B.C.)

The simultaneous occurrence of these processes makes it difficult to identify and quantify the factors affecting any single process. Second, because of the high temperature and corrosive nature of the combustion environment, *in situ* furnace sampling, for the determination of gas temperatures and concentrations, is difficult. The inability to continuously monitor

the formation of gaseous products within the furnace requires the reliance upon flue gas measurements. These measurements, however, are complicated by secondary reactions, which occur, not during combustion, but subsequent to combustion in the gas flow before flue gas detection meters.

As a result, much of the knowledge of the fundamental combustion processes of kraft black liquor has been obtained by laboratory studies. In the laboratory, individual combustion processes can be isolated. Research of this type has resulted in the development of an understanding of several individual combustion events. Examples of this work, at IPST alone, include studies describing: droplet combustion,[5] pyrolysis,[6] char combustion,[7-9] sulfur release,[10] fume deposition,[11] *etc.* In this experimental work, these studies have successfully relied upon conventional diagnostic tools for the determination of gas concentrations and temperatures; primarily thermocouples and NDIR (non-dispersive infrared) gas analyzers.

There are many questions regarding black liquor combustion which remain unresolved. For example, the consumption of char carbon in the lower furnace is a very complicated process which is not fully understood. It is believed that the carbon is consumed in three ways. First, it can undergo "combustion" by oxygen to yield CO and CO_2.[7,8,12-14] Second, in the presence of CO_2 or H_2O vapor, the char carbon can be "gasified" to produce CO and H_2.[12-15] Third, molten inorganics (Na_2SO_4, and Na_2CO_3) in contact with the solid char can lead to bed reactions resulting in the formation of CO and CO_2.[4,9,16] While rate data for some of these individual processes is available, the net interaction of all of these processes, resulting in "bed" burning, is not well understood.

Additional unresolved recovery boiler chemistry issues include fume formation, sulfur release,[17-22] NO_x formation, and gaseous HCl production. Thorough studies aimed at unravelling the chemistry involved with the production of these gaseous species, or the gaseous

intermediates responsible for their formation, have not been completed. Understanding of this chemistry is fundamental to optimizing furnace performance, reducing boiler downtime (water washes and boiler tube repairs), and reducing pollutant formation.

The development of a more complete understanding of all of these processes, requires, in part, an analysis of the chemistry which is occurring in the lower furnace. While it is difficult to make *in situ* measurements within the lower part of a recovery boiler, it is possible to simulate the char bed in the laboratory on a small scale. An analysis of the gas phase above this environment, could yield significant insight into the gaseous chemistry occurring above black liquor char beds.

IN SITU COMBUSTION DIAGNOSTICS

Experimental approaches for the analysis of the gas phase of laboratory combustion systems have included the use of non-intrusive, *in situ*, spectroscopic techniques. These techniques have been shown capable of measurements for temperatures, concentrations, soot particle size, turbulence patterns, and velocities in high temperature turbulent environments.[23] Several spectroscopic techniques are capable of measuring gas temperatures and concentrations simultaneously. These techniques include coherent anti-stokes Raman spectroscopy (CARS),[24-26] laser induced fluorescence (LIF),[27-29] spontaneous Raman scattering (SRS),[30-32] tunable diode laser absorption spectroscopy (TDLS),[33] and Fourier transform infrared absorption spectroscopy (FT-IR).[34-36] A list of these techniques, along with a brief description of each, is provided in Table 1.

Review of the literature has indicated that Fourier transform infrared (FT-IR) absorption spectroscopy may be particularly well suited for the analysis of the gas phase

Table 1. Description of several optical techniques used for the determination of gas temperatures and concentrations in combustion environments.

Spectroscopic Technique	Description
CARS (Coherent Anti-Stokes Raman Spectroscopy)[24-26]	Two relatively high-powered laser sources of frequencies w_p and w_s are focused together in a sample. As a result of the mixing of these two beams, a low intensity coherent beam of frequency $w_{as} = 2w_p - w_s$ is produced. The efficiency of the conversion to w_{as} is dependent upon the presence of molecular resonances.
LIF (Laser Induced Fluorescence)[27-29]	Analysis of radiation spontaneously emitted from an upper electronic state which was excited by the absorption of laser radiation tuned to coincide with a molecular resonance.
SRS (Spontaneous Raman Scattering)[30-32]	Analysis of scattered radiation resulting from inelastic collisions between light and gaseous molecules. The distribution of the scattered radiation frequencies from spontaneous Raman scattering is uniquely defined by the wavelength of the incident radiation and the species which produced the scattering.
TDL (Tunable Diode Laser Absorption Spectroscopy)[33]	Absorption of infrared radiation by a sample over a frequency range of 1-2 wavenumbers. A tunable diode laser is used for the infrared source.
FT-IR (Fourier Transform Infrared Absorption Spectroscopy)[34-36]	Absorption of infrared radiation by a sample over a frequency range of 4000 wavenumbers. A heated filament is used for the infrared source.

immediately above a burning black liquor char bed. This assumption is based upon a consideration of the type and concentration of the gases above a burning black liquor char bed, as well as a consideration of the effect of interferences, such as fume and emission radiation. Furthermore, FT-IR absorption spectroscopy has been used, with limited success, to obtain qualitative and quantitative gas phase information in coal combustion environments.[34-36]

FT-IR absorption spectroscopy has not previously been used for *in situ* analyses of gas concentrations and temperatures in a black liquor combustion environment. It is expected that it has the potential to yield accurate concentrations and temperatures in the gas phase directly above a burning char bed. This information is key to developing a better understanding of black liquor char consumption and in addition, has the potential to elucidate additional gaseous recovery boiler chemistry. The development of FT-IR for black liquor combustion diagnostics, however, will first require a rigorous understanding and development of the fundamentals regarding absorption of infrared radiation by high temperature gases.

BACKGROUND

INFRARED ABSORPTION FUNDAMENTALS

Infrared absorption spectroscopy has been used extensively for the identification and quantification of both organic and inorganic molecules. Its widespread use can be attributed to the large range of molecules which are infrared active, and the high degree of selectivity with which they can be analyzed. For routine analyses, it is most often used for the identification of organic liquids or solids. However, in more specialized applications, it has also been used for gas analyses. The essential components of an infrared absorption experiment, independent of sample type, are shown by the block diagram given in Fig. 2.

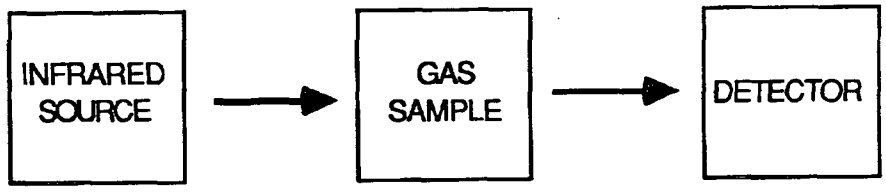

Figure 2. Simple block diagram illustrating the essential components of an infrared absorption experiment which includes the source, sample, and detector.

An infrared source is directed through a cell containing the sample. The sample absorbs part of the infrared beam and the unabsorbed radiation passes through and is measured by a detector. The ratio of the total energy reaching the detector when the beam passes through the sample, divided by the energy reaching the detector when no sample is in the cell, is plotted in a spectrum of percent transmittance vs. wavenumbers, Fig. 3. A negative spike will appear in the spectrum at a wavenumber where the sample has absorbed infrared radiation. The transmittance spectrum is often converted into the more useful format of an absorbance spectrum by using the relationship $A(\nu) = - \log_{10} [T(\nu)]$, also shown in Fig. 3. Wavenumbers are a measure of the number of waves per unit length and are related to fre-

quency by the equation $\tilde{\nu} = c \cdot \nu$, where $\tilde{\nu}$ is given in reciprocal seconds, c is the speed of light (2.998×10^{10} cm/s) and ν has units of reciprocal centimeters.

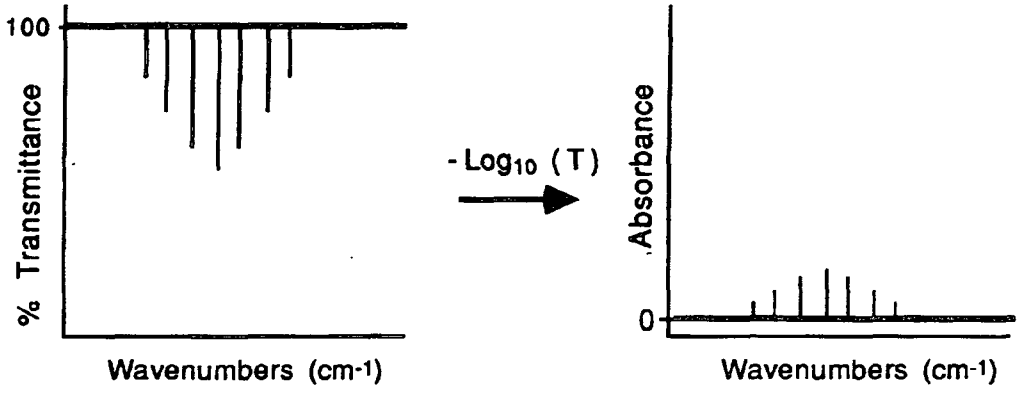

Figure 3. Illustration of data resulting from an infrared absorption experiment, the transmission spectrum, and the conversion of that data into an absorbance spectrum.

The position (wavenumber) of the peaks observed in an absorbance spectrum are dependent upon the type of molecule which is absorbing the infrared radiation. For the simple gases of interest in combustion diagnostics, CO, CO_2, H_2O, *etc.*, the frequencies of the absorption lines are well known. Observation of the peak positions, in an absorbance spectrum, permits easy identification of the molecules present in the sample. The intensity of the peaks, however, are complicated functions of gas concentration, temperature, pressure, and the presence of colliding foreign gas molecules.

VIBRATIONAL-ROTATIONAL ABSORPTION LINES

The frequency at which molecules absorb radiation, coincides with the energy required to excite the molecule from a low energy state to a higher energy state. Detailed descriptions of the theory and mathematics associated with this energy absorption, by diatomic[37] and polyatomic[38] molecules, were presented by Herzberg. Gaseous species absorbing in the mid-infrared region, each contain hundreds of absorption peaks. These absorption

peaks are called vibrational-rotational lines. When a molecule absorbs infrared radiation, it is excited from a particular rotational energy level of a given vibrational energy state, to a different rotational energy level in an excited vibrational state. Transitions of this type are designated by the notation, $(J',\upsilon' \leftarrow J'',\upsilon'')$, where J refers to a particular rotational level, υ refers to particular vibrational level, the double prime refers to the lower energy state, and the prime refers to the excited energy state. The arrow indicates that the molecule is being excited from the lower energy level J", υ" to the excited energy level, J', υ'. The energy associated with the transition is related to wavenumbers in the absorption spectrum by the relationship,

$$\Delta E = h \cdot \tilde{\nu} = h \cdot c \cdot \nu \,, \tag{1}$$

where E is the energy (Joule/s), h is Planck's constant (6.626×10^{-34} J·s), c is speed of light (2.998×10^{10} cm/s), and ν and $\tilde{\nu}$ have already been defined. The transitions which occur from one energy level to an excited level are not random. The specific allowed transitions are described by the selection rules.[39] For example, for a diatomic molecule such as CO, transitions are allowed only between vibrational levels where $\Delta\upsilon = \pm 1$, and between rotational levels where $\Delta J = \pm 1$. When $\Delta\upsilon = +1$ absorption occurs, and when $\Delta\upsilon = -1$, emission results. The rotational transitions from the ground state vibrational level, to the first vibrational excited state will consist of those from $(J''+1 \leftarrow J'')$ and $(J''-1 \leftarrow J'')$. In the absorption spectrum there are two branches. The lines resulting from $(J''+1 \leftarrow J'')$ transitions form the R branch and the $(J''-1 \leftarrow J'')$ transitions form the P branch. The allowed transitions from the ground state to the first vibrational state for a diatomic molecule are shown schematically in Fig. 4.

The selection of vibrational-rotational absorption lines for combustion diagnostics, involves identifying and choosing those lines which are most fully resolved. For example,

most of the CO lines of the P branch of the fundamental vibrational mode, occurring at wavenumbers between 2000 - 2150 cm^{-1}, are well resolved. Similarly, for CO_2 the most fully resolved lines are those on the outer wing of the CO_2 R branch of the $\tilde{\nu}_3$ normal mode of vibration. The $\tilde{\nu}_3$ normal mode of vibration, for a linear triatomic molecule such as CO_2, corresponds to an asymmetric stretch of the molecule as shown in Fig. 5.

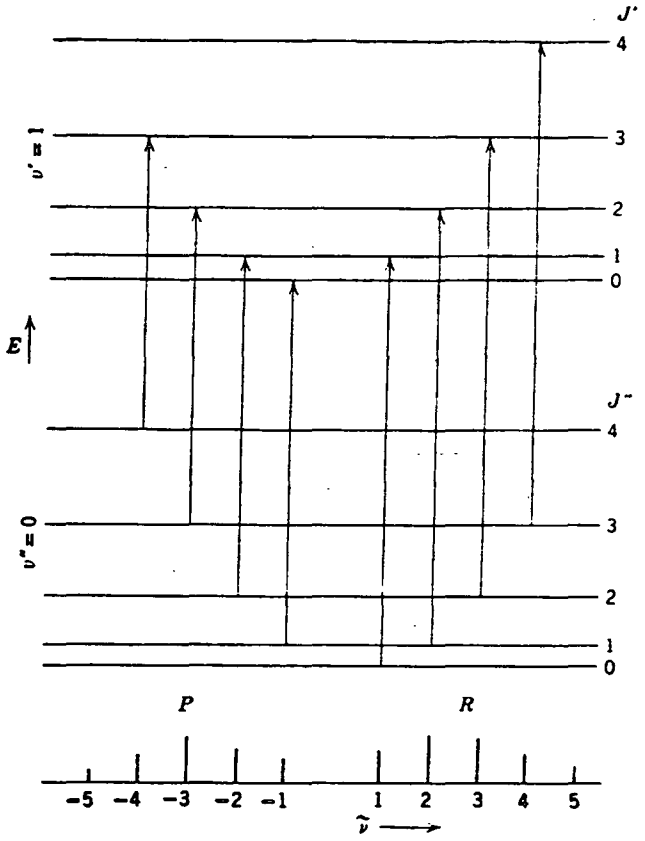

Figure 4. Allowed rotational energy level transitions from the ground state to the first excited vibrational state for a diatomic molecule. (Reprinted by permission of John Wiley & Sons, Inc., from Physical Chemistry, 6th Edition, by R. A. Alberty. Copyright© by John Wiley & Sons, Inc. 1983)

Analysis of gaseous species by infrared absorption spectroscopy is possible for many species of interest in black liquor combustion diagnostics. These species include H_2O, SO_2, H_2S, HCl, NO, NO_2, *etc.* The vibrational-rotational transitions responsible for the absorption lines of simple molecules (2-3 atoms), are easily identified. However, any molecule, re-

gardless of its size, will give an absorption spectrum, provided it has a net non-zero dipole moment. For this reason, homonuclear diatomic molecules such as O_2, N_2, H_2, *etc.* are not infrared active and do not have absorption spectra in the mid infrared region.

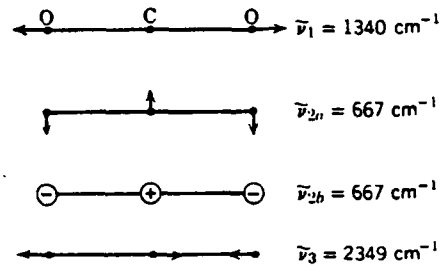

Figure 5. Normal modes of vibration for CO_2, a symmetrical, linear triatomic molecule. (Reprinted by permission of John Wiley & Sons, Inc., from Physical Chemistry, 6th Edition, by R. A. Alberty. Copyright© by John Wiley & Sons, Inc. 1983)

There are several different types of instrumentation available for the acquisition of gaseous infrared absorption spectra. The two types previously used for combustion diagnostics, include tunable diode laser spectroscopy (TDL) and Fourier transform infrared (FT-IR) spectroscopy. Although each technique is based upon the simple principles described in Fig. 2, they differ considerably in the type of source utilized, wavenumber range, and data acquisition time. The results presented in this work are based upon the use of FT-IR absorption spectroscopy, however, much of the line parameter data, and some combustion experiments, rely on TDL spectroscopy. Therefore, a brief description of each technique will be provided.

TUNABLE DIODE LASER ABSORPTION SPECTROSCOPY

A schematic diagram of a typical TDL experimental arrangement is provided in Fig. 6.[40] The experimental configuration consists of a tunable diode laser, as the infrared source, which is controlled and modulated with a dc current power supply. Out of the laser, the

beam passes through the sample (a burner in Fig. 6) and then to a monochromator. The monochromator filters out emission radiation from the burner and also eliminates unwanted laser modes from reaching the detector. From the monochromator, the infrared beam is split, half of it goes to a Fabry-Perot etalon and the other half goes to a 10 cm reference gas cell. (The etalon provides a reference, from which the half-width of the absorption line, in wavenumbers, can be determined.) The two beams are then directed to detectors, and the electrical signals from the detectors are sent to an oscilloscope or some other electronic recording device. A sample spectrum is then ratioed against a background (no gas sample), to yield either a transmission or an absorption spectrum; a typical TDL absorption spectrum is given in Fig. 7.

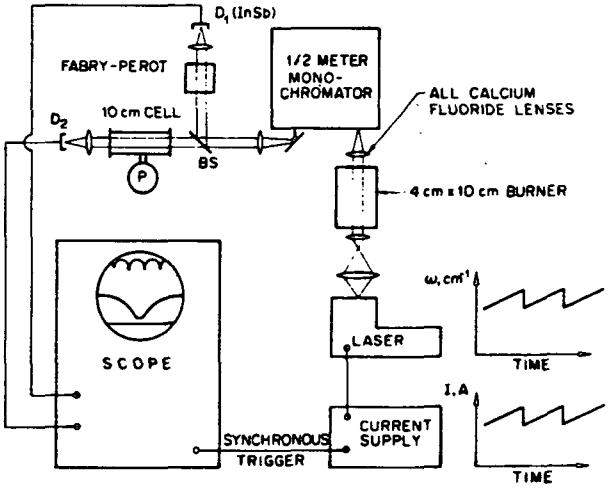

Figure 6. Experimental arrangement of a tunable diode laser spectrometer.(Reprinted from reference 40 with permission of the Optical Society of America and the principal author.)

The unique features of tunable diode laser absorption spectroscopy include the high resolution and high intensity of the source, the narrow frequency range of the laser, and the short data acquisition time. The infrared source is a tunable diode laser whose output wavelength can be rapidly changed. The tunability of a given laser source is approximately 20-100 cm^{-1} and is varied by adjusting the current supplied to the device and the tempera-

ture at which the crystal is cryogenically maintained. However, for a given experiment, the laser is able to scan only over a single laser mode, a range of 1-2 cm^{-1}. The frequency range is selected to coincide with the energy associated with a particular vibrational-rotational transition. The small frequency scanning range permits the acquisition of only 1 or 2 carefully selected absorption lines. The inability to measure multiple absorption lines, makes simultaneous multicomponent concentration measurements and/or temperature measurements difficult.

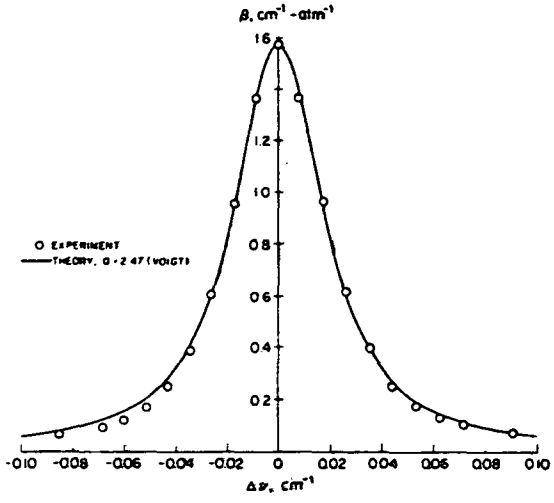

Figure 7. Spectrum of a single CO absorption line obtained from a tunable diode laser spectrometer. (Reprinted from reference 40 with permission of the Optical Society of America and the principal author.)

The disadvantages associated with the small scanning range are partially offset by the advantages associated with the instrument's high resolution, high intensity, and rapid scan rate. The resolution of the instrument, defined by the line width of the beam exiting the laser, is on the order of 3×10^{-4} cm^{-1}. The intensity of the beam, 1-4 mW, is sufficiently strong to require only a single scan, which can be obtained at scanning speeds of approximately 0.025 s. The spectrum of a single absorption line, such as that shown in Fig. 7, is of very high quality. The high degree of instrument resolution, yields spectra which are relatively unaffected by broadening from instrument distortions. Therefore, the shape of the

experimental lines, will only be a result of gas absorption and molecular interactions. As a result, the determination of line parameters such as line strengths, broadening coefficients, or half-widths from TDL absorption spectra are extremely reliable. In applications to combustion experiments, the high scanning rate and ability to require only single scans, reduces the possibility of changes to occur within the combustion environment, during the experiment, and makes combustion measurements in rapidly changing environments, such as shock tubes, possible.

FT-IR ABSORPTION SPECTROSCOPY

Fourier transform infrared spectroscopy is an alternative method for obtaining infrared absorption spectra. FT-IR spectroscopy differs most significantly from TDL spectroscopy in the type of source which is used and the method of source modulation. Compared to TDL spectroscopy, these differences significantly affect the data acquisition time, the instrument resolution, and the frequency range of the resulting spectra. A schematic diagram of the essential components of an FT-IR instrument are given in Fig. 8.[41] For high intensity instruments, an electrically heated Globar source (silicon carbide) is often used.[42] The radiation emitted from this source is collected and passed through a beam splitter which directs half of the source to a mirror with a fixed position, and the remaining half to a moving mirror; this arrangement of mirrors comprises the essential components of a Michelson interferometer. After reflecting off the mirrors, the infrared beam is recombined at the beam splitter and directed out of the interferometer. From the interferometer, it is then passed through the sample and finally onto a detector.

The Michelson interferometer, is the component which makes FT-IR spectroscopy unique among infrared absorption techniques. The interferometer is used to modulate the source. Source modulation is the process of converting the high frequency infrared radiation

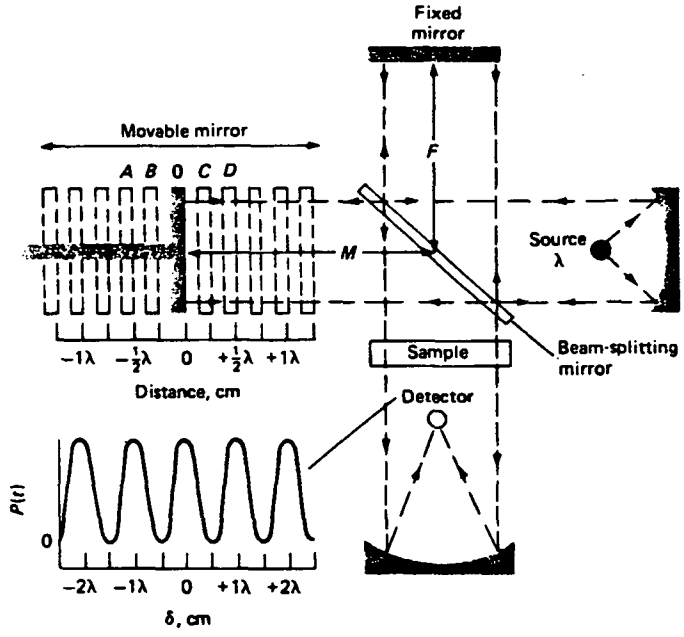

Figure 8. Schematic diagram of an FT-IR spectrometer. The diagram includes the source, beam splitter, moving and fixed mirrors, sample and detector.[41] (Figure 8-20 from PRINCIPLES OF INSTRUMENTAL ANALYSIS, Second Edition, by Douglas A. Skoog and Donald M. West, copyright © 1980 by Saunders College Publishing, reprinted by permission of the publisher.)

(for example, at 2000 cm^{-1} the frequency is 6.0×10^{13} Hz) to a lower, directly proportional, measurable frequency. Modulation by a Michelson interferometer is accomplished by the use of constructive and destructive interference. Considering first a monochromatic source, when the distance between the beam splitter and the moving mirror is the same as the distance between the beam splitter and fixed mirror, recombination of the two reflected beams will result in constructive interference, and the resulting beam will have an intensity equal to the sum of the two halves. When the adjustable mirror is moved a distance equal to one quarter a wavelength of the source, the path difference between the two reflected beams will be one half a wavelength. Recombination of these two beams will result in destructive interference, since the two are completely out of phase, and the intensity of the resulting beam will be zero. As the mirror moves an additional quarter wavelength, constructive interference will result and the intensity is again at a maximum. The intensity measured by the de-

tector is shown in Fig. 8, and consists of a cosine wave, centered at zero mirror displacement.

The source used in an FT-IR spectrometer is continuous and, therefore, all the frequencies are modulated simultaneously. At the start of data collection, the optical retardation (mirror displacement) is zero and all the frequencies reach the detector with their maximum amplitude. As the mirror moves, the coaddition of multiple cosine waves which are out of phase with respect to each other, results in a decrease of the power reaching the detector. The resulting intensity recorded by the detector, as a function of mirror displacement or time, is shown in Fig. 9 and is called an interferogram.

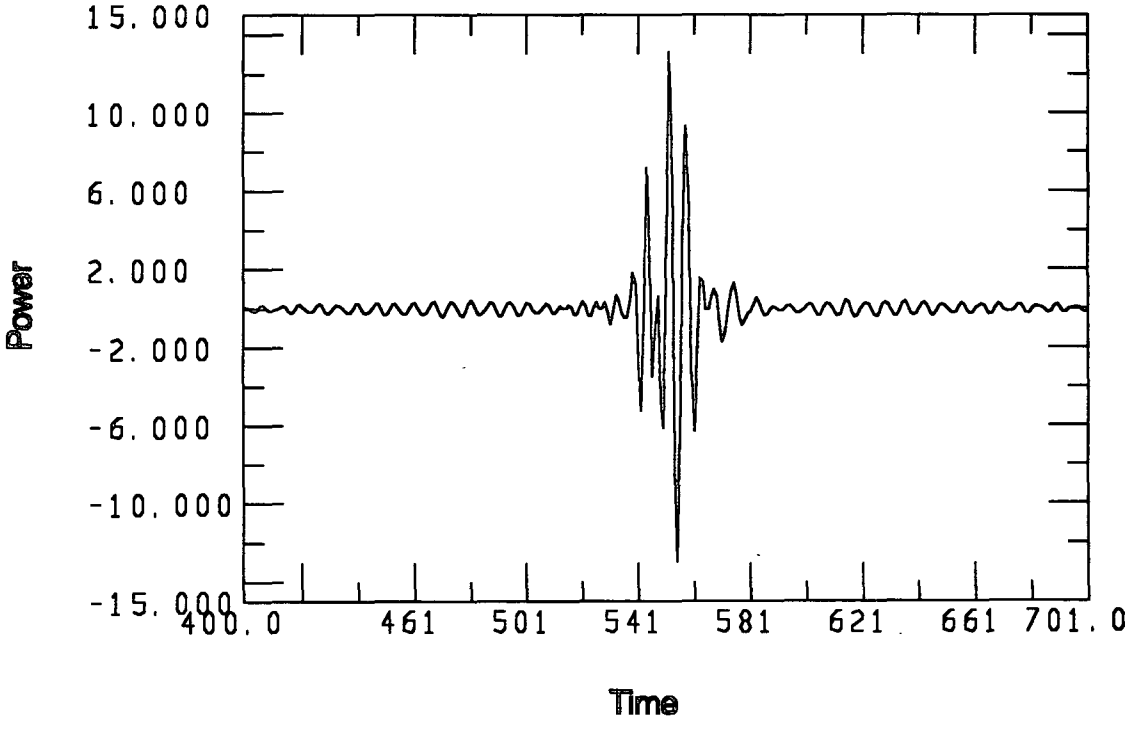

Figure 9. Intensity, $P(\delta)$, of infrared source reaching the detector as a function of mirror movement, δ, for a polychromatic source.

There would be no advantage to using a Michelson interferometer if it was only used to produce a modulated source; this could be more easily accomplished with a chopper. The

benefit of modulating the radiation with the interferometer, results from the ability to convert an interferogram, such as that shown in Fig. 9, into a spectrum of intensity versus frequency (wavenumbers). This process is accomplished mathematically. The intensity of the radiation reaching the detector for a single frequency is given by, $P(\delta)\cos 2\pi\delta\sigma$. The intensity recorded by the detector, of a polychromatic source, is given by a summation of all the frequencies. The summation can be written in the form of an integral,

$$P(\delta) = \int_{n=-\infty}^{\infty} P(\sigma) \cos 2\pi\delta\sigma_n \cdot d\delta, \tag{2}$$

where $P(\delta)$ is the time domain amplitude or power of the interferogram signal, $P(\sigma)$ is the frequency domain power incident on the interferometer, and δ is the optical retardation or mirror displacement. The data which comprise this equation are then transformed, by a Fourier transform algorithm, which converts the time domain data, into the frequency domain. The intensity is then given by,

$$P(\sigma) = \int_{n=-\infty}^{\infty} P(\delta) \cos 2\pi\sigma\delta_n \cdot d\sigma, \tag{3}$$

Plotting this data results in a measure of the detector response as a function of frequency, which is the infrared absorption spectrum. The mathematical details describing this process have been presented elsewhere.[42] Additional details describing the data collection process and instrumentation can also be found elsewhere.[41,42] The great advantage of FT-IR spectroscopy, as compared to grating instruments, is the time required to collect a single spectrum. In the case of a grating instrument, the frequency of the source passed through the sample is changed, and the intensity of absorption is measured for each individual frequency. This is a relatively slow process, in some cases requiring ten minutes or more. With FT-IR spectroscopy, all the frequencies are measured simultaneously, and the total time re-

quired to collect a single spectrum depends upon the time needed to move the mirror (resolution improves with distance of mirror displacement). The interferogram, can be recorded in approximately one second, averaging multiple interferograms results in an improvement of the signal-to-noise.

The absorption spectra obtained from FT-IR spectrometers, operating in the mid-infrared region, will contain spectral information for all wavenumbers between 400-4400 cm^{-1}. Furthermore, unlike traditional dispersive infrared instruments, all of this information will have been collected simultaneously. Application of FT-IR to a combustion environment, results in the simultaneous acquisition of infrared absorption spectra of all combustion reactants or products which are infrared active. FT-IR spectrometry is unique among all other combustion diagnostic techniques, in its ability to gather so much simultaneous spectroscopic information; other techniques have more limited spectral ranges.

The acquisition of infrared absorption spectra spanning large portions of the mid-infrared region, is not accomplished without compromise. Compared to tunable diode laser absorption spectroscopy, the data acquisition time is much longer, and the resolution of the instrument is lower. Although the entire mid-infrared region is scanned simultaneously, the Globar source used in FT-IR spectrometers is relatively weak, compared to a TDL source. In order to maintain a satisfactory signal-to-noise ratio, multiple scans (100-500) must be averaged. Averaging spectra increases data acquisition time from less than 1 second to several minutes. Unlike tunable diode laser spectroscopy, these long data acquisition times require that the experiment behave at a near steady state condition. Also, the resolution of the FT-IR instrument is much poorer than in TDL spectrometry. In order to fully resolve the rotational fine structure of gas samples such as CO or CO_2, an instrument resolution of 0.1-0.3 cm^{-1} is required. While these levels of resolution are obtainable, the acquisition of spectra at higher resolution slows down the data acquisition because the moving mirror is required to

travel longer distances. Furthermore, even though the vibrational-rotational lines are resolved, the relatively low resolution causes distortions of the spectral peaks. This distortion requires significant mathematical corrections before the spectra are useable for either temperature or concentration calculations.

TEMPERATURE DETERMINATIONS FROM ABSORPTION SPECTRA

Once an absorption spectrum has been obtained, it can be used to calculate both gas temperatures and concentrations. The determination of gas temperatures from infrared absorption spectra, is accomplished by examining the distribution of molecules populating the various rotational energy levels of a given vibrational energy state. As the temperature of a gas sample increases, the number of molecules occupying the higher rotational energy levels increases. In an absorption spectrum, changes in the distribution of molecules is evident as first, a decrease in intensity of the vibrational-rotational lines with low J" indices, and second, an increase (or appearance) of the intensity of the lines with high J" indices.

For a diatomic molecule, the number of molecules occupying a particular rotational energy level, at a given temperature, can be described mathematically,

$$S_{\upsilon'';J''}^{\upsilon';J'}(T) = S_b{}^1(T^\circ)\frac{T^\circ}{T}\frac{\nu}{\nu_b(T^\circ)}\frac{\exp\left[-\frac{hc}{kT}E(\upsilon,J)\right]}{Q(T)}\left[1-\exp\left(-\frac{hc}{kT}\nu\right)\right]$$

$$\times\ (\upsilon''+1)\,|m|\,(1+K_1 m+K_2 m^2)\,. \qquad (4)$$

A description of the terms within this equation are given in Table 2. This equation was originally derived by Herzberg,[37] but is given here in a more useful format developed by Varghese and Hanson.[43] For all the lines in a given vibrational band, the following terms which are independent of the rotational transition are, $S_b{}^1(T^\circ)$, $\frac{T^\circ}{T}$, $\frac{1}{\nu_b(T^\circ)}$, and $\frac{1}{Q(T)}$.

Table 2. Description of terms in Equation 4.

TERM	Description
T	Gas temperature (K)
T°	Reference temperature (K)
$S_{\upsilon'';\, J''}^{\upsilon';\, J'}(T)$	Line strength for (υ', $J' \leftarrow \upsilon''$, J'') transition ($1/(atm \cdot cm^2)$)
$S^1(T_o)$	Band strength ($1/(atm \cdot cm^{-2})$) for vibrational transition $1 \leftarrow 0$ at reference temperature, T°
ν	Frequency of vib-rot transition (cm^{-1})
$\nu_b(T^\circ)$	Effective band center (cm^{-1})
$E(\upsilon,J)$	Energy of initial state
$Q(T)$	Partition function at T
$\left[1-\exp\left(-\frac{hc}{kT}\nu\right)\right]$	Correction for induced emission
m	$m = -J''$ for P branch lines $m = J''+1$ for R branch lines
$(1+K_1 m+K_2 m^2)$	Herman-Wallis correction for vib-rot interaction, $K_1 = 1.73\times10^{-4}$ $K_2 = 7.3\times10^{-6}$

Each of these terms will affect the line strengths to the same extent, regardless of the specific vibrational-rotational transition. If these terms are eliminated from Equation 4, the equality is no longer applicable and must be replaced by a proportionality sign. The equation can be further simplified, if first, υ'' is set equal to zero, which is the case for first order transitions, and second, if induced emission is ignored. Finally, the line strength term, $S_{\upsilon'';\, J''}^{\upsilon';\, J'}(T)$, can be replaced by a product which is directly proportional to it, $A_{peak}(m)\cdot\gamma(m)$,[44] to yield the following proportionality,

$$A_{peak}(m)\cdot\gamma(m) \propto \nu(m)\cdot\exp\left[-\frac{hc}{kT}E(\upsilon, J)\right]\cdot|m|\cdot(1+K_1 m+K_2 m^2). \qquad (5)$$

Here, $A_{peak}(m)$ is defined as the peak maximum of the absorption line and $\gamma(m)$ is defined as the line half-width at half height (HWHH). Rearrangement of Equation 5 yields,

$$\ln \left\{ \frac{A_{peak}(m)}{(1+K_1 m+K_2 m^2)} \frac{\gamma(m)}{\nu(m)} \frac{1}{|m|} \right\} \propto -E(\upsilon,J) \frac{hc}{kT} . \qquad (6)$$

Equation 6 shows that the term on the left, called here the intensity term, is directly proportional to the product of the energy of the ground state (cm^{-1}), and the constant hc/k. The proportionality is the negative reciprocal of the gas temperature. For a given absorption spectrum, a plot can be made of the intensity term versus the corresponding energy term for each of the vibrational-rotational absorption lines. A least squares fit of these points should yield a straight line with a slope equal to -1/T.

CONCENTRATION DETERMINATIONS FROM ABSORPTION SPECTRA

In addition to gas temperatures, it is also possible to calculate the gas concentration from absorption spectra of fully resolved vibrational-rotational lines. The absorption of infrared radiation by a gas is given by the Bouguer-Lambert expression,[45]

$$T(\nu) = \exp\ [-\alpha(\nu) \cdot C \cdot L]. \qquad (7)$$

This relationship equates the transmittance, $T(\nu)$, of a single vibrational-rotational line with the negative exponential product of $\alpha(\nu)$, the absorption coefficient in units of 1/(conc·cm), C, the gas concentration, and L, the path length of the cell (cm). The relationship between transmittance, $T(\nu)$, and absorbance, $A(\nu)$, is given by,

$$A(\nu) = -\log T(\nu) . \qquad (8)$$

Substitution of Equation 8 into Equation 7 yields,

$$A(\nu) = \frac{\alpha(\nu) \cdot C \cdot L}{\ln 10} . \qquad (9)$$

The absorption coefficient, α, is dependent upon the conditions of the experiment; most importantly, the total pressure of the gas. This dependence is a result of the mechanism controlling the broadening of the vibrational-rotational line. Gross, Griffiths, and Sun[44] have given a description of the assumed profiles for various conditions. At one atmosphere pressure, molecular collisions broaden the vibrational-rotational line profile. A Lorentian line shape has been found to adequately describe the shape of a broadened absorption line,

$$\alpha(\nu) = \frac{S(m)\cdot\gamma(m)}{\left[\pi\cdot((\nu-\nu_o)^2 + \gamma(m)^2)\right]} \tag{10}$$

Here, S(m) is the line strength ($1/(atm\text{-}cm^{-2})$), γ is the halfwidth of the line (cm^{-1}), ν is the frequency, and ν_o is frequency at the line center. The line strength is dependent upon m and, therefore, is different for each line used in the concentration calculations. Substitution of the expression for the absorption coefficient, given in Equation 10, into the absorption intensity relationship, given in Equation 9, yields,

$$A(\nu) = \frac{S(m)\cdot\gamma(m)\cdot C\cdot L}{\left[\pi\cdot((\nu-\nu_o)^2 + \gamma(m)^2)\cdot\ln(10)\right]} \tag{11}$$

Solving Equation 11 to determine the gas concentration (partial pressure) can be accomplished by several different methods. The first involves a line fitting technique. Assuming that a reliable, photometrically accurate absorption spectrum of a single vibrational-rotational line has been obtained, Equation 11 can be fit by non-linear least squares to the line by adjusting the partial pressure (concentration) until agreement is obtained between the theoretical and experimental lines.

An alternate approach, involves solving Equation 11 for the peak center, ν_o,

$$A(\nu_o) = \frac{S(m) \cdot C \cdot L}{[\pi \cdot \gamma(m) \cdot \ln(10)]} \quad , \tag{12}$$

and then rearranging the equation and solving directly for C, by substitution of the parameters on the right side of this equation,

$$C = \frac{A(\nu_o) \cdot \pi \cdot \gamma(m) \cdot \ln(10)}{S(m) \cdot L} \quad . \tag{13}$$

Three factors which control the relative intensity $A(\nu_o)$ of vibrational-rotational absorption lines are 1) the absorption coefficient, $\alpha(m)$, 2) the concentration of the gas, and 3) the path length. Each of these factors is directly proportional to the absorption intensity, as described by Equation 9. While the influence of concentration and path length on absorption intensity is intuitive, the factors controlling the absorption coefficient (1) are less obvious and more complicated.

Two variables comprising the absorption coefficient are the line half-widths and the line strengths. Line strengths are strongly dependent upon the gas temperature and m. Half-widths are not only m and temperature dependent, but are also dependent upon the partial pressure of all the components in the gas phase. Explicitly accounting for both the line strength and half-widths is necessary to performing high temperature concentration calculations. A discussion of both line strengths and half-widths is provided below.

Theoretical CO and CO_2 Halfwidth Data

For gases at atmospheric pressure, collision broadening controls the line shape.[44] With this mechanism of line broadening, each species in the gas sample influences the width

of the line being observed. In addition, the half-width is influenced by the value of m and the gas temperature. Equations have been developed to describe the half-width of absorption lines, $\gamma_x(m)$, in gas mixtures, based upon the partial pressure of the gaseous components, P_x, P_y, *etc.*; the total pressure, P_t; broadening coefficients, $\gamma^o_{xx}(m)$, $\gamma^o_{xy}(m)$, *etc.*; the gas temperature, T; a reference temperature, T°; and the temperature exponents, $N_{x,x}(m)$, $N_{x,y}(m)$, *etc.*[44] For example, broadening for a two-component system consisting of species x and y is given by,

$$\gamma_x(m) = \gamma^o_{xx}(m) \cdot \left(\frac{P_x}{P_t}\right) \cdot \left(\frac{T^o}{T}\right)^{N_{x,x}(m)} + \gamma^o_{xy}(m) \cdot \left(\frac{P_y}{P_t}\right) \cdot \left(\frac{T^o}{T}\right)^{N_{x,y}(m)} \qquad (14)$$

Details describing this equation and the theories used to derive it are presented in greater detail by Gross *et al.*[44] In order to use Equation 14, either experimental, theoretical, or predicted (based upon a combination of theory and experiments) temperature and m dependent values of $\gamma^o_{xx}(m)$, $\gamma^o_{xy}(m)$, $N_{x,x}(m)$, and $N_{x,y}(m)$ are required. The most comprehensive and reliable source for this data has been found from modeling work performed by Hartmann *et al.*[46] for CO lines and by Rosenmann *et al.*[47] for CO_2 lines.

Hartmann *et al.*[46] developed a model which accounts for CO line broadening by H_2O, N_2, O_2, and CO_2. This model is based, in part, on existing high temperature experimental broadening data and upon theoretical considerations. Their calculations have yielded values of γ^o and N, including their dependence on m and temperature. This appears to be the most comprehensive data base available, from which high temperature CO half-width information can be obtained. However, these data have two limitations; first, there are minimum temperature requirements for the use of the broadening coefficients and temperature exponents, and second, the model does not yield predictions for CO self-broadening. Reliable values for room temperature nitrogen broadening coefficients of CO are reported by Varghese and

Hanson[43] and by Nakazawa and Tanaka.[48] Similarly, values of CO self-broadening coefficients have been reported by Nakazawa and Tanaka[48] and by Anderson and Griffiths.[49] With these data, the temperature exponent is assumed to be a constant, independent of both the broadening species and m value. The value of 0.75 is assumed for the temperature exponent, as described by Gross *et al.*[44]

Similarly, Rosenmann *et al.*[47] developed a model which accounts for CO_2 line broadening by CO_2, H_2O, N_2 and O_2 in the temperature range of 300-2400 K. Like the CO model, this model is again based upon both experimental broadening data and theoretical considerations. The model predicts values of γ^o and N, including its dependence on m and temperature, which can be used in Equation 14 for CO_2 half-width calculations. Unfortunately, this model does not include predictions for CO_2 line broadening by CO. Additional references describing this interaction have not been found in the literature.

Theoretical Temperature Dependence of Line Strengths

The two factors dominating the line strength of a vibrational-rotational absorption line are the gas temperature and the magnitude of the partition function (see Equation 4). Both factors are inversely proportional to the line strength and the partition function increases with increasing temperature. The combined effect of these two factors on the line strength is not intuitive. For lines which are relatively intense at room temperature, those with lower values of J", the line strength tends to decrease, nearly exponentially, as the temperature increases, this is true for CO lines with m indexes of -5 to -10. For lines with higher indexes (CO lines with $|m|$ values greater than 21 and most CO_2 lines on the wing of a band) the line strength tends to increase with increasing temperature up to approximately 600 K, and then either decrease or remains constant.

There are very little experimental data that accurately describe the temperature dependence of CO or CO_2 line strengths in the mid-infrared. These can be calculated, however, if accurate absorption lines can be obtained experimentally. The calculation of line strengths, from absorption spectra, is made by solving Equation 12 for S(m) instead of gas concentrations. The revised equation is

$$S(m) = \frac{A(\nu_o) \cdot C \cdot L}{[\pi \cdot \gamma(m) \cdot \ln(10)]} . \qquad (15)$$

Solving this equation requires accurate values for the corrected peak heights, $A(\nu_o)$, half-widths, γ, gas concentration, C, and the cell path length, L. The line strength, for a specific vibrational-rotational line, is independent of the gas concentration at a given gas temperature. Therefore, the line strength calculated from several different spectra recorded at different gas concentrations, should yield the same value for S(m). Furthermore, the Bouguer-Lambert law, given by Equation 7, suggests that there should be a linear relationship between peak heights and gas concentrations for spectra recorded at the same gas temperature but different gas concentrations. These conditions can be used to check the accuracy of the calculated line strength values. First, the variability (variance or standard deviation) of measured values of S(m) at different gas concentrations, at the same gas temperature, can be determined. Second, plots of gas concentrations versus corrected peak heights can be made to validate the assumption that the linearity of the Bouguer-Lambert law is maintained.

The accuracy of the calculated line strengths can also be checked by comparisons with the limited available experimental results and with theoretical predictions. The experimental data for CO peaks includes one study,[45] in which the temperature dependence of the P(6) line of CO was evaluated between 300-800 K. There have been several articles describ-

ing the theoretical temperature dependence of line strengths.[43,50] The first of these, by Chackerian *et al.*,[50] describes the temperature dependence of line strengths relative to the line strength at some reference temperature. The second, by Varghese and Hanson,[43] describes the temperature dependence relative to the band strength; this is Equation 4 presented earlier. Other theoretical descriptions of the temperature dependence of CO line strengths have been presented; however, they are based upon calculations similar to either those of Chackerian *et al.*[50] or by Varghese and Hanson.[43] Similar calculations are possible for CO_2 absorption lines. While the equation describing the temperature dependence is identical to that used for CO, the calculation of partition functions and transition energies is much more difficult.

PHOTOMETRIC ERRORS RESULTING FROM FT-IR INSTRUMENTS

The determination of gas concentrations and temperatures from infrared absorption spectra, recorded at moderate resolution (0.125-1.0 cm^{-1}), is significantly complicated by spectral distortions resulting from the finite resolution of the instrument. These distortions occur because the intensity measured by the instrument at any given frequency is actually an average intensity of all the frequencies within the spectral bandpass of the instrument. The extent of this error is dependent upon the resolution of the instrument and the half-width of the absorption line. Anderson and Griffiths[51] have given a thorough theoretical analysis of this phenomenon.

The mathematical relationship between experimentally obtained (apparent) peak heights (A^a_{peak}) and true peak heights (A^t_{peak}) is given by Equation 16,

$$A^a_{peak} = -\log\left[\, 2\int_0^\infty \frac{\sin^2(\pi\cdot y)}{(\pi\cdot y)^2}\cdot\exp\left(\frac{-\ln 10\cdot A^t_{peak}}{(1+4\rho^2y^2)}\right) dy\right] . \qquad (16)$$

The variables y and ρ are defined as,

$$y = \frac{(\nu - \nu_o)}{R_i} \tag{17}$$

$$\rho = \frac{R_i}{2 \cdot \gamma(m)} \tag{18}$$

where $(\nu-\nu_o)$ is the frequency difference between ν and the peak maximum frequency, ν_o, R_i is the resolution of the spectrometer and $\gamma(m)$ is the half-width of the line at half height. The experimental peak heights are the peak values recorded by the FT-IR instrument; the true peak heights are the peak heights due only to absorption of infrared radiation by the gas. Anderson and Griffiths' analysis (Equation 16) describes the experimentally measured peak heights as the convolution of two functional parts. The first part, $\frac{\sin^2(\pi \cdot y)}{(\pi \cdot y)^2}$, is known as the line shape. The line shape function describes the response of the instrument to radiation of frequency ν when the instrument is measuring at frequency ν_i. The functionality of the line shape changes with the type of apodization applied to the interferogram before transformation. The equation for the line shape given in Equation 16, is a result of triangular apodization.[42] The second part, $\exp\left(\frac{-\ln 10 \cdot A^t_{peak}}{(1+4\rho^2 y^2)}\right)$, describes the absorption of infrared radiation by the sample assuming a Lorentzian line shape. This relationship has already been discussed in the description of gas concentration determinations.

The relationship between A^t_{peak} and A^a_{peak}, with triangular apodization, is illustrated in Fig. 10 for three different values of ρ. For an instrument resolution of 0.25, and for line widths typical of atmospherically broadened CO and CO_2 lines, the value of ρ is between 1 and 10.

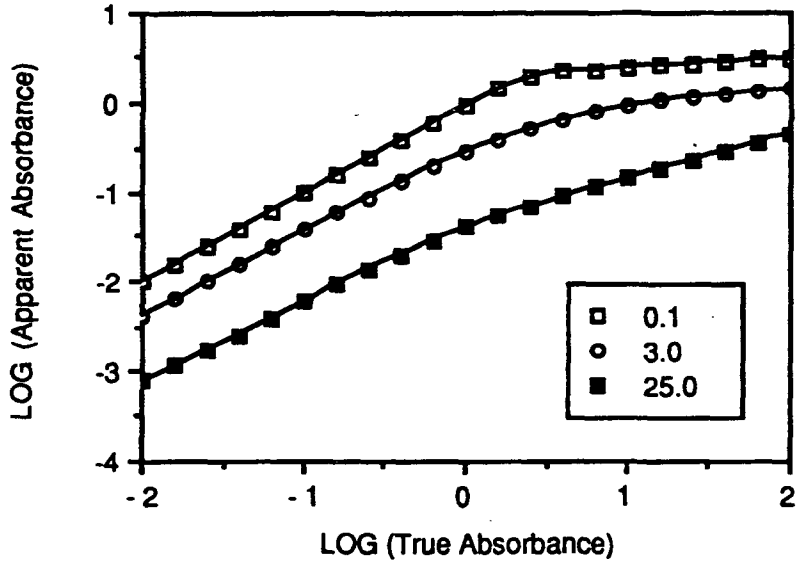

Figure 10. Plot of Log(A^a_{peak}) versus Log(A^t_{peak}) for resolution parameters, ρ = 0.1, 3.0, 25. Calculations based on the methods of Anderson and Griffiths.[51]

PREVIOUS WORK

DETERMINATION OF GAS TEMPERATURES FROM IR ABSORPTION SPECTRA

The theoretical concepts associated with the determination of gas temperatures, from an analysis of absorption spectra, have been presented in a previous section. The application of these fundamentals, follows in the section below. The review of this literature is divided into two groups; those determinations of gas temperatures made in pure gases or gas mixtures (non-combustion) environments and those made in combustion environments. In all cases, FT-IR absorption spectroscopy was used to generate the spectra required for these analyses.

Experiments with Pure Gases or Gas Mixtures

Anderson and Griffiths[49] were the first to use FT-IR absorption spectroscopy for the determination of gas temperatures in a pure gas environment. Their work takes into account the distortions resulting from the finite resolution of the FT-IR instrument, as well as the changes occurring with the line half-widths as a result of temperature and foreign gas broadening. In this work, these authors actually presented two different methods for calculating gas temperatures. The first method is computationally more complex, although it is generally more applicable. The second, although simpler, does not completely account for instrument distortions. They began the description of the first method with Equation 6, and made the appropriate substitutions into the proportionality for the case of m = 1, to obtain

$$A^{t}_{peak}(1) \propto F(1)\frac{\nu(1)}{\gamma(1)}, \tag{19}$$

where F(1) is the Herman-Wallis factor, E(1) = 0, and $\nu(1)$ and $\gamma(1)$ are the frequency and

half-width of the m=1 line, respectively. Since the constant of proportionality between the specific case of Equation 19, and the general case of Equation 6 is the same, the two can be combined to form the equality,

$$A^t_{peak}(m) = \frac{A^t_{peak}(1)F(m)\nu(m)\gamma(1)\exp(-E(m)/kT)}{F(1)\nu(1)\gamma(m)}. \qquad (20)$$

Using a non-linear least squares routine, Anderson and Griffiths then solved, in series, Equation 20, and Equation 16, which describes the functional relationship between experimental (apparent) peaks and true peaks, to calculate the gas temperature. They began by assuming values for $A^t_{peak}(1)$ and T. With these assumed values, they were able to calculate the true peak height for any line, $A^t_{peak}(m)$, using Equation 20. With the assumed value of T, they then calculated the line half-width, $\gamma(m)$, from knowledge of the gas composition and Equation 14. With a calculated value of, $\gamma(1)$, they were able to calculate ρ from Equation 18, which then enabled them to calculate the experimental peak height, A^a_{peak}, by using the calculated values of ρ and A^t_{peak} in Equation 16. They then varied, $A^t_{peak}(1)$ and T, until the calculated values of A^a_{peak} best reproduced the experimental peaks. The value of T which yielded the best reproduction of the experimental lines (evaluated by least squares), was then considered the gas temperature.

The second calculation methodology they developed is simpler; however, it does not fully account for instrument distortions resulting from the finite resolution of the FT-IR instrument. In this approach, they began with the assumption that,

$$A^a_{peak} \approx \frac{1.1\sqrt{A^t_{peak}}}{\rho}, \qquad (21)$$

which is true when 1) triangular apodization is used, 2) ρ is "large" (true for gas phase spec-

tra), 3) A^t_{peak} is greater than about 3, and 4) A^a_{peak} is less than about 1. Under these conditions, A^t_{peak} can be calculated from Equation 21 and substituted directly into Equation 6, to yield,

$$(A^a_{peak}(m))^2 \propto |m|\ F(m)\ \nu(m)\ \gamma(m)\ \exp\left(\frac{-E(m)}{kT}\right) \qquad (22)$$

Similar to the method described earlier, a plot of $\left[\ln\frac{(A^a_{peak})^2}{|m|F(m)\nu(m)\gamma(m)}\right]$ versus E(m) was made for each of the vibrational-rotational lines, and the slope of the resulting plot was equated with -1/kT.

In evaluating the accuracy of these methodologies, calculated temperatures from 12 spectra, collected at temperatures between 303-424 K, were presented. The gas samples were recorded in either pure CO or in CO/air mixtures; the results of these experiments are given in Table 3. Included in this table are the absolute and the percent errors associated with the calculations. At room temperature, both methods yielded excellent results, with the percent difference between measured and calculated values only 0.50 and 0.65% for methods I and II, respectively. As the gas temperature increased, the results became progressively worse for both methods; for those spectra at approximately 350 K the errors for each method were 2.05 and 2.22%, respectively and at 420 K the errors were 3.8 and 4.16 %.

The authors attributed the poorer results at higher temperatures to a lack of reliable CO line width data at temperatures greater than 295 K. There was no suggestion that the theoretical concepts applicable at room temperature were compromised, as the gas temperature increased.

Table 3. Results of Anderson and Griffiths temperature calculation experiments.[49]

Sample No.	T (K)	Pressure CO (Torr)	Pressure Air (Torr)	Method I $T-T_{calc}$, (% Diff.)	Method II $T-T_{calc}$, (% Diff.)
1	303.8	108.8	0.0	2.8 (0.92%)	1.3 (0.43%)
2	304.6	63.1	0.0	0.8 (0.26%)	0.7 (0.23%)
3	304.6	34.2	0.0	-1.0 (0.33%)	-1.1 (0.36%)
4	304.6	101.6	0.0	1.3 (0.43%)	-4.7 (1.54%)
5	304.7	52.3	0.0	-0.9 (0.29%)	-2.0 (0.66%)
6	366.2	129.5	0.0	-4.8 (1.31%)	-4.9 (1.34%)
7	358.2	76.3	0.0	-8.2 (2.29%)	-6.8 (1.90%)
8	424.2	150.0	0.0	-12.0 (2.83%)	-14.4 (3.39%)
9	423.2	90.2	0.0	-15.5 (3.66%)	-16.0 (3.78%)
10	305.0	34.2	710.3	2.4 (0.79%)	-2.1 (0.69%)
11	357.7	45.3	682.5	-9.1 (2.54%)	-12.2 (3.41%)
12	423.2	53.6	807.5	-21.1 (4.98%)	-22.5 (5.32%)

Presented in Fig. 11 is a plot of $\left(\ln\frac{(A^a_{peak})^2}{|m|F(m)\nu(m)\gamma(m)}\right)$ versus E(m) from which Anderson and Griffiths calculated the gas temperature of one spectrum, using method II. The top line excludes the m dependence of γ. The bottom plot was calculated using experimental peaks, A^a_{peak}, instead of peaks corrected by Equation 21. The middle plot includes both the m dependence of γ and the peak height corrections. While there is little effect from excluding the m dependence of γ, the line is significantly curved when no corrections are made for the finite resolution of the instrument. The temperature calculated from this uncorrected plot was 48% in error, compared to thermocouple measurements.

The pioneering work presented by Anderson and Griffiths is significant for three reasons. First, it describes the theoretical considerations required for the determination of gas temperatures from absorption spectra. Second, it identified the importance of photometric error corrections in the determination of gas temperatures from absorption spectra. Finally, it revealed the importance of accurate half-width data for these measurements.

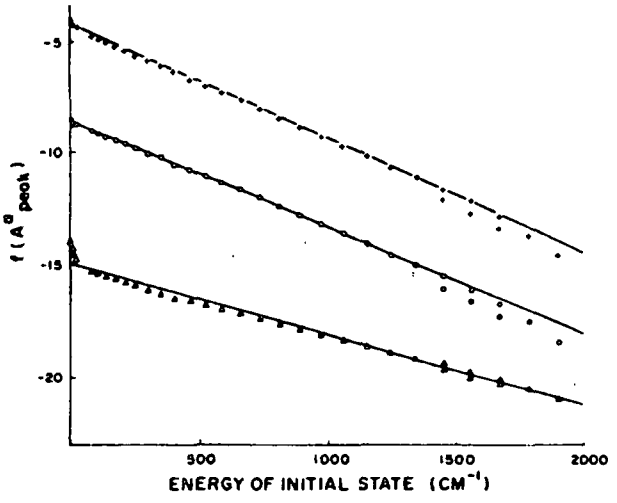

Figure 11. Plot of peak intensity versus energy for data presented by Anderson and Griffiths.[49] The top plot excludes the m dependence of the half-widths, the bottom plot excludes corrections for instrument distortions. The middle plot includes corrections for both of these factors. (Reprinted with permission from reference 27, Copyright 1977, Pergamon Press plc. and the principal author).

In evaluating the potential of using either of these techniques for the determination of gas temperatures in a combustion environment, there are several difficulties. First, temperature calculation methodology I, requires prior knowledge of the gas composition in order to calculate accurate half-widths. In a combustion environment, this information will not be known in advance. In method II, the peak heights must follow four stringent criteria (triangular apodization, ρ is large, $A^t_{peak} > 3$, $A^a_{peak} < 1$), which will not always be applicable for gas samples recorded at combustion conditions. Finally, although the results at room temperature were excellent, the calculated temperatures at only 420 K were already 4% in error. If the error continues to increase with higher temperatures, the results will become poor at temperatures of interest in black liquor char combustion, 950-1300 K.

The extension of Anderson and Griffiths' work to higher gas temperatures has recently been accomplished by McNesby and Fifer.[52] These authors used a calculation technique similar to method II. They assumed that corrections for the finite resolution of

the FT-IR instrument could be approximated by an equation similar in form to Equation 21,

$$A^t_{peak} = K_3 \cdot (A^a_{peak})^x \cdot \rho^y , \tag{23}$$

where in Equation 21, x and y are approximately equal to 2. Using the results of numerically integrating Equation 16 for the case of gases below 800 K, A^t_{peak}'s between 1 and 5, optical retardation of 1 cm, and line widths between 0.01 and 0.1 cm^{-1}, the authors found the best fit values of K_3, x and y to be 0.122, 1.818, and 1.748, respectively. Equation 23 was then substituted into Equation 6, to yield

$$\frac{(A^a_{peak})^x}{\{(2\Delta\gamma_{mo})^{y-1}|m|F(m)\nu_m\}} \propto \exp\{\frac{-E(m)}{kT}\} . \tag{24}$$

The familiar plot of $\frac{(A^a_{peak})^x}{\{(2\Delta\gamma_{mo})^{y-1}|m|F(m)\nu_m\}}$ versus E(m) was then made and the slope resulting from a weighted least squares routine was equated with -1/T.

To determine the accuracy of this technique, the authors calculated gas temperatures from 32 absorption spectra recorded between 302-773 K. With the exception of one spectrum, all the calculated gas temperatures were within 5% of the actual temperatures. The single outlier was within 10% of the actual temperature. The best results were obtained at 400 K, where actual and calculated temperatures were within 1% of each other. It is interesting to note that these authors obtained the best results at the temperature Anderson and Griffiths' results were the worse. McNesby and Fifer explained that this was likely a result of their distortion correction methodology being more accurate with the A^t_{peak}'s less than 3, which is not the case with the lower temperature spectra. These authors attributed the inaccuracies of their work to the approximate nature of the peak corrections and to a lesser extent, to the lack of line broadening data at temperatures greater than 295 K.

In addition to this work, these authors also calculated gas temperatures in a low-pressure (64 Torr) CH_4/N_2O flame. They reported calculated temperatures from CO absorption spectra between 1524-1704 K. However, they did not make any independent temperature measurements (such as thermocouple measurements) to verify the accuracy of the calculated gas temperatures. Therefore, the only criteria which can be used to evaluate the accuracy of the results is from a consideration of the linearity of the intensity verses energy plots, which were very good. This result suggests a relative insensitivity for several factors which they excluded from their calculations, these included not correcting for baseline shifts, or broadening by foreign gases. Furthermore, they assumed that the gas would absorb with a Lorentzian line profile; however, at 64 Torr, a Voight profile (combination of Gaussian and Lorentzian) is more appropriate.[44]

The work presented by these authors reveals the potential accuracy of Anderson and Griffiths' temperature calculation methodology (II), at higher temperatures. The errors observed in the results can easily be attributed to the approximations made in the peak corrections or in the determinations of line half-widths. Their results also suggest that a more rigorous application of the technique to higher temperature spectra will yield accurate results. The more rigorous technique would include a complete description of the finite resolution of the instrument, and the use of better linewidth and broadening data. Furthermore, the inaccuracies of their work reveal, as did Anderson and Griffiths' results, that accurate determinations of linewidths is critical to reliable temperature calculations. Too few details of the flame experiments were presented to suggest anything regarding the accuracies at higher temperatures. However, the ability to record absorption spectra at these temperatures is significant itself.

Combustion Environments

Infrared absorption spectroscopy has also been used for the determination of gas temperatures in process environments including combustion, flame, and dissociation environments. Cleland and Hess[53], studied the dissociation of N_2O in a radio frequency glow discharge. These authors made low temperature gas phase measurements from the rotational absorption spectra of N_2O. Their theoretical approach is identical to that presented in the Background chapter. However, in all cases the pressure of the glow discharge environment was less than 1 Torr. Doppler broadening is the predominate molecular broadening mechanism occurring at these pressures; therefore, the line shape will have a Gaussian profile rather than a Lorentzian. This changes the relationship between A^t_{peak} and A^a_{peak} and it also changes the equation describing the half-widths of the lines. The equation given for the relationship between A^t_{peak} and A^a_{peak}, assuming triangular apodization is given by,

$$A^a_{peak} = -\log\left[\, 2\int_0^{\infty} \frac{\sin^2(\pi\cdot y)}{(\pi\cdot y)^2}\cdot\exp\{(A^t_{peak}\cdot\exp[-4\cdot\ln(2)\cdot(\rho y)^2]\}\, dy\right] . \qquad (25)$$

The Doppler broadened line width is simply given by,

$$\gamma_d = 3.58\times10^{-7}\tilde{\nu}_o\sqrt{\frac{T}{MW}} \qquad (26)$$

where $\tilde{\nu}_o$ is the peak center, T is the gas temperature, and MW is the molecular weight in grams per gram-mole. At these conditions, the line width is independent of the presence of foreign gas species.

Having made the appropriate changes to account for the lower gas pressure, these authors first corrected peak heights by calculating ρ and using this value, along with a range of values for A^t_{peak}, to determined the functional relationship between A^t_{peak} and A^a_{peak}. From

this relationship the A^t_{peak} which corresponded to the experimental line of interest could be determined. Then the plot of ln $\left[\frac{\gamma_d \cdot A^t_{peak}}{|m|\tilde{\nu}(m)F(m)}\right]$ versus E(m) was made, from which the slope and the gas temperature were determined.

These authors presented calculated temperatures for only four spectra. These spectra were all collected without the discharge turned on, instead the walls of the cell were simply heated; heating the gas sample by conduction. From each spectrum they calculated the temperature from two different bands, the $\nu_1+\nu_3$ and $2\nu_1$ bands. The results are presented in Table 4.

Table 4. Gas temperature calculation results from Cleland and Hess.[31]

Sample No.	Pressure (Torr)	T (K)	Calculated Temp. $\nu_1+\nu_3$ band	Calculated Temp. $2\nu_1$ band
1	500	298	307±7 (3.02%)	295 ±3 (1.01%)
2	300	298	311±7 (4.36%)	308±3 (3.35%)
3	500	323	333±8 (3.09%)	306±3 (5.26%)
4	500	355	361±9 (1.69%)	336±4 (5.35%)

Despite the rigorous attempts to correct experimental peaks for the errors resulting from the finite resolution of the instrument, the results presented here are no better than the more approximate methods used by Anderson and Griffiths' (method II) and McNesby and Fifer. Cleland and Hess offered no explanation for the discrepancies observed between actual and calculated temperatures. For the results calculated from the $\nu_1+\nu_3$ band the uncertainties derived from the standard deviation in the slope were high relative to those obtained by others.[49,52] This suggests that perhaps the signal to noise of the spectra was poor or that the peaks were not fully resolved. It is also possible that there were temperature gradients along the path of the infrared beam. The cell was heated by wrapping the vertical side walls of the reactor with heating tape. Other parts of the reactor, in contact with the

gas, were not heated. This might have contributed to the high level of error observed with the higher temperature data from the harmonic band, $2\nu_1$, but it would not explain the problems associated with the room temperature data.

Temperature determinations have also been made in environments which more closely approximate the combustion of black liquor char. These results illustrate the use of FT-IR at higher temperatures and in environments which contain small particles and emission from other higher temperature species. Ottesen and coworkers[34-36] have made temperature measurements in hydrocarbon flames and during coal combustion. Ottesen and Stephenson[34] calculated the gas temperature as a function of distance above the burner for a propane/air diffusion flame. These reports[34,35] provided few details regarding the calculation methodology or a comparison of results with thermocouple measurements.

In more quantitative work, Ottesen and Thorne[36] made gas phase temperature measurements in hydrocarbon flames and during pulverized coal combustion. They used the familiar technique of plotting an "intensity term" versus the transition energy and then calculated the slope to determine the gas temperature. However, their assumed proportionality simply consisted of,

$$I \propto (J'+J''+1)\cdot\exp\left(\frac{-E(J'')}{kT}\right) \quad , \tag{27}$$

where I is the peak intensity which they equated with the peak height (H). They plotted $\ln\left[\frac{H}{(J'+J''+1)}\right]$ versus E(J") to obtain the gas temperature. They reported only a single calculation result, based upon a vibrational-rotational spectrum of CO_2. The reported temperature was 1546 K (±47); the associated uncertainty was based upon the statistical uncertainty of the points relative to the least squares fit of the data to the line. They made no comparison of this value to temperatures measured by some alternative technique.

It is not possible to comment upon the accuracy of this approach given the limited amount of data which they have presented. However, their approach has neglected several factors which others have considered important. First, in their proportionality, they have not included the Herman-Wallis correction factor or the frequency term which should appear in the denominator of the left side of this equation. Second, they have equated peak intensities (I) directly with experimental peak heights. As stated earlier, for Lorentzian lines, intensities are directly proportional to the product of peak heights and their corresponding half-width; here, the half-width term has been ignored. Finally, these authors have used the experimental peaks directly without making corrections for photometric errors.

In a final article, Ottesen and Thorne[35] presented calculations of gas temperatures from CO_2 absorption spectra recorded during pulverized coal combustion. The temperature range of the reported values was from 776 to 1484 K. The statistical uncertainty associated with these calculations was on the order of ± 35 K. The uncertainty was based upon the deviation of the points around the fitted line. Once again there were no comparisons made with temperatures recorded by some other technique. Furthermore, the calculation methodology used in this work was identical to that presented above. The problems associated with this methodology have already been discussed and those comments are applicable to this work as well. Despite these difficulties, this work is significant in that relatively high temperature spectra were recorded in a combustion environment without interference from small particles. These process conditions are similar to those expected in a black liquor char combustion environment.

One final application of FT-IR absorption spectroscopy for temperature determinations was made by Solomon, *et al.*[54] They used the technique to study the pyrolysis of coal in an entrained flow reactor. Part of their study included the determination of gas temperatures from the vibrational-rotational absorption spectrum of CO. The theoretical equation

they used is familiar, although simplified,

$$A_{int} = K_i \cdot (2J''+1) \cdot \exp\left[\frac{J''(J''+1) \cdot B}{kT}\right] \qquad (28)$$

where A is the integrated absorbance of the line, K_i is a constant, B is the rotational constant for CO, and all other terms have been previously defined. Similar to previous work, these authors plotted $\ln\left(\frac{A_{int}}{(2J''+1)}\right)$ versus $J''(J''+1)$ to obtain a slope equal to $\frac{-B}{kT}$, from which the temperature of the gas could be determined. Although several unfamiliar terms have been included in this equation, this approach is identical to others, already described. The use of an integrated absorbance, in place of a peak height, actually more closely approximates the intensity term used in the original derivation, Equation 4. The substitution of $B \cdot J''(J''+1)$ for E(m) is also valid, since the two are equivalent. However, this equation is not without assumptions. First, these authors have combined, the frequency term (ν) and the Herman-Wallis factor and called it a constant, which is only approximately true. More seriously, however, the authors did not correct the experimental peaks for the finite resolution of the instrument. Despite the fact that they are using an integrated area, corrections are still required. In addition, the corrections are more difficult in this case since the true peak height must be calculated for each point along the absorption line, instead of only at the peak maximum.

Using this equation, these authors reported temperature calculations for only two spectra. The first, a room temperature CO spectrum, yielded a calculated temperature of 303 K which agrees reasonably well with the known gas temperature. The second, yielded a calculated gas temperature of 1323 K, while the measured temperature (using a suction pyrometer) was approximately 9.97% lower, at 1203 K. Figure 12 includes the original spectra and the plots of integrated peak area versus energy. The plot of peak area versus energy is

linear for the room temperature spectra, while it is significantly curved at the higher temperature.

Solomon, *et al.* explained these results by suggesting that the curvature was a result of three factors. First, a contribution from lower temperature CO which may exist near the reactor tube walls, second, saturation effects in the high intensity lines, and third, a nonlinear contribution from interference from the next highest vibrational transitions. For this final reason, they used only the filled (black) ovals to calculate the slope and obtain the gas temperature. The effect of a nonuniform temperature profile is difficult to predict since it depends on the shape of the temperature profile. However, if the spectrum was affected by a lower temperature gas, it is likely that the calculated gas temperature would be lower then expected, not higher as observed with these results. It is also unlikely that the detector is saturated at such relatively low absorbances (less than 0.2), unless there is a significant amount of stray radiation reaching the detector from the reactor. Finally, it is also unlikely that the interference from the second order transitions are affecting these lines, since the highest degree of curvature is not at the point where these second order transitions absorb most strongly.

The curvature displayed in these plots is most probably a result of distortions resulting from the finite resolution of the instrument. This curvature was clearly illustrated in similar plots made by Anderson and Griffiths,[49] presented in Fig. 11. In their work, the curvature was completely eliminated after making photometric error corrections. Solomon's room temperature spectrum in Fig. 12, does not display these same non-linearities because the absorbance intensity is very low. Recall from Fig. 10, that the corrections become more important at higher apparent (experimental) peak intensities.

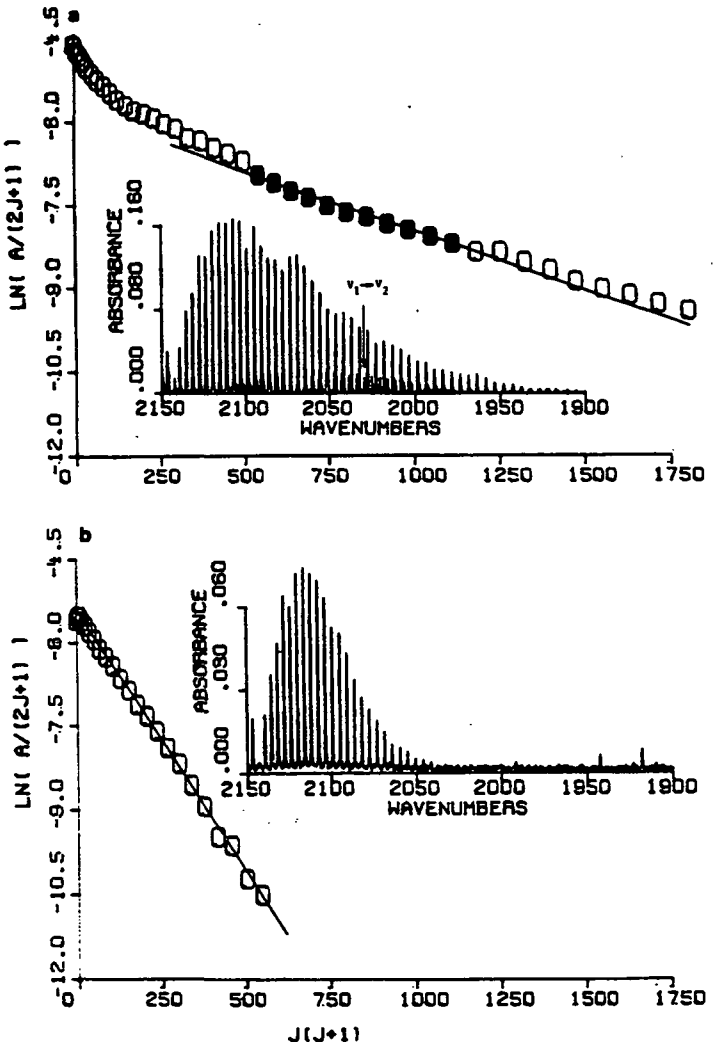

Figure 12. CO absorption spectra recorded at 1203 K (top spectrum) and at room temperature (bottom spectrum). Also included are the plots of integrated areas versus energy from which the temperature was determined. (Reprinted with permission from the President of the Combustion Institute, H.F. Calcote)

DETERMINATION OF GAS CONCENTRATIONS FROM IR ABSORPTION SPECTRA

The theoretical concepts associated with the determination of gas concentrations from infrared absorption spectra have already been presented. Unlike the determination of gas temperatures, there have been few applications of these equations at temperatures above 300 K. It has been difficult to apply these techniques because there is a lack of high temper-

ature line strength, S(m), and linewidth, $\gamma_{x,x}$, data. This information is critical to the successful determination of gas concentrations from infrared absorption spectra. As a result, research in this area has focused on the generation of this data, rather than the determination of gas concentrations.

As described before, the absorption of infrared radiation by a gas is dependent upon the line strength, the linewidth, the gas concentration, the path length, and the frequency. This dependence was given by Equation 11 and is rewritten here,

$$A(\nu) = \frac{S(m)\cdot\gamma(m)\cdot C\cdot L}{\left[\pi\cdot((\nu-\nu_o)^2 + \gamma(m)^2)\cdot\ln(10)\right]}. \qquad (11)$$

Both the line strength and linewidth are temperature and m dependent, therefore, absorption by the gas will also be dependent upon these variables. Furthermore, the line widths are dependent upon the broadening by foreign gases.

Review of the literature describing the absorption behavior of the vibrational-rotational lines comprising the fundamental band of CO and the ν_3 fundamental band of CO_2, has provided no single comprehensive source which examines each of these variables for either band. Instead, much of the literature describes absorption behavior of only a few lines (or one), and then only describes the dependence of one variable, line strength, temperature, or line width, while making assumptions regarding the remaining variables. Given the total number of combinations of these variables, the literature is very incomplete, most especially regarding the temperature dependence of line strengths.

Table 5 is a tabulation of the literature pertinent to this work. It includes references for line strengths, self and foreign broadened line widths and temperature exponents (N) of the vibrational-rotational lines used here. Also included are the temperature and pressure

ranges at which the results were recorded, the type of environment of the experiment (pure gas, shock tube, *etc.*) and the spectroscopic method employed for the data acquisition. Because of the large amounts of data included in these articles, the actual values have not been presented in Table 5. Instead, they will be included throughout the remainder of the text in the form of comparison results, or tables of spectroscopic data used for calculations.

The techniques used for the acquisition of this data, have included grating infrared spectrometry, FT-IR spectroscopy, and tunable diode laser spectroscopy. The majority of the recent work, and nearly all the high temperature results have been obtained using tunable diode laser spectroscopy. The theoretical methods employed for the evaluation of these quantities are the same as those provided earlier. In many cases, however, the gas pressure of the sample was relatively low (< 100 Torr). In these cases, either a Voight or Gaussian profile was required to describe the line shape, rather than a Lorentzian profile.[44]

Table 5. Listing of reported values of line strengths, self and foreign broadened line widths, and temperature exponents (N) for several CO and CO_2 lines.

Author(s)	Ref.	Reported Values	CO Lines m=...	CO_2 Lines m=...	Temp. (K)	Press (Torr)	Environ.	Spec. Method
Sell	45	S(m) γ_{CO-N_2}	-6	-	303-783	760	Pure Gas/ Gas Mixture	TDLS
Anderson, Griffiths	49	γ_{CO-CO}	|1-38|	-	297	-	Pure Gas/ Gas Mixture	Compiled
Hartmann, *et al.*	46	γ_{CO-N_2} γ_{CO-CO_2} N_{CO-CO_2} N_{CO-N_2}	|1-77|	-	200-3000	-	Pure Gas/ Gas Mixture	Modeled
Rosenmann, *et al.*	47	$\gamma_{CO_2-N_2}$ $\gamma_{CO_2-CO_2}$ $N_{CO_2-CO_2}$ $N_{CO_2-N_2}$	-	|1-101|	300-2400	-	Pure Gas/ Gas Mixture	Modeled

Author(s)	Ref.	Reported Values	CO Lines m=..	CO_2 Lines m=..	Temp. (K)	Press (Torr)	Environ.	Spec. Method
Nakazawa, Tanaka	48	γ_{CO-CO} γ_{CO-N_2} γ_{CO-CO_2} S(m)	1-20	-	300	-	Pure Gas/ Gas Mixture	Grating
Chackerian, *et al.*	50	S(m)	|1-40|	-	297		Pure Gas/ Gas Mixture	Calculated
Varghese, Hanson	43	γ_{CO-N_2} S(m)	-(10) - (26)	-	300	100	Pure Gas/ Gas Mixture	TDLS
Sun, Griffiths	57	γ_{CO-CO} N_{CO-CO}	-(25) - (-31)	-	293-453	50-500	Pure Gas/ Gas Mixture	TDLS
Sun, Griffiths	58	γ_{CO-N_2} N_{CO-N_2}	-25	-	274-413	50-500	Pure Gas/ Gas Mixture	TDLS
Varanasi, Sarangi	59	S(m)	-1,-3,-4,-5, -7,-11,-12, -27,-28	-	298	50-2280	Pure Gas/ Gas Mixture	Grating
Varghese, Hanson	60	γ_{CO-Mix} N_{CO-Mix}	-(1) - (-28)	-	300 1850	760	Combustion	TDLS
Bonamy, *et al.*	61	γ_{CO-N_2} N_{CO-N_2}	-3,-6,-7 -12,-22	-	300-2000	-	Pure Gas/ Gas Mixture	Modeled
Lowry, Fisher	62	γ_{CO-CO_2} N_{CO-CO_2}	-2,-3, -7,-8	-	300-1826	258-775	Pure Gas, Combustion	TDLS
Hanson, *et al.*	63	γ_{CO-N_2} γ_{CO-Mix}	1,-7	-	294, 1850	51,760	Pure Gas, Flat Flame	TDLS
Hanson	64	S(m)	-11	-	300-3500	-	Shock Tube	TDLS
Malathy Devi, *et al.*	65	S(m) $\gamma_{CO_2-N_2}$ $\gamma_{CO_2-CO_2}$ $N_{CO_2-CO_2}$ $N_{CO_2-N_2}$	-	24-78	300	0.015-10 40-140 70-120 40-70	Pure Gas/ Gas Mixture	TDLS
Cousin, *et al.*	66	S(m) $\gamma_{CO_2-N_2}$ $\gamma_{CO_2-CO_2}$	-	53-89	296	-	Pure Gas	Grating
Johns	67	S(m) $\gamma_{CO_2-N_2}$ $\gamma_{CO_2-CO_2}$	-	1-91	300,320	-	Pure Gas	FT-IR
Johns	68	S(m)	-	1-79	300-320	0.19-100	Pure Gas	FT-IR
Johns	69	S(m)	-	63-87	300-320	1-100	Pure Gas	FT-IR
Fridovich	70	S(m)	-	47-91	246-338	0.16-100	Pure Gas	Grating

It is difficult to discuss the accuracy or reliability of the data presented. Experimental uncertainties are presented by some authors. However, there are few standards by which

experimental results can be compared. Even theoretical results, which can be used as a basis of comparison, require some measured quantities for their calculation. When the actual values are used later in the text, some measure of their reliability will be presented.

Unlike gas temperature measurements, there have been very few studies which use infrared absorption spectroscopy for the determination of gas concentrations at temperatures greater than 295 K. Some of the authors mentioned above have used the data they generated, along with Equation 11, for the determination of gas concentrations at high temperatures. No literature has been found, however, which describes a study designed to evaluate the accuracy or feasibility of these types of measurements.

While the calculation methodology is well known, there is insufficient experimental line strength data to make high temperature gas concentration measurements. This suggests that either theoretical values will be required, or these values will have to be experimentally determined in this work before concentration calculations can be performed.

PROBLEM ANALYSIS AND OBJECTIVES

The combustion chemistry occurring within a recovery furnace is complex and difficult to analyze. The harsh nature of the recovery boiler environment hinders efforts directed at *in situ* monitoring of gas concentrations in the lower furnace. Furthermore, the simultaneous occurrence of multiple combustion, drying and fuming events, makes it difficult to identify and quantify the factors affecting any single process. As a result, black liquor combustion research has been performed, to a great extent, in the laboratory. Here, individual events can be isolated and the factors controlling the process can be identified.

Previous laboratory studies have yielded a wealth of knowledge regarding the fundamentals of black liquor combustion. However, there remain many unresolved questions. For example, a clear understanding of char bed burning has not been established nor is there a thorough understanding of the formation of pollutant species (sulfur species, HCl, NO_x, *etc.*). Both char bed burning and the formation of pollutant species involve gas phase chemistry. If these processes are adequately simulated in the laboratory, an analysis of the gas phase above this environment could provide insight into the chemical events occurring in the lower part of a recovery boiler.

INFRARED ABSORPTION CAPABILITIES

Infrared absorption spectroscopy has been used for the determination of gas temperatures and, to a limited extent, gas concentrations at temperatures greater than 300 K. Two techniques, tunable diode laser absorption spectroscopy and Fourier transform infrared absorption spectroscopy, have been used to generate the absorption spectra required for these concentration and temperature determinations. While TDLS has significantly higher resolution and shorter data acquisition times, the frequency range of a single TDLS spectrum is limited to approximately 1 cm^{-1}. This limited range makes simultaneous multicomponent

gas analyses or temperature determinations difficult, or depending upon the species, impossible. Conversely, FT-IR offers relatively low resolution and longer data acquisition times. However, in a single absorption spectrum, the entire mid-infrared region, 400-4400 cm^{-1}, can be analyzed, which permits simultaneous multicomponent concentration and temperature determinations. Char combustion studies, require the simultaneous determination of CO, CO_2, and gas phase temperatures, eliminating TDLS as a potential technique for these measurements.

The application of FT-IR for the analysis of the gas phase directly above a burning black liquor char bed is not straight forward; there are several potential sources of difficulty. It is difficult to record infrared absorption spectra in either a pure gas or a combustion environment at temperatures as high as 1250 K. The spectra which are recorded require corrections for photometric errors resulting from the finite resolution of the FT-IR spectrometer. Calculation methodologies must be developed to obtain concentration and temperature information from corrected spectra.

There are numerous problems associated with recording infrared absorption spectra at high temperatures. These difficulties include designing and constructing reactors suitable for high temperature pure gas and combustion analyses, directing the spectrometer's infrared beam to these reactors, finding suitable high temperature windows for the reactor, and controlling the radiation emitted from the high temperature gas samples.

Once the spectra have been obtained, it has been shown that they require significant corrections to account for the photometric errors associated with the limited resolution of the instrument. These corrections require the development of numerical methods to convert the experimental peaks into photometrically accurate peaks.

After the absorption peaks have been corrected, calculation methodologies must be

developed to determine gas temperatures and concentrations. Systematic studies, designed to evaluate the potential of determining gas temperatures from absorption spectra, have been performed for spectra recorded at temperatures up to 750 K. However, with the exception of a few calculations with unknown degrees of accuracy, these methodologies have not been applied to temperatures of interest in black liquor combustion, 1000-1300 K. There has been considerably less work regarding the determination of gas concentrations at these temperatures. There has been no systematic study identifying the accuracy of concentration calculations using infrared absorption spectroscopy at these temperatures. Furthermore, there is a substantial lack of fundamental data required for these calculations.

Despite these difficulties, FT-IR absorption spectroscopy appears to be a viable technique for the determination of gas temperatures and concentrations in a black liquor combustion environment. In addition to the analysis of CO and CO_2 gas concentrations, important to char combustion studies, the technique is capable of recording absorption spectra of all infrared active species in the mid-infrared region. These species include the gaseous intermediates critical to understanding the chemical mechanisms occurring during black liquor combustion.

THESIS OBJECTIVES

Considering the spectroscopic needs of black liquor research, and the capabilities of Fourier transform infrared absorption spectroscopy, a thesis was proposed which involved the development of experimental and mathematical methodologies which will enable the use of Fourier transform infrared absorption spectrometry for the *in situ* analysis of black liquor combustion. In order to focus this work into a specific, manageable project, the following objective was established:

"The objective of this thesis is to quantitatively evaluate the gas phase above a burning, lab-scale black liquor char bed using a nonintrusive, *in situ*, spectroscopic technique. Quantitative measurements of the concentrations of CO and CO_2, as well as the gas phase temperature will be made in this evaluation. Fourier transform infrared absorption spectroscopy (FT-IR) will be the spectroscopic technique used in this environment for these analyses."

It is expected that this work will provide the foundation for later studies, which will use these techniques to provide insight into specific combustion problems.

EXPERIMENTAL APPROACH

In order to accomplish the stated thesis objective, an experimental plan was proposed, consisting of three parts. First, methodologies were developed (experimental and mathematical) which provide for the determination of gas temperatures from absorption spectra recorded at temperatures up to 1250 K. Second, methods were developed to permit the determination of gas concentrations (CO and CO_2) from absorption spectra also recorded at temperatures up to 1250 K. Finally, these techniques were applied to spectra recorded in a black liquor combustion environment to permit the evaluation of gas temperatures and concentrations during black liquor char combustion.

Temperature Determinations in a Pure Gas Environment

In the first part of the experimental program, methodologies were established for the determination of gas temperatures from infrared absorption spectra. This work first required the development of experimental procedures which permit the acquisition of infrared absorption spectra in a CO/N_2 pure gas environment at temperatures up 1250 K. In this phase of the work, it was necessary to purchase an FT-IR spectrometer, build a high temperature gas cell, and direct the infrared beam from the interferometer through the gas cell and to a detector. Once spectra were obtained, mathematical procedures were developed

which were necessary for the correction of these spectra for photometric errors, resulting from the finite resolution of the instrument. These methods were based upon the work of Anderson and Griffiths.[51] Finally, based in part upon previous work,[49] calculation methods were developed for the determination of gas temperatures from the corrected spectra. Once the experimental and mathematical methods were established, a detailed experimental program, designed to determine the accuracy of temperature calculations from absorption spectra, was initiated. This program consisted of calculating the gas temperature from a large number of CO spectra, recorded in a pure CO/N_2 environment, at various temperatures between 300-1250 K. The accuracy of the technique was established from these calculations.

CO and CO_2 Concentration Determinations in a Pure Gas Environment

In the second part of this thesis, mathematical methods were developed for the determination of CO and CO_2 gas concentrations from absorption spectra. The experimental procedures, established in the first part of this work, were used to obtain absorption spectra of various CO and CO_2 gas mixtures in nitrogen at temperatures between 295-1250 K. The mathematical procedures developed for the correction of absorption spectra for photometric errors were applied to these spectra. These spectra were then used to evaluate the temperature dependence of line strengths for several CO and CO_2 lines. These values were compared to both the existing limited experimental data, as well as to theoretical predictions. This information was then used to determine gas concentrations from additional spectra. A large number of spectra was recorded, and the CO and CO_2 gas concentrations were calculated. These calculated values were compared to measured concentrations, which was used to establish the expected accuracy of these techniques.

Concentration and Temperature Determinations in a Combustion Environment

After the calculation methods were developed for the determination of CO and CO_2 concentrations and gas temperatures in a pure gas environment, they were applied to spectra recorded in a black liquor char combustion environment. This work first required designing and constructing a reactor which was suitable for the combustion of char carbon and which permitted the acquisition of infrared absorption spectra. Using this reactor, absorption spectra were recorded in the combustion environment. The gas temperatures and concentrations were then calculated using the procedures described above. The calculated values were compared to the measured values recorded with thermocouples and NDIR instruments.

EXPERIMENTAL EQUIPMENT AND METHODS

The experimental equipment and methods, developed for the completion of the thesis objectives, can be divided into three categories. First, experimental equipment has been purchased and methods have been developed which are related to the FT-IR instrument. Second, a high temperature gas cell has been constructed, and finally, a char combustion reactor has been built. The details associated with the experimental aspects of each of these areas are discussed below.

FT-IR INSTRUMENTATION

A Laser Precision Analytical RFX-75 Fourier transform infrared spectrometer has been purchased for this work. The initial efforts of this thesis were dedicated primarily to this instrumentation. First, the instrument was selected. Second, an optical configuration was established to direct the infrared beam to external reactors. Third, methods were developed for aligning the instrument. Fourth, operating parameters were established for optimizing spectrum quality. Finally, methods were established for determining the instrument resolution.

Instrument Description

The Laser Precision Analytical RFX-75 FT-IR spectrometer is a high resolution research grade instrument capable of a maximum resolution of 0.125 cm^{-1}. It consists of two modules one optical and one electronic, a detector, external optics, and a computer. A summary of the instrument's optical features are provided in Table 6.

The optical module houses the source, interferometer, and laser. This module generates and modulates the infrared source, and uses the laser to trigger the sample intervals

along the interferogram. The source is a high intensity water cooled Globar coil, controlled by a 24-26 volt power supply. The interferometer consists of two mirrors, one moving and one fixed, and a beam splitter. The moving mirror is mounted on a ceramic air bearing. Both mirrors are cube corners, rather than the more conventional plane mirrors. The beam splitter is made of KBr. The frequency range of the interferometer is in the mid-infrared, between 400-4400 cm^{-1}. The laser is a class IIIa, 5 mW Helium-Neon laser manufactured by Siemens (Munich, Germany).

Table 6. Description of optical components and dimensions of the FT-IR spectrometer used in this work.

ITEM	DESCRIPTION
Manufacturer	Laser Precision Analytical
Model Number	RFX-75
Maximum Resolution	0.125 cm^{-1}
Detector	Wide Band (0.25mm), Mercury-Cadmium-Telluride (MCT)
Bearing Type	Ceramic Air Bearing
Interferometer Type	OMNISEPT® Cube Assembly
Interferometer Frequency Range	4400-400 cm^{-1}
Infrared Source	Water Cooled, High Output
External Optics	Optibus® Components
Optical Module Dimensions	7.5"x14"x10.5" (Height,Length,Width)
Electronic Module Dimensions	9"x9.5"x13" (Height,Length,Width)

The electronics module of the instrument performs several functions. First, it converts the analogue detector signal into a digitized signal. Second, it is connected to the computer and serves as the interface between the user-inputted commands (acquire interferogram, change aperature setting, adjust gain, *etc.*) and the interferometer response. Finally, it performs the data collection and signal processing functions of the instrument.

The detector converts the infrared radiation into an electrical signal, whose intensity is proportional to the intensity of the modulated infrared beam. The instrument's detector

is a wide band mercury-cadmium-telluride (MCT) detector. The MCT detector was selected because it offers greater sensitivity than the more conventional pyroelectric detectors such as a DTGS (deuterated triglycine sulfate) detector.

External optics attached to the optical module provide a means for directing the infrared beam from the interferometer to the high temperature gas cell or char combustion reactor, and finally to the detector. This beam transfer is accomplished by the use of optical parts manufactured by Laser Precision Analytical, called Optibus® components. The Optibus® components offer a flexible means of transferring the infrared beam through a series of prealigned mirrors and hollow tubes. The mirror focal lengths are purchased in either standard or customized dimensions. The mirrors are gold-coated aluminum and are housed in hollow 2" cubes. The hollow tubes (no mirrors) are rectangular solids, 2" by 2" by x" where x" is some specified length. For this work, 8" focal length mirrors, hollow tubes (x = 13") and flat mirrors have been combined for the beam transfer. The components are attached and held tight by clamps.

The optical and electronics modules, Optibus® components, detector, and gas cell or char combustion reactor are all mounted on a 36"x48" air supported, vibration isolation optical bench (Technical Manufacturing Corp, Peabody, Massachusetts). The bench provides a stable base which is required for accurate high resolution data collection. Furthermore, it offers a convenient means of moving the instrument to other combustion experiments without instrument realignment.

The instrument's computer is the user's interface for controlling the interferometer, collecting and viewing data, transforming interferograms, and manipulating spectra. It is located on a desk 5-10 feet away from the instrument. It is connected to the electronics module via a LAN (Local Area Network) cable. The computer is a TeleVideo 386 powered by

an Intel 80386 microprocessor and an Intel 80387 math co-processor. The computer's operating system is MS/DOS® which permits easy conversion of spectral data into formats required for subsequent use for concentration and temperature calculations. All the systems hardware components are IBM PC® compatible which offers inexpensive flexibility for hardware modifications. For example, dual IOMega 20 MByte 5 1/4" Bernoulli drives were added to the system as a means of mass data storage. The computational features of the instrument are summarized in Table 7.

Table 7. Computational equipment associated with the Laser Precision Analytical RFX-75, FT-IR spectrometer.

COMPONENT	DESCRIPTION
Computer	TeleVideo 386
Processor	Intel 80386
Math Co-processor	Intel 80387
Processor Speed	16 MHz Clock
Operating System	MS/DOS
Monitor	AST Research inc., EGA
Hard Drive	80 MBytes
Floppy	1 - 1.2 Mbytes High Density
External Memory Storage	IOMega Dual 20 MByte 5 1/4" Bernoulli Drives
Printer	PCPI Laser Printer (HP LaserJet Plus Compatible)
Modem	Internal

Instrument Selection

The Laser Precision Analytical instrument was selected after the optical requirements for this work were evaluated, and the available instrumentation was considered. Although an extensive list of criteria was established for the selection of the instrument (see Appendix I), the key variables included instrument resolution, external optics, and portability. First, the resolution required for resolving the most closely spaced lines, the high J" valued lines of the R branch of the v_3 fundamental CO_2 band, is 0.5 cm^{-1}. Therefore, an in-

strument capable of this level of resolution was required. Second, the instrument needed to be readily adaptable to performing measurements through a nonconventional sample cell. Directing the infrared beam from the interferometer through a furnace/gas cell and to a detector was non-trivial for some instruments. Finally, it was also critically important that the instrument was sufficiently portable to permit its movement to other combustion environments, such as the Institute's DOE-funded in flight reactor.

Given these criteria, the Laser Precision Analytical (LPA) RFX-75, was found to be particularly well suited for this work. However, before it was ordered, its performance in a black liquor combustion environment was tested. For this demonstration, a reactor was constructed (described later), which was suitable for the combustion of black liquor char and which provided optical accessibility to the gaseous phase immediately above the char bed surface. The reactor was shipped to LPA's test facilities. The RFX-75 was successfully used to record absorption spectra through the combustion environment during char combustion.

Optical Configuration

Because of the furnace size and the high temperatures, no conventional sample compartment could be used to contain either the high temperature gas cell or the char combustion reactor. Instead, the beam is directed from the interferometer to the cell/reactor by a series of mirrors, as shown in Fig. 13.

After exiting the interferometer as a collimated beam, the infrared source is gathered and focused by an 8" focal length parabolic mirror. The beam, traveling through a hollow Optibus® tube, is then focused through an 0.8-1.6 mm aperture and is received by a second 8" focal length mirror (located 16" away from the first) which sends the beam collimated to a third 8" focal length mirror. This third mirror directs the beam through the gas cell. The

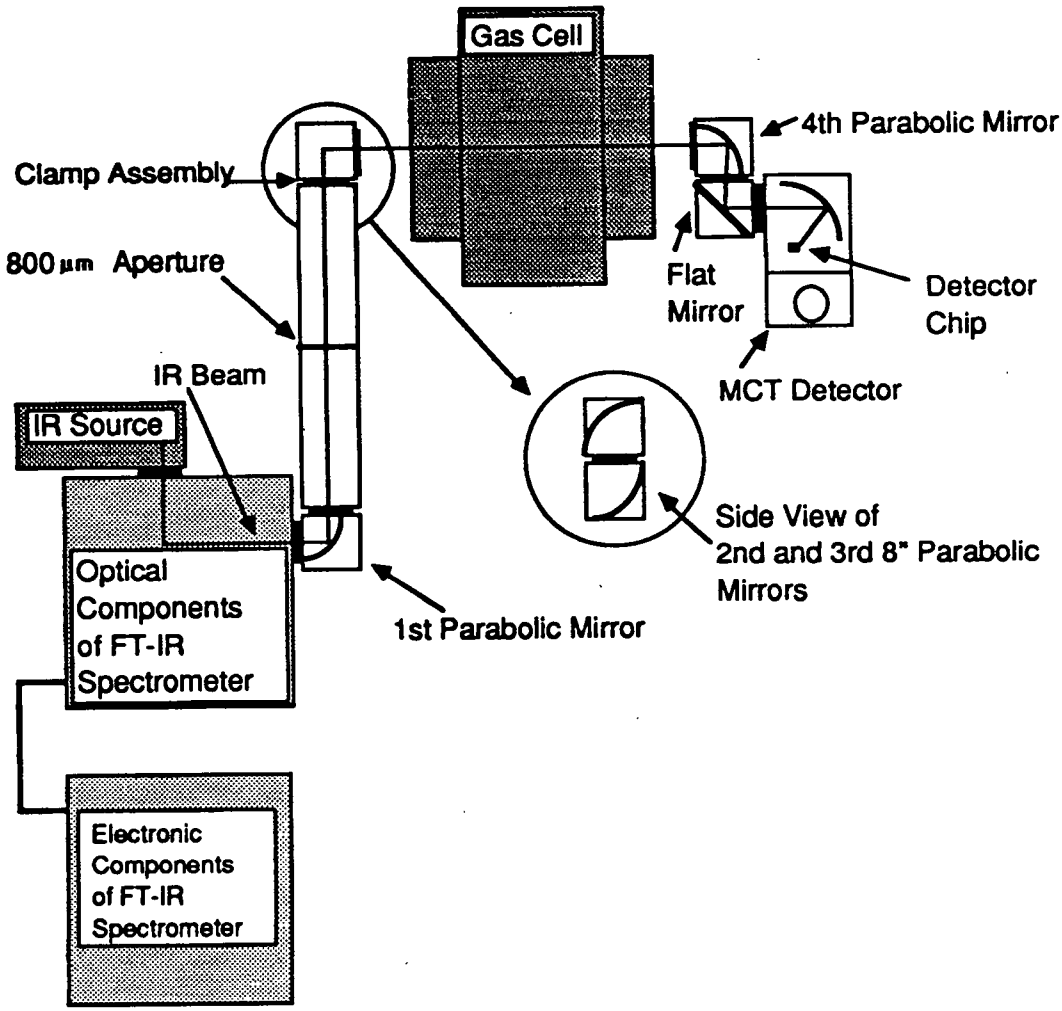

Figure 13. Overhead diagram of optical configuration including the FT-IR, Optibus® components, high temperature gas cell, and MCT detector.

beam is then picked up on the other side of the gas cell by a fourth 8" mirror which sends the beam collimated to a flat mirror which directs the beam into a wide band, 0.25 mm, MCT detector. Inside the detector, the collimated beam strikes one final mirror which focuses it onto the detector chip. This optical configuration keeps the furnace sufficiently far from the interferometer while minimizing the number of reflections. All the mirrors and the hollow tube were obtained from Laser Precisions Analytical and were part of the external optical component system called Optibus®.

The aperture located between the first and second mirrors is used to reduce the effect of stray emission on the absorption spectra. Without the aperture, emission from the gas sample can go back through the Optibus components to the interferometer, become modulated, and then go back through the mirrors, through the cell and to the detector. This emission radiation has been observed in absorption spectra recorded in the absence of the aperture, see Results and Discussion. Placement of the aperture between the first and second mirrors eliminated this source of error.

Instrument Alignment

Once the modulated radiation is produced in the interferometer, it is essential that the optical path be aligned to most efficiently transfer the beam from the optical module, through the Optibus® components, through the reference cell and finally to the detector. Misalignment of the beam will result in a reduced signal intensity. Aligning the system actually refers to two processes, first, adjusting the position of the aperture, mirrors, and detector until the infrared signal has been maximized; and second, adjusting the position of the gas cell or reactor until a maximum infrared signal is obtained. A detailed procedure of the alignment process is given in Appendix II. Alignment of the infrared beam begins with proper alignment of the interferometer, which should only be done by a LPA technician. Assuming that the interferometer is aligned, the individual Optibus® components and aperture are then aligned using a laser jig. The detector mirror stages are then adjusted until the intensity of the infrared beam reaching the detector is maximized. Finally, the height and position of the detector is slightly adjusted until the signal reaching the detector is maximized. The infrared signal is monitored by attaching an oscilloscope to the electronics module of the instrument and monitoring the output of the detector. The electronic signal recorded by the oscilloscope is in the form of an interferogram, the same signal which is sent to the computer for subsequent averaging and Fourier transformation. The maximum intensity of the

interferogram is marked on the scope and the mirror adjustments are made and the changes in peak height of the interferogram are observed. If the peak height of the interferogram increases, the system is considered to be in better optical alignment.

Once the alignment of the infrared beam has been completed, the gas cell or reactor is put into the path of the infrared beam and aligned. A white light within the interferometer is turned on and used to indicate the approximate path of the infrared beam, relative to the windows of the gas cell. The height and position of the gas cell are adjusted until the white light passes through the cell. The white light is then turned off and a fine adjustment of the cell position and height is made by examining the intensity of the infrared beam using the oscilloscope as described above.

Instrument Operating Conditions

An understanding of proper instrument operation has been developed by experimenting with the various instrument settings. These instrument variables include gain, the size of the Jacquinot stop, apodization function, resolution, zero filling, number of scans, and the interferogram step. Several of these settings fundamentally affect the shape of the final spectrum; these have been characterized as non-adjustable parameters. The others influence the signal-to-noise ratio of the final spectrum, and have been designated as adjustable. Before each of these parameters is briefly discussed, the method of data collection and transformation will first be reviewed.

Data Collection

All the data has been collected using the AQIG (Acquire Interferogram) command which directs the interferometer to collect and average some number of interferograms. This is done with only nitrogen in the reference cell (background interferogram) and then

again after the sample gas has been added (sample interferogram). A background interferogram was always collected immediately before the sample interferogram in order to reduce errors resulting from the changing transmittance of the windows or the different stray emission which results from the furnace at different temperatures. The resulting interferograms are not transformed and ratioed at the time of data collection, since the Fourier transformation process can take as long as 45 minutes to complete. Instead, all the data is collected first and then the transformations are done at a later time (usually overnight) using DOS batch files. After transformation, the spectra are baseline corrected and the experimental peak heights are determined. The specific instrument commands and calculation parameters for the data collection, transformation, baseline correction and peak height determinations are given in Appendix III.

Non-Adjustable Parameters

Several of the instrument parameters which have been adjusted throughout the course of this work have a significant effect on either the resolution or mathematical shape of the final spectrum. In general, these parameters should not be routinely adjusted. Instead, these should only be adjusted when a different experimental line shap is desired. These parameters include the Jacquinot setting, the apodization function, the instruments nominal resolution, the level of zero filling, and the interferogram step.

The diameter of the aperture between the source and the interferometer is known as the Jacquinot setting. This aperture is opened or closed allowing more or less radiation to reach the interferometer. The setting of this aperture is dependent upon the nominal resolution setting of the instrument. For example, at a resolution of 0.25 cm^{-1}, the Jacquinot stop should be set at a diameter of 0.4 mm, or a nominal setting of five. The system has been designed to coordinate the Jacquinot settings with specific nominal instrument resolu-

tions. Although it is desirable to increase the aperture to allow additional infrared radiation to get through the sample when the signal/noise is poor, this practice should be avoided. It has been observed that this radiation does not provide the photometric accuracy required to maintain high resolution.

The choice of apodization functions is extremely important, particularly when corrections for photometric errors are made. The type of apodization used controls the instrument line shape. The instrument line shape is a key parameter in the equations for determining true peak heights from experimental peak heights. From the photometric error corrections, it has been determined that the triangular apodization function (resulting in a $\sin^2(x)/x^2$ instrument line shape) is well behaved during numerical integration. It has therefore been used throughout this work.

Instrument resolution is defined in two ways. First, the nominal resolution is the setting of the instrument which is used to direct the movable mirror to travel a specified distance. Second, the actual resolution is the measured resolution which is determined by a separate series of experiments. Although the two should be nearly the same, there are differences which must be considered. At higher levels of resolution, the movable mirror travels farther and collects more data. This additional data adds detail to the transformed spectrum and increases its capacity to resolve lines which are closely spaced together. For making temperature and concentration calculations from spectra, it is important that adjacent peaks are well resolved. This includes separating lower intensity peaks resulting from ^{13}CO absorption of ^{12}CO second order transitions. In order to achieve this high level of line separation, the instrument must be run at nominal resolutions of 0.125 or 0.25 cm^{-1}.

The degree to which a spectrum is zero-filled dictates the point to point accuracy of the line which is fit to the data points comprising the spectrum. For example, at a low level

of zero filling, the shape of an absorption peak will appear chopped and noncontinuous. At higher levels of zero filling, the spectrum takes on a more smooth shape. Although the smoother line contains no more true spectral information, the accurate determination of the maximum peak height is a function of the smoothness of the peak. Therefore, a high degree of zero filling (15X) has been used in this work.

A helium-neon laser inside the interferometer is used as a means to trigger the sampling intervals along the interferogram. The frequency of this laser, which is used to provide a reproducible sampling interval along the interferogram, influences the peak accuracy of the observed peaks compared to known positions. It was determined early in this work, that the frequency used for the transformation calculations should be 0.63294 μm instead of 0.632991μm as originally designated with the instrument. The new value provided spectra with the highest degree of peak to peak accuracy.

These non-adjustable paramter settings are summarized in Table 8. Included in this table are both the LPA code for the setting as well as the acutal value.

Table 8. The instrument parameters which were kept constant throughout the data collection process of this work.

Parameter	LPA Code	Setting
Nominal Resolution	5	0.25 cm^{-1}
Apodization Function	8	Triangular
Jacquinot Stop	5	0.4 mm
Zero Filling	4	15 zeroes/int. point
Interferogram Step	-	0.63294 μm

Adjustable Parameters

During the data collection process, the intensity of the infrared signal reaching the detector was closely monitored. It was important that the signal was neither too intense nor

too weak. A signal, which was too intense, resulted in detector saturation and subsequent nonlinear response from the detector, while a signal which was too weak, resulted in a poor signal to noise ratio. Detector saturation was determined by examining the background interferogram, LPA command TSTB. A saturated condition was apparent when the background transmittance intensity was not zero where the optical cut-off of the windows dictates that the signal should be zero (with sapphire windows 1700-0 cm^{-1}). In all cases the assessment of good signal to noise was made by visual inspection of the final spectra.

The intensity of the signal reaching the detector was more quantitatively evaluated by running the instrument command, TSTI (Test Interferogram), which plots the interferogram intensity as a function of mirror displacement. The optimum interferogram height was found to be between 15-30 units on the y-axis of this scale. A saturated condition was likely to exist if the interferogram peak height was substantially higher (30-50). A poor signal-to-noise ratio was likely to occur when the interferogram peak heights were less than 10.

In the case of detector saturation, the instrument was first set to the lowest level of gain, 1. If the detector was still saturated, a metal screen which blocked approximately 50-75% of the radiation was placed between the Optibus® tube and the reactor. In all cases, these screens were successful in getting the instrument out of a saturated state.

If the energy reaching the detector was too low, resulting in a poor signal-to-noise ratio, the number of scans averaged was increased. The improvement in signal/noise resulting from increasing the number of scan is proportional to $\sqrt{n}$, where n is the numbers of scans.[41] Increasing the gain does not improve the signal-to-noise ratio. However, it is important to increase the gain until the interferogram height is between 15-30. If the interferogram intensity is too low, the instrument is not able to process the interferogram and "scan errors" result.

In this work, the gain was adjusted between 1-8x. The number of scans varied from 100-500. At low temperatures, the amount of infrared radiation reaching the detector was very high and screens were often used to reduce the signal intensity and only 100 scans were required to obtain good spectra. At higher temperatures, the signal-to-noise ratio was reduced because of the reduced transmission through the gas cell windows, and therefore the intensity reaching the detector was very weak. At these temperatures, 250-500 spectra were coaveraged and the gain was between 4-8x.

Instrument Resolution

Knowledge of the resolution of the instrument is essential for making corrections for the finite resolution of the instrument. The nominal resolution of the instrument is nearly the same as the actual resolution. However, differences between the two have been observed with changes in the optical alignment. Therefore, before spectra were recorded, the resolution of the instrument was determined by measuring the full width at half height of low pressure spectra. If the pressure is maintained sufficiently low, instrument broadening will be the dominant mechanism controlling the line shape. At these pressures, molecular interactions are not significantly influencing the line shape. Furthermore, Doppler broadening is insignificantly small, relative to instrument broadening at these pressures.

The resolution of the instrument, for a given optical alignment, was determined by first measuring the full width at half height (FWHH) of triangularly apodized, low pressure CO absorption lines. These spectra were recorded using a standard 10 cm, dual stopcock, gas cell with 25 x 4 mm CaF_2 windows (Janos Technology, Inc.). The sample was prepared by first evacuating the cell with a vacuum pump, to less than 1 Torr (measured with a mercury absolute pressure gauge). A small amount of CO was introduced into the cell by filling a rubber balloon and holding it over one of the two stopcocks. The stopcock was opened for

a fraction of second, and some of the CO was drawn into the gas cell. A background spectrum of the sample was viewed, and the presence of CO was usually observed. The sample was then reattached to the vacuum pump through one of the two stopcocks. The stopcock was again opened, for a brief second. A background spectrum of the sample was again examined. If CO was still observed in the background, additional gas was withdrawn from the cell. The entire process was continued until no CO was visible in the background spectrum. Although it was not observable, there was still generally enough CO left in the cell to make the measurement. From this spectrum, the resolution of the instrument was calculated as discussed in the Mathematical Methods chapter. Generally, 3-5 low pressure spectra were recorded for each resolution test.

HIGH TEMPERATURE GAS CELL

A high temperature gas cell has been designed and constructed for use in this work. This cell has provided a controlled environment from which infrared absorption spectra at known gas concentrations, temperatures, and pressures could be recorded. The development of this cell has been critically important for obtaining reference spectra from which temperature and concentration determination procedures have been developed and fundamental line strength data have been obtained. In the subsequent sections, a physical description of the cell will be given along with a description of the cell heating equipment, gas preheating methodology, and cell window selection. In addition, the methods for metering gases into the cell, monitoring the gases out of the cell, and measuring the gas cell pressure will be given. Finally, the determination of the actual gas temperatures relative to furnace set point temperatures will be discussed.

Description of Apparatus

For these studies the gas cell shown in Fig. 14 was designed and constructed. It permits the acquisition of absorption spectra of gases at atmospheric pressure and at temperatures between 298 and 1273 K. The cell consists of a stainless steel tube with end caps; the inside diameter of the cell is 3.875" and the inside length is 3.75". Holes 0.625" in diameter are drilled through each end cap to allow the infrared beam to pass through the cell. The cell walls and end caps are constructed of 0.187" thick, 304 stainless steel. Windows, 1" in diameter, are contained in 2" diameter stainless steel window-holders and placed over the holes in each end cap. Ceramic paper insulation (not shown in Fig. 14) is used around the windows and between the window-holders and the gas cell to seal the gas sample in the cell. Each window-holder is fastened to the end cap by stainless steel screws.

Inlet and outlet 0.157" I.D. stainless steel tubes were put into the cell to allow a continuous stream of gas to flow through the cell. The inlet tube consists of a coil 72" long wound on the inside of the gas cell to preheat the gas to the cell temperature. Heat transfer calculations have shown that the gas pre-heating is accomplished in the first few inches of the coil. The additional length of coil assures that the gas in the coil will reach the furnace temperature before entering the gas cell. A flow of gas continuously exits the cell through the outlet tube; this tube is open to the room so that the internal cell pressure is maintained at atmospheric pressure.

The gas cell is heated by placing it inside an electric tube furnace obtained from American Test Systems (ATS model 3110). The furnace has a maximum continuous temperature rating of 1273 K, a heated length of 4", an overall length of 5", an inside diameter of 4.5", and an overall diameter of 12". The temperature of the furnace is controlled by an LFE

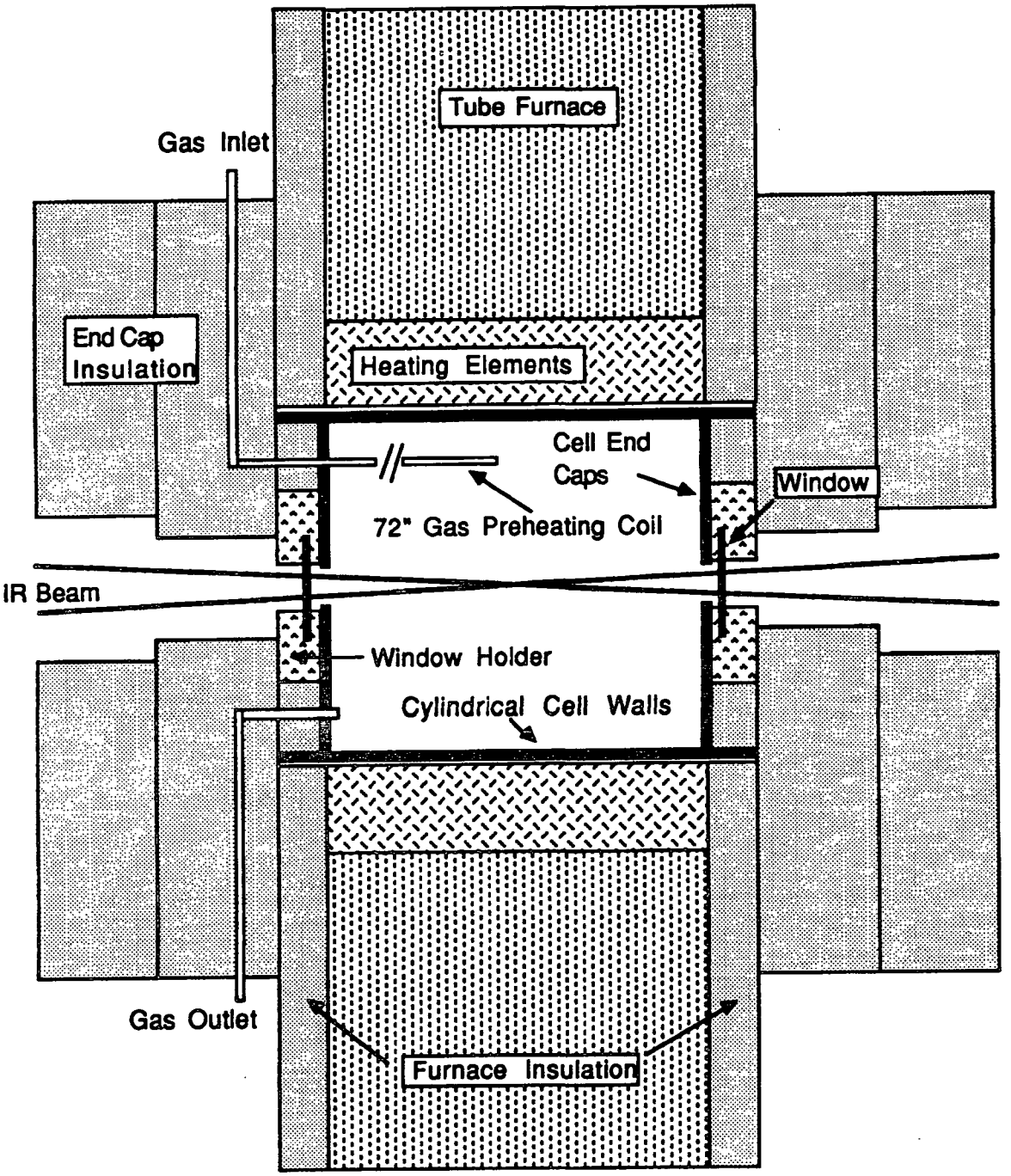

Figure 14. Schematic diagram of high temperature gas cell. Also shown is the tube furnace, heating elements, end cap insulation, and the path of the infrared beam.

model 2010 time-proportioned temperature controller. Once inside the furnace, the ends of the gas cell are insulated with two discs made of B&W Kaowool HS-45 board insulation placed over each of the end caps. The insulation was machined to an outside diameter of 8" and a thickness of 3". Holes through the center of each disc allow the infrared beam to pass through the cell. The insulation on the end caps was necessary to reduce energy loss through the ends of the cell.

Window Selection

Two materials have been successfully used for the gas cell windows; sapphire and yttrium oxide (Y_2O_3). These materials were selected for both their optical and thermal properties. First, they are transparent in the region between 1900-2500 cm^{-1}. Second, they are thermally stable at these high temperatures.

Industrial sapphire is relatively inexpensive and can be easily manufactured in windows of the necessary dimension. Sapphire is a good high temperature material with respect to its thermal stability at 1273 K, however, its optical properties are not ideal. Sapphire is only 40-60% transparent in the range of 1800-4400 cm^{-1} at room temperature; at high temperatures, 800-1273 K, the transmittance decreases. In addition, the optical cut-off increases to nearly 1900 cm^{-1} at these higher temperatures. As a result, high temperature spectra become very noisy near the outer wing of the CO P branch.

Because of the poor optical properties of sapphire, yttrium oxide has also been used. This experimental material, made by Raytheon in Lexington, MA, is as thermally stable as sapphire, but has better optical properties. First, it is transparent between 1200-4400 cm^{-1} and it has a higher percent transmittance than sapphire. Second, it maintains this high degree of transmission at elevated temperatures. The disadvantages of this material include

its high cost and the deterioration of its optical transmittance with long term exposure to high temperatures. The first samples of this material were given to us at no charge by Raytheon. As these samples deteriorated, and needed to be replaced, sapphire was used. The difficulties arising from the poor signal-to-noise ratios with sapphire were partly overcome by increasing the number of spectra averaged for each spectrum.

Regardless of the material, the windows must be wedged. Wedging is the process of grinding one face of a plano-plano window at an angle with respect to the other face. It is necessary to wedge the windows in order to eliminate artifacts which would otherwise appear in the absorption spectrum. These artifacts are manifested as sinusoidal waves which propagate throughout the absorption spectrum. Wedge angles of 0.7-2.0° have been used in this work. While the 0.7° wedge was sufficient, windows with higher wedge angles were often purchased because of pricing and availability.

Measurement of Gas Cell Flow Rates, Concentrations, and Pressure

All the gas samples consisted of mixtures of either CO and N_2 or CO, CO_2 and N_2. A total volumetric flow rate of 1 slpm was continuously passed through the cell. The gases used consisted of research grade CO and CO_2 (minimum purities of 99.997% and 99.998%, respectively) and prepurified (minimum purity 99.998%) or technical grade N_2. The volumetric flow of individual CO, CO_2 and N_2 streams were measured either by mass flow meters (Teledyne, Hastings-Raydist, Model NALL-1, 10 K) or rotameters (Brooks model 1355-V). Corrections to the mass flow meter readings were made for temperature, pressure, and gas species. No corrections were required for the rotameters which were operated at the same conditions as their calibration. The accuracy of all the meters was validated by comparisons with dry gas meters. The standard deviation for the CO and CO_2 rotameters is $\pm$ 0.0005 l/min and for the N_2 rotameter is $\pm$ 0.01 l/min. The accuracy of the gas analyzers

was established by calibration curves. The standard deviation of the points comprising these curves was $\pm$ 0.031 l/min for CO and $\pm$ 0.051 l/min for CO_2. After being measured, the gases were combined in a "T" and mixed in the tubing (6') between the respective metering devices and the gas cell.

After exiting the gas cell, the gas composition was rechecked using a NDIR CO/CO_2 duel gas analyzer (Infrared Industries, Inc., Model 702, CO Range 0-6%, CO_2 Range 0-20%). Good agreement between the metered gas concentrations and the NDIR instrument was obtained from gas samples at room temperature. At higher temperatures, however, the agreement between metered concentrations and NDIR analyzer measurements was very poor. It was later realized that some of the CO in the cell was oxidized to CO_2; thereby, changing the inputted gas composition (see Appendix X). Therefore, only the NDIR gas concentration measurements were used for samples at temperatures greater than room temperature.

A pressure transducer (Omega Corp., Model PX425-030AV) and a digital pressure indicator (Omega Corp., DP 2000-S7) have been obtained to measure the absolute pressure in the cell. The calibration of this device has been made by first zeroing the instrument with a vacuum pump. The middle range of the instrument was calibrated to local weather service barometric measurements.

Temperature Profiling

Knowledge of the actual gas temperature through the center of the gas cell is critically important to the development of temperature calculation methodologies. The actual value of the gas serves as a reference to evaluate the accuracy of calculated temperatures. Because of the spatial separation, the temperature of the gas in the center of the cell is dif-

ferent than the temperature indicated by the thermocouple controlling the furnace. Furthermore, despite the end cap insulation, some energy loss occurs through the ends of the cell. Therefore, a nonlinear temperature profile along the path of the infrared beam may be expected. It is also possible that the presence of the gas preheating coil affects the temperature of the gas through the center of the cell.

In an effort to identify and quantify these gradients, the temperature profile inside the cell was measured. This was accomplished by placing the gas cell inside the tube furnace and putting ceramic paper windows in place of the normal sapphire or yttria windows. A thermocouple was placed through a small hole in one of the ceramic paper windows. The thermocouple, supported by two ring stands, was slid in and out of the furnace to any position within the cell. The thermocouple had an exposed junction and was obtained from the Omega Company (model XC1B-K-233). A schematic diagram of this experimental arrangement is given in Fig. 15.

A series of preliminary studies evaluated the magnitude of thermocouple errors resulting from radiative, conductive, and convective heat transfer to and from the thermocouple junction. No significant errors (less than 1%) resulted from either radiation or convection. Radiative errors were checked by comparisons with a single layered shielded thermocouple. Convective errors were checked by varying the gas flow rate through the cell.

Thermocouple errors, resulting from conduction along the shaft of the thermocouple, were found to be significant. These errors were manifested as lower measured temperatures for the first inch of thermocouple insertion into the cell. When only a small part of the entire thermocouple was inserted into the cell, there was a significant temperature gradient along the thermocouple shaft. This temperature gradient caused an energy transfer down the length of the shaft from the thermocouple junction.[71] As a result, the temperature read

by the thermocouple was lower than the actual gas temperature. In order to account for this error, temperature measurements for the first inch of thermocouple insertion were not used and the total temperature profile of the cell was obtained by recording the profile twice; the thermocouple was inserted from a different side of the cell in each profile.

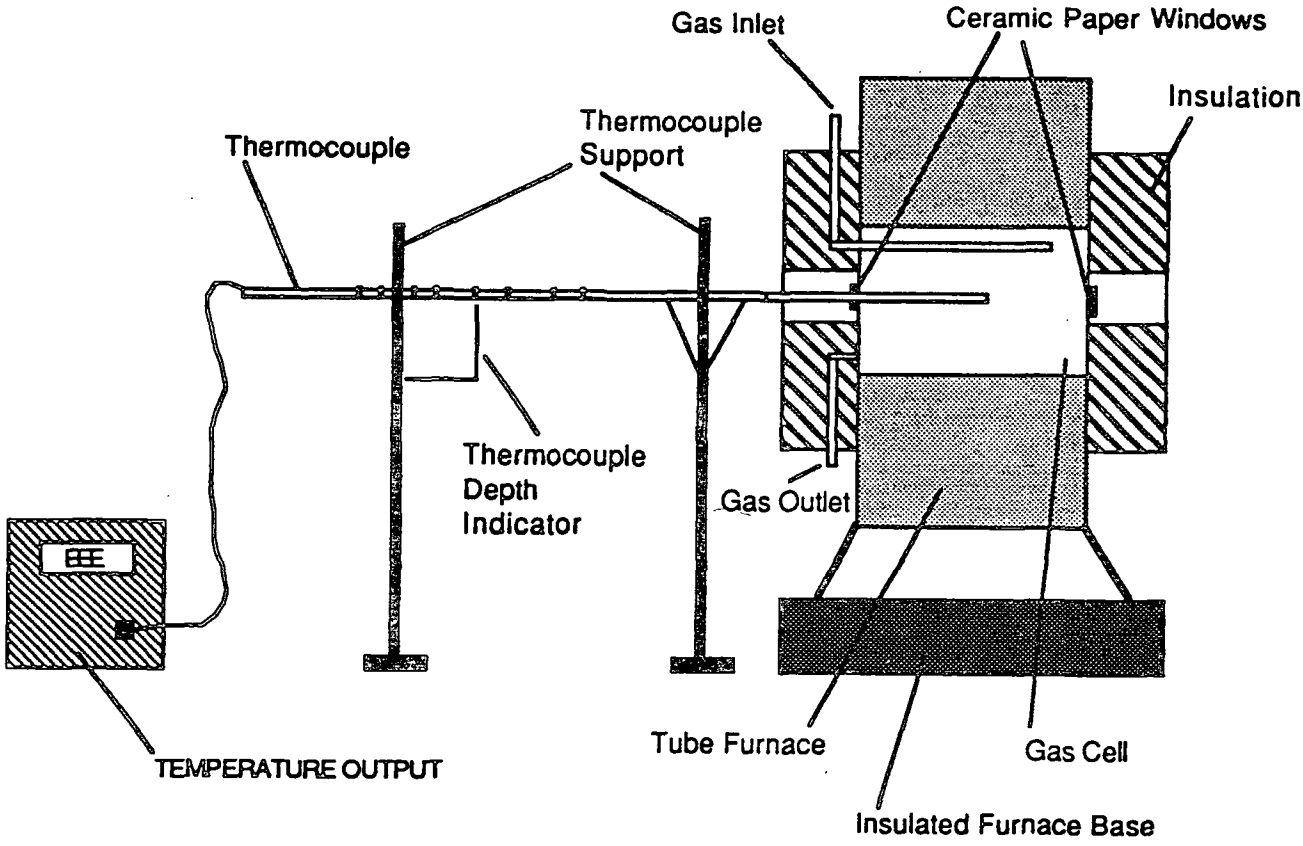

Figure 15. Experimental arrangement for temperature profiling experiments within the gas cell.

Temperature profiles of the gas within the cell were obtained at seven different furnace set point temperatures: 373, 573, 773, 973, 1073, 1173, and 1273 K. Approximately ten temperatures were recorded along the cell center line. These measurements were replicated three times, and an average profile was calculated. Measurements were then made to calculate a second average profile. This time the thermocouple originated from the other window. A complete temperature profile (both average profiles combined), recorded at a furnace set

point temperature of 1173 K, is given in Fig. 16. The experimentally obtained profiles at all seven furnace set point temperatures are given in Appendix IV.

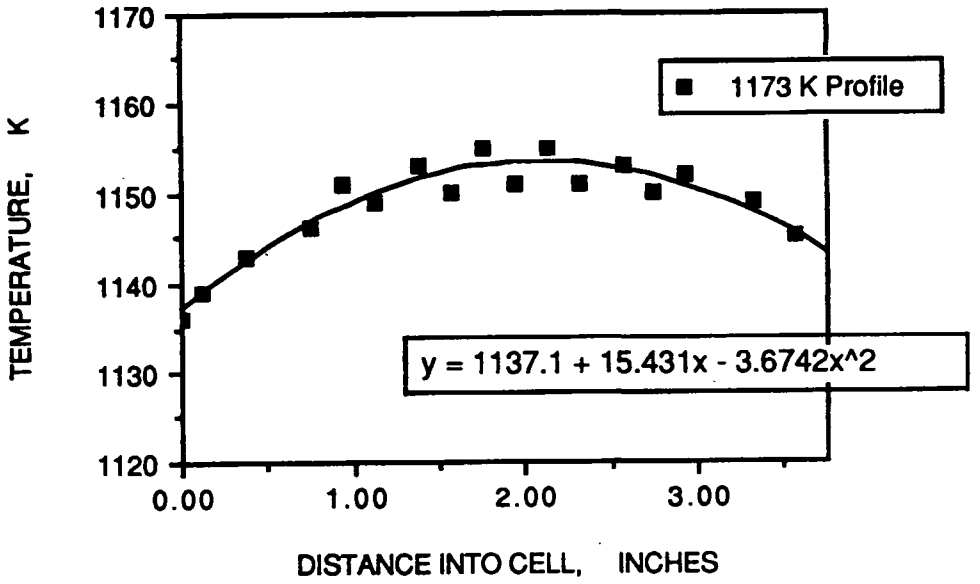

Figure 16. Experimentally obtained temperature profile within the gas cell at a furnace set-point temperature of 1173 K.

The shape of the profiles were similar at all temperatures, except for the 373 K profile which was flat. The temperature profile is parabolic and nearly symmetrical with respect to the cell geometry. In the worst case (1250 K), the difference between the maximum and minimum temperature along the profile was about 10-20 K.

An empirical equation was fit to each profile at each furnace set point temperature. These equations were integrated to obtain average temperatures[72] which are used as a basis for comparison with the temperatures calculated from absorption spectra. The empirical equation for each furnace set point temperature, as well as the integrated average cell temperature, are given in Table 9.

Table 9. Empirical equations fit to the experimentally obtained temperature profiles and the corresponding calculated average temperature resulting from integration of these equations.

Furnace Set-Point (K)	Empirical Equation	Calculated Average Profile Temperature (K)
373	$y = 359.94 + 0.34x$	361
573	$y = 539.79 + 9.56x - 2.34x^2$	547
773	$y = 736.42 + 13.79x - 3.50x^2$	746
973	$y = 937.32 + 13.28x - 3.10x^2$	948
1073	$y = 1037.06 + 13.65x - 3.23x^2$	1048
1173	$y = 1137.14 + 15.43x - 3.67x^2$	1149
1273	$y = 1239.0 + 13.68 - 3.88x^2$	1247

To determine if the shape of the parabolic, experimentally obtained, temperature profile could be explained by the temperature difference between the cylinder wall and the cylinder end caps, the heat transfer within the cell was mathematically modeled. The model, given in Appendix V, assumes that heat transfer to the gas was accomplished by conduction alone. The mathematical results for the case of the furnace set point at 1273 K are given in Appendix V. These results have been plotted in Fig. 17, along with the experimentally obtained profile. As shown in this figure, good agreement between mathematical and experimental results have been obtained. This is indirect evidence that the observed temperature profiles were the result of the slight difference between the cylinder wall temperature and the cylinder end caps.

CHAR COMBUSTION REACTOR

A reactor, suitable for the combustion of a black liquor char bed and which permits optical accessibility to the gas phase directly above the burning bed surface, has been designed and constructed. The construction of this reactor has been critical to providing a lab-scale device, which simulates the recovery furnace process of char bed burning. This environment is necessary to establish the feasibility of making *in situ*, concentration and

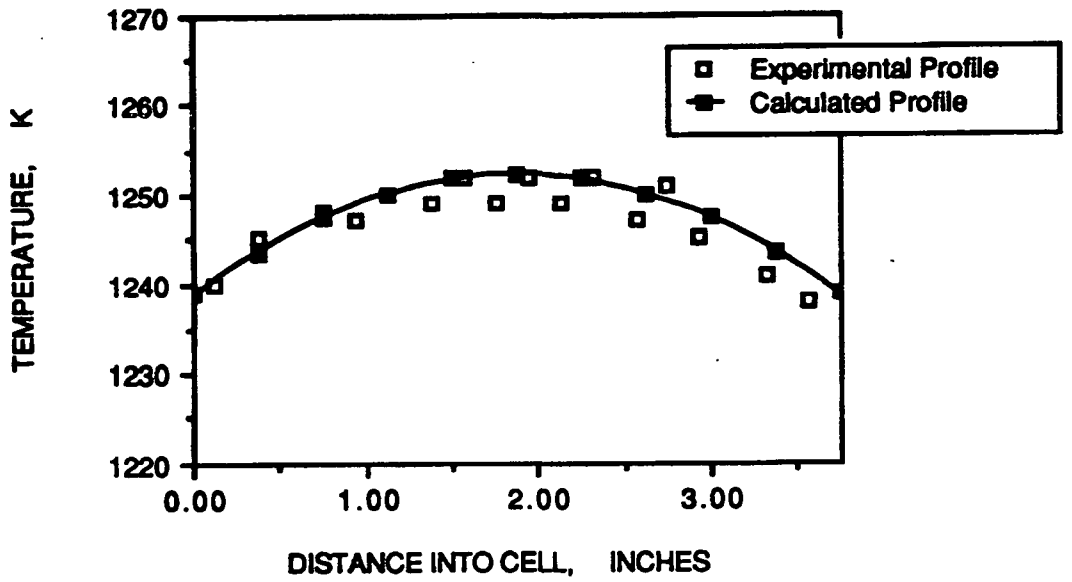

Figure 17. Comparison of experimentally obtained temperature profile in the gas cell at 1273 K, and a mathematically calculated profile. The calculations are presented in Appendix V.

temperature measurements during char combustion, using FT-IR absorption spectroscopy. A description of this reactor, along with a brief description of the char preparation, is provided below.

Description of Apparatus

Schematic diagrams of the reactor are provided in Figs. 18 and 19. The first one emphasizes the path of the infrared beam through the reactor, while the second emphasizes the flow of combustion air to the char bed surface. There are three primary sections to the reactor, each of which is described in greater detail below; first, the lower reactor section, which contains the sample and supplies the energy to heat the char; second, the mid section of the reactor which provides optical accessibility to the gas above the char surface, and which contains the jets which direct air onto the char surface; and finally, the upper reactor section which contains a crucible lift mechanism.

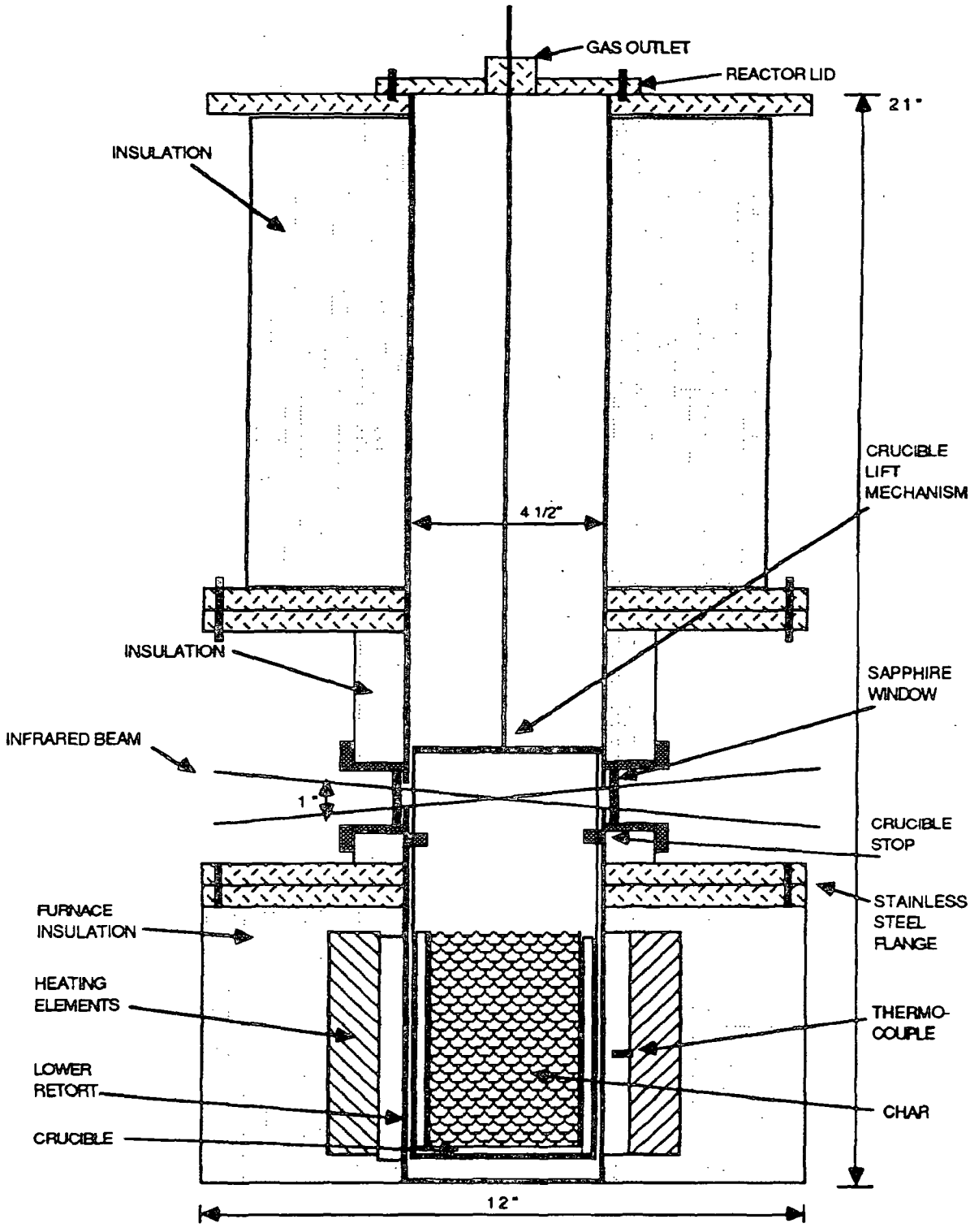

Figure 18. Schematic diagram of char combustion reactor, emphasizing the optical path above the char sample.

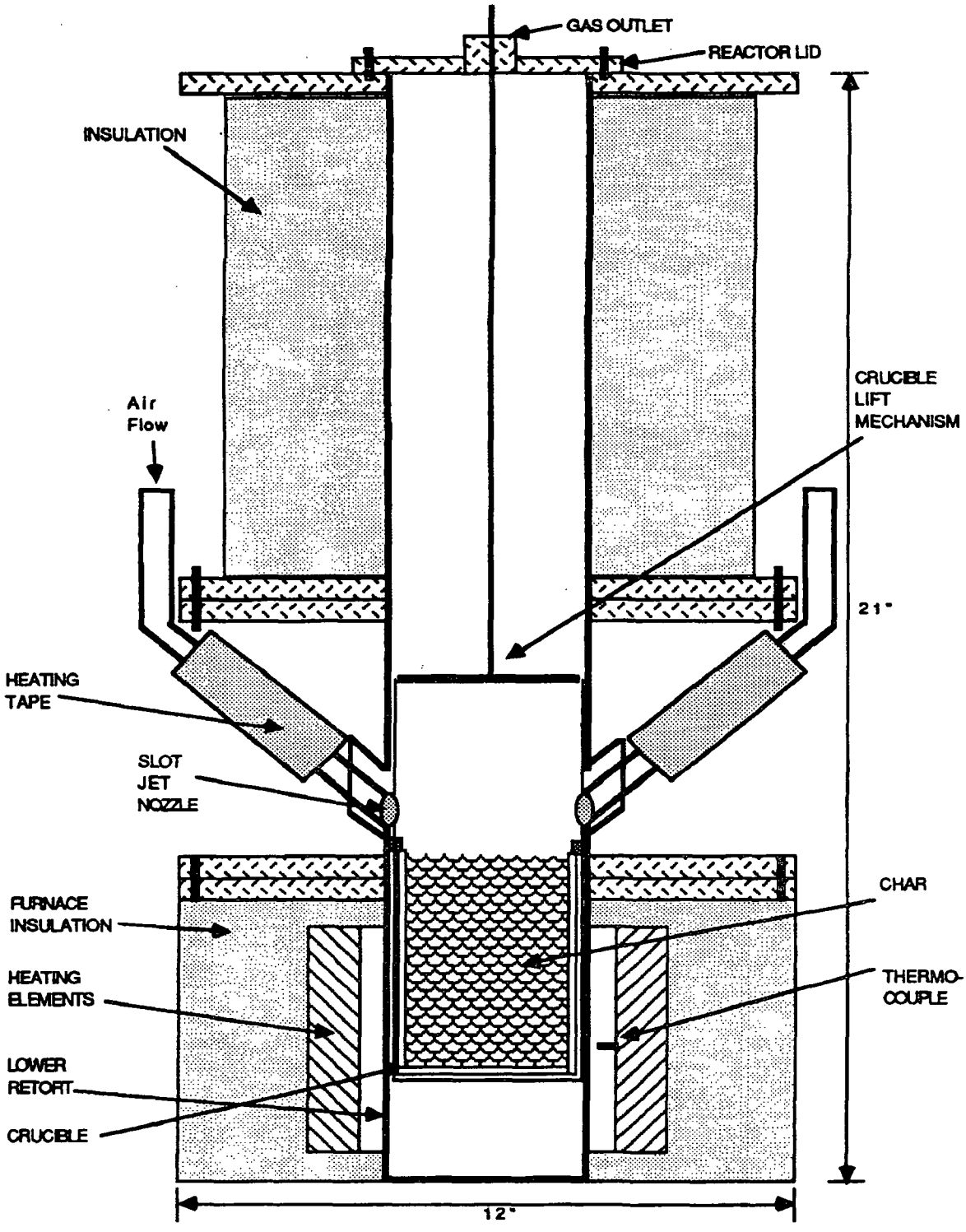

Figure 19. Schematic diagram of char combustion reactor, emphasizing the air ports and the position of the char bed during combustion.

The lower part of the reactor has two functions; it contains the black liquor char sample, and it supplies energy to the sample. This section is comprised of a tube furnace, a stainless steel retort and a crucible. In addition to supplying energy to the char sample, the furnace, which is mounted on a steel frame (not shown in these figures), supports the reactor. The retort serves to support the char bed and protects the furnace from accidental crucible failure. Inside the retort, a crucible contains the char sample. The furnace is the same ATS Series 3110 tube furnace used to heat the gas cell. It is controlled by a LFE model 2010 time-proportioned temperature controller. Both of these have been described earlier. Unlike its use previously, it is mounted with the hole through the furnace vertical, rather than horizontal. The retort consists of a 4.5" diameter stainless steel (316) tube, approximately 0.0625" thick. The tube is closed on the bottom by a 0.125" thick plate. Attached to the other end of the tube is a stainless steel flange which provides an air-tight point of attachment to the middle part of the reactor. This flange is 0.375" thick and has an outside diameter of 12" and an inside diameter of 4.5". The crucible is constructed of aluminum oxide (McDanel Refractory Co) and has a geometry consisting of a 2.5" tube body with one hemispherical closed end; the overall crucible length is 4".

The middle section of the reactor also has two functions; first it permits optical accessibility through the gas phase above the char bed and second, it introduces the O_2/N_2 gas mixture to support combustion. This section is comprised of the reactor tube, windows, window ports, air nozzles, and air heaters. The optical ports and air inlet jets are located at approximately the same height in the reactor. The position, relative to each other is more clearly illustrated in Fig. 20.

The reactor tube supplies a point of anchor to mount the window ports and air nozzles. The window ports permit optical accessibility to the gas phase above the char. The air ports and nozzles provide a continuous stream of gas to support the combustion. The reac-

tor tube consists of a 4.5" diameter stainless steel tube which is 0.125" thick. On each end of the tube are flanges which are 12" in diameter and 0.375" thick. The flanges provide air tight attachment points between the upper and lower sections of the reactor. The entire mid reactor section is insulated with 1" thick ceramic fiber insulation (Cotronics Model 372-Wrap-It Moldable, Wet Felts). The path of the infrared beam through the reactor is shown in Figs. 18 and 20. Holes, 5/8" in diameter, are drilled through this middle part of the reactor to allow the beam to pass through the reactor. Sapphire windows, 1" diameter and wedged 0.7-2.0°, (General Ruby and Sapphire Corp.) are compressed between the reactor tube wall and an insert in the window port. The inserts are slid against the windows to secure them in place. Ceramic paper insulation is placed on both sides of the windows to minimize air leaks through the window ports.

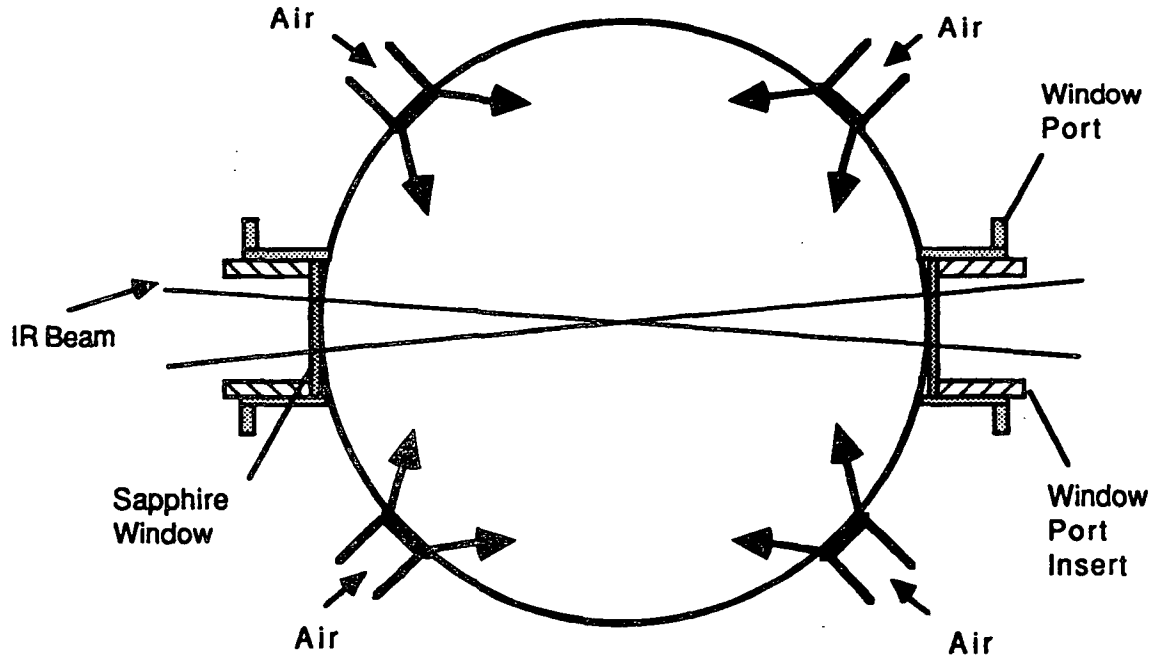

Figure 20. Overhead diagram of mid reactor section. The position of the windows relative to the air jets is illustrated as well as the direction of air flow from the nozzles, the windows, window ports, and window port inserts.

The air flow onto the char bed is illustrated in Fig. 19. The air or O_2/N_2 gas mixture is directed onto the char surface through 4 tubes shown in Fig. 20. The four air inlet tubes are connected to nozzles which are located slightly below the optical ports, and which are aimed onto the char bed at a 35° angle, with respect to the char surface. The nozzles (Spraying Systems Model 1/4T-SS+L-SS) are slot jets producing an angular flow pattern, see Fig. 20. The positioning of these nozzles was established by experimentation which included flow visualization aids (dry ice/acetone mixture or smoke). Before the gas is directed onto the char surface, it is preheated by four Omega heating tapes (OmegaLux® Ultra High Temperature Heating Tapes, Model STH051-020) controlled by 120 V voltage regulators. These tapes preheat the gas to a maximum temperature of 750 K before it exits the jets.

The upper part of the reactor has two functions; first, it directs the combustion gases out of the reactor with a minimum of recirculation back onto the char bed surface, and second, it provides the means for raising the char bed after it has been preheated. This section is comprised of the reactor tube and the crucible lift mechanism. The reactor tube is a long hollow tube which allows the gases to continue their ascent from the char bed surface to the gas outlet. It has been designed particularly long, so that any recirculation which occurs will result only in small recirculation zones at the top of the reactor and not produce recirculated flows back onto the char bed surface. The crucible lift supplies a means for raising the char bed closer to the optical ports after it has first been preheated inside the furnace cavity. It is then possible to make gas phase measurements closer to the char bed surface. The lift mechanism is constructed of threaded stainless steel rods, and supports the char bed from the bottom. The bed is raised by turning a threaded rod out of the gas outlet elbow (not shown in the figures).

The gases which flow in and out of the reactor are monitored by the same rotameters, mass flow meters and gas analyzers described for use with the gas cell. A 5% mixture of CO

in nitrogen covers the char during heat-up to reduce char consumption by sodium carbonate in the bed. Either prepurified air, or air diluted with nitrogen was used to support the combustion.

Char Preparation

Preparation of the char burned in this reactor began in the Institute's DOE-funded inflight reactor. Details describing this reactor have been presented elsewhere.[73] This reactor was used to form dried and partially pyrolyzed char particles. This material was then more fully pyrolyzed by heating it in the char reactor, described above. Here it was heated to 725-800° C for 1 hour after an initial 1 hour heat-up. A 5% mixture of CO in nitrogen was run over the char during heat-up, pyrolysis, and during the cool-down to reduce char consumption by sodium carbonate decomposition. The black liquor used for this work was obtained from the Weyerhaeuser Company, in New Bern, North Carolina. The liquor was produced by the kraft pulping process.

MATHEMATICAL METHODS

In addition to experimental procedures, this work has also required the development of mathematical methods. First, a simple means of determining the instrument resolution has been developed. Second, computational methods have been developed for the determination of "true" peak heights, gas concentrations, and gas temperatures from CO and CO_2 absorption spectra. The techniques used for each of these will be discussed in the sections that follow.

DETERMINATION OF INSTRUMENT RESOLUTION

The resolution of the instrument is a key parameter in the correction of experimental absorption peaks for the photometric errors resulting from the finite resolution of the spectrometer. While many definitions of instrument resolution are used in the literature, Anderson and Griffiths[51] have defined instrument resolution, for a sinc squared instrument line shape (ILS), as the point where the ILS first touches the baseline. In order to experimentally and computationally evaluate the instrument line shape, low pressure CO absorption spectra have been acquired and the half-width at half height (HWHH) of individual vibrational-rotational lines have been measured. These lines were then described mathematically. From this description, the resolution of the instrument could be obtained.

The procedures used for the acquisition of low pressure CO absorption spectra have already been described in the Experimental chapter. After acquiring and transforming these spectra, the P branch lines with J" indexes of 8, 9, and 10 were plotted and the HWHH of each was measured. It is assumed that the width of these lines is due only to instrument broadening.[44] Because triangular apodization was used in the transformation process, the instrument line shape is a sinc squared function.[42,51]

The sinc squared instrument line shape, $\sigma(\nu-\nu_i)$, is given mathematically by,

$$\sigma(\nu-\nu_i) = \frac{\sin^2(\pi\Delta(\nu-\nu_i))}{(\pi\Delta(\nu-\nu_i))^2}, \tag{30}$$

and is presented graphically in Fig. 21. The instrument resolution was determined by making plots similar to these. Using a spreadsheet, the functional relationship between $\sigma(\nu-\nu_i)$ and $\frac{\sin^2(\pi\Delta(\nu-\nu_i))}{(\pi\Delta(\nu-\nu_i))^2}$ was plotted. The value of Δ, the maximum optical retardation, was then varied until the HWHH of the calculated ILS was equal to the HWHH experimentally obtained from the low pressure CO absorption spectra. When the proper fit was obtained, the instrument resolution was simply evaluated by graphically determining where the ILS first reached the baseline, or by calculating the inverse of Δ, since $R_i = \frac{1}{\Delta}$, where R_i is the instrument resolution.

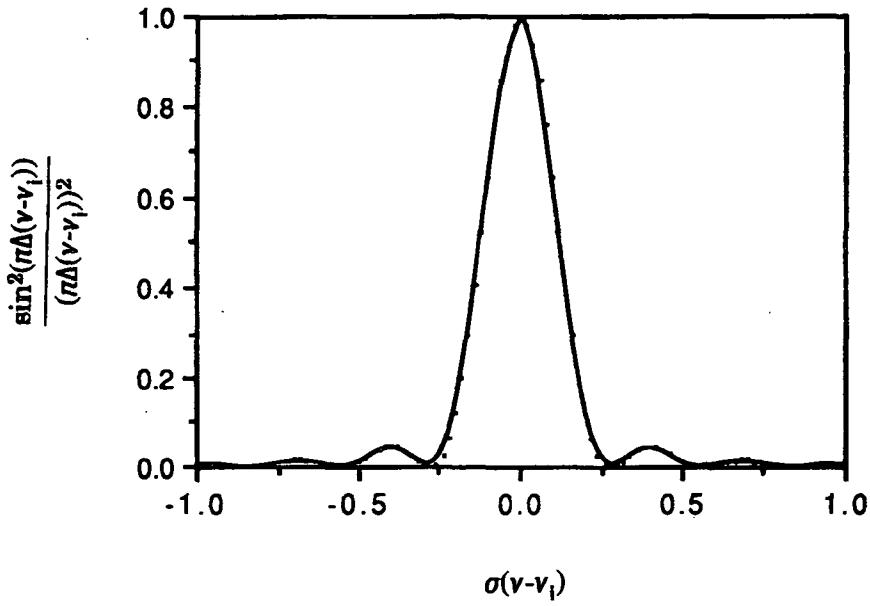

Figure 21. Plot of sinc squared instrument line shape, resulting from triangular apodization.

GAS TEMPERATURE AND CONCENTRATION CALCULATION METHODOLOGY

The results presented in this work involve the calculation of gas temperatures, line strengths and concentrations from infrared absorption spectra. Before these calculations can be made, the spectra must be corrected for photometric errors resulting from the finite resolution of the spectrometer. However, peak corrections require prior knowledge of the gas temperature and the concentration of all the species present in the gas phase. The interdependence between these two has been resolved by solving for gas temperatures, concentrations, and true peak heights iteratively. A Pascal program has been written to perform these calculations; the code has been included in Appendix VI. In the section that follows, an overview of the calculation methodology will be presented, including a more detailed description of the individual procedures used for calculating photometric error corrections, temperatures, line strengths, and gas concentrations.

A flow diagram of the program, called *SpecAnal* (Spectrum Analysis), is provided in Fig. 22. This diagram illustrates the calculation methodology, without providing calculation details. The program begins by initializing the computational environment, which includes setting the level of calculation precision, identifying subroutines, establishing the type of error trapping, *etc.* It then asks the user a series of questions which reveal how the program will be run; single file or batch mode, with or without CO concentration calculations, and with or without CO_2 concentrations. After this data input, the variables which will be used throughout the program are then initialized using the Pascal unit, *GlobVar* (Global Variables). A Pascal unit is similar to a FORTRAN subroutine.

Control of the program is then transferred to the unit, *SpAnUser* (Spectral Analysis User) which asks the user specific questions. These questions include; name(s) of the data and output file(s), the instrument resolution, initial temperature estimate, the partial pressure of CO, CO_2, and N_2 (known values are given if line strengths are calculated

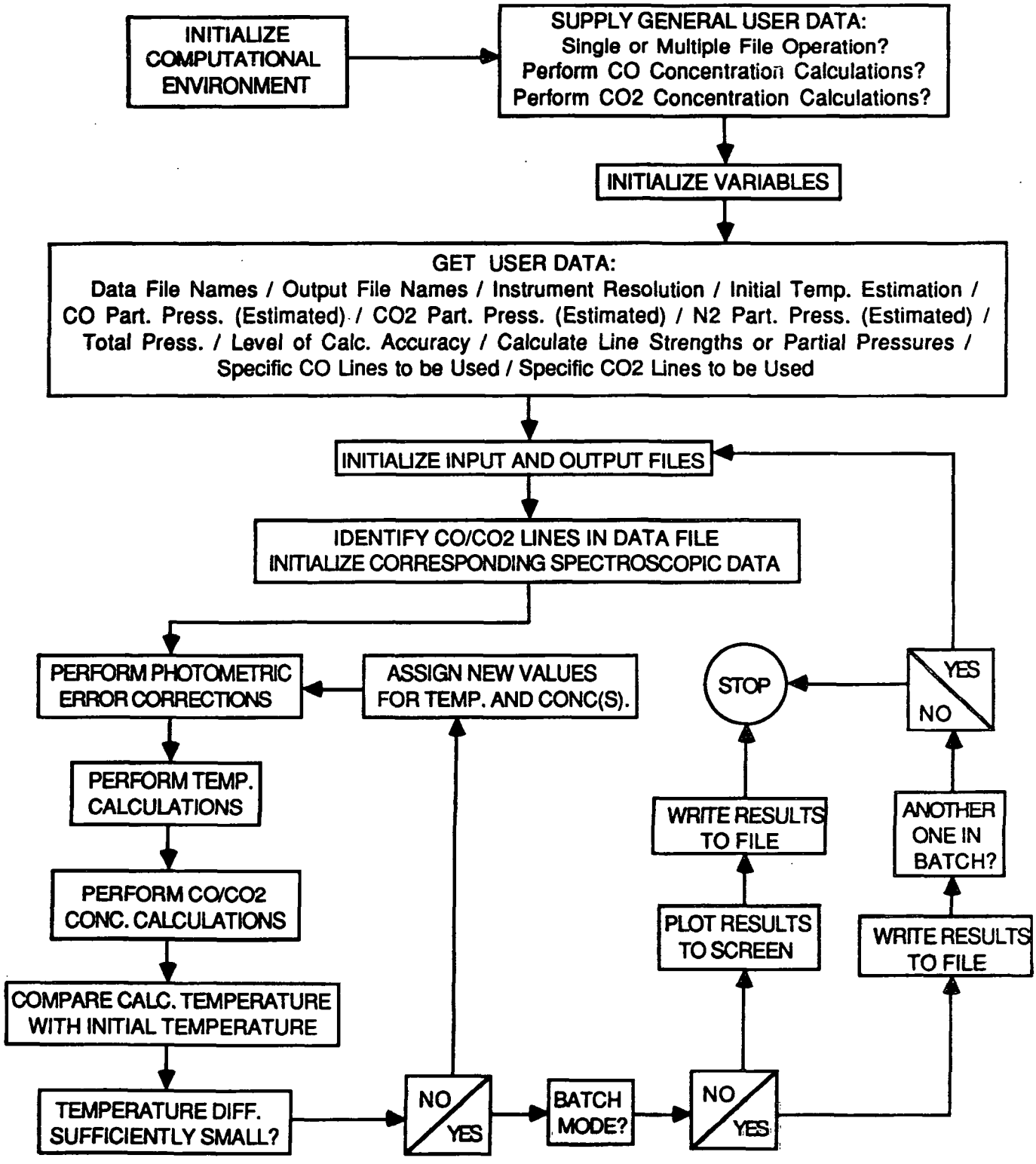

Figure 22. Flow diagram of calculation methodology used by the Pascal program, SpecAnal.Pas.

otherwise the values are estimated), the total pressure of the gas, the level of calculation accuracy (acceptable difference between calculated and estimated temperatures), the type of calculations which are to be performed (line strength or partial pressure), and finally the specific absorptions lines which are to be used for the calculations.

The files which have been designated for input (data) and output (results) are then initialized. The data file is the listing of experimental peak heights and positions which is generated after the spectrum is collected, see Appendix III. The file is read by the program and the peaks corresponding to CO and CO_2 absorption are identified. In this work, only well resolved lines were used. The CO lines used for gas phase temperature determinations and CO concentration determinations included the P branch lines from the ground state to the first vibrationally excited state with J" indexes between 5 and 35, excluding 10, 16, 17, 18, 19, 20, 24, 32, and 33. CO_2 concentration calculations were made with the R branch band of the $\tilde{\nu}_3$ normal mode of vibration. The specific lines used had J" values between 62 and 88. A listing of both the CO and CO_2 lines used in this work, as well as their position, is provided in Appendix VII. After these lines are identified, the spectroscopic data corresponding to each is initialized, which includes theoretical peak centers, and broadening coefficients. The peak identification, and data initialization, is performed in the Pascal unit *SpAnData* (Spectral Analysis Data).

After these preliminary procedures, the calculations begin. For the first iteration, the gas temperature and concentrations required throughout the calculations are the ones supplied as initial estimates by the user. Using these values, the experimental peak heights are corrected for the finite resolution of the instrument, gas temperatures are then calculated from the CO absorption spectrum, and finally, gas concentrations or line strengths are calculated. These procedures are detailed in the section below. The calculated gas temperature is then compared to the initial estimate. If the difference between the two is suffi-

ciently small, in this work less than 0.1 K, the calculations are complete. Otherwise, a second iteration begins. The second iteration starts by assigning new values for the gas temperature and concentration. The new gas temperature is the one just calculated. If CO and CO_2 gas concentrations have been made, these calculated values are used for the next iteration. When line strengths are calculated, the concentrations initially inputted into the program are used throughout all the iterations. In the second iteration, again, the experimental peaks are first corrected for photometric errors, then gas temperature, concentrations, and/or line strengths are calculated. The iterative process is continued until the convergence criteria is met. Generally 3-5 iterations are required for these calculations, which requires approximately 10-20 minutes on a 16 Mhz 80386 personal computer.

After the calculations are complete, the program follows one of two paths. If the program is operated in single file mode, the peak intensity versus transition energy is plotted on the screen, and the results are written to a data file. If the program is operated in batch mode, the results are simply written to a file and calculations are started on the next file in the batch. Writing the results to output files is accomplished using the unit *Output*.

Photometric Error Corrections

Correcting experimentally obtained absorption peak heights, for distortions resulting from the finite resolution of the instrument, are made in the Pascal unit called *PeakCor* (Peak Correction). Peak corrections are made for each line, individually. This unit begins by calculating a resolution parameter, ρ, using Equation 18 and the linewidth data found in references 43, 44, 46 and 48. The data found in reference 46 are preferred if the initial estimate of temperature is in the range where these data apply, *i.e.*, above 500 K. Equation 16 is then used to calculate twenty values of A^a_{peak} given twenty different values of A^t_{peak}. These calculations are done by an adaptive Gaussian numerical integration routine. The

range of A^t_{peak} values used, yield A^a_{peak} values which cover the range of possible apparent peak heights recorded by the instrument. This series of numerical integrations yields the functional relationship between apparent and true peaks, given a specific resolution parameter. A cubic spline interpolation routine is then used to get the specific true peak height which corresponds to the experimental peak. Once the true peak height is known for the first line, the calculations are repeated to obtain a half-width, a resolution parameter, and a true peak height for the next line. This procedure is continued until the true peak heights are calculated for all the carbon monoxide and carbon dioxide lines which were designated by the user to be included in these calculations.

Gas Temperature Calculations

Once the true peak heights of all the lines are known, the temperature of the gas is calculated using the Pascal unit, *TempCalc* (Temperature Calculation). Gas temperatures are determined by first calculating the terms, given by Equation 6, $\ln \left\{ \frac{A_{peak}(m)}{(1+K_1 m+K_2 m^2)} \frac{\gamma(m)}{\nu(m)} \frac{1}{|m|} \right\}$ and $-E(\upsilon, J)\frac{hc}{k}$ for each line of a given CO spectrum. A plot of these data points should yield a straight line with a slope equal to -1/T. A linear least squares routine is used to fit the calculated data points to an equation for a straight line. Before this plot can be made, the Pascal unit must first calculate values for the Herman-Wallis correction factor, $(1 + K_1 m + K_2 m^2)$, the line halfwidth, and the energy of the transition. The constants given by Anderson and Griffiths[49] ($K_1 = 1.77\times10^{-4}$, $K_2 = 6.67\times10^{-6}$) are used to calculate the Herman-Wallis correction factor. The energy of the transitions are calculated from the relationship,[74,75]

$$E = B'' J''(J''+1) - D'' J''^2(J''+1)^2 \qquad (29)$$

where B'' is the rotational constant (1.922529), and D'' is the centrifugal distortion constant

(6.1193×10^{-6}). The halfwidths are calculated by Equation 14, and using the data in references 43, 44, 46, and 48. Both weighted and non-weighted linear least squares procedures were used to fit the data to a straight line. In some cases, additional terms were included to account for induced emission.

Gas Concentration Calculations

Gas concentration calculations are made by incorporating the theoretical concepts presented in Equations 7-15 into other Pascal units called, *COConc* and *CO2Conc* (CO and CO_2 Concentration). After the CO and CO_2 peak corrections have been made, and the gas temperature has been calculated, the corrected peaks are substituted into Equation 12 which can be rearranged to directly calculate either the gas concentration, Equation 13, or the line strength, Equation 15. Experimental values for lines strengths were calculated initially. The initial line strength calculations yielded the temperature dependence of the line strengths for nearly forty CO and CO_2 absorption lines. This data was incorporated into the program, in the form of paired arrays; an average gas temperature corresponding to an average line strength. When a line strength value is required for a concentration calculation, a cubic spline interpolation is performed from the corresponding pair of arrays. Concentration measurements are made from as many CO and CO_2 lines as possible, and the final reported concentration value is an average of all the lines used in the calculations. When concentration calculations are requested, from a spectrum, the estimated values for CO and CO_2 partial pressure are used for the first iteration to facilitate the calculation of peak corrections. However, on subsequent iterations, the most recently calculated CO and CO_2 gas concentrations are used throughout the program.

RESULTS AND DISCUSSION

A presentation of the experimental data and a discussion of results, is given in the following five sections. In section 1, the qualitative characteristics of experimentally obtained CO and CO_2 absorption spectra, recorded in the high temperature gas cell, are presented and discussed. Furthermore, the effectiveness of mathematical peak height corrections, accounting for the finite resolution of the spectrometer, are illustrated. In section 2, data are presented which illustrate the accuracy of gas temperature calculations from CO absorption spectra. In section 3, experimental data are presented which describe the temperature dependence of line strengths for 22 CO and 19 CO_2 absorption lines. In section 4, the accuracy of gas concentration calculations, from absorption spectra, are presented. In section 5, results obtained for the determination of gas temperatures and concentrations in a black liquor char combustion environment are presented.

1. CO AND CO_2 ABSORPTION SPECTRA AND PEAK HEIGHT CORRECTIONS

Key preliminary steps in this work include the development of experimental systems which permit the acquisition of high temperature absorption spectra and also the development of a mathematical approach which corrects the experimental peak heights for photometric errors which result from the finite resolution of the spectrometer. A discussion and presentation of results related to each of these topics is given below.

CO and CO_2 Absorption Spectra

The high temperature gas cell, described earlier, has been used to provide a means for recording infrared CO and CO_2 absorption spectra, at temperatures between 295-1250 K. The environment is well defined with respect to gas temperature, pressure, and concentration. It is desired that the spectra recorded in this cell have a high signal-to-noise ratio and

that they are free of spectral distortions resulting from either, multiple reflections of the infrared beam through the cell windows or, modulated emission radiation from the hot gases.

Throughout the early phases of this work, difficulties were experienced from each of these factors. Poor signal-to-noise ratios were overcome by improving the alignment of the optical components which direct the infrared beam through the gas cell. The improved alignment was made possible by the acquisition and use of a laser jig which permitted the precise alignment of the Optibus® mirrors. The spectra recorded in the early part of this work were also effected by spectral artifacts resulting from the use of plano-plano windows. The parallel faces of the windows provided a means for the infrared beam to undergo multiple reflections through the window. The effect of this beam displacement resulted in small sinusoidal waves propagating throughout the entire absorption spectrum. The intensity of the wave was several times greater than the noise, resulting in a distortion of the measured peak intensities of the CO and CO_2 lines. These distortions were eliminated by the use of wedged (0.7-2.0°) windows.

A more difficult spectral distortion, more unique to the high temperature nature of this work, resulted from the emission from the high temperature gases. While emission radiation from the gas cell which is unmodulated merely reduces the signal-to-noise ratio of the spectra, modulated emission from the gas cell results in more serious spectral distortions. Emission radiation from the gas can pass through the optical tubes, to the interferometer, become modulated and then pass through the sample and to the detector. The modulated emission radiation appears in an absorption spectrum as negative peaks, shifted in wavenumber, but very near the corresponding absorption peak. A spectrum affected by this distortion is shown in Fig. 23. Distortions resulting from this effect were eliminated by placing an aperture at a focal point between the first and second 8" focal length mirrors (see Fig. 13). With the aperture in place, radiation emitted from the cell is blocked from the in-

terferometer and is unable to become modulated.

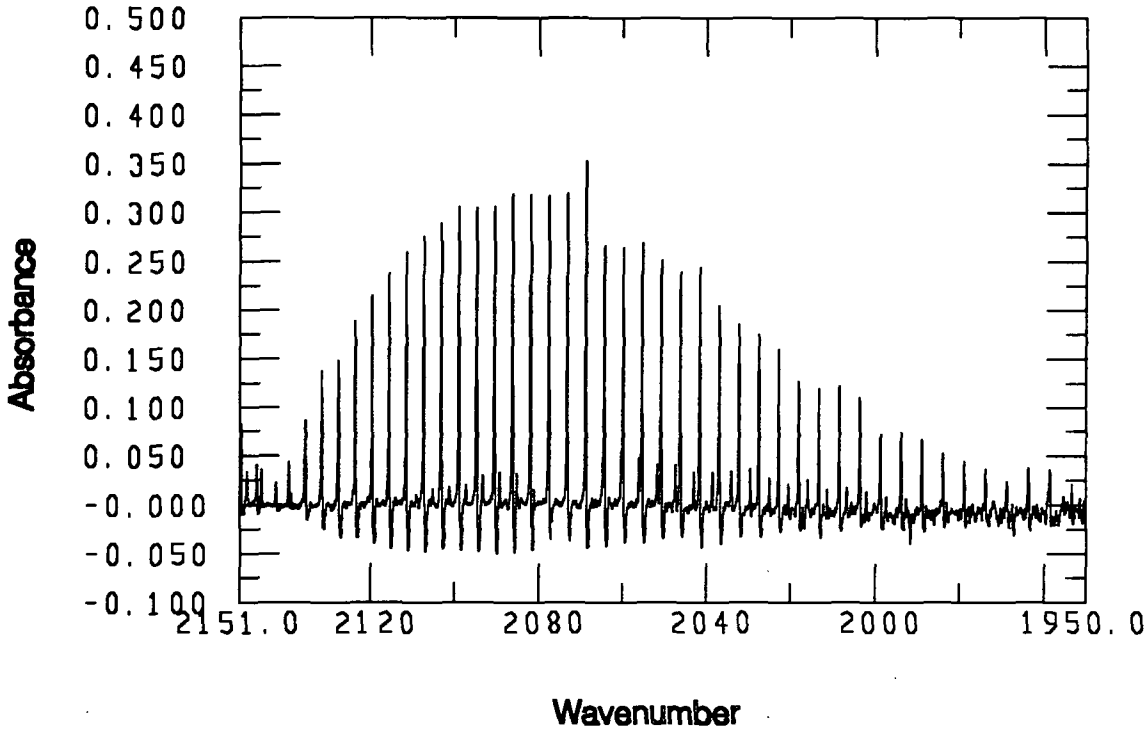

Figure 23. Infrared absorption spectrum distorted by modulated emission radiation emitted from the gas sample.

With the elimination of spectral distortions, it was then possible to acquire high quality, high temperature CO or CO_2 absorption spectra in the gas cell. Figs. 24 and 25 provide examples of pairs of CO and CO_2 absorption spectra recorded at 295 and 1250 K. Complete sets of spectra recorded at each of eight furnace temperatures (298, 361, 547, 746, 948, 1048, 1149, and 1247 K), for both CO and CO_2 are provided in Appendix VIII. These spectra, combined with the data from the temperature profiling experiments and the data provided by the pressure gauge and gas analyzers provide a unique and previously unreported set of CO and CO_2 absorption spectra at known gas conditions (temperature, pressure and concentration). The four spectra shown in these figures are representative of the quality of the spectra recorded throughout the course of this work.

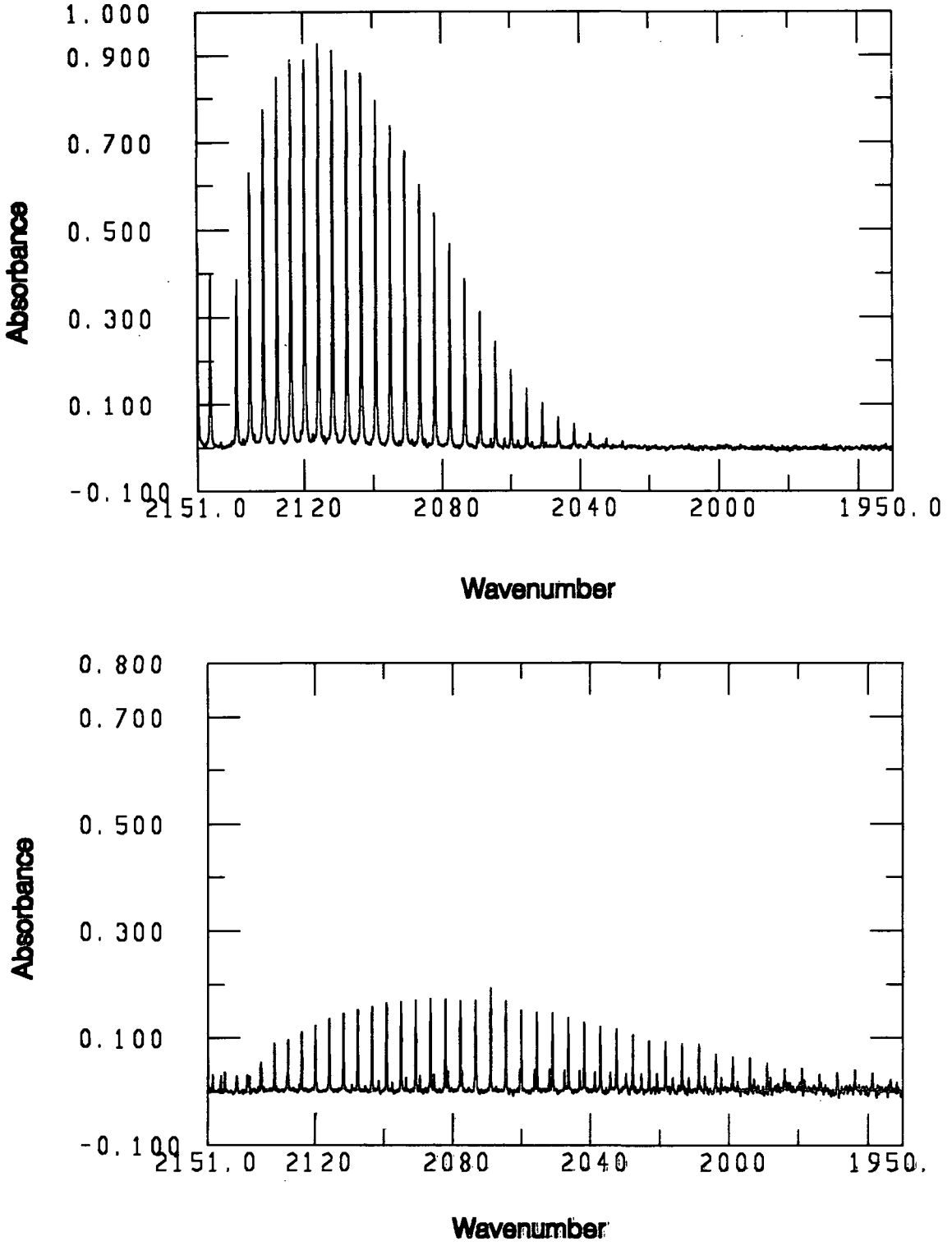

Figure 24. CO absorption spectra recorded at 295 K (top) and 1250 K (bottom). Both spectra were recorded from samples of 1.5% CO in nitrogen.

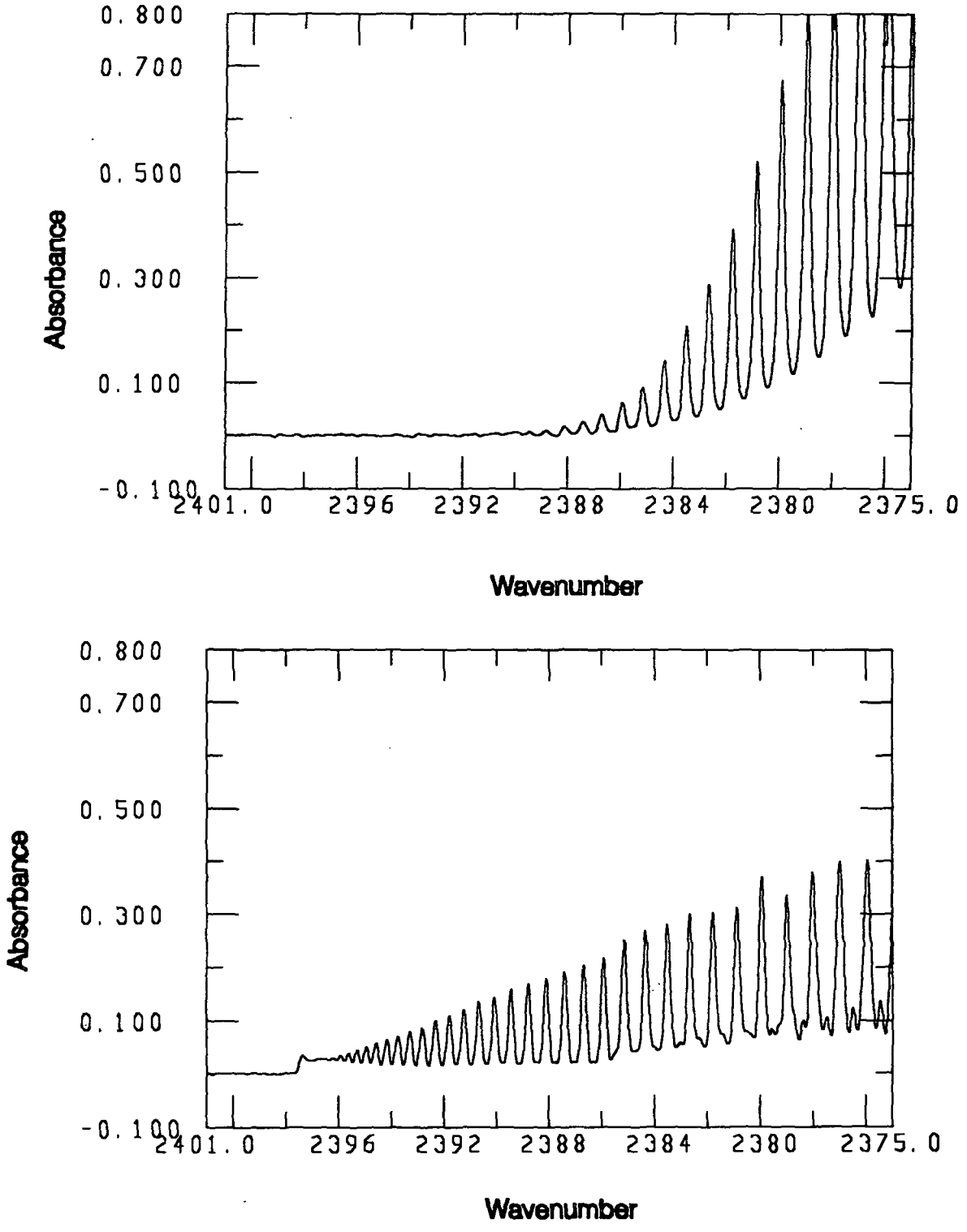

Figure 25. CO_2 absorption spectra recorded at 295 K (top) and 1250 K (bottom). Both spectra were recorded from samples of 1.5% CO_2 in nitrogen.

The spectra shown in Figs. 24 and 25 (and in Appendix VIII) illustrate both the changes in absorption behavior which occur at increasing temperatures and the effects of some experimental factors. First, among the experimental effects, the signal-to-noise ratio decreased as the temperature increased. This is a result of the diminished transmission of infrared radiation through the yttrium oxide or sapphire windows at higher temperatures. The changing transmission properties of the windows require that background spectra be recorded at the same temperature as the sample spectra. For these spectra, a new background spectrum was collected before each sample spectrum. Increased emission radiation from the gas cell at higher temperatures may also contribute to the reduction in the signal-to-noise ratio observed at higher cell temperatures. This stray radiation provides a high level background d.c. source which can reduce the sensitivity of the MCT detector.

The spectra shown in these figures also illustrate the changing absorption behavior of CO and CO_2 at increasing temperatures. First, as the temperature of the gas increases, the intensity of second order transitions also increase; these are transitions from the first vibrationally excited state to the second excited state. In the case of the CO lines, these lines appear as a P branch band with a shape that is similar to the first order band, but with lower absorption intensities and with frequencies shifted to lower wavenumbers. Second, as the temperature increases, the number of molecules populating the higher energy levels, corresponding to higher $|m|$ values, increases; and the number of molecules populating the lower energy levels decreases. Therefore, the higher temperature spectra show an increase in the number of lines observed on the outer wing of each band.

Figures 24-25 also illustrate the need for selectivity in choosing absorption lines for temperature and concentration calculations. In the case of the CO branch, as the second order transitions increase in intensity, second order lines which are not fully resolved from the

first order lines will influence the peak heights of the first order peaks. Note, for example, the m = -18 line (2068.847 cm^{-1}) in Fig. 24. At 295 K this peak is not significantly higher then neighboring lines, while at 1250 K this peak is clearly distorted by the second order m = -12 peak (2068.803 cm^{-1}). Inclusion of this peak in the temperature calculations will result in incorrect temperature determinations. In general, first order CO peaks which were within 0.5 cm^{-1} of either a ^{13}CO or second order ^{12}CO peak were excluded from temperature calculations.

In the case of the CO_2 R branch, the lines used in this work had m indices between 53 and 89, with corresponding frequencies of 2381.622 to 2394.021 cm^{-1}, respectively. These lines were selected since they are the most fully resolved CO_2 lines at temperatures between 295-1250 K in the frequency range between 1800 and 4400 cm^{-1}. However, there are two factors which still distort these lines. First, none of these lines are fully resolved from their nearest neighboring CO_2 line. Second, at higher temperatures, there is some overlap of the lower lines (53-65) by a neighboring CO_2 R branch band. Unlike the CO lines, no CO_2 lines have been excluded from use because of peak overlap. Instead, additional steps (described later) have been taken to calculate the distortions resulting from the overlap of neighboring lines.

Photometric Error Corrections

In addition to distortions of spectral peaks resulting from overlap of neighboring lines, the peak heights recorded by the spectrometer are also distorted by the finite resolution of the instrument. The theoretical basis of this distortion has already been discussed. A computational method of correcting peak heights has been developed. As discussed in the Mathematical Methods chapter, these corrections are based upon the use of Equation 16 which describes the functional relationship between the experimental peaks and the true

peak height for a given type of apodization. Initial temperature calculations from CO absorption spectra did not include these corrections. The plots of peak intensity versus peak energy, which are theoretically predicted to be linear, were significantly skewed. Furthermore, the linear Beer's law relationship expected from plots of peak intensity versus gas concentration also displayed significant nonlinear behavior. Examples, of these distortions are shown in the plots given in Figs. 26 and 27.

The plots given in Figs. 28 and 29 illustrate the improvements resulting from correcting experimental peaks for the finite resolution of the spectrometer. These plots show clearly that the peak corrections are necessary and indicate that the corrections have been properly made. Additional verification of the accuracy of these calculations will be presented later when line strength results are presented.

While the methods used for the correction of CO peaks have yielded satisfactory results, these same techniques alone are inadequate for the CO_2 lines. The calculation technique presented in the Mathematical Methods chapter assumes that the peaks are well resolved from neighboring lines. This assumption is not valid for the CO_2 lines used in this work, as illustrated in Fig. 25. Therefore, additional steps are required for these lines. These additional steps involve first correcting the experimental peak maxima for the overlap from neighboring lines, before using the values in calculations to determine the peak heights corrected for the finite resolution of the spectrometer. The calculation methodology is described below.

For the first iteration, the peak heights are performed in a manner identical to those for the CO lines. These calculations result in approximate values of the true peak heights, A^t_{peak}. At the start of the second iteration the original experimentally obtained CO_2 peak heights, designated as A^a_{peak}, are corrected for the overlap from the two neighboring lines,

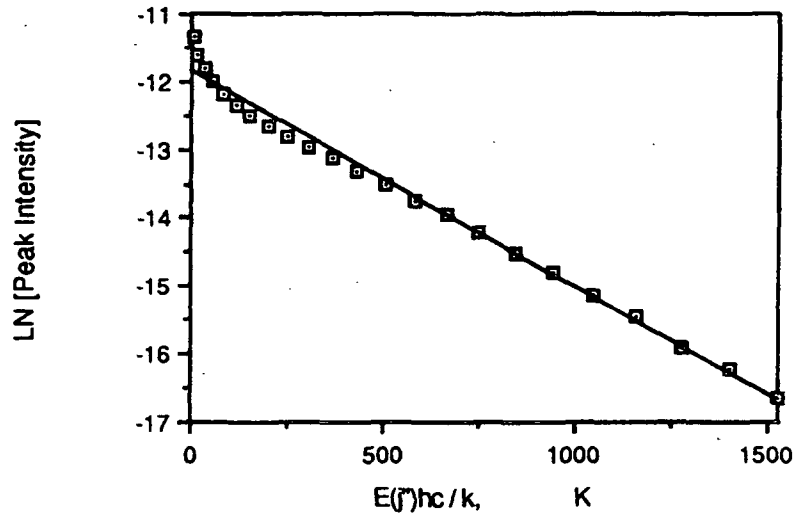

Figure 26. Plot of peak intensity, $\ln \left\{ \frac{A_{peak}(m)}{(1+K_1 m+K_2 m^2)} \frac{\gamma(m)}{\nu(m)} \frac{1}{|m|} \right\}$, versus $E(J'') \frac{hc}{k}$ for a 297 K CO absorption spectrum using uncorrected absorption peaks. Calculated gas temperature from the slope is 298 K.

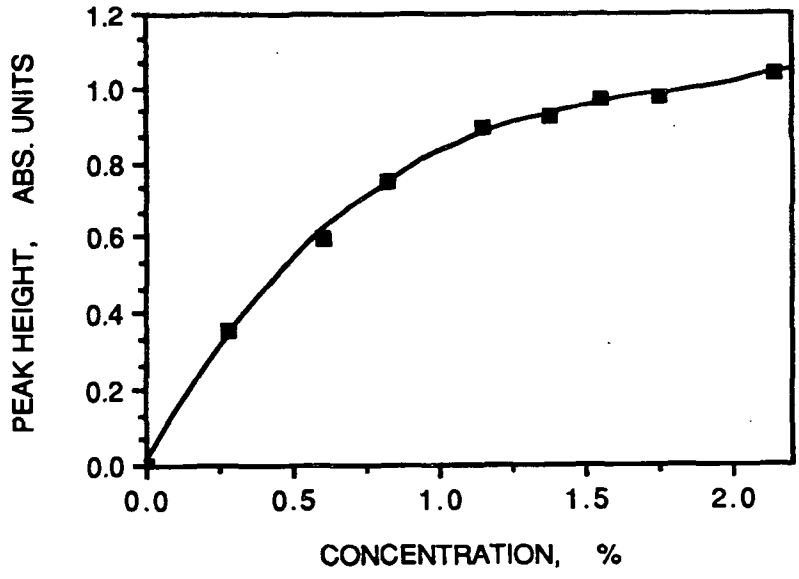

Figure 27. Peak height of P(6) line versus CO gas concentration for 8 296 K CO absorption spectra. The peak heights have not been corrected for photometric errors resulting from the finite resolution of the FT-IR instrument.

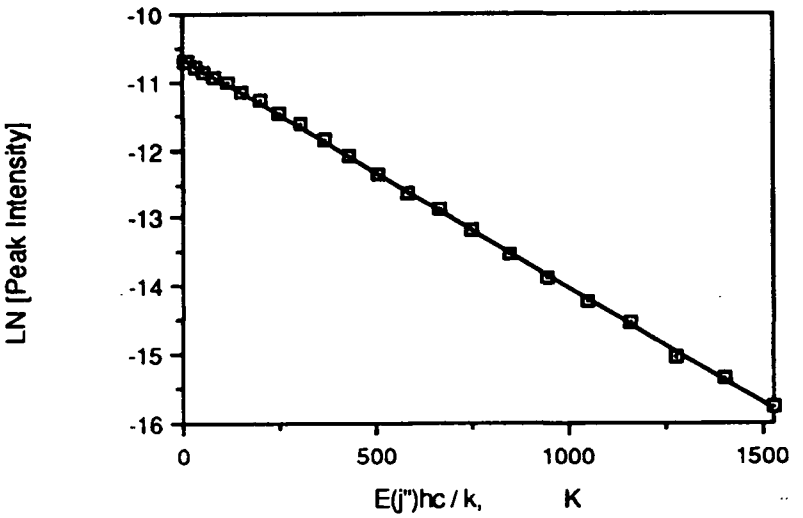

Figure 28. Plot of peak intensity, $\ln \left\{ \frac{A_{peak}(m)}{(1+K_1 m+K_2 m^2)} \frac{\gamma(m)}{\nu(m)} \frac{1}{|m|} \right\}$, versus $E(J'') \frac{hc}{k}$ for a 297 K CO absorption spectrum using corrected absorption peaks. Calculated gas temperature from the slope is 298 K.

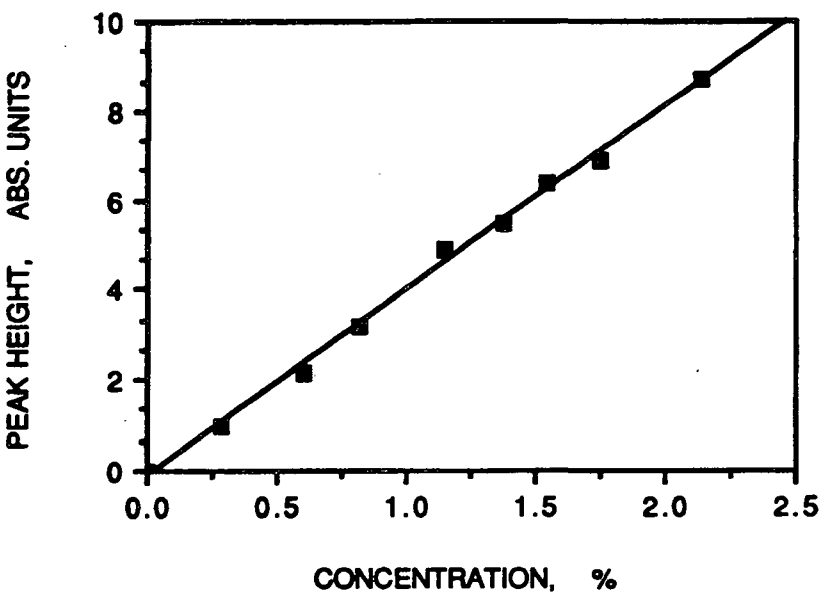

Figure 29. Peak height of P(6) line versus CO gas concentration for 8 296 K CO absorption spectra. The peak heights have been corrected for photometric errors resulting from the finite resolution of the FT-IR instrument.

resulting in a corrected peak, designated as A'^{a}_{peak}. These calculations are based upon the following set of equations, which are given below by example for line m=65,

$$A'^{a}_{peak}(65) = A^{a}_{peak}(65) - A^{a}_{x}(63) - A^{a}_{z}(67), \tag{30}$$

where x is the distance between the peak maxima of the m= 63 and 65 lines (which are the neighboring lines) and z is the distance between the m= 65 and 67 lines. This equation equates the overlap corrected experimental peak height with the original experimental peak minus the contribution of the lines on each side of it. The contributions from the neighboring lines is given by,

$$A^{a}_{x}(63) = -\log\left[\int_0^{\infty} \frac{\sin^2(\pi\cdot R_i\cdot(y-x))}{(\pi\cdot R_i\cdot(y-x))^2}\cdot\exp\left(\frac{-\ln 10\cdot A^{t}_{peak}(63)\cdot\gamma^2}{(x^2+\gamma^2)}\right)dy \Big/ \int_0^{\infty} \frac{\sin^2(\pi\cdot R_i\cdot(y-x))}{(\pi\cdot R_i\cdot(y-x))^2}\,dy\right] \tag{31}$$

$$A^{a}_{z}(67) = -\log\left[\int_0^{\infty} \frac{\sin^2(\pi\cdot R_i\cdot(y-z))}{(\pi\cdot R_i\cdot(y-z))^2}\cdot\exp\left(\frac{-\ln 10\cdot A^{t}_{peak}(67)\cdot\gamma^2}{(z^2+\gamma^2)}\right)dy \Big/ \int_0^{\infty} \frac{\sin^2(\pi\cdot R_i\cdot(y-z))}{(\pi\cdot R_i\cdot(y-z))^2}\,dy\right] \tag{32}$$

where R is the resolution of the instrument, y is a variable of integration, and γ is the line halfwidth at half height. These equations are similar to Equation 16, except that they are solved at a point other than the peak maximum. Resulting from this series of integrations is a new set of "experimental" or apparent peak maxima. These new values are then used in the standard calculations, described previously, for the determination of true peak heights (corrected for the finite resolution of the spectrometer). With each successive iteration the corrected peak heights, A'^{a}_{peak}, improve as the values of the true peak height A^{t}_{peak} improve. The accuracy of these calculation will be assessed later in the discussion of line strengths.

Significance of Results

In the overall scope of this work, the acquisition of high temperature absorption

spectra in the gas cell, and the correction of the experimental peaks for distortions resulting from the finite resolution of the spectrometer are key preliminary steps. The gas cell will be used for the collection of data in subsequent sections and the peak height correction methodology will be used for all spectra collected in this work, including those in a combustion environment. However, these results have additional significance. Few spectra, for CO and CO_2 at these combustion temperatures, similar to those reported here and in Appendix VIII, have been reported previously in the literature. The valuable line strength information which can be derived from these spectra will be presented later.

The correction of peak heights for the photometric error resulting from the finite resolution of the spectrometer is not unique to this thesis. Although the mathematical techniques developed for this work have not been previously reported in the literature, similar methods have been employed by others. Unique to this thesis, however, are the corrections made for the CO_2 peaks which required correction for multiple sources of distortion.

These preliminary steps, will provide the foundation from which addition calculations can be made, including gas temperature determinations, line strength calculations, and gas concentration calculations.

2. GAS TEMPERATURE DETERMINATIONS

The first phase of experimental work which uses the preliminary results described above, was a study directed towards the determination of gas temperatures from absorption spectra. The specific objective of this part of the thesis was to demonstrate the feasibility of calculating gas temperatures from CO absorption spectra in a high temperature environment. This objective was met by comparing spectroscopically measured gas temperatures with measurements made by a thermocouple.

In achieving this objective, sixty absorption spectra of a CO/N_2 gas mixtures were recorded at furnace set-point temperatures of 297, 373, 573, 773, 973, 1073, 1173, and 1273 K. The gas temperatures corresponding to the furnace set-points were 297, 361, 547, 746, 948, 1048, 1149, and 1247 K, respectively, as measured by a thermocouple. Six spectra were recorded at each temperature except at 297 K and 1273 K at which twelve spectra were recorded. Figure 24 in the previous section and Figs. A8-1 to A8-8 show typical absorption spectra of the P branch of CO at each of the furnace temperatures. In general, the spectra had an excellent signal-to-noise ratio, the peaks were very well resolved, and there was no evidence of emission peaks. The CO concentration metered into the cell was varied between 1 and 10% in nitrogen. The actual gas concentrations in the cell were significantly different, however, as a result of oxidative reactions occurring within the cell (discussed in greater detail in Appendix X). The resulting gas composition was a $CO/CO_2/N_2$ mixture. Over the course of all the data collection, the concentrations varied from 0.4-2.9% for CO and 0-6.2% for CO_2. (These concentrations were determined spectroscopically, after the gas concentration methodology was completed.)

Gas temperatures were calculated from the sixty spectra using the calculation methodology described in the Mathematical Methods chapter. Included in these calculations were calculations to account for induced emission, see Equation 4. Results averaged for the

6 or 12 spectra recorded at each furnace temperature are presented in Table 10. Included in this table is a comparison of the spectroscopically determined gas temperatures with gas temperatures measured by a thermocouple. The difference between the two is reported as both an average ΔT and an average percent difference. This table also includes the statistical information (high, low, mean, and standard deviation) regarding the replicates at each temperature. The average error associated with the least squares fit (LSF), at each furnace temperature, is also presented in this table. The original data is included in Appendix IX.

Table 10. Results of temperature calculations from CO absorption spectra.

Furnace Set Point (K)	Number of Spectra	Average Meas. Temp (K).	Average Calc. Temp.	Average Absolute Difference (K)	Average % Absolute Difference	Low (K)	High (K)	SD, (K)	Average Standard Error LSF
297	12	296	296	1.4	0.5 %	294	300	1.6	0.6
373	6	361	353	8	2.1 %	348	357	2.9	0.9
573	6	547	532	15	2.7 %	529	534	1.5	1.0
773	6	746	724	22	3.0 %	720	727	2.7	2.0
973	6	948	925	23	2.4 %	920	933	4.4	3.5
1073	6	1048	1032	16	1.5 %	1021	1042	7.5	4.8
1173	6	1149	1152	13	1.1 %	1130	1161	16	7.8
1273	12	1247	1272	33	2.7 %	1229	1386	48	18.3

Good agreement between thermocouple and spectroscopic temperatures was observed. The average percent differences between the two vary between 0.5 and 3.0%. At temperatures below 1149 K, the standard deviation among the six or twelve spectra recorded at each temperature did not exceed 8 K. At higher temperatures, 1149 and 1251 K, the standard deviation increased to 16 and 48 K, respectively. The increase of standard deviations at higher temperatures is a result of the reduced signal-to-noise ratio in these spectra and the corresponding increased random variation of experimental peak heights. This variation is evident in the 1250 K spectrum shown in Fig. 24. The significantly higher standard deviation for the 12 spectra at 1250 K, is primarily a result of one spectrum with a calculated temperature of 1386 K. A test for outliers (maximum normed residuals) was per-

formed on this value and it was shown that it could not be rejected at the 95% confidence level; therefore, it has been included in the tabulated results.

Table 10 also lists the error associated with the fit of the least squares line. The standard error associated with the least squares fit, for each spectrum, is included in the data presented in Appendix IX. This error is an indication of the scatter of the data points around the least squares fitted line. Predictably, the error increases at the higher temperatures where the signal-to-noise decreases.

Presented in Figs. 30 and 31 are representative samples of $\ln \left\{ \frac{A_{peak}(m)}{(1+K_1 m+K_2 m^2)} \frac{\gamma(m)}{\nu(m)} \frac{1}{|m|} \right\}$ versus $E(J'') \frac{hc}{k}$ plots at each furnace set-point temperature. It was from plots similar to these that the gas temperatures were calculated from each spectrum. Figure 30 contains plots for spectra recorded at furnace set-point temperatures of 296, 373, 573, and 773 K, and Fig. 31 contains plots for spectra recorded at temperatures of 973, 1073, 1173, and 1273 K. An arbitrary constant has been added to the y-coordinates of several of the data sets, comprising the lines in these two figures, in order to separate the lines for visual clarity. In Fig. 31, the constants -1, 2.5 and 4.5 have been added to the y-coordinates in the 297, 573, and 773 K plots, respectively. In Fig. 31, the constants -1.5, 1.5, and 2.5 have been added to the y-coordinates in the 973, 1173, and 1273 K plots, respectively. The differences between the slopes, which correspond to the different temperatures, are made more obvious by the separation.

As theoretically predicted, at all temperatures these plots are quite linear. The spectra recorded at the higher temperatures resulted in plots which deviate slightly from this high degree of linearity. This is a result of the reduced signal-to-noise ratio present in these spectra and the corresponding increases in random variations of the peak heights. It should be noted that this linear behavior was obtained only after correcting for photometric errors

and line broadening. As illustrated in the previous section, prior to making these corrections, the plots were linear over a limited range of $E(J'')\frac{hc}{k}$, but exhibited significant nonlinearities at the extreme lower values of $E(J'')\frac{hc}{k}$. The calculation of slopes from these nonlinear plots yielded calculated temperatures which were in error by as much as 20% of the true temperature.

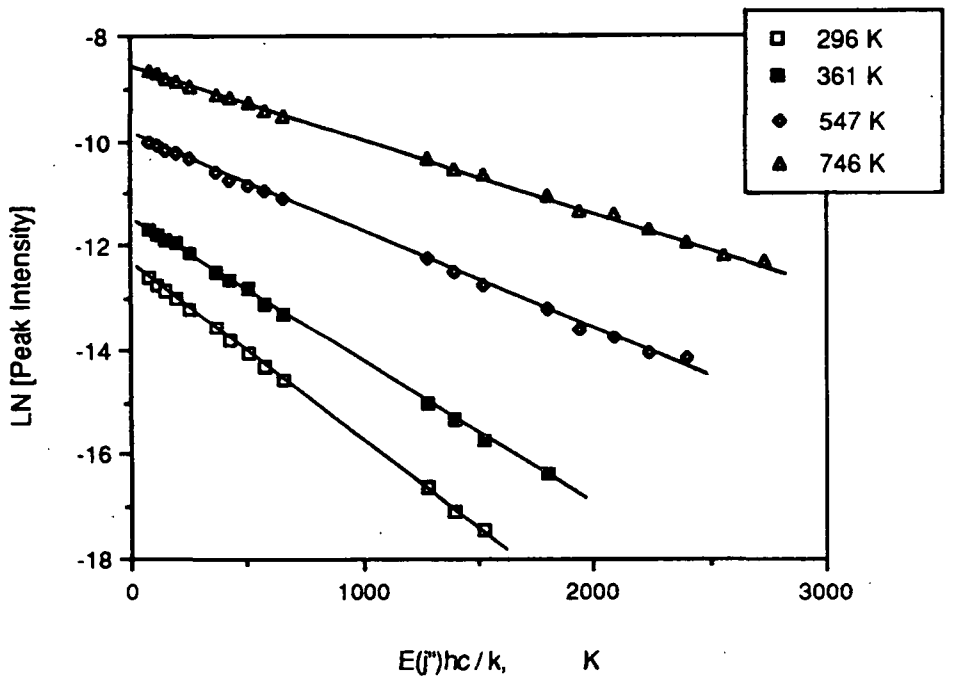

Figure 30. Plot of $\ln\left\{\frac{A_{peak}(m)}{(1+K_1 m+K_2 m^2)}\frac{\gamma(m)}{\nu(m)}\frac{1}{|m|}\right\}$ versus $E(J'')\frac{hc}{k}$ for representative spectra recorded at furnace set-point temperatures of 297, 373, 573, and 773 K.

In addition to the spectroscopic sample variation presented in Table 10, error is also associated with the gas temperature measurements recorded by the thermocouples, to which the spectroscopic measurements are compared. The source of this error arises first, from the K type thermocouples used for the temperature profiling which have an uncertainty of $\pm$ 0.75% (as reported by the thermocouple manufacturer). Second, variations in packing the

insulation around the gas cell can lead to variation in the energy loss, which can change the temperature profile. The combined error associated with the thermocouple uncertainty and insulation was evaluated by determining the temperature profile with a thermocouple at a furnace set-point temperature of 1273 K in five different experiments. The gas temperatures from these profiles were 1254, 1253, 1251, 1245, and 1249 K, which yielded an average value of 1250 K with a standard deviation of 13 K. Since both the thermocouple variance and the heat loss variance are greatest at the highest furnace temperature, the 13 K standard deviation is considered a maximum value for all the furnace temperatures considered. While this variation is sufficiently large to account for some of the average absolute temperature differences shown in Table 10, it cannot account for the variation at all the furnace temperatures considered especially those at the two highest temperatures.

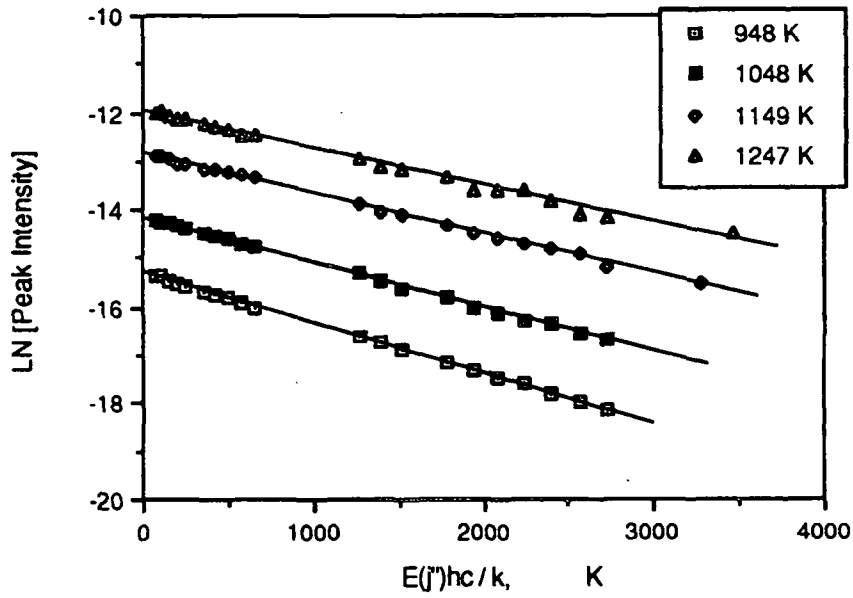

Figure 31. Plot of $\ln\left\{\frac{A_{peak}(m)}{(1+K_1 m+K_2 m^2)}\frac{\gamma(m)}{\nu(m)}\frac{1}{|m|}\right\}$ versus $E(J'')\frac{hc}{k}$ for representative spectra recorded at furnace set-point temperatures of 973, 1073, 1173, and 1273 K.

Although the thermocouple and spectroscopic measurements are in good agreement,

(< 3% average error at all temperatures) neither variations in thermocouple measurements nor random sample variations alone can account for the differences calculated at all furnace temperatures. Nor can such errors account for the tendency of all the calculated temperatures, except at 1150 and 1250 K, to be lower than the gas temperatures measured by the thermocouple. Additional sources of error need to be considered.

It has been suggested[49] that the use of a linear least squares fit of the data can lead to inaccuracies in temperature calculations since the standard deviation of the y term (*i.e.*, the ordinate term) in the temperature plots of $\ln \left\{ \frac{A_{peak}(m)}{(1+K_1 m+K_2 m^2)} \frac{\gamma(m)}{\nu(m)} \frac{1}{|m|} \right\}$ versus $E(J'') \frac{hc}{k}$, varies with $E(J'') \frac{hc}{k}$. The linear least squares model assumes that all the variances for the y components are equal. Generally, the y terms are weighted to compensate for this deviation to meet the model requirements. In an effort to determine the importance of weighting, the y-components of some plots were weighted by the inverse of the variance of y. The temperatures were then recalculated for several of the spectra. The weighting resulted in only minor changes in the calculated temperatures. However, these differences were not always in the direction closer to the temperatures measured by a thermocouple. Therefore, it appears unlikely that the use of an unweighted least squares is responsible for the systematic lowering of the calculated temperatures.

It was also possible that modulated emission from the gas samples, if it reached the detector, might be biasing the data. The aperture placed between the gas cell and the interferometer was effective in eliminating most of the emission radiation which becomes modulated. The importance of the remaining emission which reached the detector, if any, was evaluated by performing calculations with theoretical spectra. Two spectra were calculated, one for CO absorption and the other for emission, each at 1273 K. The emission spectrum peak heights were normalized to reduce their heights to 25% of the intensity of the absorp-

tion peaks. The emission peaks (negative peaks) were then added to the absorption spectrum, and the temperature of the resulting spectrum was calculated. The calculated temperature was higher than 1273 K, while the plot of $\ln \left\{ \frac{A_{peak}(m)}{(1+K_1 m+K_2 m^2)} \frac{\gamma(m)}{\nu(m)} \frac{1}{|m|} \right\}$ versus $E(J'') \frac{hc}{k}$ remained linear. This would suggest that the deviations observed in the calculated temperatures, which are in the opposite direction, are not a result of emission. However, it is possible that the 1149 and 1251 K spectra are slightly affected by modulated emission, which has resulted in raising the calculated temperatures closer to the measured gas temperatures. The higher temperature spectra would be more affected by emission, since it is at these temperatures that emission from the gas sample is greatest.

The significance of emission was further explored by considering the results of changing the aperture diameter used to block the modulated emission from reaching the detector. As the diameter of the aperture was increased, the calculated temperatures also increased. With no aperture in place, the calculated temperatures were 50-100 K above the measured temperatures at the higher furnace set point temperatures. Therefore, it is unlikely that emission from the gas sample is causing the lowering of the calculated temperatures. However, it is possible that it is responsible for reducing the difference between calculated and measured gas temperatures at the higher furnace set point temperatures.

Of the eight temperatures examined, the best results were obtained at room temperature. The high degree of accuracy obtained at this temperature suggests that the calculation methodology is correct. This is also the only temperature at which line widths have been experimentally measured. At all other temperatures, a model[46] is used to estimate the widths of the lines. It is possible that inaccuracies in the estimates of the line widths are responsible for the deviations between calculated and measured gas temperatures. The temperature calculation program is very sensitive to changes in ρ, the ratio of the instrument

resolution to the line width. The line width data of Hartmann *et al.*[46] has a reported accuracy of $\pm$10%. Altering only a few of the line widths by this amount was shown to result in significant changes in the calculated temperatures ($\pm$ 20 K). Changes of line widths of this magnitude could account for the discrepancies between calculated and measured gas temperatures.

Reliable half-width broadening data from Hartmann *et al.*[46] has been a key component towards the accurate results shown in Figs. 30 and 31. Although some of the error of these calculations has been attributed to the inaccuracies of this model ($\pm$ 10%), in general the model has done an adequate job of predicting CO line broadening by nitrogen. This model appears to be the most comprehensive and accurate source of high temperature CO line broadening information available in the literature.

Significance of Results

Temperature calculations have been successfully derived from CO absorption spectra at temperatures up to 1273 K. These calculations had accuracies of 3.0% or better as compared to thermocouple measurements (accuracy of $\pm$ 0.75%) and were found to be independent of CO concentration. The accuracy of these calculations met the expectations of the technique in this high temperature environment and will be sufficiently reliable to be used in combustion research. The success of these calculations can be attributed to two factors; first, the high degree of linearity of the lines in Figs. 30 and 31, and second, control of the emission from the hot gases. The high degree of linearity of the lines in these figures has resulted from correctly accounting for the photometric error. Before these corrections were made, the plots of $\ln \left\{ \frac{A_{peak}(m)}{(1+K_1 m+K_2 m^2)} \frac{\gamma(m)}{\nu(m)} \frac{1}{|m|} \right\}$ versus $E(J'') \frac{hc}{k}$ were significantly curved. A fitted straight line to these plots resulted in poor regression coefficients and calculated temperatures in error by 10-20%. The linearity of these plots can also be attributed, in

part, to the accuracy of the half-width broadening data from Hartmann, *et al.*[46]

The second key component for accurate temperature calculations has been the control of emission from the hot gases. The use of an aperture in the optical path has eliminated the presence of emission peaks in the absorption spectra and has significantly reduced calculation errors resulting from the use of absorption spectra with absorption peaks convoluted with emission lines.

These calculations represent only the first phase of work in a project whose ultimate objective is to use FT-IR absorption spectroscopy for the *in situ* determination of gas temperatures and concentrations above a burning black liquor char bed. The success of these results, however, is essential for subsequent work.

3. LINE STRENGTH RESULTS

The determination of gas concentrations from absorption spectra requires knowledge of the line strengths of the individual vibrational-rotational lines. In a linear plot of peak absorption versus concentration, the line strength is equal to the slope of the line (see Equation 15). The line strength of an absorption peak is a fundamental parameter of the line, and at room temperature, has been studied thoroughly for the various CO and CO_2 lines considered in this work. However, in addition to displaying m dependence, line strengths are also strongly temperature dependent. The temperature dependence of these values has received little experimental evaluation. For the accurate determination of gas concentrations at temperatures greater than 300 K, knowledge of the temperature dependence of these values is essential.

In the following subsections, experimental data describing the temperature dependence of 22 CO and 19 CO_2 lines will be presented. The accuracy of this data will be evaluated by considering the statistical variability among replicates and by error analysis calculations. The data will also be evaluated by comparisons with other experimental line strength data as well as theoretical calculations which predict the temperature dependence of these values.

Line Strength Data

For the determination of the temperature dependence of the line strength of 22 CO and 19 CO_2 vibrational-rotational lines, 52 spectra were recorded from $CO/CO_2/N_2$ gas samples at eight different temperatures in the high temperature gas cell. Ten spectra were recorded at room temperature (296 K) and six each at furnace set point temperatures of 373, 573, 773, 973, 1073, 1173, and 1273 K. Like the spectra recorded for the determination of gas temperatures in the cell, all the spectra recorded for this work were of high quality, dis-

playing excellent signal-to-noise and were free of emission peaks. The gas concentrations of all the spectra were measured by a CO/CO_2 gas analyzer at the exit of the high temperature gas cell and by measurements with mass flow meters and rotameters before the gases entered the cell.

At furnace set point temperatures greater then 373 K, the agreement between the metered gas concentrations into the cell and the measurements from the gas analyzer were very poor. In general, there was less CO and more CO_2, measured by the analyzer, compared to the mass flow meters and rotameters. The difference between the two measurements is a result of a CO/CO_2 equilibration reaction and also a reaction between the gas mixture and the stainless steel. A more detailed discussion of these reactions is provided in Appendix X. The net result of these two reactions, however, is a change in the composition of the gas, from the quantities metered into the cell, to NDIR measured quantities at the exit of the cell. Since these reactions begin to occur at temperatures near 500 K, the metered gas concentrations were used for the first two furnace set point temperatures, 296 and 373 K. At higher temperatures the gas composition was more accurately measured by the NDIR instrument.

With a knowledge of the gas composition, the Pascal program described in the Mathematical Methods chapter was run on each of the 52 spectra, resulting in the determination of both the gas temperatures and the line strengths. The method of gas temperature determination has already been described. The determination of line strengths was based upon Equation 15, reproduced below,

$$S(m) = \frac{A(\nu_o)\cdot\pi\cdot\gamma(m,T)\cdot\ln(10)}{C\cdot L}, \qquad (15)$$

where S(m) is the line strength, $A(\nu_o)$ is the peak height (corrected for both the finite reso-

lution of the spectrometer and overlap of neighboring lines), $\gamma(m,T)$ is the m and temperature dependent line halfwidth at half height, C is the partial pressure of the gas, and L is the path length of the cell. The calculated results from the temperature and line strength calculations are given in Appendix XI. Included in this Appendix, is first, a sample output from the Pascal program, and then tables of compiled results containing the calculated line strengths for the 41 CO and CO_2 absorption lines for each spectrum at each furnace set point temperature. Also included in these tables are average line strengths, the standard deviation of the line strengths among the six (or ten) spectra, and the relative percent of the standard deviation (relative percent of S.D. = 100* S.D./Average Line Strength).

The data presented in Appendix XI have been summarized in the tables below. First, Table 11 shows the results of the temperature calculations. This table is similar to that presented in the previous section. It has been included here to reiterate the temperature determination accuracy and to emphasize that the quality of these spectra is as good as those previously obtained. The results presented in Tables 12 and 16 are the average line strengths at each furnace set point temperature and for each of the 22 CO and 19 CO_2 lines, respectively. The temperatures reported at the top of these two tables are the averaged temperatures calculated from the spectra.

Evaluation of the accuracy and precision of the line strengths which have been presented in these tables is accomplished in four ways: 1) by consideration of the variation among samples and a calculation of the standard deviation based upon error analysis calculations, 2) by evaluation of the Bouguer-Lambert relationship for this data, 3) by comparison with existing room temperature and high temperature measurements, and 4) by comparison with theoretical predictions. In the following two subsections, the data in Tables 12 and 16 will be evaluated by a consideration of each of these four criteria.

Table 11. Results of temperature calculations from CO absorption spectra from the data set collected to measure absorption line strengths.

Furnace Set Point (K)	Number of Spectra	Average Measured Temp.(K).	Average Calc. Temp.(K)	Average Absolute Difference (K)	Average % Absolute Difference	Low (K)	High (K)	SD (K)	Average Standard Error LSF
297	10	296	294	3.1	1.0 %	290	298	2.5	1.4
373	6	361	353	8	2.2 %	345	361	5.6	2.1
573	6	547	535	12	2.2 %	527	542	5.1	2.7
773	6	746	720	26	3.5 %	715	734	8.8	4.4
973	6	948	936	14	1.4 %	928	954	8.9	2.5
1073	6	1048	1034	18	1.8 %	1014	1061	18	4.8
1173	6	1149	1144	30	2.6 %	1114	1201	35	8.0
1273	6	1247	1226	36	2.9 %	1191	1293	36	15.4

CO Absorption Lines

The temperature dependent line strengths, calculated from the CO P branch of the 52 spectra described above, are presented in Table 12. It was not possible to calculate line strengths from some lines, at the lowest three temperatures, because the peak intensities were too low. Additional lines have been excluded at all temperatures for lines with m indices of -1, -2, -3, -4, -10, -16, -17, -18, -19, -20, -24, -32, and -33. These lines were not fully resolved from either ^{13}C isotopic CO lines or hot band CO lines (the small peaks adjacent to the major absorption lines shown in Fig. 24).

Table 12. Results of line strength calculations for 22 CO absorption lines recorded at temperatures between 295-1250K. Calculated values of S(m) are in units of 1/(atm-cm^2).

Line (m)	S(m) 295 K	S(m) 353 K	S(m) 535 K	S(m) 720 K	S(m) 936 K	S(m) 1034 K	S(m) 1144 K	S(m) 1226 K
-35	-	-	-	0.111	0.183	0.210	0.209	0.236
-34	-	-	-	0.154	0.215	0.235	0.266	0.225
-31	-	-	0.140	0.307	0.378	0.397	0.374	0.372
-30	-	-	0.178	0.333	0.428	0.432	0.437	0.376
-29	-	-	0.248	0.431	0.496	0.488	0.482	0.468
-28	-	-	0.306	0.520	0.571	0.556	0.533	0.522
-27	-	0.130	0.402	0.635	0.647	0.629	0.594	0.541
-26	-	0.185	0.491	0.735	0.731	0.679	0.640	0.582

Line (m)	S(m) 295 K	S(m) 353 K	S(m) 535 K	S(m) 720 K	S(m) 936 K	S(m) 1034 K	S(m) 1144 K	S(m) 1226 K
-25	0.154	0.303	0.656	0.905	0.826	0.773	0.705	0.673
-23	0.346	0.539	0.986	1.182	1.022	0.916	0.829	0.752
-22	0.493	0.779	1.197	1.312	1.119	1.014	0.875	0.759
-21	0.704	1.010	1.420	1.503	1.219	1.094	0.947	0.860
-15	4.113	4.069	3.301	2.598	1.680	1.413	1.179	1.003
-14	5.031	4.856	3.629	2.719	1.728	1.442	1.202	0.994
-13	6.196	5.794	3.874	2.800	1.728	1.437	1.176	0.982
-12	7.347	6.552	4.085	2.864	1.741	1.427	1.155	0.966
-11	8.472	7.155	4.275	2.854	1.712	1.387	1.109	0.926
-9	10.364	8.500	4.373	2.814	1.581	1.283	1.025	0.834
-8	11.241	8.567	4.267	2.626	1.511	1.207	0.928	0.771
-7	11.367	8.378	4.088	2.510	1.391	1.106	0.878	0.724
-6	11.013	8.198	3.787	2.306	1.271	1.001	0.780	0.653
-5	10.522	7.538	3.425	2.021	1.096	0.875	0.661	0.546

Although the six (or ten) values of line strength calculated for each line at each temperature were recorded at a different concentration, the line strengths should be the same. Therefore, a first measure of the precision of these line strengths is simply a calculation of the standard deviation of all calculated values at each temperature. The standard deviations are reported in Appendix XI for the calculated average line strengths at all the furnace set point temperatures. These values, along with the calculated relative percent standard deviations, are provided in Table 13 at three furnace temperatures. Generally, the standard deviation of these values is low, equaling between 3-6% of the average value for most lines at all three temperatures. Furthermore, there appears to be no significant dependence of the relative percent standard deviations on m or the gas temperature.

The individual factors which contribute to the variability of these results can be evaluated in two ways; first, by plots of peak height versus concentration, the Bouguer-Lambert relationship, and second, by error analysis. The Bouguer-Lambert relationship requires a linear relationship between peak height and concentration. If either the peak height or concentration values are significantly in error, it will appear as deviations from linearity in these plots. Corrected peak heights versus CO concentration plots are given in Figs. 32-34

for furnace temperatures of 295, 720, and 1225 K.

Table 13. Standard deviations and relative percent standard deviations for the replicated line strengths calculated at temperatures of 295, 720, and 1226 K.

Line (m)	S.D. 295 K	Relative % S.D.	S.D. 720 K	Relative % S.D.	S.D. 1225 K	Relative % S.D.
-35	-	-	0.011	9.11	0.044	18.49
-34	-	-	0.017	11.21	0.011	4.70
-31	-	-	0.014	4.49	0.022	5.89
-30	-	-	0.018	5.35	0.021	5.57
-29	-	-	0.022	5.02	0.033	7.03
-28	-	-	0.021	4.12	0.051	9.74
-27	-	-	0.056	8.75	0.040	7.41
-26	-	-	0.017	2.37	0.024	4.20
-25	0.010	6.41	0.037	4.13	0.045	6.72
-23	0.023	6.70	0.083	6.99	0.042	5.63
-22	0.015	3.12	0.073	5.56	0.032	4.24
-21	0.041	5.81	0.094	6.22	0.046	5.34
-15	0.217	5.28	0.105	4.04	0.059	5.91
-14	0.231	4.59	0.115	4.22	0.029	2.88
-13	0.410	6.61	0.164	5.85	0.044	4.52
-12	0.431	5.86	0.171	5.97	0.031	3.22
-11	0.482	5.68	0.098	3.43	0.047	5.04
-9	0.656	6.33	0.177	6.27	0.045	5.41
-8	0.691	6.14	0.137	5.21	0.028	3.65
-7	0.762	6.71	0.091	3.61	0.027	3.74
-6	0.500	4.54	0.111	4.81	0.038	5.89
-5	0.689	6.27	0.106	5.24	0.031	5.60

All of the lines plotted in these figures display a high degree of linearity. Furthermore, there appears to be no significant deviations from this trend at higher temperatures or at different values of m. The importance of the linearity of these plots to the line strength data is simply that it suggest that gas concentrations have been measured accurately and that the peak height corrections have been performed correctly. The importance of peak height corrections has already been emphasized by the data presented in Figs. 27 and 29. However, it is also very significant that gas concentrations have been measured accurately,

since the reactions occurring within the cell, under some conditions, changed the initial gas composition very significantly, 20-50%. Accurate knowledge of each of these factors is critical to line strength calculations since each is either directly (peak height) or inversely (concentration) proportional to the line strength.

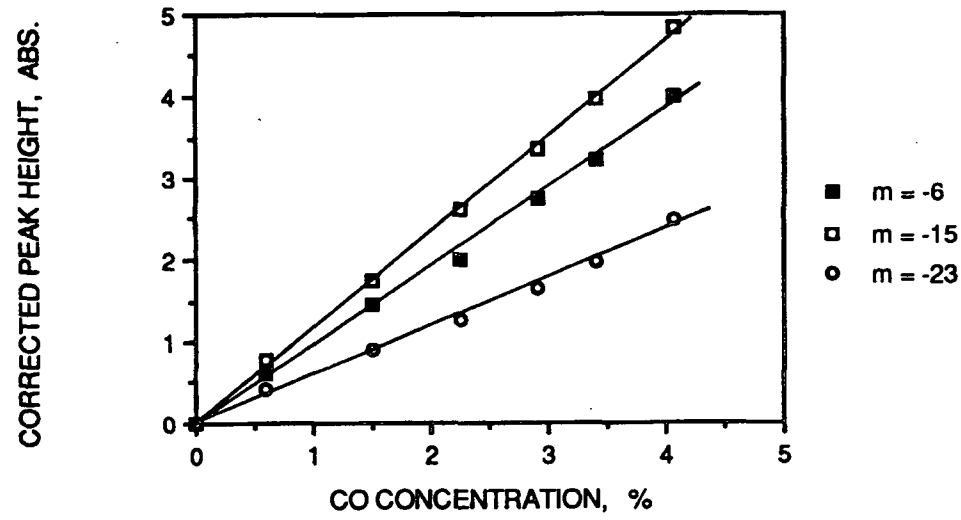

Figure 32. Plot of peak height versus concentration for the m = -6, -15, and -23 CO lines at a temperature of 295 K.

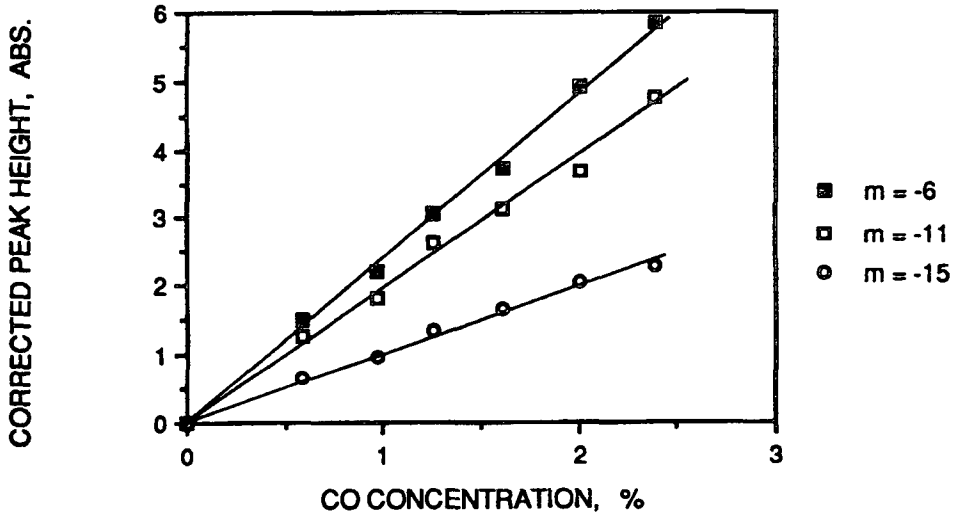

Figure 33. Plot of peak height versus concentration for the m = -6, -15, and -30 CO lines at a temperature of 720 K.

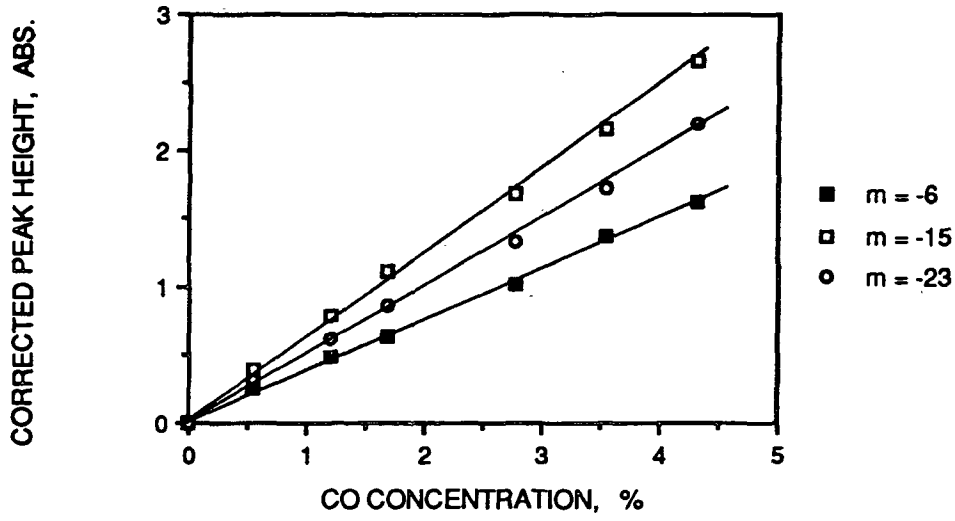

Figure 34. Plot of peak height versus concentration for the m = -6, -15, and -30 CO lines at a temperature of 1225 K.

A more direct determination of the precision of the calculated line strengths can be obtained from an error analysis based upon a consideration of the standard deviations of all the components used in the calculations of line strengths.[41] These calculations have been done on one line from one spectrum at each of the gas temperatures. These calculations yield a standard deviation of the calculated value based upon a summation of the products of the variance of each measurement, multiplied by the square of the partial derivative of the equation with respect to that value. For example, for a measurement of x which is dependent upon p, q, and r, the variance of x is given by,

$$\sigma_x^2 = \left(\frac{\delta x}{\delta p}\right)^2 \sigma_p^2 + \left(\frac{\delta x}{\delta q}\right)^2 \sigma_q^2 + \left(\frac{\delta x}{\delta r}\right)^2 \sigma_r^2 \qquad (33)$$

Using equations 15 and 33, and the measured variances of all the quantities comprising this equation, the standard deviation of the calculated line strengths were determined. The calculated values are provided in Table 14.

Table 14. Results of error analysis calculations for the determination of line strengths. Calculations were performed for the CO m = -15 line.

Temp. (K)	Calculated Line Strength (1/atm-cm^2)	Calculated Standard Deviation	Relative % Standard Deviation
298	4.23	0.51	12.1
348	4.35	0.52	11.8
534	3.37	0.39	11.5
719	2.56	0.29	11.5
936	1.71	0.20	11.5
1038	1.41	0.16	11.6
1173	1.22	0.14	11.6
1199	1.05	0.04	11.5

The standard deviations calculated from the analysis were all between 11.5 and 12.1% of the average line strengths. Additional calculations were performed for multiple lines from the same spectrum; among the different lines from each spectrum, there was no calculated difference in the relative percent standard deviations. The percent contributions to the calculated variance for the line strengths was approximately 68% for the line half widths, 20% for the peak heights, 11% for the concentration and <1% for the path length. The single largest factor contributing to the total error was the deviation associated with the line half-widths. The standard deviation used to calculate the relative contribution of error by the half-widths, 10%, was based on that reported by Hartmann, *et al.*[46]. This value was so high, however, that it dominated the error analysis results, leaving the calculations relatively insensitive to the other factors (line height, concentration, and path length). When the error associated with the half-widths was artificially reduced by an order of magnitude, the remaining factors resulted in calculated standard deviation which were approximately 5% of the calculated line strengths. This level of relative standard deviation is much closer to the variability observed between replicates at each temperature.

Additional methods for determining the accuracy of the line strengths involves direct comparison of the calculated values with both theoretical predictions and other experimental values. Figures 35-37 show plots of the calculated theoretical predictions of the temperature dependent line strengths of the m = -6, -15, and -30 lines, based upon Equation 4. Also included in each of these plots are the experimentally determined line strengths.

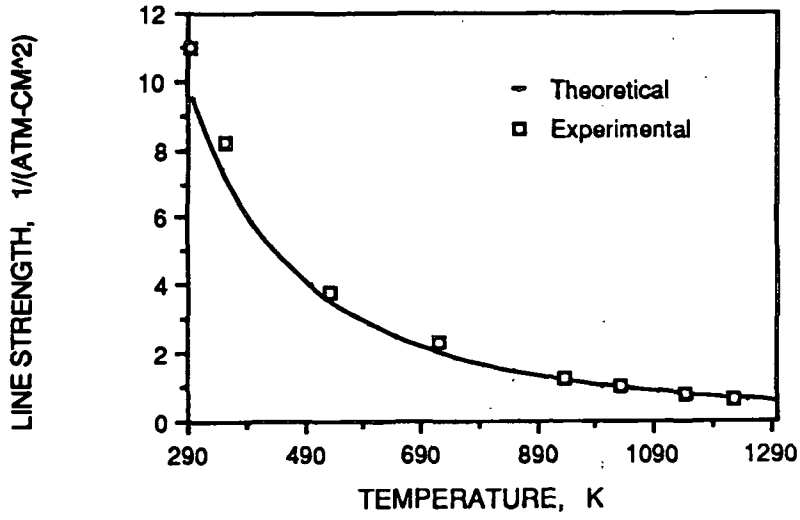

Figure 35. Comparison of experimental and theoretically calculated line strengths as a function of temperature for the m = -6 CO line.

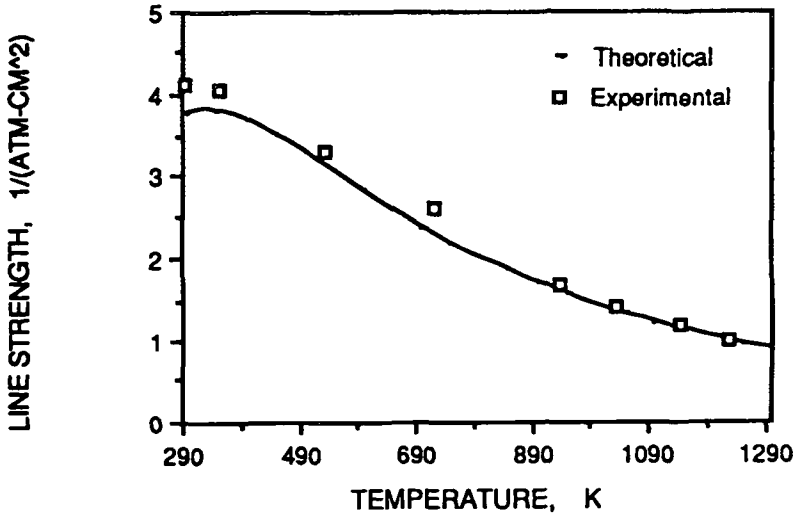

Figure 36. Comparison of experimental and theoretically calculated line strengths as a function of temperature for the m = -15 CO line.

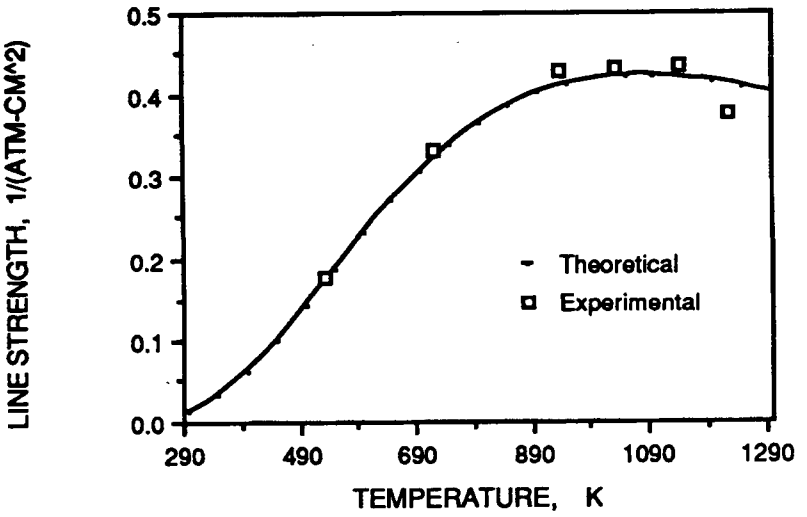

Figure 37. Comparison of experimental and theoretically calculated line strengths as a function of temperature for the m = -30 CO line.

The agreement between the theoretical predictions and the experimental values is excellent. Regardless of the absorption line, the experimental values closely follow the contour of the theoretically predicted lines. The percent differences between theoretical and calculated values is less then 10% for some of the worse values and less than 5% for most of the others. In addition to the accuracy of the experimental results, the agreement between these two can also be attributed to the ability to make accurate theoretical predictions of line strengths. The method used for this work is based on Equation 4 and the methods described by Varghese and Hanson[43] to calculate line energies and partition functions. In addition to these calculated parameters, one experimental parameter, the band intensity, which is directly proportional to the line intensity, has also been required for these calculations. The good agreement between experimental and theoretical predictions presented in these results reflects positively on the accuracy of that value.

Evaluation of the accuracy of the calculated line strengths can also be accomplished by comparisons with existing experimental data. Table 15 presents a comparison of the ex-

perimental room temperature line strengths, calculated in this work, with those presented by two others.[50,59] In addition, Fig. 38 shows a comparison of high temperature line strengths from this work and from data presented by Sell[45] for the m = -6 CO line. Sell presented his line strengths in units of 1/(ppm-cm). These values were converted to atmospheres and multiplied by the half-widths used in this work to obtain lines strengths which were in units of 1/(atm-cm^2).

Table 15. Comparison of experimental room temperature CO line strengths with values presented in the literature.

Line (m)	S(m) from This Work	S(m) from Chackerian, *et al.*[50]	S(m) from Varanasi and Sarangi[59]
-5	10.522	8.980	-
-6	11.013	9.618	-
-7	11.367	9.832	-
-8	11.241	9.664	8.44
-9	10.361	9.178	9.49
-11	8.472	7.561	7.23
-12	7.347	6.586	6.44
-13	6.196	5.592	-
-14	5.031	4.633	-
-15	4.113	3.749	-
-21	0.704	0.660	-
-22	0.493	0.459	-
-23	0.346	0.313	-
-25	0.154	0.136	-

Comparison of the line strengths measured in this work, to those given in the literature, resulted in good agreement for both the room temperature and high temperature results. At room temperature, the difference between the two is approximately 10%. While this is higher than the variability obtained for the relative standard deviation of the replicates at each furnace temperature, it is not higher then the calculated standard deviations based upon the error analysis calculations. It is interesting to note, however, that in all cases the values reported in this work are higher then those reported by others. Considering

the error analysis results, the line half-widths should have the greatest influence on these results. In evaluating the accuracy of the half-width results, it was found that Hartmann *et al.*[46] examined the difference between the predicted half-widths and those experimentally measured. At room temperature, the nitrogen broadened half-widths obtained from the calculations were consistently 10% higher then experimental values (for lines with |m| indices between 5 and 20). Since the half-widths are directly proportional to line strengths, these errors will affect the line strengths calculated in this work to an equivalent extent. This difference may be responsible for some of the discrepancies observed in the absolute intensities of the room temperature line strength data. Because of the limited amount of high temperature half-width data available, Hartmann *et al.*[46] did not present similar evaluations of their model predictions for the higher temperature results.

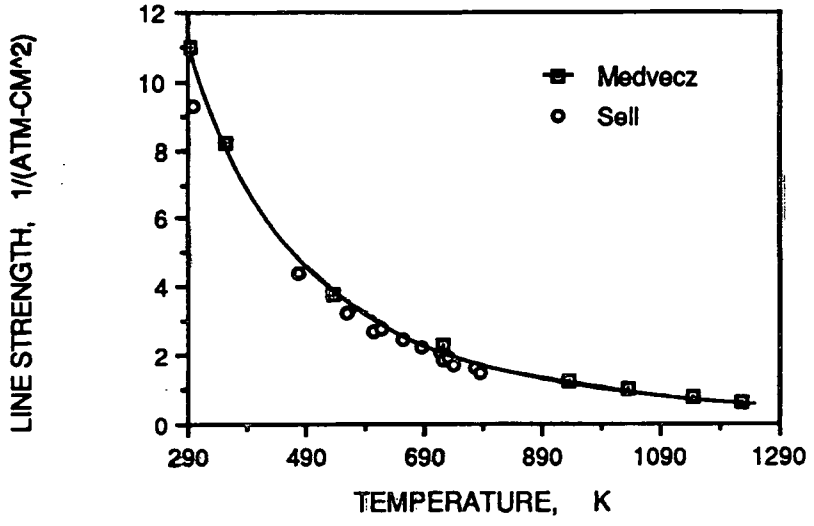

Figure 38. Plot comparing the experimentally determined temperature dependence of the m = -6 CO line measured in this work and measured by Sell[45].

The agreement between the temperature dependence of the line strength for the m = -6 CO line, measured in this work, with Sell's experimental results is also very good. At 295 K, the results vary by nearly 10%, however, at higher temperatures the agreement is much better.

CO_2 Absorption Lines

The average temperature dependent line strengths, calculated from the 52 CO_2 R branch spectra of the ν_3 fundamental band, are given in Table 16. This table includes calculated line strengths for absorption lines with m indices between 53 and 89. Values are missing for the higher m indices at the lowest temperatures; the experimental peak intensities of these values was below the threshold, 0.025.

Table 16. Results of line strength calculations for 19 CO_2 absorption lines recorded at temperatures between 295 and 1250K. Calculated values of S(m) are in units of $1/(atm\text{-}cm^2)$.

Line (m)	S (m) 294 K	S (m) 353 K	S (m) 535 K	S (m) 720 K	S (m) 936 K	S (m) 1034 K	S (m) 1144 K	S (m) 1226 K
53	2.776	4.426	6.695	5.936	4.056	3.513	2.996	2.462
55	1.919	3.246	5.692	5.505	3.694	3.293	2.900	2.444
57	1.284	2.321	4.497	4.515	3.356	3.047	2.723	2.281
59	0.854	1.678	3.555	3.845	2.979	2.734	2.478	2.111
61	0.560	1.187	2.835	3.176	2.496	2.287	2.098	1.812
63	0.367	0.832	2.251	2.679	2.119	1.865	1.604	1.303
65	0.228	0.576	1.734	2.290	1.882	1.696	1.464	1.194
67	0.145	0.395	1.363	1.856	1.655	1.504	1.333	1.092
69	-	0.246	1.072	1.568	1.463	1.346	1.198	0.999
71	-	0.175	0.832	1.314	1.278	1.208	1.095	0.915
73	-	-	0.623	1.085	1.106	1.063	0.987	0.838
75	-	-	0.476	0.892	0.969	0.951	0.882	0.752
77	-	-	0.326	0.707	0.692	0.702	0.684	0.593
79	-	-	0.196	0.465	0.596	0.612	0.598	0.530
81	-	-	0.142	0.372	0.494	0.515	0.522	0.477
83	-	-	0.101	0.293	0.419	0.455	0.452	0.411
85	-	-	-	0.231	0.348	0.381	0.399	0.367
87	-	-	-	0.183	0.303	0.336	0.350	0.329
89	-	-	-	0.142	0.243	0.280	0.303	0.287

All of the experimental peak intensities used in the line strength calculations were corrected for both the finite resolution of the spectrometer and for peak overlap resulting from neigh-

boring CO_2 lines. No lines were excluded from the calculations because of overlap from other transitions. However, from the spectra shown in Fig. 25, at high temperatures, the far wing of the R branch of another CO_2 band overlaps some of these lines (53-61).

Evaluation of the accuracy and precision of these line strengths can be accomplished by the same criteria considered for the CO lines. The standard deviation of all the calculated values at each temperature is used as the first measure of the precision of the data. The standard deviations and relative percent standard deviations are included for three furnace temperatures, 295, 720 and 1226 K in Table 17, and for all the data in Appendix XI.

Table 17. Standard deviations and relative percent standard deviations for the replicated CO_2 line strengths calculated at temperatures of 295, 720, and 1226 K.

Line (m)	S.D. 294 K	Relative % S.D.	S.D. 720 K	Relative % S.D.	S.D. 1225 K	Relative % S.D.
53	0.071	2.57	0.809	13.63	0.387	15.73
55	0.052	2.72	0.879	15.97	0.341	13.94
57	0.029	2.25	0.590	13.08	0.380	16.67
59	0.027	3.12	0.373	9.71	0.339	16.05
61	0.021	3.77	0.256	8.07	0.228	12.59
63	0.021	5.61	0.206	7.69	0.092	7.05
65	0.006	2.62	0.142	6.20	0.073	6.08
67	0.005	3.65	0.121	6.49	0.064	5.88
69	-	-	0.077	4.89	0.061	6.11
71	-	-	0.057	4.37	0.045	4.92
73	-	-	0.048	4.41	0.043	5.09
75	-	-	0.030	3.40	0.039	5.24
77	-	-	0.081	11.51	0.027	4.60
79	-	-	0.013	2.71	0.027	5.03
81	-	-	0.008	2.21	0.021	4.35
83	-	-	0.011	3.67	0.018	4.47
85	-	-	0.010	4.29	0.016	4.36
87	-	-	0.007	3.65	0.017	5.05
89	-	-	0.006	4.37	0.014	4.74

In general the standard deviations are low, 3-5% of the average values, for all the

room temperature lines and most of the lines at the higher temperatures. However, there is a strong deviation from this trend for the first six lines (53-61) at the higher temperatures. The relative percent standard deviations calculated for these results is at, or above, 10%. The increased error associated with these values is a result of the influence of the R branch of the neighboring CO_2 band mentioned earlier. The overlap of this neighboring band destroys the concentration independence expected for these results. As the CO_2 concentration increases, the overlap causes the line strengths to increase, rather then remain constant. The increase in calculated line strengths can be more than 20% at a given furnace temperature. It is certain that the accuracy, as well as the precision, of the calculated line strengths is compromised by this overlapping CO_2 band. Peak height corrections have not included a consideration of the overlap resulting from this band, since none of these lines are sufficiently resolved to permit such calculations.

A better understanding of the individual factors which contribute to the variability of the calculated standard deviations can be evaluated by the Bouguer-Lambert plots and by error analysis calculations. The Bouguer-Lambert plots (corrected peak height versus concentration) are presented in Figs. 39-41. Each of these figures illustrates the dependence of peak height as a function of concentration, for three lines, at a given furnace temperature. At room temperature the data from lines with m indices of 53, 57, and 63 are given. At a furnace temperature of 720 K the m = 53, 63, and 71 lines are plotted and at 1225 K, data from lines 53, 71 and 89 are given.

The data presented in these plots agree well with the calculated standard deviations. At room temperature, where the calculated relative percent standard deviations were low, the lines are highly linear. At 720 K, the m = 53 and 63 lines, which had calculated relative standard deviations of 13.6 and 7.7%, respectively, yielded plots which are slightly curved upward. At this same temperature, the m = 71 line had a lower relative standard deviation

of 4.4% and a correspondingly higher degree of linearity, shown in Fig. 40. The same trend is evident for the 1225 K data, in Fig. 41. These data support the theory that the unusually high relative percent standard deviations calculated for some of the CO_2 lines (53-65) is a result of inaccurate peak heights.

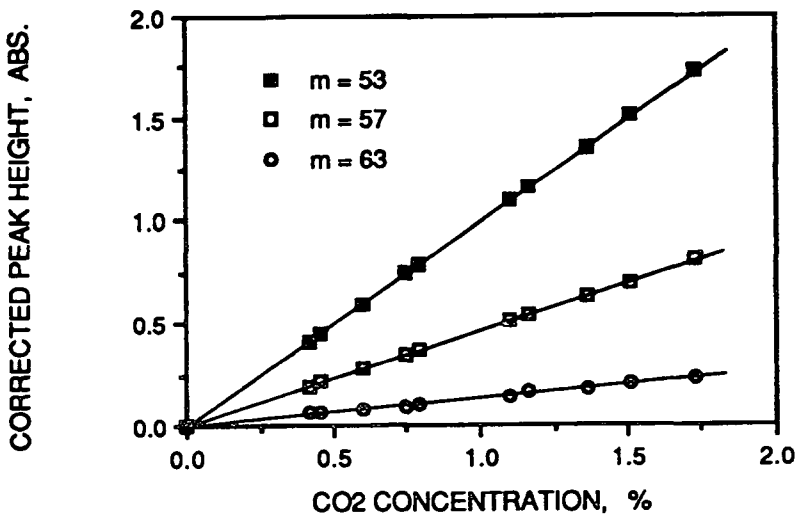

Figure 39. Plot of peak height versus CO_2 concentration for the m = 53, 57 and 61 lines at a temperature of 296 K.

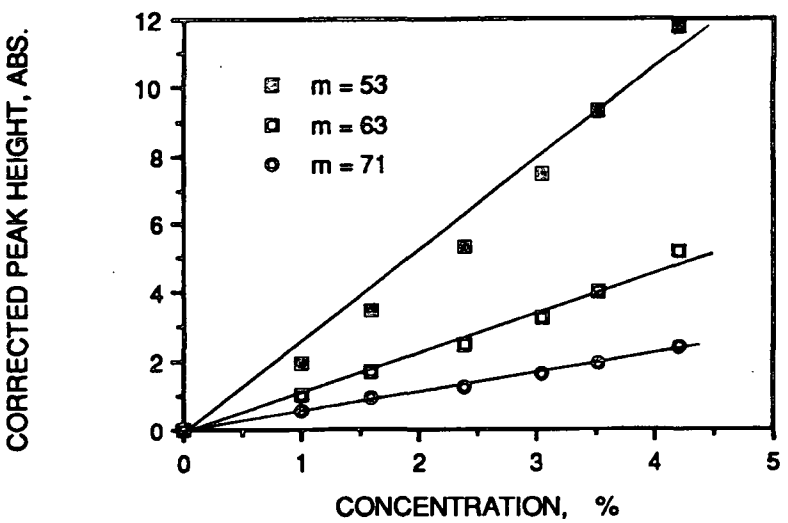

Figure 40. Plot of peak height versus CO_2 concentration for the m = 53, 71, and 89 lines at a temperature of 720 K.

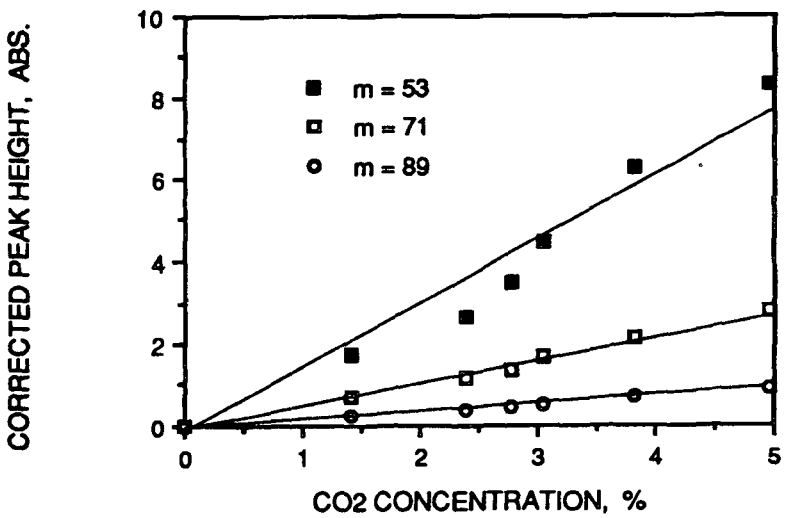

Figure 41. Plot of peak height versus CO_2 concentration for the m = 53, 71, and 89 lines at a temperature of 1225 K.

Error analysis calculations, similar to those performed for the CO lines, were also used to quantify the factors effecting the variability of the line strengths calculated in Table 17. The calculations were performed on one line of one spectrum from each furnace set point temperature. These calculations yielded a standard deviation based upon the error associated with each term in the equation used to calculate line strengths. The results of these calculations are presented in Table 18.

The standard deviations resulting from these calculations yielded relative percent standard deviations which were between 4-5%. Additional calculations were performed for several lines from the same spectrum; the error analysis calculations yielded the same relative percent standard deviations for each line considered. These results are significantly lower then those calculated for the CO lines. The primary difference between the two sets of calculations is the error associated with the half-widths. Rosenmann *et al.*[47] reported standard deviations for the half-width data which were between 1 and 4%, instead of 10%, re-

ported for the CO lines. The percent contributions from the individual parameters toward the total variance, for the 534 K spectrum, were 44% for the half-widths, 28% for the peak heights, 23% for the concentration, and 3% for the path length. The other lines had similar distributions for the error contributions. The contribution from each parameter is more evenly distributed in these calculations compared to the CO results.

Table 18. Results of error analysis calculations for the determination of standard deviations associated with the calculation of CO_2 line strengths.

Line (m)	Temp. (K)	Calculated Line Strength (1/atm-cm^2)	Calculated Standard Deviation	Relative % Standard Deviation
61	298	0.529	0.026	4.86
71	348	0.177	0.008	4.64
71	534	0.809	0.043	5.23
71	719	1.275	0.060	4.72
71	936	1.193	0.053	4.42
71	1038	1.162	0.051	4.34
71	1173	1.072	0.044	4.07
71	1199	0.883	0.035	4.02

The variability calculated by this technique is very close to that calculated for the variability between spectra (except for the case where the peaks are influenced by overlap). This suggests that the variability calculated between samples can be described by the uncertainties associated with the individual measurements comprising the line strength calculations. Note that these calculations do not predict high standard deviations for lines which are affected by peak overlap. The standard deviations for peak heights used in these calculations were based on the systematic errors associated with peak maxima selection, base line correction, and peak height corrections. Overlap from lines of a neighboring band will add to the peak height of a given line but will not change the precision with which it can be measured.

Evaluation of the accuracy of the CO_2 line strength results can also be made by direct comparison with both theoretical predictions and other experimental results. Figures 42-44 provide the theoretically predicted temperature dependence of lines with m values of 53, 71 and 89, respectively. Also included in each of these plots are the experimentally determined line strengths from this work. The error bars associated with the data points in the y-direction, simply represent 10% of the y value. They have been included here to more easily quantify the absolute difference between the experimental and theoretically predicted line strengths.

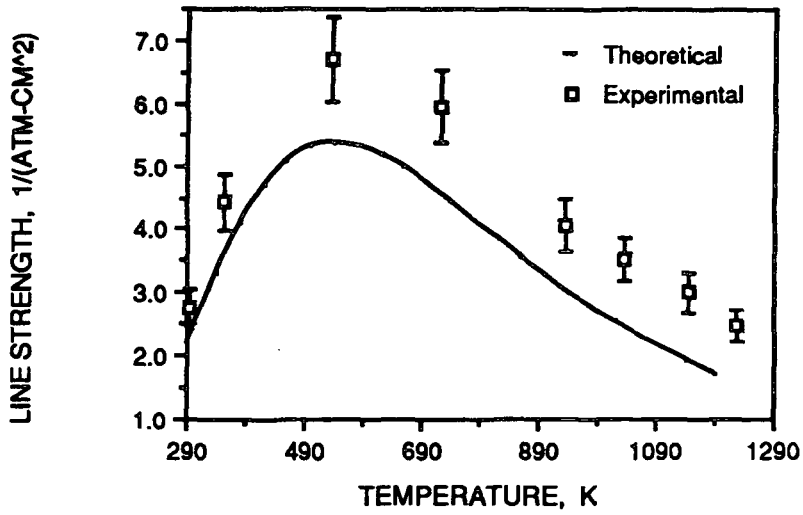

Figure 42. Comparison of experimental and theoretically calculated line strengths as a function of temperature for the m = 53 CO_2 line.

Despite the differences in absolute measurements, there is excellent agreement in the expected temperature dependent profiles for all three lines considered. Furthermore, the magnitude of the difference between theoretical predictions and experimental results decreases with increasing values of m. These results are consistent with expectations, given the influence of the overlap of the neighboring CO_2 band. In addition to reducing the precision of the line strength results, the accuracy of the results are compromised as well. The

overlapping peaks increase the corrected peak heights which result in unexpectedly high values for line strengths. As this overlap decreases, with increasing values of m, the effect diminishes and the calculated results more closely approach theoretical predictions.

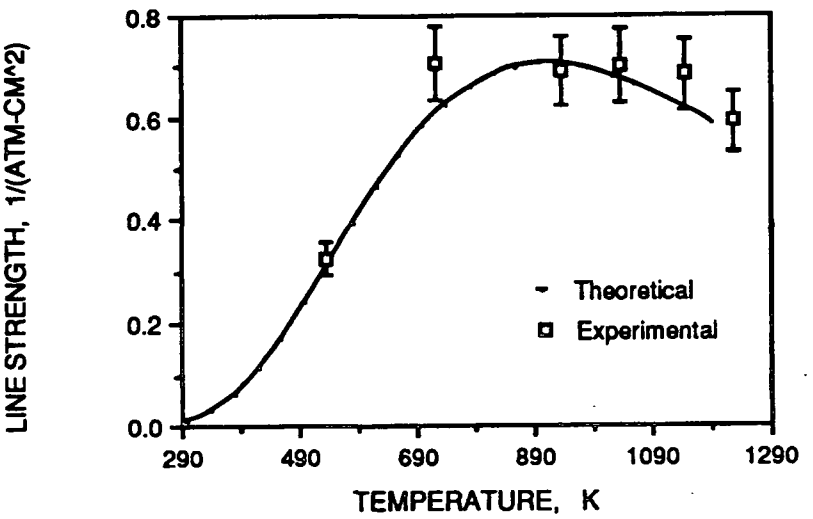

Figure 43. Comparison of experimental and theoretically calculated line strengths as a function of temperature for the m = 71 CO_2 line.

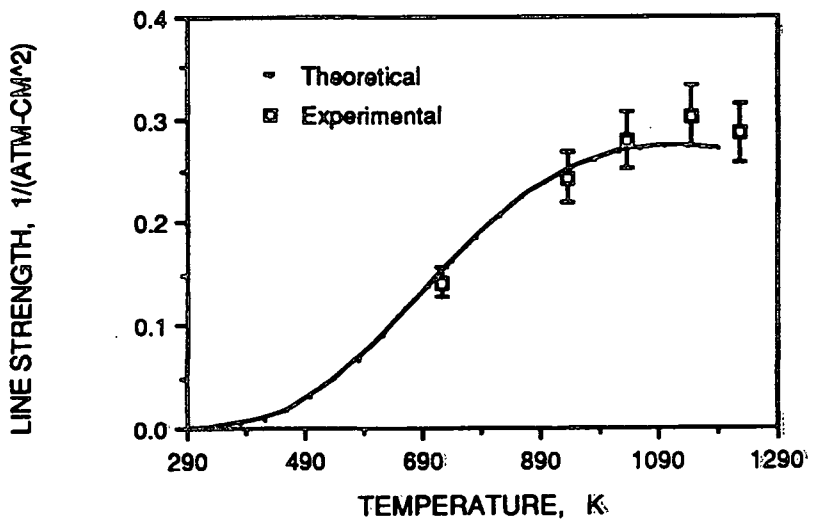

Figure 44. Comparison of experimental and theoretically calculated line strengths as a function of temperature for the m = 89 CO_2 line.

Despite the influence of the overlapping peak heights, the theoretical calculations still tend to under predict the line strengths. This assertion is based upon an evaluation of the accuracy of theoretical predictions for room temperature data, which are not influenced significantly by the neighboring band. As shown in Fig. 42, even the room temperature m = 53 line is under predicted by ten percent or more. Considering the excellent agreement between this experimental value and other experimentally obtained values described below, it is unlikely that these discrepancies of more then 10% is due solely to the experimental measurements. Instead, it is likely that a significant portion of the discrepancies between the theoretical line strengths and experimental values results from uncertainties associated with the theoretical predictions. The theoretical predictions made for these plots were based on Equation 4. Data required for the calculations were taken from a number of sources; partition functions were obtained from Gray and Selvidge,[76] band strength and band center data was obtained from Malathy-Devi *et al.*[65], and line intensities, centers and energies were obtained from Rothman[77]. Unfortunately, uncertainty levels have not been provided with this data, which would permit error analysis calculations.

One final method of evaluating the accuracy of the experimental results is to make direct comparisons with previously reported experimental data. There have been several reports of the line strengths of these CO_2 lines at room temperature, although there has been no experimental data found describing their temperature dependence. Room temperature experimental results from the literature, as well as the data from this work, are presented in Table 19.

The agreement between the room temperature line strength results from this work and those presented previously in the literature is very good. An average line strength was calculated for each line from the literature values and the percent difference between that average value and the results from this work were calculated. The percent differences were

found to be 1.8, 2.9, 1.0, 5.6, 0.4, 0.5, and 0.6% for lines 53-67, respectively. Unfortunately, there is no high temperature data available to make similar comparisons. The agreement between the room temperature experimental results of this work, compared to those presented by others, provides confidence in the methodologies used to calculate line strengths from the absorption spectra.

Table 19. Comparison of experimental room temperature CO_2 line strengths with values presented in the literature. (Line strength units, $1/(atm\text{-}cm^2)$).

Line (m)	S(m) from this work	S(m) from ref. 65	S(m) from ref. 66	S(m) from ref. 67	S(m) from ref. 69	S(m) from ref. 70
53	2.776	2.775	2.50	2.579	-	3.049
55	1.919	-	-	1.791	-	1.936
57	1.284	1.278	1.17	1.229	-	1.407
59	0.854	0.796	0.769	0.832	-	0.827
61	0.560	0.554	0.510	0.552	-	0.615
63	0.367	0.353	-	0.361	0.352	0.382
65	0.228	0.224	0.211	0.233	0.228	0.237
67	0.145	0.140	0.132	0.147	0.144	0.157

Significance of Results

The experimental line strength results presented in this work are important for two reasons. First, they provide an understanding of the absorption behavior of over 40 CO and CO_2 vibrational-rotational absorption lines. This understanding can be used for high temperature gas concentration determinations. Second, they represent a relatively large data base of high temperature line strength information, not previously reported in the literature, from which existing theoretical predictions can be compared. While the former is essential for this work, the latter will find more significance by others in the field.

The results in this section have also made other subtle, although equally important, contributions. First, agreement of the room temperature line intensities with previously

measured results illustrate that the peak height corrections, for the finite resolution of the spectrometer, have been made correctly on an absolute basis as well as a relative basis, as already shown in the temperature results. This is significant, since in some cases, the peak heights have changed by more than an order of magnitude as a result of these corrections, *i.e.*, from 0.8 to 10.0 absorbance units. The accuracy of these results suggest that the calculation methodology used to correct for neighboring peak overlap has also been done correctly. Second, the high degree of linearity of the Bouguer-Lambert plots are also significant, since they offer additional evidence that the gas concentrations are being accurately measured in the gas cell, despite significant conversion of these species. The reliability of these concentration results will be essential in the following sections.

4. CONCENTRATION DETERMINATIONS FROM ABSORPTION SPECTRA

In addition to performing gas temperature and line strength measurements from infrared absorption spectra, another key objective of this thesis is the determination of gas concentrations. The theoretical considerations necessary for these measurements have been thoroughly described in the literature. However, there have been few experimental studies describing gas concentration analyses, at high temperatures, of either gas mixtures or in a particle laden combustion environment. Of the work which has been reported, nearly all of it is based on the determination of the gas concentration from a single, well resolved line, recorded with a tunable diode laser. The ability of FT-IR absorption spectroscopy to make gas concentration determinations at high temperatures has not been rigorously proved.

As a preliminary step to pursuing concentration measurements in a combustion environment, it has been necessary to first establish the concentration calculation methodology in a well controlled gas environment. This same approach was used to establish the accuracy of the methods used for temperature analyses. The following sections describe the results of concentration determinations in the high temperature gas cell. The results from the gas cell are divided into three groups; the division is based upon how the spectra were recorded. In the first group, the spectra used for line strength measurements are used again here to measure gas concentrations. In the second group, the gas concentrations are recorded from a different set of spectra, although recorded at the same temperatures as those used for line strength calculations. Finally, concentrations are measured from a third set of spectra, recorded at temperatures intermediate to those in the first two groups.

Description of Spectra Recorded for Concentration Calculations

One hundred and twenty eight spectra have been recorded in the high temperature gas cell to establish the accuracy of the calculation methodology. These spectra have been

recorded at temperatures between 295 and 1250 K. One hundred of the spectra have been recorded at furnace set point temperatures of 295, 373, 573, 773, 973, 1073, 1173 and 1273 K. These are the same furnace set point temperatures at which the gas cell was calibrated, the temperature determination accuracy was established, and line strengths were measured. The remaining spectra were recorded at furnace set point temperatures of 338, 473, 673, 873, 1023, 1123 and 1223 K. All of the spectra recorded in the cell were of a high quality; the spectra presented in Appendix VIII are representative of the quality of the spectra recorded here. The concentration of the CO and CO_2 within the cell was determined by metered quantities, at furnace set point temperatures of 296, 338, and 373 K. At higher temperatures, because of the conversion reactions discussed in Appendix X, the gas concentration was evaluated by a NDIR gas analyzer, attached to the exit of the flow-through gas cell.

With a knowledge of the temperature dependence of the line strengths for many CO and CO_2 absorption lines, the Pascal program, described in the Mathematical Methods chapter, *SpecAnal*, was run on each of the 128 spectra. Resulting from these calculations were both the gas temperature and the CO and CO_2 gas concentration. The gas concentration was determined by the use of Equation 13, reproduced below,

$$C = \frac{A(\nu_o) \cdot \pi \cdot \gamma(m) \cdot \ln(10)}{S(m) \cdot L} , \qquad (13)$$

where C is the gas concentration, $A(\nu_o)$ is the corrected peak height, $\gamma(m)$ is the half-width at half height, S(m) is the temperature dependent line strength, and L is the path length. Resulting from this equation is the gas concentration, as measured by one absorption line. Since there are twenty-one CO and nineteen CO_2 lines available for these measurements, from each spectrum, the gas concentration reported was actually an average value from all the lines with sufficiently high peak intensities. The line strengths required for these calcu-

lations were obtained from the data presented in the previous section. This data was put into *SpecAnal* in the form of ordered pairs of numbers for each line. For each line, there were 5-8 pairs which were comprised of an average line strength and an average gas temperature. These ordered pairs described the temperature dependence of the line strength for each individual absorption line.

The results obtained from these calculations are presented in Appendix XII. Included in this appendix is first a sample results file, produced by *SpecAnal,* illustrating a typical output for these calculations. Following this file are the calculation results for each spectrum, from each of the three data sets. Reported for each file, is the spectrum name, pressure, measured gas concentrations and temperature, calculated gas concentrations and temperatures, and percent differences between the measured and calculated concentrations and temperatures. The concentration results have been consolidated by averaging each furnace set point temperature and are reported in the tables below. No description of the accuracy of the temperature calculation results is provided in detail. The temperature results obtained from these spectra were as good as those previously reported.

Concentration Determination Results

The results of the concentration calculations are presented in Tables 20, 21, and 23-26. Each of these tables first includes general data regarding the spectra, including; the furnace set point temperature, the number of spectra recorded at that temperature, the measured concentration range, and the average calculated temperature. Measurements of the accuracy of the concentration calculations are given in the three columns that follow. In the first of these columns is presented the average absolute percent concentration difference. The calculation of the percent difference is defined by the following equation,

$$\% \text{ Difference CO Concentration} = \frac{100 \cdot (\text{Measured CO - Calculated CO})}{\text{Measured CO}} \quad (34)$$

The average absolute percent difference is the numerical average of the absolute percent difference calculated for each spectrum at each of the furnace set point temperatures. The last two columns contain the low and high calculated percent differences from each group of spectra at each furnace set point temperature.

The gas concentration is measured from each absorption line. The concentration reported from each spectrum is an average of the calculated concentrations from each line in that spectrum. The variability among the lines comprising the average was calculated as a standard deviation in units of percentage (% concentration). The average standard deviation, reported in the final column, is calculated by averaging the standard deviations from each of the spectra at a given furnace set point temperature.

Concentration Results from Data Set 66

The concentration of CO and CO_2 was first determined from the 52 spectra recorded to measure the line strengths. The results of these calculations are presented in Tables 20 and 21, for CO and CO_2, respectively.

The average absolute percent differences for both CO and CO_2, ranged between 1 and 5% at all temperatures, except for the CO_2 1273 K spectra which had an average value of 8.8%. The low and high values comprising each set were negative and positive respectively, for most temperatures, indicating that the data were not biased on either side of zero. Among the individual spectra, the variability ranged from a worse case low value of -15.97% to the worse case high value of 11.67%.

Table 20. Results of CO gas concentration calculations from the spectra recorded for data set 66.

Furnace Set Point Temp. (K)	# of Spectra	Measured Conc. Range (%)	Calculated Avg. Gas Temp. (K)	Average Abs. % Diff of Calc.CO Conc.	Low (%)	High (%)	Variability Among Lines Avg. SD (%)
295	10	0.59-2.38	294	3.84	-7.2	6.8	0.04
373	6	0.78-2.94	353	3.30	-5.2	6.0	0.05
573	6	0.79-3.83	535	1.24	-2.5	3.1	0.06
773	6	0.60-4.06	720	2.93	-3.6	8.3	0.06
973	6	0.55-4.27	936	4.09	-4.9	10.9	0.03
1073	6	0.55-3.25	1034	1.32	-4.0	2.0	0.03
1173	6	0.58-3.94	1144	4.70	-10.1	7.6	0.04
1273	5	1.21-4.32	1227	3.86	-5.0	-4.32	0.08

Table 21. Results of CO_2 gas concentration calculations from the spectra recorded for data set 66.

Furnace Set Point Temp. (K)	# of Spectra	Measured Conc. Range (%)	Calculated Avg. Gas Temp. (K)	Average Abs. % Diff of Calc.CO_2 Conc.	Low (%)	High (%)	Variability Among Lines Avg. SD (%)
295	6	0.72-2.87	294	3.69	-10.45	3.90	0.03
373	6	0.85-2.78	353	3.30	-5.88	8.63	0.03
573	6	0.81-3.91	535	4.76	-7.41	10.23	0.10
773	6	1.01-4.20	720	4.73	-8.91	11.67	0.09
973	6	1.00-4.29	936	4.23	-7.14	7.69	0.07
1073	6	1.02-4.86	1034	2.85	-3.89	4.32	0.07
1173	6	1.29-4.77	1144	4.10	-5.03	5.45	0.10
1273	5	1.40-4.96	1227	8.80	-15.97	7.86	0.08

The standard deviation for the variability among the lines at each furnace temperature ranged between 0.03-0.10%. To provide additional details regarding these values, the individual standard deviations of the six 773 K spectra comprising the average value presented in Table 20 are presented in Table 22. These results indicate that the variability of the calculated concentrations, among the lines, is relatively low - less than 5%. This suggests that there is good agreement among the lines regarding the actual gas concentration of the sample. The calculated relative percent errors for these values are typical for the other

temperatures as well.

Table 22. Measured and calculated concentrations for the six spectra recorded at a furnace temperature of 773 K. Also included are the standard deviations and the relative percent standard deviations of the lines which have been averaged to obtain the average concentration from the spectrum.

Measured CO Conc. (%)	Calculated CO Conc. (%)	Standard Deviation (%)	Relative Percent Standard Deviation
0.60	0.65	0.02	3.3%
1.51	1.52	0.07	4.6%
2.24	2.16	0.06	2.8%
2.90	2.81	0.06	2.1%
3.40	3.36	0.05	1.5%
4.06	4.03	0.13	3.2%

The deviations between measured and calculated concentrations for the spectra of data set 66, are small; overall average of 3.2% and 4.6% for CO and CO_2, respectively. The deviations which have been observed result from the deviation of the line strengths about the average line strength, and the deviations resulting from the cubic spline interpolations.

Concentration Results from Data Set 68

Results for the CO and CO_2 concentration calculations, from the 48 spectra of data set 68, are presented in Tables 23 and 24. These spectra were recorded under the same conditions, and at the same furnace set point temperatures as those in data set 66.

The average absolute percent differences ranged between 1.8-4.0% for the CO spectra and between 2.5-5.1% for the CO_2. Among the individual results, the lowest percent difference among both the CO and CO_2 data was -9.6% and the highest was 13.9%. The calculations for the average standard deviations among the lines ranged between 0.04-0.16%. The low and high values for each furnace set point temperature were negative and positive, re-

spectively, again indicating no bias among the calculated results.

Table 23. Results of CO gas concentration calculations from the spectra recorded for data set 68.

Furnace Set Point Temp. (K)	# of Spectra	Measured Conc. Range (%)	Calculated Avg. Gas Temp. (K)	Average Abs. % Diff of Calc.CO Conc.	Low (%)	High (%)	Variability Among Lines Avg. SD.
295	6	0.73-2.44	295	2.83	-3.74	5.48	0.06
373	6	0.96-2.91	352	2.11	-4.17	1.82	0.09
573	6	0.99-3.96	532	2.69	-5.05	5.05	0.08
773	6	0.87-4.58	723	1.80	-2.30	4.07	0.11
973	6	0.81-4.49	930	2.70	-4.82	-1.23	0.04
1073	6	0.78-4.20	1033	3.04	-5.63	0.00	0.04
1173	4	0.89-4.28	1130	2.83	-6.27	0.89	0.07
1273	4	2.31-4.49	1248	4.01	-5.54	-2.45	0.18

Table 24. Results of CO_2 gas concentration calculations from the spectra recorded for data set 68.

Furnace Set Point Temp. (K)	# of Spectra	Measured Conc. Range (%)	Calculated Avg. Gas Temp. (K)	Average Abs. % Diff of Calc.CO_2 Conc.	Low (%)	High (%)	Variability Among Lines Avg. SD.
295	6	0.86-3.24	295	4.48	-9.65	0.37	0.04
373	6	1.05-3.06	352	5.13	-9.52	6.54	0.05
573	6	1.10-4.10	532	4.87	-4.55	13.90	0.16
773	6	1.12-4.58	723	5.05	-4.71	10.92	0.13
973	6	1.12-4.48	930	2.50	-1.17	7.37	0.07
1073	6	1.18-4.86	1033	3.70	-3.23	8.23	0.10
1173	4	1.21-4.53	1130	3.35	-7.10	1.77	0.08
1273	4	2.57-4.86	1248	4.24	0.78	8.85	0.13

The results obtained from this set are as good as those described in set 66; the overall percent differences are 2.7 and 4.2% for CO and CO_2, respectively. There appears to be no bias in the calculation methodology with regard to the gas temperature. The similarity of these results with those of data set 66 are additional evidence that the line strengths have been accurately measured.

Concentration Results from Data Set 70

The concentration methodology was evaluated by a third data set. In this set, 28 spectra were recorded at temperatures intermediate to those used for the line strength data. The results of these calculations are shown in Tables 25 and 26.

Table 25. Results of CO gas concentration calculations from the spectra recorded for data set 70.

Furnace Set Point Temp. (K)	# of Spectra	Measured Conc. Range (%)	Calculated Avg. Gas Temp. (K)	Average Abs. % Diff of Calc.CO Conc.	Low (%)	High (%)	Variability Among Lines Avg. SD.
338	4	0.99-2.68	330	7.72	-10.98	-4.08	0.06
473	4	0.99-3.83	441	4.22	-8.77	-1.31	0.09
673	4	0.58-3.61	634	8.16	-6.37	14.33	0.08
873	3	1.34-3.62	854	5.02	-2.22	11.66	0.11
1073	4	0.52-3.11	978	4.94	-1.92	10.51	0.04
1123	4	0.58-2.83	1081	3.43	-7.02	-0.10	0.04
1223	4	0.703.50	1213	3.03	-1.88	4.99	0.08

Table 26. Results of CO_2 gas concentration calculations from the spectra recorded for data set 70.

Furnace Set Point Temp. (K)	# of Spectra	Measured Conc. Range (%)	Calculated Avg. Gas Temp. (K)	Average Abs. % Diff of Calc.CO_2 Conc.	Low (%)	High (%)	Variability Among Lines Avg. SD.
338	4	1.09-2.68	330	12.62	-16.89	-9.75	0.05
473	4	0.99-3.72	441	3.92	-6.17	-1.59	0.10
673	4	1.35-3.72	634	7.44	-11.35	-2.67	0.17
873	4	1.36-4.10	854	5.96	-8.97	7.05	0.12
1073	4	1.33-3.81	978	5.24	-8.03	2.76	0.06
1123	4	1.29-4.20	1081	4.34	-6.42	-2.09	0.07
1223	4	1.28-3.81	1213	4.60	-1.24	8.82	0.07

For these spectra, the average absolute concentration differences varied between 3.0-8.16% for the CO spectra and between 3.9-12.6% for the CO_2. The low and high values

among all the spectra were, at the worse case, -16.9 and 14.3%, respectively. The calculations of the variability among lines yielded average standard deviations which were between 0.04 and 0.17%. The overall average percent deviations for both the CO and CO_2 results are 5.2 and 6.3%, respectively. The average absolute percent differences presented from this set are only slightly higher than those presented in the previous two data sets.

The data from this set show a slight bias towards under predicting the gas concentrations. This is most evident for the CO_2 338 K spectra. It is likely that this error is a result of the inabilities of the line strength correlation to adequately account for the influence of peak overlap. This is consistent with the fact that the lines with lower m values are most strongly influenced by overlap and that at low temperatures fewer high m valued lines are available to offset this effect.

Despite this slight increase in the calculated percent differences, the results presented from this data set are still very good. These data reveal that the calculation methodology is capable of accurately predicting gas concentrations at temperatures different than those where the line strengths have been measured. These results further suggest that the cubic spline interpolation routine, which has been used for these analyses, can be used to accurately describe the temperature dependence of the line strengths.

Significance of Results

The data presented in this section illustrate the potential of FT-IR absorption spectroscopy for the determination of gas concentrations in a high temperature environment. In general, the results have been very good. The overall accuracy is between 3-7%, for spectra at temperatures between 295-1250 K and at concentrations between 0.5-5% percent. These results are the most thorough illustration of the potential of FT-IR absorption spectroscopy

for the determination of gas concentrations at high temperatures.

The success of these results are a product of the rigor used in the many preliminary steps; most importantly, the correction of peak heights for the finite resolution of the spectrometer and peak overlap. The combined ability to determine the gas temperature and concentration from absorption recorded in a pure gas environment provides the methodology to make similar measurements in a combustion environment.

5. CHAR COMBUSTION

The use of FT-IR as a diagnostic tool for the elucidation of the chemical events occurring in a combustion environment, requires first, that well resolved absorption spectra can be recorded, and second, that gas temperatures and concentrations can be accurately determined from the absorption spectra. There have been few reports of FT-IR absorption spectra, recorded in combustion environments. From these spectra, there have been even fewer descriptions of accurate temperature and concentration calculations.

In the first of the following three sections, spectra recorded in a black liquor char combustion environment will be presented. It will be shown that these spectra contain high quality CO and CO_2 absorption lines from which gas temperatures and concentrations can be made. It will also be shown that a large part of the mid infrared region, 800-4400 cm^{-1}, is available for the identification and quantification of additional gaseous species which absorb in this region. In the second section, the gas temperature will be measured from spectra recorded during black liquor char combustion experiments. The accuracy of these measurements will be established by comparisons with temperatures recorded simultaneously with a suction pyrometer. In the final section, gas concentrations will be calculated from a number of spectra recorded under various combustion conditions. The spectroscopically measured concentrations will be compared to those determined by an NDIR instrument. From these comparisons, the accuracy of CO and CO_2 gas concentration measurements, in a black liquor char combustion environment, will be established.

Absorption Spectra Recorded During Black Liquor Pyrolysis and Char Combustion

The combustion reactor, described in the Experimental Methods chapter, has been used to record absorption spectra during char combustion, and to a lesser extent, during pyrolysis. This reactor has provided the means to first, heat black liquor solids to tempera-

tures up to 1250 K and second, to record the infrared absorption spectra of the gases directly above the sample surface. The black liquor solids are burned in the reactor in a bed configuration, and the experiments are run in a batch mode. The black liquor samples have been comprised of either partially or fully pyrolyzed kraft liquor. The spectra have been recorded at heights of 0.75-3.0 inches above the bed surface.

In Figs. 45 and 46 two spectra are presented; the first, Fig. 45 was recorded near the end of pyrolysis and the second, Fig. 46, was recorded during char combustion. The quality of these spectra are representative of all those recorded in the reactor. The signal to noise is very good and there are no obvious distortions resulting from the presence of fume. These spectra provide an easy means of qualitatively identifying the infrared active components present in the gas phase. For example, in the case of the spectrum recorded during pyrolysis, Fig. 45, three components are readily visible: CO absorbing in the region between 2000 and 2250 cm^{-1}; CO_2 absorbing in the region of 2250-2400 cm^{-1}; and water vapor, absorbing in the regions of 1000-2000 cm^{-1} and 3500-4000 cm^{-1}. There are no additional components visible at this point of the pyrolysis. The pyrolysis products such as H_2S, have already been released from the black liquor solids, or are absorbing in regions under the water vapor lines. In the second spectrum, Fig. 46, only two components can be identified, CO and CO_2. The CO absorbs in the region of 1900-2250 cm^{-1} and the CO_2 absorbs in the region from 2250-2400 cm^{-1}. The two additional bands centered at 3600 and 3700 cm^{-1} are also CO_2 absorption lines.

On a qualitative basis, these spectra demonstrate the potential of FT-IR absorption spectroscopy to yield information regarding the gas composition above a combusting sample. Efforts have not been made to vary the state of the black liquor to effect a change of composition in the gas phase. For example, if spectra were recorded during the early phases of pyrolysis, and if the spectra were more closely examined, additional products of pyrolysis might

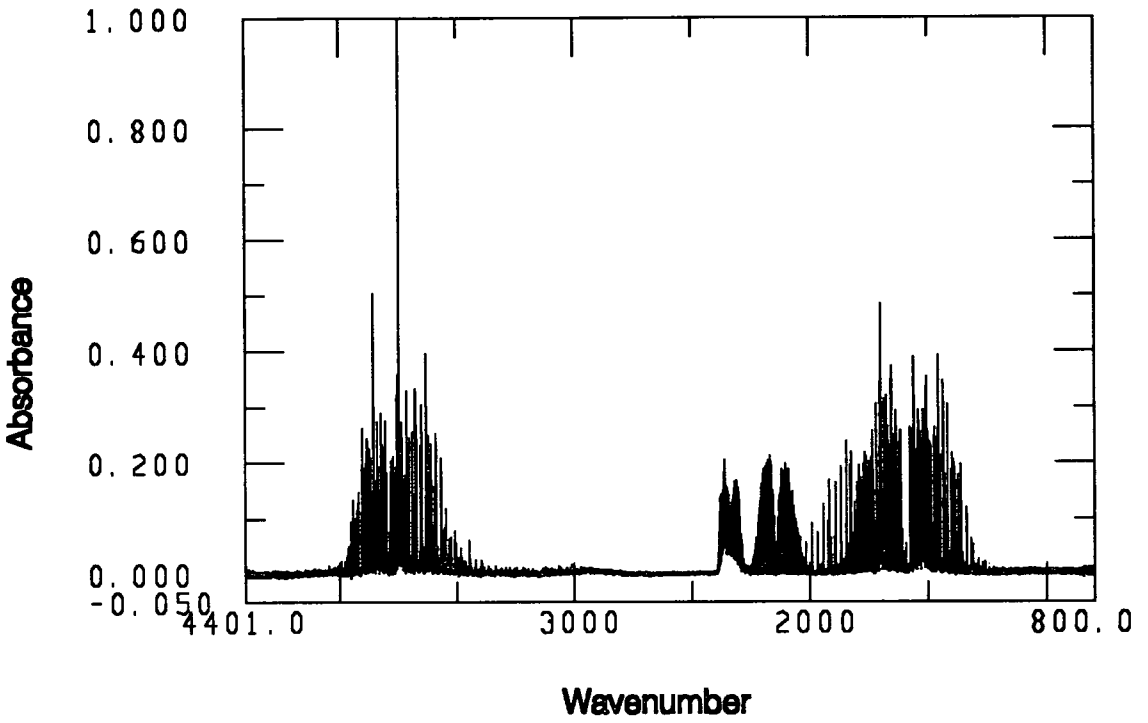

Figure 45. Absorption spectrum recorded during pyrolysis. The species absorbing in the spectrum are CO (2000-2250 cm-1), CO_2 (2250-2400 cm^{-1}) and water vapor (1000-2000 and 3500-4000 cm^{-1}).

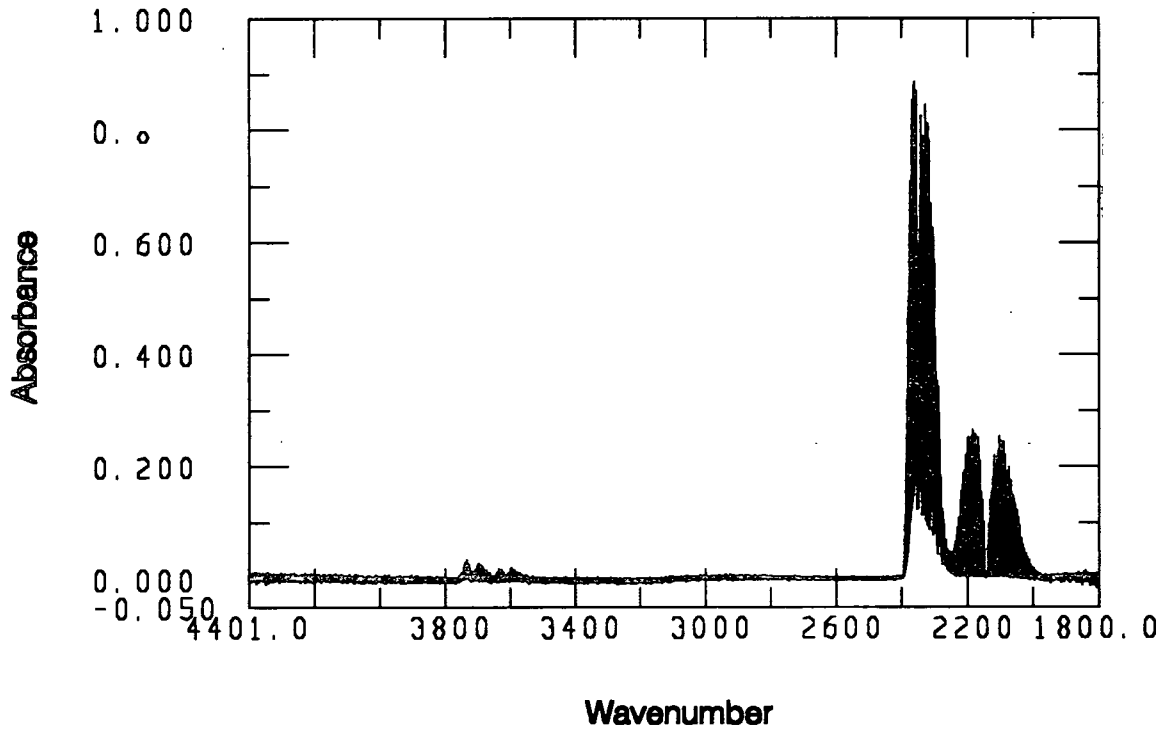

Figure 46. Absorption spectrum recorded during char combustion; CO (1900-2250 cm^{-1}) and CO_2 (2250-2400 cm^{-1}) absorbing species.

be visible. The focus of the black liquor combustion work of this thesis has been the verification that gas temperature and concentration measurements can be made during char combustion.

The use of these spectra, for gas temperature and concentration determinations, requires that the individual absorption lines are well resolved and free from interfering peaks. The spectra provided in Figs. 47 and 48 are the CO and CO_2 lines from Fig. 46. The quality of these spectra are as good as those obtained in the gas cell gas environment.

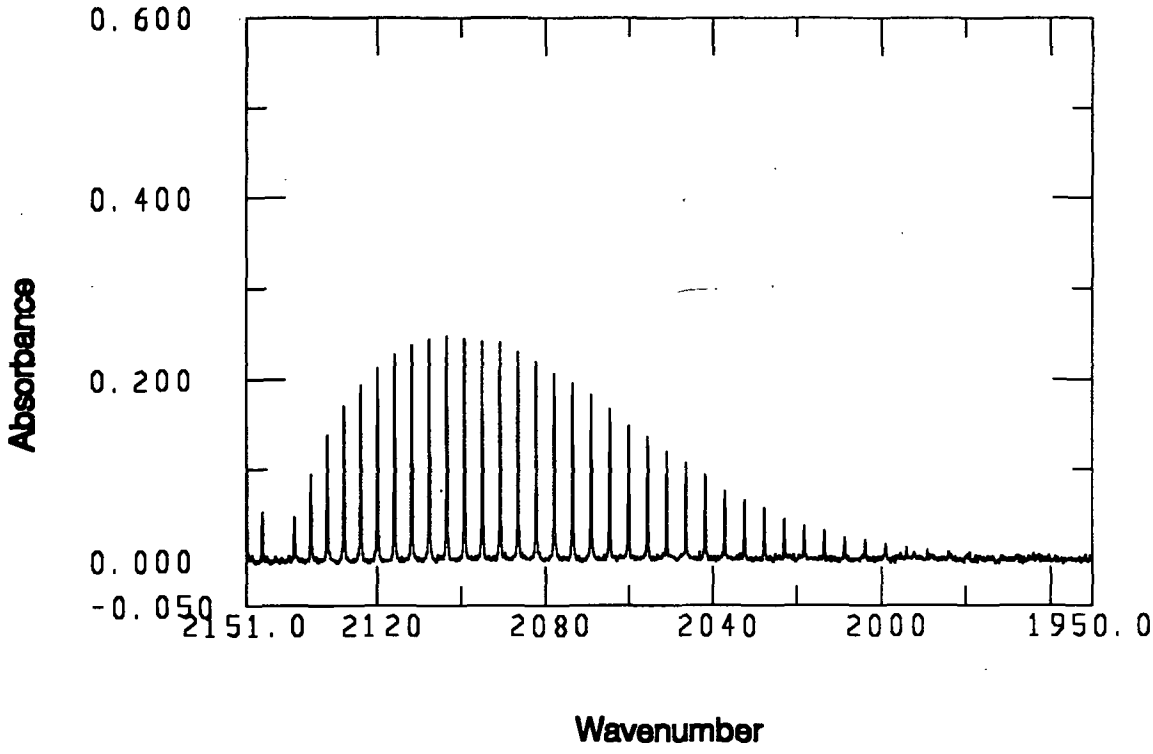

Figure 47. CO absorption spectrum recorded during char combustion above a burning black liquor char bed.

The acquisition of absorption spectra in a black liquor combustion environment has been no more difficult then recording spectra in the high temperature gas cell. Furthermore, the windows in the reactor do not get as hot as those of the gas cell, which improves the transmission of the infrared beam through the reactor. With higher transmission

through the reactor, the signal to noise ratio of the spectra improves. Also, early concerns regarding the influence of fume have not been warranted. The fume does not significantly attenuate the infrared beam, and no broad $NaCO_3$ or $NaSO_4$ bands are seen in the absorption spectrum. The implications of the absence of these bands in the spectra have not been considered in light of elucidating fume formation mechanisms using FT-IR.

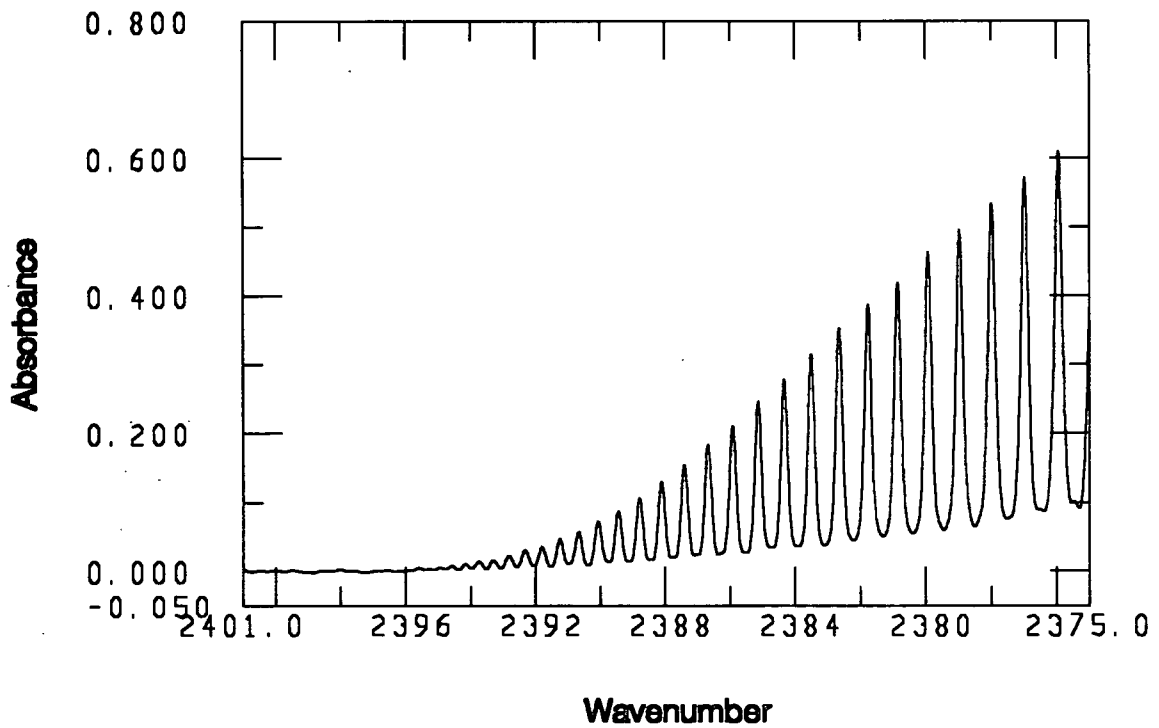

Figure 48. CO_2 absorption spectrum recorded during char combustion above a burning black liquor char bed.

Gas Phase Temperature Determinations

Infrared absorption spectra, recorded in a black liquor combustion environment, have been used to determine the gas temperature above a burning black liquor char bed. The accuracy of these measurements has been established by comparisons with thermocouple measurements. The char combustion reactor has been used to provide the environment in which black liquor char can be burned and absorption spectra recorded.

The char samples consisted of 15-20 grams of fully dried and pyrolyzed softwood black liquor droplets. They were preheated to 1273 K in the lower part of the reactor for two hours. While the char was preheated, the sample was covered with a stream of gas containing 5% CO in nitrogen. The gas mixture was used to suppress the consumption of char carbon by carbonate,[4]

$$Na_2CO_3 + 2C \leftrightarrow 2\,Na + 3\,CO\,. \qquad (35)$$

Before combustion was started, the crucible containing the sample was raised several inches upward, into the middle of the reactor. The bed was moved to increase the proximity of the spectroscopic analysis relative to the char surface; 0.5-1.0 inches at the start of combustion. The time required for complete combustion of the char was approximately two hours. The rate of char combustion was controlled by the oxygen flow rate and concentration. The combustion gas, comprised of 5% O_2 in nitrogen, was preheated to 773-873 K, and was fed into the reactor at a rate of 3 L/min. This rate was selected to provide a product gas stream which contained CO and CO_2 concentrations in the range between 0.5-5%.

The gas temperature above the char was measured during combustion by a suction pyrometer. The thermocouple was placed at the same height in the reactor as the infrared beam. The pyrometer consisted of a K type thermocouple and was shielded by both stainless steel and ceramic shields. The gas from the reactor was drawn through the stainless steel tube. The thermocouple tip was heated by convection of the gas past the thermocouple junction.

Absorption spectra were recorded above three different char beds. Ten spectra were recorded during combustion of the first burn, nine during the second, and six during the third. The Pascal program, *SpecAnal*, was run on each of the spectra to yield a calculated

gas temperature. The results of the temperatures calculated from the absorption spectra are presented in Table 27. Also included in the table are the gas temperatures recorded by the thermocouple, as well as the relative and absolute difference between the thermocouple and spectroscopic measurements.

The agreement between spectroscopic and thermocouple measurements are very good. The average percent differences for each of the three burns was 2.2, 2.0 and 1.0%, respectively. The largest percent difference, for any one spectrum was 4.9%. These results are as good as those obtained in the pure gas environment, at similar temperatures. As expected, there is no evidence that the combustion environment has affected the accuracy of the calculation methodology. These results also support the conclusion that the absorption spectra recorded in the reactor are photometrically accurate.

Despite the excellent agreement between the thermocouple and spectroscopic measurements, the temperatures which have been recorded in the reactor are very low. Furthermore, in each of the three trials, the gas temperature increases as the burn progresses (the data from each char burn in Table 27 are in chronological order). Qualitatively, these observations can be explained. The combustion gas which is supplied to the reactor is heated by four high temperature heating tapes. Each tape heats the outside of a 5 inch stainless steel pipe to about 750 K. Given the flow rate of gas, approximately 0.5-1.0 L/Min (STP), the tubing is sufficiently long to heat the gas to the outside wall temperature. In fact, heat transfer calculations have shown that the tubing need only be about one inch long. After leaving the heated section of tubing, the gas does not immediately flow into the reactor, instead it travels at least one inch through a slot jet nozzle which is not heated, only insulated. Because the nozzles are at a significantly lower temperature, the gas decreases in temperature through the slot jet. After exiting the jet, it is directed downward onto the char surface.

Table 27. Comparison of spectroscopic (calculated) and thermocouple (measured) determinations of the gas temperature above three different char combustion experiments.

Spectrum	Spectroscopic Temp. (K)	Thermocouple Temp. (K)	Temp. Diff. (K) (Calc.- Meas.)	Absolute Percent Difference (%)
Char Burn #1				
C75A	433	441	-8	1.8
C75B	575	589	-14	2.4
C75C	590	573	17	3.0
C75D	588	567	21	3.7
C75E	594	566	28	4.9
C75F	584	578	6	1.0
C75G	589	589	0	0.0
C75H	653	645	8	1.2
C75I	656	667	-11	1.6
				Average = 2.2%
Char Burn #2				
C76A	564	560	4	0.7
C76B	576	555	21	3.8
C76C	573	559	14	2.5
C76D	573	576	-3	0.5
C76E	598	581	17	2.9
C76F	608	602	6	1.0
C76G	636	628	8	1.3
C76H	648	656	-8	1.2
C76I	703	673	30	4.4
				Average = 2.0%
Char Burn #3				
C78A	569	567	2	0.3
C78B	588	581	7	1.2
C78C	583	585	-2	0.3
C78D	598	603	-5	0.8
C76E	639	628	11	1.7
C78F	652	665	-13	1.9
				Average = 1.0%

The only heating elements in the furnace are those around the crucible. When the sample is lifted closer towards the infrared beam, only a part of the crucible is exposed to the heating elements of the furnace. After the combustion air leaves the jets, it travels to the char surface, supplies oxygen to support char combustion, and is then directed upwards out

of the furnace. Throughout this process, energy from the heated gas is lost to the surrounding reactor walls. There is relatively little energy obtained from the char surface, although the combustion reactions are exothermic. The net effect of these processes is a further decline in the gas temperature.

During the course of the two hour combustion process, the nozzles are continually heated by conduction from the heated pipes, and the bed surface sinks further into the crucible. Therefore, as the burn progresses, the combustion gas enters the reactor at a higher temperature, and once inside the reactor it has the opportunity to go further into the crucible which is directly exposed to the furnace heating elements. The net effect of these processes is an increase in the gas temperature as the burn progresses.

The excellent agreement between spectroscopic and thermocouple measurements indicates that gas temperatures can be accurately measured in a combustion environment using FT-IR absorption spectroscopy. Although the temperatures were relatively low, there is no indication that the accuracy should be less for similar measurements recorded at higher gas temperatures. The ability to use similar spectra to make CO and CO_2 gas concentration measurements, during char combustion, will be illustrated in the following section.

Gas Concentration Determinations

In addition to gas temperatures, spectroscopic CO and CO_2 concentration measurements have also been made during black liquor combustion. These measurements were made from CO and CO_2 absorption spectra, recorded through the reactor, during char combustion. The accuracy of these measurements was evaluated by comparing the calculated concentrations with measurements recorded on the outside of the reactor with a CO/CO_2 gas analyzer.

Room Temperature Concentration Calculations in the Reactor

Before experiments were run during char combustion, room temperature absorption spectra of $CO/CO_2/N_2$ gas mixtures were recorded in the reactor. These spectra were collected to verify that concentration measurements could be accurately made in a different cell, under controlled conditions. Twenty six room temperature spectra were recorded in the reactor in three separate trials. Nine spectra were recorded in each of the first two trials and eight were recorded in the third. The concentration accuracy, evaluated by comparison with the metered quantities, is presented in Tables 28 and 29 for CO and CO_2, respectively.

Table 28. Results of CO gas concentration calculations from the spectra recorded at room temperature in the char reactor.

Trial #	# of Spectra	Measured Conc. Range (%)	Calculated Avg. Gas Temp. (K)	Average Abs. % Diff of Calc.CO Conc.	Low (%)	High (%)
1	9	0.41-2.34	290	3.32	-4.42	8.46
2	9	0.33-1.42	296	3.60	-5.38	10.32
3	8	0.34-1.65	294	3.54	-2.32	14.88

Table 29. Results of CO_2 gas concentration calculations from the spectra recorded at room temperature in the char reactor.

Trial #	# of Spectra	Measured Conc. Range (%)	Calculated Avg. Gas Temp. (K)	Average Abs. % Diff of Calc.CO_2 Conc.	Low (%)	High (%)
1	9	0.40-1.89	290	9.45	-15.65	-3.65
2	9	0.34-1.56	296	7.65	-16.45	-2.70
3	8	0.37-1.59	294	9.60	-15.95	8.05

The agreement between the calculated and metered CO gas concentrations is very good. The average absolute percent difference is between 3-4% which agrees well with the calculation accuracy reported for the gas cell. In addition, the low and high values are both

negative and positive, respectively, indicating no bias among the results towards over or under predicting the gas concentration. The room temperature CO_2 results, however, are not as good. The average absolute percent difference between calculated and metered gas concentrations was between 7-10%, and all but one of the 26 spectra had a calculated gas concentration which was lower than the metered concentration. In the gas cell, the average absolute percent difference for CO_2 at room temperature was between 3-5%.

The accuracy of the results from the room temperature CO calculations, suggest that the increased error with the CO_2 is not due to differences between the gas cell and the reactor. Instead, an explanation for the differences is derived from a comparison of the CO_2 individual results, obtained in the gas cell, at room temperature. The overall accuracy of the CO_2 results, in the gas cell, was between 3-5%. However, this average value included calculations from spectra with a broad range of concentrations (0.72-3.24%). Among the spectra recorded at lower concentrations, 0.5-1.5% (similar to 90% of those in Table 29), all but one of the calculated CO_2 concentrations were less than the measured values (3.60, -6.02, -4.17, -4.00, -10.45, -9.30, and -9.65). Among these values, the average absolute percent difference was 6.7%. These results suggest that the calculation accuracy is concentration dependent.

Part of the reason for the lower accuracies obtained from the CO_2 data may be linked to the concentration dependence of the CO_2 line strengths. A concentration dependence for line strengths has already been shown for higher temperature spectra. This was not expected among the lower temperature spectra, however, because of the excellent agreement between the room temperature line strengths calculated in this work, compared to those reported in the literature. Table 30 is a listing of the calculated lines strengths of lines 53-61, along with the concentration for each of the spectra, from which each the line strengths were calculated.

Table 30. Illustration of the concentration dependence of CO_2 lines 53-61 at room temperature. Line strengths are in units of 1/(atm-cm^2).

Conc. (%)	Line Strength = 53	Line Strength = 55	Line Strength = 57	Line Strength = 59	Line Strength = 61
0.72	2.695	1.887	1.275	0.832	0.535
0.77	2.785	1.955	1.299	0.890	0.587
1.33	2.640	1.809	1.210	0.798	0.530
1.34	2.720	1.881	1.295	0.849	0.529
1.82	2.805	1.958	1.301	0.861	0.572
1.89	2.868	1.988	1.314	0.888	0.581
2.24	2.815	1.899	1.279	0.845	0.563
2.46	2.853	1.963	1.290	0.865	0.564
2.87	2.802	1.926	1.302	0.857	0.564

The line strengths presented in this table show a slight concentration dependence. The average of the line strengths, calculated at concentrations between 1.82-2.24%, was 2.1-5.9% higher than the line strengths calculated at concentrations between 0.72-1.34%. The reason for this dependence is the overlap of the neighboring R branch band and/or incomplete correction for the overlap of neighboring lines. The net effect of these errors is an increase in the average line strengths for each line. These conclusions are supported by the observation that the room temperature theoretical line strengths, presented earlier, were lower then those calculated in this work.

Because relatively few lines are available for CO_2 concentration calculations at room temperature, the lines known to have temperature dependent line strengths, have not been excluded and the calculations repeated. The errors which have been described here are relatively small. In general, the results suggest that accurate concentrations can be measured from absorption spectra recorded in the reactor. In the next set of experiments, gas concentrations are calculated from spectra recorded during char combustion.

Concentration Calculations During Char Combustion

Absorption spectra were recorded in the reactor during the combustion of six char samples. The char samples and combustion conditions were the same as those described for the temperature results, except for the following; the char bed was not lifted after the pre-heating period for trials 4, 5, and 6, and the char was only heated to temperatures of 1173 and 1073 K, respectively, in trials 5 and 6. These changes provided some variability in the CO and CO_2 gas concentration, among the trials. For each trial, 6-9 spectra were recorded during the combustion of each char sample. The concentration accuracy, evaluated by comparison with NDIR measured quantities is presented in Tables 31 and 32 for CO and CO_2, respectively.

Table 31. Results of CO gas concentration calculations from the spectra recorded during char combustion.

Trial #	# of Spectra	Measured Conc. Range (%)	Average Calculated Gas Temp. (K)	Average Abs. % Diff of Calc.CO Conc.	Low (%)	High (%)
1	8	0.41-1.99	586	4.50	-6.68	12.36
2	9	0.21-0.93	609	6.56	-15.66	-0.01
3	7	0.65-0.86	611	10.42	-11.78	-9.05
4	7	0.42-1.21	676	8.89	-11.19	-5.72
5	6	0.37-0.99	644	4.91	-9.31	0.70
6	6	0.26-0.60	594	4.32	-7.06	2.86

Among the trials, the difference between the average calculated CO concentration and NDIR measured concentrations varied from 4.3-10.4%, while the CO_2 results varied from 8.6-17.0%. Both the CO and CO_2 data are biased toward under predicting the gas concentration. In the case of the CO data, with the exception of trial #3, the range of error predicted from the gas cell work was only slightly higher than those measured in the gas cell (2-5%).

Table 32. Results of CO_2 gas concentration calculations from the spectra recorded during char combustion.

Trial #	# of Spectra	Measured Conc. Range (%)	Average Calculated Gas Temp. (K)	Average Abs. % Diff of Calc.CO_2 Conc.	Low (%)	High (%)
1	8	0.51-0.81	586	8.60	-14.88	-2.96
2	9	0.55-1.10	609	13.06	-16.36	-9.00
3	7	0.53-1.01	611	17.00	-19.37	-16.34
4	7	0.52-0.90	676	13.36	-15.99	-6.38
5	6	0.55-0.91	644	11.11	-13.65	-9.48
6	6	0.59-1.04	594	9.20	-11.94	-3.78

The CO_2 data recorded during char combustion are similar to the room temperature reactor results. An explanation for the relatively high percent errors from these spectra can again be derived from a consideration of the concentration dependence of the line strengths. The line strengths determined in the gas cell (reported in Section 3) were calculated over a wide range of CO_2 concentrations (0.81-3.91). The line strengths which were recorded at the higher concentrations are affected to a greater extent by peak overlaps from the neighboring CO_2 band. This band raises the average line strengths, for lines with lower values of m. Table 33 lists the calculated line strengths as a function of concentration for lines 53-67.

Table 33. Illustration of the concentration dependence of CO_2 lines 53-67, at 573 K. Line strengths are in units of 1/(atm-cm^2).

Conc. (%)	L.S. m = 53	L.S. m = 55	L.S. m = 57	L.S. m = 59	L.S. m = 61	L.S. m = 63	L.S. m = 65	L.S. m = 67
0.81	5.860	5.125	4.124	3.353	2.747	2.222	1.702	1.352
1.32	6.130	5.266	4.256	3.372	2.700	2.194	1.743	1.366
2.00	6.506	5.255	4.426	3.365	2.722	2.207	1.710	1.358
2.29	6.772	5.457	4.327	3.570	2.747	2.197	1.698	1.329
3.10	7.391	6.169	4.614	3.708	2.975	2.348	1.774	1.402
3.91	7.513	6.882	5.232	3.960	3.118	2.339	1.776	1.372

Only the first of the six spectra in Table 33 were recorded at a concentration within the range of the concentrations calculated in the reactor. The percent difference between the

line strength calculated at a CO_2 concentration of 0.81%, compared to the average line strength calculated from the other five spectra, was 14.6, 11.7, 9.8, 6.7, 3.7, 1.5, 2.2 and 1.0% respectively, for lines 53-67. These calculations clearly illustrate the effect of concentration on the line strength. The error diminishes as the lines move out toward the wing, because the lines are further from the overlap of the neighboring R branch band and because the peak intensity of the lines is decreasing, reducing the effect of overlap from neighboring CO_2 lines.

To test the importance of the concentration dependence of line strength on the results in Table 33, the calculations were repeated. This time, however, lines 53-67 were excluded from the calculations. In addition, line 77 was excluded, since it yielded calculated concentrations which were 10-20% lower than the other lines. The results of these calculations are presented in Table 34.

Table 34. Results of CO_2 gas concentration calculations from the spectra recorded during char combustion. Lines 53-67 have been excluded from the calculations because of the concentration dependence of line strength for these lines.

Trial #	# of Spectra	Measured Conc. Range (%)	Average Calculated Gas Temp. (K)	Average Abs. % Diff of Calc.CO_2 Conc.	Low (%)	High (%)
1	8	0.51-0.81	586	6.62	-13.71	1.56
2	9	0.55-1.10	609	9.25	-14.58	-3.75
3	7	0.53-1.01	611	12.25	-15.62	-7.02
4	7	0.52-0.90	676	10.09	-14.08	-2.13
5	6	0.55-0.91	644	7.57	-10.37	-5.8
6	6	0.59-1.04	594	5.97	-8.32	-0.86

The results presented in this table show a significant reduction in the average absolute difference between the calculated and measured CO_2 concentrations. The overall average percent difference, calculated prior to the exclusion of lines 53-65 and 77, was 12.0% and after

exclusion of these lines it has been reduced to 8.6%. Clearly, the temperature dependence of the line strengths has affected the concentration calculation accuracy. The level of accuracy reported for CO_2, after these corrections, approaches that obtained in the gas cell.

The results presented in this table still show a bias toward under predicting the actual concentrations. It is unlikely that the observed concentration differences between the spectroscopic measurements and the analyzer values are a result of a secondary CO oxidation reaction,

$$CO + 1/2\, O_2 \rightarrow CO_2 \quad . \tag{36}$$

First, the gas temperature is very low which prohibits this reaction, and second, an increase in CO_2 concentration at the NDIR meter should be coupled with a corresponding decrease in the CO concentration at the meter. However, this has not been observed.

The overall accuracy of the char combustion concentration calculations is 6.6 and 8.6% for the CO and CO_2, respectively. The calculated concentrations of CO and CO_2, were between 0.3-1.2%. This is the most difficult range of concentrations to make accurate measurements, since relatively small deviations in the concentration, $\pm$ 0.05%, result in relative large percent errors, 16.7- 4.0%. As the concentration of the gas increases, with faster rates of char combustion, it is likely that the accuracy will improve.

Significance of Results

Results have been presented in this section which described the acquisition of absorption spectra in a combustion environment, and the determination of gas concentrations and temperatures from these spectra. The quality of the absorption spectra is as good as those obtained in the gas cell, and no problems have been encountered in the transition from the

gas cell to the combustion environment. Furthermore, these spectra have demonstrated that a large window of the mid infrared region is available for both qualitative and quantitative analysis of multi component gaseous systems.

The quantitative accuracy of these spectra has also been demonstrated by gas temperature and concentration measurements. The gas temperature measurements have been shown to be accurate to within 2-4% of thermocouple measurements, while the gas concentration measurements have demonstrated accuracies of better than 5-10%.

There have been several examples, in the literature, of the acquisition of FT-IR absorption spectra in combustion environments. However, these spectra have only been used to a limited extent for the determination of gas concentrations and temperatures. FT-IR has been demonstrated in this work, to not only yield qualitative information regarding the composition of the gas phase above a combustion environment, but has also been shown to yield accurate quantitative information as well.

It is recognized that the gas temperatures in the char combustion environment are lower than desired for char combustion or gasification studies. However, there is no indication that either the qualitative or quantitative reliability of these spectra should decrease with increasing gas temperatures. The results of this thesis indicate that FT-IR absorption spectroscopy has been developed sufficiently to be useful for the quantitative evaluation of the events occurring during black liquor combustion.

CONCLUSIONS

The results of this thesis have demonstrated that the gas phase of a combustion environment can be qualitatively and quantitatively evaluated using Fourier transform infrared absorption spectroscopy. Qualitative evaluations lead to an identification of the gaseous components present above a burning char bed, while quantitative results provide gas temperature and concentration information in the high temperature combustion environment. In developing both the mathematical and experimental methods for these capabilities, several key conclusions have been reported. These conclusions are enumerated below.

1. High temperature absorption spectra can be routinely recorded in a gas cell at temperatures up to 1250 K, provided the emission radiation from the gases are adequately controlled. In this work, a strategically placed aperture has been used to block the interfering effects of this radiation source.

2. The infrared absorption spectra recorded by a moderate resolution (0.25 cm^{-1}) spectrometer, are significantly distorted by the finite resolution of the instrument. The distortions can be adequately described mathematically, and numerical corrections have yielded "corrected" spectra which follow the theoretical principles expected from diatomic and linear triatomic molecules.

3. A slight temperature gradient exists along the path of the infrared beam through the gas cell. Thermocouple profiling and heat transfer calculations have been used to describe the profile and to yield an average gas temperature which can be correlated to furnace set point temperatures.

4. With the corrected absorption peaks, the gas temperature of CO absorption spectra can be determined at temperatures between 295-1250 K. The accuracy of these calculations shows little temperature dependence, and in the worse case the average difference between spectroscopic measurements and thermocouple measurements is 3.5 %.

4. At temperatures greater than 360 K, the composition of $CO/CO_2/N_2$ gas mixtures in the gas cell are significantly altered by both $CO/CO_2/C_{gr}$ equilibration reactions and by oxidative reactions with the metals comprising 304 stainless steel. Accurate "average" gas concentrations can be obtained from the cell by analysis of the gas composition exiting the cell with a NDIR instrument.

5. Knowledge of the gas composition and peak intensities of corrected CO and CO_2 spectra has resulted in the experimental evaluation of the temperature dependence of 22 CO and 19 CO_2 vibrational-rotational absorption lines. The accuracy of these values was established by comparisons with other experimental values reported in the literature and with theoretical calculations; in general, the agreement was very good.
For CO: At 295 K, line strengths determined in this work, have been approximately 10% higher than both other experimental values and theoretical predictions. At temperatures greater than 295 K, the agreement between both other experimental results and theoretical predictions has been between 5-10%.
For CO_2: At 295 K, the experimentally determined line strengths from this work are within 2% (average) of experimental results previously presented in the literature. The theoretically calculated line strengths, at room temperature, are 10% lower than those reported here. At temperatures between 295-1250 K, the agreement is between 5-10% of theoretical predictions; no experimental reports of high temperature line strengths have been found in the literature. At all temperatures, although more significantly above 295 K, the calculated line intensities are distorted by incomplete resolution of lines from a neighboring CO_2 band or from neighboring lines in the same band. As a result, the experimental line strengths have displayed a concentration dependence. In the worse case, this dependence caused line strengths, calculated from low concentration spectra, to vary by 15% from line strengths calculated from higher concentration spectra.

6. The line strengths experimentally determined in this work have been used to calculate CO and CO_2 gas concentrations in the high temperature gas cell. The spectroscopically determined concentrations of CO and CO_2, for the concentration range 0.5-5.0%, agree, on average, with both metered and NDIR measurements to within 3.6 and 4.9%, respectively.

7. The char combustion reactor can be used to record high quality infrared absorption spectra above black liquor pyrolysis or combustion. From these spectra, qualitative evaluations have been made of the gas phase above a char bed near the end of pyrolysis and during char combustion. CO, CO_2, and water vapor were identified during pyrolysis. CO and CO_2 were also identified during char combustion.

8. The char combustion reactor can also be used to record spectra which can be used for quantitative evaluations of the gas phase during char combustion. In this environment, gas temperatures have been measured with an accuracy of 2-3% at temperatures between 450-750 K. Gas concentrations have been measured with accuracies of better than 10% at concentrations between 0.3-1.3%.

SUGGESTIONS FOR FUTURE WORK

With the spectroscopic foundation established in this thesis, there is now ample opportunity to supplement current black liquor combustion studies with the additional insight that FT-IR absorption spectroscopy can provide. Two areas of research are particularly attractive for future spectroscopic studies. These include char combustion/gasification studies, and second, studies directed towards the elucidation of additional furnace chemistry. Knowledge of the rates of char combustion and gasification by oxygen, carbon dioxide, and water vapor, is important in understanding black liquor burning rates and the development of accurate mathematical models of the lower furnace. The reactor developed in this work is well suited for this type of experimentation, with one exception. It should be modified to raise the gas temperature above the char bed. This modification could easily be made by adding heating elements to the middle section of the reactor. These heating elements would neither influence transmission of the infrared beam through the reactor, nor affect the accuracy with which CO, CO_2 or gas temperatures could be measured. With this modification, the combustion or gasification of black liquor char could be studied in a bed configuration, with combustion air (or CO_2 or H_20), passed directly on the char surface. With the analysis of the gaseous products made directly above the char surface, the interfering effects of secondary CO oxidation reactions or $CO/CO_2/C_{gr}$ equilibration reactions could be minimized.

The second area of black liquor combustion research which might benefit from FT-IR absorption spectroscopy, is the elucidation of furnace chemistry during black liquor combustion. There are several areas of research in which the furnace chemistry is not well known, these include; sulfur release, fume formation, the fate of chlorinated compounds during combustion, and NO_x formation. In each case, the expected amount of each species is small and the absorption intensities of the molecules are much weaker than those of CO, CO_2 and water vapor. However, methods have been developed which are directed towards

the elucidation of very small absorption peaks from FT-IR absorption spectra.[78] The application of these techniques, in conjunction with the char combustion reactor might lend additional insight into recovery boiler chemistry.

NOMENCLATURE

SYMBOLS

$A(\nu)$	Frequency specific absorbance
$A_{peak}(m)$	Peak maximum of absorption line m
$A^a_{peak}(m)$	Experimentally measured or apparent absorption peak maximum
$A^t_{peak}(m)$	True absorption peak maximum
A_{int}	Integrated absorbance of line
B	Rotational constant
c	Speed of light
C	Concentration
D	Centrifugal distortion constant
E	Energy
F	Herman-Wallis correction factor
h	Planck's constant
H	Peak height (experimental)
I	Peak intensity, same as S(m)
J"	Lower rotational energy level of vib-rot transition
J'	Upper rotational energy level of vib-rot transition
k	Boltzman constant
K_i	Constant
L	Path length
m	Index of line (equal to -J" for P branch lines, equal to J"+1 for R branch lines)
MW	Molecular weight
N_{xy}	Temperature exponent for molecule x broadened by molecule y
P	Branch of absorption lines comprising (J"-1 ← J") vib-rot transitions
P_x	Partial pressure of species x
P_t	Total pressure
$P(\delta)$	Time domain amplitude of interferogram
$P(\sigma)$	Frequency domain amplitude of interferogram
Q(T)	Partition function at temperature T
R	Branch of absorption lines comprising (J"+1 ← J") vib-rot transitions
R_i	Instrument resolution
S(m)	Line strength of absorption line m
S_b	Band strength
T	Temperature
$T(\nu)$	Frequency specific transmission

GREEK SYMBOLS

$\alpha(\nu)$	Absorption coefficient
$\gamma(m)$	Line half-width at half height
γ°_{xy}	Broadening coefficient for molecule x by molecule y
γ_d	Doppler broadened line width
δ	Optical retardation or mirror displacement
Δ	Maximum optical retardation
ν	Frequency (wavenumber)
$\tilde{\nu}$	Frequency (1/sec)
ν_b	Effective frequency of band center
ρ	Resolution parameter
σ	Frequency (used in interferogram description)
υ''	Lower vibrational energy level of vib-rot transition
υ'	Upper vibrational energy level of vib-rot transition

ABBREVIATIONS

CARS	Coherent Anti-Stokes Raman Spectroscopy
FWHH	Full Width at Half Height
FT-IR	Fourier Transform Infrared
HWHH	Half-Width at Half Height
ILS	Instrument Line Shape
LIF	Laser Induced Fluorescence
LPA	Laser Precision Analytical
LSF	Least Squares Fit
MCT	Mercury Cadmium Telluride
NDIR	Non-Dispersive Infrared
SD	Standard Deviation
SRS	Spontaneous Raman Scattering
TDL(S)	Tunable Diode Laser (Spectroscopy)

ACKNOWLEDGEMENTS

Completion of this work was made possible by the assistance of numerous individuals and organizations; to all those who contributed, I am sincerely grateful. I am particularly thankful for the technical advice of the faculty, for the financial assistance of the Institute, and for the emotional support of friends and family. Without their combined efforts, I would not have had the technical expertise to guide me, the finances to support me, and the personal love and support to sustain me.

Among the faculty, I have been significantly influenced, and I am especially indebted to my primary advisor, Dr. Ken Nichols, to former advisors, Dr. David Clay and Dr. Rajai Atalla, and to committee members Dr. Jeff Lindsay and Dr. James de Haseth. For financial assistance I am grateful to the Institute of Paper Science and Technology along with its member companies, and the U.S. Department of Energy (grant DE-ACO2-83CE40637).

I am also very thankful for the many friendships which I have established while attending the Institute. While many will not survive the strain of distance and time, they have all added greatly to my enjoyment of the time spent completing this work. I am especially grateful for the friendship of fellow student Tom Spielbauer and for the friendship and support of brothers, Dave and Bob.

Finally, I will always be indebted to my parents. In addition to the gift of life, they provided me with a stable and nurturing environment as a youth, and by their exemplary life style, have unknowingly instilled in me a desire to work to the best of my abilities.

LITERATURE CITED

1. Walsh, A. R. A Computer Model for In-Flight Black Liquor Combustion in a Kraft Recovery Furnace. Doctoral Dissertation. Appleton, WI, The Institute of Paper Chemistry, 1989.
2. Jones, A. K. A Model of the Kraft Recovery Furnace. Doctoral Dissertation. Appleton, WI, The Institute of Paper Chemistry, 1989.
3. Sumnicht, D.W. A Computer Model of a Kraft Char Bed. Doctoral Dissertation. Appleton, WI, The Institute of Paper Chemistry, 1989.
4. Blackwell, B.; King, T. Chemical Reactions In Kraft Recovery Boilers. Vancouver, B.C., Sandwell and Company Limited, 1985.
5. Kulas, K. A. An Overall Model of the Combustion of a Single Droplet of Kraft Black Liquor. Doctoral Dissertation. Appleton, WI, The Institute of Paper Chemistry, 1990.
6. Miller, P. T. Swelling of Kraft Black Liquor. An Understanding of the Associated Phenomena During Pyrolysis. Doctoral Dissertation. Appleton, WI, The Institute of Paper Chemistry, 1986.
7. Aiken, G. W. The Use of a Char Pile Reactor to Study Char Bed Processes. Doctoral Dissertation. Appleton, WI, The Institute of Paper Chemistry, 1988.
8. Brown, C. A.; Grace, T. M.; Lien, S. J.; Clay, D. T. Char Bed Burning Rates - Experimental Results. Conference Proceedings from the 1989 International Chemical Recovery Conference, p. 65.
9. Grace, T. M.; Cameron, J. H.; Clay, D. T. Role of the Sulfate-Sulfide Cycle in Char Burning: Experimental Results and Implications. Tappi Journal 69(10):108-113(1986).
10. Harper, F. D. Sulfur Release During the Pyrolysis of Kraft Black Liquor. Doctoral Dissertation. Appleton, WI, The Institute of Paper Chemistry, 1989.
11. Goerg, K. A. A Study of Fume Particle Deposition. Doctoral Dissertation. Appleton, WI, The Institute of Paper Chemistry, 1989.
12. Merriam, R. L. Simulation Analysis of Liquor-Firing and Combustion Processes in Kraft Recovery Furnaces. Tappi Journal 65(9):112-116(1982).
13. Laurendeau, N. M. Heterogeneous Kinetics of Coal Char Gasification and Combustion. Progress in Energy Combustion Science 4:221-270(1978).
14. Milanova, E.; Kubes, G. J. The Combustion of Kraft Liquor Chars. International Chemical Recovery Conference, New Orleans, 363-370, (1985).
15. Li, J.; Van Heiningen, A. R. P. Mass Transfer Limitations in Gasification of Black Liquor Char by CO_2. International Chemical Recovery Conference, New Orleans, 459-464, 1985.
16. Cameron, J. H.; Grace, T. M. Kinetic Study of Sulfate Reduction with Carbon. Industrial and Engineering Chemistry Fundamentals 22(4):486-494(1983).
17. Feuerstein, D. L.; Thomas, J. F.; Brink, D. L. Malodorous Products from the Combustion of Kraft Black Liquor. I. Pyrolysis and Combustion Aspects. Tappi Journal 50(6):258-

262(1967).

18. Brink, D. L.; Thomas, J. F.; Feuerstein, D. L. Malodorous Products from the Combustion of Kraft Black Liquor. II. Analytic Aspects. Tappi Journal 50(6):276-285(1967).

19. Brink, D. L.; Pohlman, A. A.; Thomas, J. F. Analysis of Sulfur-Containing and Sulfur-Free Organic Products formed in Kraft Black Liquor Pyrolysis. Tappi Journal 54(5):714-720(1971).

20. Iatridis, B.; Gavalas, G. R. Pyrolysis of a Precipitated Kraft Lignin. Industrial and Engineering Chemistry Product Research and Development 18(2):127-130(1979).

21. Bjorkman, A. Significance of Pyrolysis from Gasification. International Conference on Recovery of Pulping Chemicals, 3-7, (1981).

22. Bhattacharya, P. K.; Parthiban, V.; Kunzru, D. Pyrolysis of Black Liquor Solids. Industrial and Engineering Chemistry Product Research and Development 25(2):420-426(1986).

23. Penner, S. S.; Wang, C. P.; Bahadori, M. Y. Laser Diagnostics Applied to Combustion Systems. Twentieth International Symposium on Combustion, 1149-1179 (1984).

24. Tolles, W. M.; Nibler, J. W.; McDonald, J. R.; Harvey, A. B. A Review of the Theory and Application of Coherent Anti-Stokes Raman Spectroscopy (CARS). Applied Spectroscopy 31(4):253-272(1977).

25. Hall, R. J. Coherent Anti-Stokes Raman Spectroscopic Modeling for Combustion Diagnostics. Optical Engineering 22(3):322-329(1983).

26. England, W. A.; Milne, J. M.; Jenny, S. N.; Greenhalgh, D. A. Application of CARS to an Operating Chemical Reactor. Applied Spectroscopy 38(6):867-876(1984).

27. Eckbreth, A. C.; Bonczyk, P. A.; Verdieck, J. F. Combustion Diagnostics by Laser Raman and Fluorescence Techniques. Progress in Energy and Combustion Science 5(4):253-322(1979).

28. Daily, J. W. Laser-Induced Fluorescence Spectroscopy in Flames. ACS Symposium Series 134:61-83(1980).

29. Schofield, K.; Steinberg, M. Quantitative Atomic and Molecular Laser Fluorescence in the Study of Detailed Combustion Processes. Optical Engineering 20(4):501-510(1981).

30. Lapp, M.; Hartley, D. L. Raman Scattering Studies of Combustion. Combustion Science and Technology 13(1-6):199-210(1976).

31. Stephenson, D. A. High-Temperature Raman Spectra of Carbon Dioxide and Water for Combustion Diagnostics. Applied Spectroscopy 35(6):582-584(1981).

32. Zur Loye, A.; Santavicca, D. A. Temperature and Concentration Measurements in an Internal Combustion Engine Using Laser Raman Spectroscopy. Progress in Astronautics and Aeronautics 92:255-269(1984).

33. Hanson, R. K.; Kuntz Falcone, P. Temperature Measurement Technique for High Temperature Gases using a Tunable Diode Laser. Applied Optics 17(16):2477-2480(1978).

34. Ottesen, D. K.; Stephenson, D. A. Fourier Transform Infrared (FT-IR) Measurements in Sooting Flames. Combustion and Flame 46(1):95-114(1982).

35. Ottesen, D. K.; Thorne, L. R. *In Situ* Studies of Pulverized Coal Combustion by Fourier Transform Infrared Spectrometry. Proceedings of the 3rd International Conference on Coal Science, pp. 351-354, (1985).

36. Thorne, L. R.; Ottesen, D. K. Fourier Transform Infrared (FT-IR) Spectroscopic Measurements of *In Situ* Coal Combustion. Proc. from the Western States Section of the Combustion Institute, Jet Propulsion Lab., Paper WSS/CI 83-17, Pasadena, CA, (1983).

37. Herzberg, G. Molecular Spectra and Molecular Structure. I. Spectra of Diatomic Molecules. New York, Van Nostrand Reinhold Company, 1950.

38. Herzberg, G. Molecular Spectra and Molecular Structure. II. Infrared and Raman Spectra of Polyatomic Molecules. Princeton, New Jersey, D. Van Nostrand Company, Inc., 1945.

39. Alberty, R. A. Physical Chemistry. 6th Edition. New York. New York, John Wiley & Sons, 1983:448-454.

40. Hanson, R. K.; Kuntz, P. A.; Kruger, C. H. High-resolution Spectroscopy of Combustion Gases Using a Tunable IR Diode Laser. Applied Optics 16(8):2045-2047(1977).

41. Skoog, D.A.; West, D.M. Principles of Instrumental Analysis, Second Edition. Philadelphia, PA, Holt, Rinehart and Winston, 1980.

42. Griffiths P.R.; de Haseth, J.A. Fourier Transform Infrared Spectrometry. New York, New York, John Wiley & Sons, 1986.

43. Varghese, P. L.; Hanson, R. K. Tunable Infrared Diode Laser Measurements of Line Strengths and Collision Widths of $^{12}C^{16}O$ at Room Temperature. Journal of Quantitative Spectroscopy and Radiative Transfer 24:479-489(1980).

44. Gross, L. A.; Griffiths, P. R.; Sun, J. N.-P., "Temperature Measurement by Infrared Spectrometry," in Infrared Methods for Gaseous Measurements, J. Wormhoudt, Ed., Marcel Dekker, Inc., New York, New York, 1985, 1985, Chap. 3.

45. Sell, J. A. Temperature Dependence of the Absorption Coefficient and Half-width of the P(6) Line of Carbon Monoxide. Journal of Quantitative Spectroscopy and Radiative Transfer 23:595-598(1980).

46. Hartmann, J. M.; Rosenmann, L.; Perrin, M. Y.; Taine, J. Accurate Calculated Tabulations of CO Line Broadening by H_2O, N_2, O_2, and CO_2 in the 200-3000 K Temperature Range, Applied Optics 27(15):3063-3065(1988).

47. Rosenmann, L.; Hartmann, J. M.; Perrin, M. Y.; Taine, J. Accurate Calculated Tabulations of IR and Raman CO2 Line Broadening by CO2, H2O, N2, O2 in the 300-2400 K Temperature Range. Applied Optics 27(18):3902-3907(1988).

48. Nakazawa, T.; Tanaka, M. Measurements of Intensities and Self- and Foreign-Gas-Broadened Half-Widths of Spectral Lines in the CO Fundamental Band. Journal of Quantitative Spectroscopy and Radiative Transfer 28:409-416(1982).

49. Anderson, R. J.; Griffiths, P. R. Determination of Rotational Temperatures of Diatomic Molecules From Absorption Spectra Measured at Moderate Resolution. Journal of Quantitative Spectroscopy and Radiative Transfer 17:393-401(1977).

50. Chackerian, C.; Guelachnili, G.; Tipping, R. H. CO 1-0 Isotopic Lines as Intensity Standards. Journal of Quantitative Spectroscopy and Radiative Transfer 30:107-112(1983).

51. Anderson, R. J.; Griffiths, P. R. Errors in Absorbance Measurements in Infrared Fourier Transform Spectrometry, because of Limited Instrument Resolution. Analytical Chemistry 47(14):2339-2347(1975).

52. McNesby, K. L.; Fifer, R. A. Rotational Temperature Estimation of CO at High Temperatures by Graphical Methods Using FT-IR Spectrometry. Applied Spectroscopy 45(1):61-67(1991).

53. Cleland, T. A.; Hess, D. W. Measurement of Rotational Temperature and Dissociation in N_2O Glow Discharges Using *in situ* Fourier Transform Infrared Spectroscopy. Journal of Applied Physics 64(3):1068-1077(1988).

54. Solomon, P. R.; Hamblen, D. G.; Carangelo, R. M.; Krause, J. L. Coal Thermal Decomposition in an Entrained Flow Reactor: Experiments and Theory. Nineteenth Symposium (International) on Combustion. The Combustion Institute, pp.1139-1149, 1982.

55. Hunt, R. H.; Toth, R. A.; Plyler, E. K. Journal of Chemical Physics 49:3909(1968).

56. Bouanich, J. P.; Brodbeck, C. Journal of Quantitative Spectroscopy and Radiative Transfer 13:1(1973).

57. Sun, J. N-P.; Griffiths, P. R. Temperature Dependence of the Self-broadening Coefficients for the Fundamental Band of Carbon Monoxide. Applied Optics 20(9):1691-1695(1981).

58. Sun, J. N-P.; Griffiths, P.R. Nitrogen-broadening Coefficient of Vibrational-Rotational Lines of Carbon Monoxide. Applied Optics 20(14):2332-2334(1981).

59. Varanasi, P.; Sarangi, S. Measurements of Intensities and Nitrogen-Broadened Linewidths in the CO Fundamental at Low Temperatures. Journal of Quantitative Spectroscopy and Radiative Transfer 15:473-482(1975).

60. Varghese, P. L.; Hanson, R. K. Collision Width Measurements of CO in Combustion Gases Using a Tunable Diode Laser. Journal of Quantitative Spectroscopy and Radiative Transfer 26(4):339-347(1981).

61. Bonamy, J.; Robert, D.; Boulet Simplified Models for the Temperature Dependence of Linewidths at elevated Temperatures and Applications to CO Broadened by Ar and N_2. Journal of Quantitative Spectroscopy and Radiative Transfer 31(1):23-34:1984.

62. Lowry, H. S.; Fisher, C. J. Line Parameter Measurements and Calculations of CO Broadened by H_2O and CO_2 at Elevated Temperatures. Journal of Quantitative Spectroscopy and Radiative Transfer 31(6):575-581(1984).

63. Hanson, R. K.; Varghese, P. L.; Schoenung, S. M.; Falcone, P. K. Absorption Spectroscopy of Combustion Gases Using a Tunable Diode Laser. ACS Symp. Series, 134(Laser Probes Combustion Chemistry) 413-426, 1980.

64. Hanson, R. K. Tunable Diode Laser Measurements in Combustion Gases. Proc. SPIE-Int. Soc. Opt. Eng. 438(Tunable Diode Laser Dev. Spectrosc. Apl.) 75-83, 1983.

65. Malathy-Devi, V.; Fridovich, B.; Jones, G. D.; Snyder, D. G. Diode Laser Measurements of

Strengths, Half-Widths, and Temperature Dependence of Half-Widths for CO_2 Spectral Lines Near 4.2 μm. Journal of Molecular Spectroscopy 105:61-69(1984).

66. Cousin, C.; Le Doucen, R.; Houdeau, J. P.; Boulet, C.; Henry, A. Air Broadened Linewidths, Intensities, and Spectral Line Shapes for CO_2 at 4.3 μm in the Region of the AMTS Instrument. Applied Optics 25(14):2434-2439(1986).

67. Johns, J. W. C. Absolute Intensity and Pressure Broadening Measurements of CO_2 in the 4.3-μm Region. Journal of Molecular Spectroscopy 125:442-464(1987).

68. Johns, J. W. C. High Resolution and the Accurate Measurement of Intensities. Mikrochim. Acta [Wien] III:171-188(1987).

69. Johns, J. W. C. Absolute Intensities in CO2: The 4.3- and 2.7-μm Regions Revisited. Journal of Molecular Spectroscopy 134:433-439(1989).

70. Fridovich, B.; Braun, W. C.; Smith, G. R.; Champion, E. E. Strengths of Single Lines in the $^{12}C^{16}O_2$ ν_3 Band at 4.3 μm. Journal of Molecular Spectroscopy 81:248-255(1980).

71. Chedaille, J.; Braud, Y. Volume 1. Measurements in Flames. London, England, Edward Arnold (Publishers) Limited, 1972:13. Part of series with general editions: Beer, J. M.; Thring, M. W. Industrial Flames. London England, Edward Arnold (Publishers) Limited.

72. Swokowski, E. W. Calculus With Analytic Geometry. Second Edition. Boston, MA, Prindle, Weber & Schmidt, 1979:243.

73. Clay, D. T. *et al.* Fundamental Studies of Black Liquor Combustion. Phase 1, 2 and 3. Report No. 3. DOE/CE/40637-T7, April 1989.

74. Alberty, R. A. Physical Chemistry. 6th Edition. New York, New York, John Wiley & Sons, pp. 436-438, 1983.

75. Allen, H. C.; Cross, P. C. Molecular Vib-Rotors, The Theory and Interpretation of High Resolution Infrared Spectra. New York, New York, John Wiley & Sons, p. 113, 1963.

76. Gray, L. D.; Selvidge, J. E. Relative Intensity Calculations for Carbon Dioxide. Journal of Quantitative Spectroscopy and Radiative Transfer 5:291-301:1965.

77. Rothman, L. S. AFGL Atmospheric Absorption Line Parameters Compilation: 1980 Version. Applied Optics, 20(5):791-795(1981).

78. Haaland, D. M.; Easterling, R. G. Improved Sensitivity of Infrared Spectroscopy by the Application of Least Squares Methods. Applied Spectroscopy 34(5):539-548(1980).

79. Ozisik, M. N. Heat Transfer, A Basic Approach. New York, New York, McGraw-Hill Book Company, 1985:30.

80. O'Neil, P. V. Advanced Engineering Mathematics. Second Edition. Belmont, CA, Wadsworth Publishing Co., 1987:302-312.

81. Fontana, M. G. Corrosion Engineering. 3rd Edition. New York, New York, McGraw-Hill Book Company, p.533, 1986.

82. Cox, A. R. The High Temperature Reactions of CO with Iron, Nickel, and Austenitic Stainless Steel. M.S. Thesis. Atlanta, Georgia, The Georgia Institute of Technology, 1963.

APPENDIX I

FT-IR SPECTROMETER SELECTION

The purchase of a FT-IR spectrometer was one of the first tasks completed for this thesis. The search and selection of an instrument was accomplished by assessing anticipated system requirements and comparing those requirements with available instrumentation. Representatives from each of the major FT-IR spectrometer manufactures were brought to the Institute and interviewed regarding their instruments. Following the interviews, each manufactured presented an instrument package, which they felt best fit our needs. The data from these recommendations was assembled, Table A1-1, and the system which offered the most attractive solution was selected, Laser Precision Analytical.

Table A1-1 Comparison data used to evaluate FT-IR spectrometers for this work. Data presented in this table was supplied by representatives of each of the respective instrument manufacturers.

MANUFACTURER	LPA (LASER PRECISION ANALYTICAL)	DIGILAB	MATTSON	NICOLET
Model	RFX-75	FTS-40	Cygnus 100	20SXC (Demo.)
Base Price	$52,000	$53,000	$40,500	$54,950
System Features				
Resolution	0.125 cm^{-1}	0.1 cm^{-1}	0.125 cm^{-1}	0.5 cm^{-1}
Bearing Type	air	air	Mechanical	Air
Detector	Narrow band MCT	Narrow band MCT	Narrow band MCT	Narrow band MCT
Detector Charge	$0	$5,000	$7,000	$0
Interferometer	Cube Assembly	Plane Mirror	Cube-Corner	Plane Mirror
Source	Water Cooled	Water Cooled	Water Cooled	
Source Charge	$0	$0	$3,000	$0
External Optics				
Demo. Optics	Optibus	Use Coll. Beam	Charge/LPA	Nicolet
Optic Design	Optibus	Digilab	Mattson	Nicolet
Availability	LPA Stock	Digilab/Order	Mattson/Ordr	Stock
Assembly	LPA/IPST	Digilab	Mattson	Nicolet
Charge (Approx.)	$0	$2,000-$4,000	$2,000-$4,000	$0

MANUFACTURER	LPA (LASER PRECISION ANA-LYTICAL)	DIGILAB	MATTSON	NICOLET
Computer				
Processor	80386 32-Bit	68000	68020 32-Bit	620 Super-Mini
Operating System	MS/DOS	IDRIS, UNIX LInk	Unix	Nicolet
Processor Speed	16-20 MHz	12 MHz	16-20 MHz	40 MHz
Quant. Software	Optional	Optional	Standard	Standard
Stand. Equipment	2 MByte Ram	3 MByte Ram	2 MByte Ram	1.28 MByte Ram
	1 Floppy Drive	1 Floppy Drive	1 Flopp Drive	2 Floppy Drives
	50 MByte Hard Drive	26 MByte Hard Drive	Color Graphics	50 Mbyte Hard Drive
	EGA Graphics	Color Graphics	Mouse	Plotter
	Mouse	Plotter		Color Graphics
	Modem			
Add. Equipment				
	Printer/Plotter	68020 32-Bit	86 MByte HD	
			Plotter	
Charge	$2,5000	$4,000	$5,000	$0
Add. Software				
	Multicomp	Quantitative	Kermit	J-Camp
	JCamp-A		JCamp-DX	
Charge	$1,500	$2,000	$800	$700
Optical Bench	Standard	Optional	Optional	Optional
Training Program	3 Days	5 Days	2 Days	5 Days
Char Combustion Demonstration	YES	Limited Optics	Charge	YES
Warranty	1 Year P/L	90 Days P/L 2.5%/ 3 Months	90 Days P/L 12 Months "MOM" 5 Years Bearing	6 Months
Location	California	Massachusetts	Wisconsin	Wisconsin
Delivery Time	8-12 Weeks	8-12 Weeks	6-8 Weeks	8-12 Weeks
Total Cost	**$57,000**	**$67,000**	**$60,100**	**$55,650**

The companies and instruments were evaluated on the following criterion; resolution, bearing type, detector type, interferometer type, external optics, willingness to perform char combustion demonstration, level of assistance with external optics, computer processor, computer operating system, processor speed, quantitative software, data accessibility, multi-tasking potential, standard computer hardware, necessary optional hardware, training pro-

grams, warranty, deliver time, and cost. Before the final decision to purchase the instrument was made, the instrument was demonstrated with conventional samples (at an LPA office in Chicago), second, other LPA customers were contacted and questioned, and finally, the usefulness of the instrument in a combustion environment was proven during a demonstration with the char combustion reactor at their manufacturing facilities (Irvine, CA).

APPENDIX II

INSTRUMENT ALIGNMENT PROCEDURE

A step by step description of the instrument alignment procedure is given below. The instrument alignment should be checked anytime the instrument optical configuration has been altered. After instrument alignment, the resolution of the instrument should be re-measured, as described in the Experimental chapter. If the optical configuration of the instrument is not frequently adjusted, it should not be necessary to perform this alignment very often.

PRELIMINARIES

1. View the background spectrum with no sample cell in place by using the LPA command TSTB (test background). Observe the intensities of the high wavenumber transmittance region. Compare the transmittance between 3500-4400 cm^{-1} with the transmittance between 2500-3500 cm^{-1}.
2. Compare this background with the one printed on page 2-102 of the users manual. Note that there is only a slight decrease in the transmittance of the higher wavenumber region in this background. If the transmittance of the background at the higher wavenumbers is significantly lower than the transmittance between 2500-3500 cm^{-1}, replace the source.
3. If replacing the source has not improved the background shape, contact the LPA service center. They may suggest that the interferometer needs to be realigned.
4. If the background looks good, proceed with the next section.

OPTIBUS® COMPONENT ALIGNMENT

5. Remove all Optibus® tubes from the instrument and detector. Note the directionality of each component, *i.e.,* beam entrance and exit.
6. Attach the first 8" mirror to the laser jig and laser target. The entrance port of the mirror should be attached to the laser jig. The laser target should be attached to the exit port.
7. Turn on laser.
8. Adjust set screws on mirror until the laser strikes the center of the target.
9. Remove laser target and attach 13" hollow Optibus® tube to beam exit of first mirror. Attach laser target to exit of hollow tube.
10. Readjust the mirror screws until the laser strikes the target.

11. Put aperture in place. Adjust aperture position until the laser beam strikes the target unaffected by the aperture. Tighten aperture into position with set screw.
12. Remove laser target and put second 8" mirror on hollow tube. Put laser target on the output of second 8" mirror.
13. Align second 8" mirror.
14. Remove laser target and put on third 8" mirror. Put laser target on the output of third 8" mirror.
15. Align third 8" mirror.
16. Remove laser target and put on hollow 13" Optibus® tube. Put laser target on exit of hollow tube. Realign third 8" mirror.
17. Remove laser target and put fourth 8" mirror on hollow tube. Put laser target on exit of fourth tube.
18. Align fourth 8" mirror.
19. Remove laser target and put flat mirror on the fourth 8" mirror. Put laser target on exit of flat mirror.
19. Align flat mirror.

DETECTOR ALIGNMENT

20. Remove laser jig from first mirror and target from flat mirror. Keeping the optical components together, attach first mirror (end) to interferometer and flat mirror (end) to the detector.
21. Attach oscilloscope to "Alignment" port on the electronics module. Adjust oscilloscope until the interferogram is observed.
22. Adjust mirror stages in the detector until the signal reaching the detector is maximized. Hand-tighten detector to the optical bench.

GAS CELL/REACTOR ALIGNMENT

23. Remove hollow Optibus® tube between the third and fourth 8" mirrors without significantly disrupting the position of the detector. Loosen the clamps between the first mirror and the interferometer, and the flat mirror and the detector.
24. Put cell/reactor in place of tube.
25. Turn on white light from the interferometer, LPA command AQPARM ALIGN=2.
26. Adjust height of Optibus® arm, by pivoting it at the interferometer attachment until the white light strikes the center of the cell/reactor window.
27. Adjust cell/reactor until the white light passes through both windows.
28. Tighten clamp between the first mirror and the interferometer. Support the optical tubes

under the second 8" mirror with an adjustable-height support. Turn off white light, LPA command AQPARM ALIGN=1.

29. Remove the cell/reactor.

30. Reattach oscilloscope to detector output. Adjust the height and position of the detector until the infrared signal is maximized. It is helpful to replace hollow 13" tube to find the approximate detector position. The energy measured on oscilloscope should not be significantly different than that measured earlier when the detector mirrors were adjusted.

31. Tighten the clamp between the flat mirror and the detector.

32. Tighten the detector jack to the optical bench and tighten the detector to the detector jack.

33. Replace cell/reactor. Adjust its position until the infrared signal has been maximized.

APPENDIX III

INSTRUMENT COMMANDS FOR DATA COLLECTION AND SPECTRA CONVERSION

The spectra recorded in this work have all been collected by recording interferograms, backgrounds and samples, and then later transforming and ratioing these separately. This has been done to reduce the data collection time. A standard naming procedure was established to simplify identification of the interferograms. This procedure, as well as, the commands used for data collection and transformation are given below.

Data Acquisition command:

AQIG SPNTEMLT

Where AQIG is the LPA acquire interferogram command, S distinguishes the file as an experimentally derived spectrum instead of a calculated spectrum, PN refers to the last two digits of the notebook page where the spectra are recorded, TEM is the furnace set point temperature (999 was used for a furnace set point temperature of 1000°C), L is the letter of the spectrum which corresponds to the notebook assignment, and T is type of the interferogram, S is used for sample interferograms and B is used for background interferograms.

An example of this notation is given below,

AQIG S38700AS

Here, the spectrum refers to sample A on page 38 (or 138) of the notebook, the furnace set point temperature was 700 degrees and the interferogram was a gas sample (S), not a background (B).

After data collection, a DOS batch file is written to perform the transformations and ratioing. A typical batch file is given below,

(1) IG2SP S38700AS.AIF,TEMP1.ASF,8,4
(2) IG2SP S38700AB.AIF,TEMP2.ASF,8,4
(3) DVDR TEMP1.ASF,TEMP2.ASF,TEMP3.ASF
(4) ABSB TEMP3.ASF,C38700A.ASF
(5) ERASE TEMP1.ASF
(6) ERASE TEMP2.ASF
(7) ERASE TEMP3.ASF

Line (1) and (2) of this batch file convert the interferograms (.AIF) to frequency domain spectra (.ASF) using triangular apodization (LPA code 8) and a zero fill level of 15 zeroes per interferogram point (LPA code 4). The transformed spectra are stored in temporary files TEMP1.ASF and TEMP2.ASF, respectively. Line (3) ratios TEMP1.ASF and TEMP2.ASF and stores the resulting spectrum into TEMP3.ASF. Line (4) converts the spectrum from transmittance into absorption units and stores the resulting spectrum with a recognizable name. Finally, lines (5)-(7) erase the temporary files. Generally, these seven steps were repeated in the same batch file to perform multiple spectra transformations. Additional details regarding the LPA commands are provided in the users manual.

INSTRUMENT COMMANDS FOR SPECTRA CONVERSION

The goal of spectra conversion is to reduce an absorption spectrum to a listing of the peak heights, and corresponding positions, for all the CO and CO_2 absorption lines between 1800 and 2500 cm^{-1}. This listing of peak heights, in the form of an ASCII file, can then be read by another program, Turbo Pascal, to calculate gas temperatures and concentrations. After the data have been collected and transformed, the spectra are extracted, baseline corrects are made, and the peak heights are determined. It is important that the spectra are first baseline corrected, otherwise, inaccurate temperature and concentration calculations will result. The extraction procedure is needed to reduce the spectrum size from 4000 cm^{-1} to 700 cm^{-1}. The baseline correction program can only handle a spectrum of this smaller size.

Spectra Extraction is simply accomplished by the LPA command, EXTRACT, for example,

```
EXTRACT C38700A.ASF,XC38700A.ASF,1800,2500.
```

Where C38700A.ASF is the source file, XC38700A.ASF is the destination file, and the upper and lower limits of the extraction are 2500 and 1800 cm^{-1}, respectively.

Once the spectrum has been reduced to a smaller size, the baseline is corrected. This is accomplished by the LPA command BSLN, for example,

```
BSLN XC38700A.ASF,CC38700A.ASF,A.
```

Here, XC38700A.ASF is the source file name, CC38700A.ASF is the destination file name and A

indicates that the procedure should be performed automatically.

After the base line correction, an ASCII listing of peak maxima and the corresponding wavenumber positions is generated. This is again accomplished automatically by an LPA command, PEAK. A typical use of this command is given below,

```
PEAK CC38700A.ASF,1800,2500,0.025,,E:\TURBO\C38700A.DAT
```

Here, the baseline corrected source file, CC38700A.ASF, is given along with the upper and lower limits of the frequency range 2500 and 1800 cm^{-1}, the minimum peak height, 0.025 absorbance units, and the destination file, C38700A.DAT. The destination file is sent to the sub directory where temperature and concentration calculations are made.

A typical data file is given below (only the first 5 peaks are listed),

```
CC38700A.ASF
1800.00  2499.99  0.0250  0.5000
2050.87    0.0714
2055.39    0.1012
2059.89    0.1412
2064.38    0.1904
2068.83    0.2414
etc . . .
```

The first two lines of the data file, list the source file and peak selection criteria, respectively. Following these lines, the peak maxima and their corresponding positions are listed.

APPENDIX IV

EXPERIMENTALLY OBTAINED TEMPERATURE PROFILES IN THE GAS CELL

Temperature profiles within the gas cell, at various furnace set-point temperatures, have been measured and are presented here. These figures contain the data from two profiling experiments; the first experiment had the thermocouple entering the cell from the front, while in the second the thermocouple entered from the back. The first two data points from each profile have been removed, since the thermocouple measurements were affected by a conduction error.

A least squares routine has been used to fit a second order polynomial equation to each set of experimental data. A linear profile was fit to the data recorded at 373 K. These empirical equations have been used to calculate average gas temperatures for each furnace set point temperature.

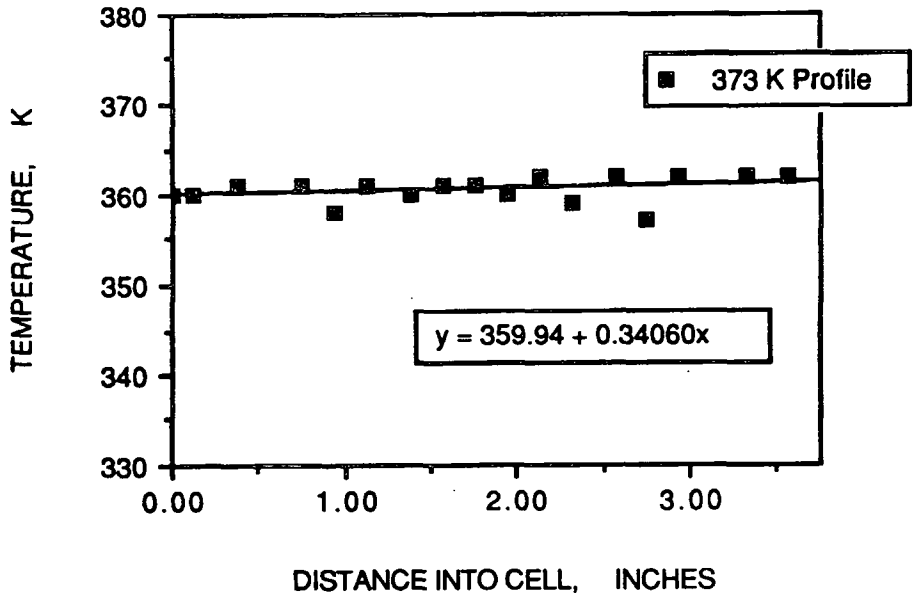

Figure A4-1. Experimentally obtained temperature profile within the gas cell at a furnace set-point temperature of 373 K. Also presented is an empirical fit of the data to a first order polynomial.

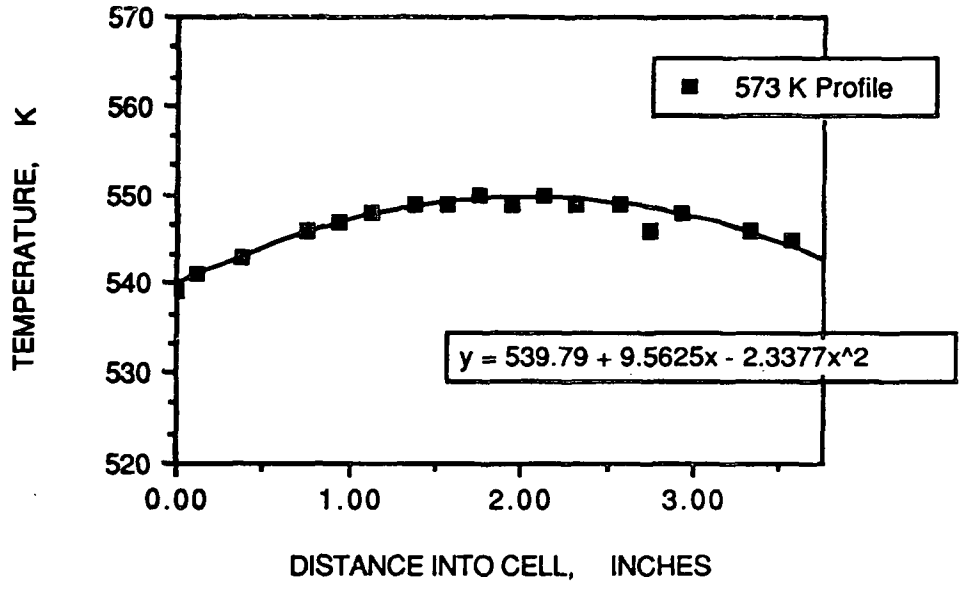

Figure A4-2. Experimentally obtained temperature profile within the gas cell at a furnace set-point temperature of 573 K. Also presented is an empirical fit of the data to a second order polynomial.

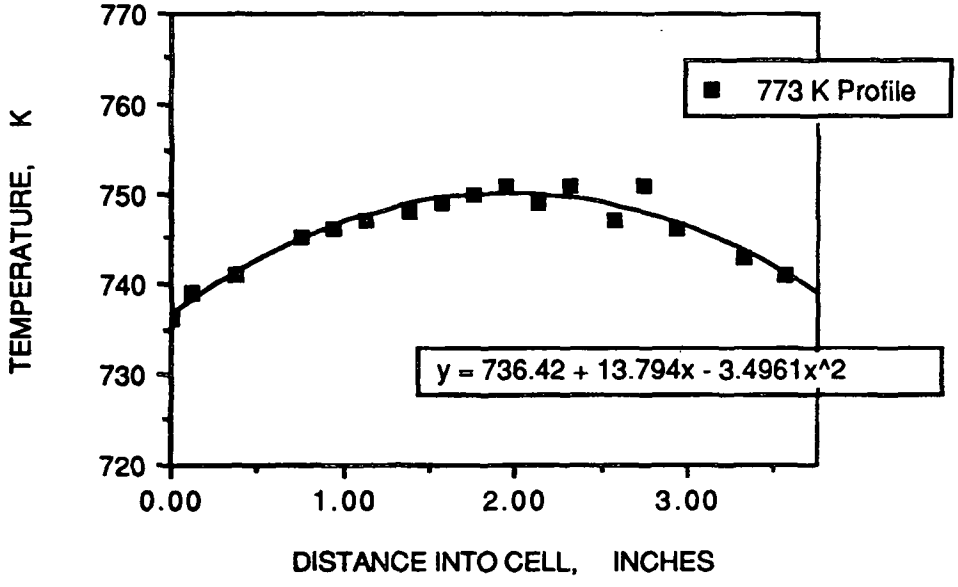

Figure A4-3. Experimentally obtained temperature profile within the gas cell at a furnace set-point temperature of 773 K. Also presented is an empirical fit of the data to a second order polynomial.

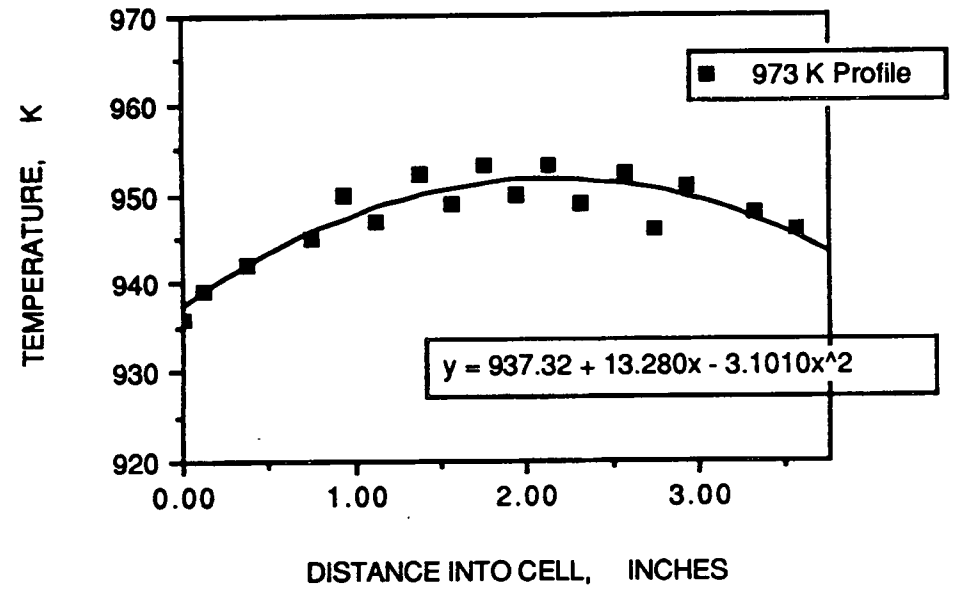

Figure A4-4. Experimentally obtained temperature profile within the gas cell at a furnace set-point temperature of 973 K. Also presented is an empirical fit of the data to a second order polynomial.

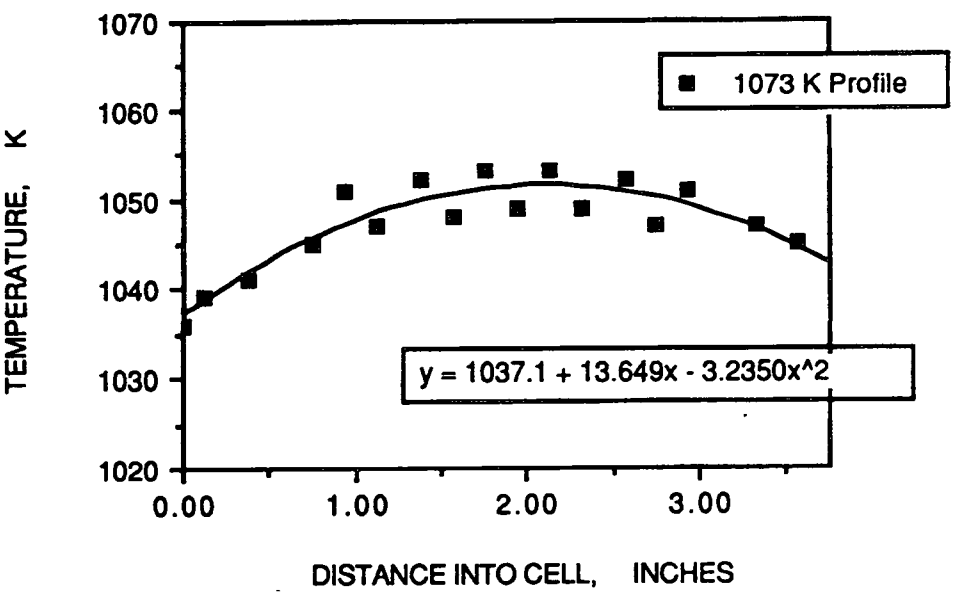

Figure A4-5. Experimentally obtained temperature profile within the gas cell at a furnace set-point temperature of 1073 K. Also presented is an empirical fit of the data to a second order polynomial.

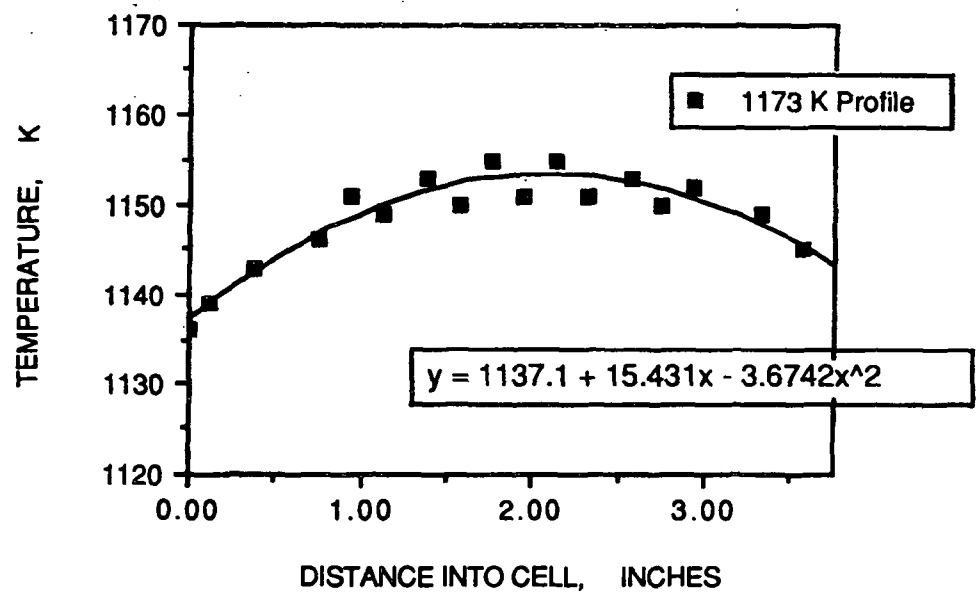

Figure A4-6. Experimentally obtained temperature profile within the gas cell at a furnace set-point temperature of 1173 K. Also presented is an empirical fit of the data to a second order polynomial.

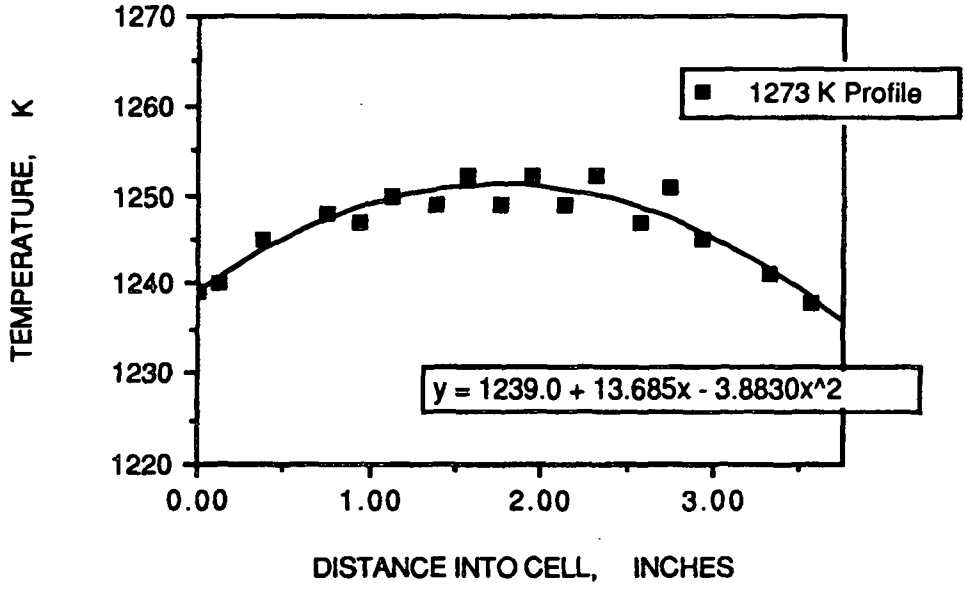

Figure A4-7. Experimentally obtained temperature profile within the gas cell at a furnace set-point temperature of 1273 K. Also presented is an empirical fit of the data to a second order polynomial.

APPENDIX V

HEAT TRANSFER CALCULATIONS IN THE GAS CELL

A mathematical description of the temperature profile expected within the gas cell is presented. The dominant mode of heat transfer to the gas is by conduction; the gas is in contact with the heated stainless steel walls. Nitrogen, the major species within the gas cell does not significantly absorb infrared radiation, eliminating radiation as a means of heat transfer to the gas. Thermocouple experimentation has shown that the cylinder wall temperature is hotter than the end caps.

The mathematical description of the heat transfer to the gas begins with the assignment of a coordinate system, illustrated below.

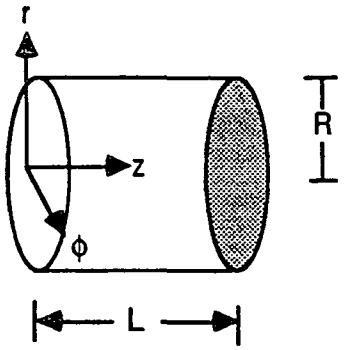

Figure A5-1. Coordinate system for heat transfer calculations.

The equation for three dimensional heat transfer by conduction is given by,[79]

$$\frac{1}{r}\cdot\frac{\delta}{\delta r}\left(r\cdot\frac{\delta T}{\delta r}\right)+\frac{1}{r^2}\cdot\frac{\delta^2 T}{\delta\phi^2}+\frac{\delta^2 T}{\delta z^2}+\frac{g}{k}=\frac{1}{\alpha}\cdot\frac{\delta T}{\delta t} \qquad \text{(A5-1)}$$

where g is heat generated, t is time, and α is the thermal diffusivity. If it is assumed that there is no variation of temperature in the ϕ-direction, and if there is no heat generated (g =

0), and if the process is assumed to be at steady state, Equation A5-1 reduces to,

$$\frac{1}{r}\cdot\frac{\delta}{\delta r}\left(r\cdot\frac{\delta T}{\delta r}\right)+\frac{\delta^2 T}{\delta z^2}=0 \qquad \text{(A5-2)}$$

with boundary conditions $T(r,0) = T_o$, $T(r,L) = T_o$, $T(R,z) = T_1$ and $T(r,z)|_{r=0}$ = finite, where T_o and T_1 are the end cap and cell wall temperatures, respectively.

This second order differential equation can be solved analytically by using the separation of variables technique. Assume that the temperature, T(r,z), can be described by, $\theta(r,z)$, where,

$$\theta(r,z) = \Psi(r)\cdot\Gamma(z) \qquad \text{(A5-3)}$$

and $\theta(r,z) = T(r,z) - T_o$. After the variable change, Equation A5-2 becomes,

$$\frac{1}{r\cdot\Psi(r)}\cdot\left[\frac{\delta\Psi(r)}{\delta r}+r\cdot\frac{\delta^2\Psi(r)}{\delta r^2}\right]+\frac{1}{\Gamma(z)}\cdot\frac{\delta^2\Gamma(z)}{\delta z^2}=0 \qquad \text{(A5-4)}$$

Equation A5-4 is set equal to a constant, λ^2, and like terms are separated resulting in the formation of two second order differential equations. The boundary conditions are modified to account for the variable change. The two differential equations are solved resulting in equations for $\Psi(r)$ and $\Gamma(z)$, which are substituted back into Equation A5-3. The equation for T(r,z) is then obtained from, $\theta(r,z)$, by the relationship $T(r,z) = \theta(r,z) + T_o$,

$$T(r,z) = To + \sum_{n=1}^{\infty}\frac{2}{n\pi}\cdot(T_1 - T_o)\cdot(1 - \cos(n\pi))\cdot\sin(\lambda_n z)\cdot\frac{I_o(\lambda_n r)}{I_o(\lambda_n R)} \qquad \text{(A5-5)}$$

where I_o is a modified Bessel function of the first kind of order zero[80] and $\lambda_n = \frac{n\cdot\pi}{L}$. Equation A5-5 gives the temperature at any point in the gas cell when T_o and T_1 are known. A

Pascal program was written to solve this equation for eleven different values across the cell, along the z direction, at r = 0. The theoretical temperature profile was calculated for one experiment, where the end cap and cell wall temperatures were recorded at a furnace set point temperature of 1273 K. At this temperature, T_o was 1239 K and T_1 was 1258 K. Using Equation A5-5, the temperatures along the center of the cylinder at various distances from the end caps were calculated; the results are given below.

Table A5-1. Table of calculated gas temperatures at various positions along the center line of the gas cell using Equation A4-5 and assuming T_o = 1239 and T_1 = 1258.

Distance into Cell (in.)	Gas Temperature (K)
0	1239.0
0.375	1243.4
0.750	1247.3
1.125	1250.1
1.500	1251.8
1.875	1252.3
2.250	1251.8
2.625	1250.1
3.000	1247.3
3.375	1243.4
3.750	1239.0

A comparison of these theoretically predicted values with an experimentally obtained temperature profile in given in the Experimental section of this report.

APPENDIX VI

PASCAL CODE FOR PEAK CORRECTIONS AND GAS TEMPERATURE AND CONCENTRATION DETERMINATIONS

```
Program SpecAnal;

{ ********************************************************************************************************************** }
{ *****                                                                                                            ***** }
{ *****    The Pascal program SpecAnal.pas is written to convert experimental Carbon Monoxide and                 ***** }
{ *****    Carbon Dioxide FT-IR absorption data into gas temperature and concentration information.               ***** }
{ *****    The program accomplishes this object by the following:                                                ***** }
{ *****                                                                                                            ***** }
{ *****       1.  The computation environment is initialized.                                                     ***** }
{ *****       2.  The user supplies general information including:                                                ***** }
{ *****            a.  Program operation single or multiple file?                                                 ***** }
{ *****            b.  Perform CO Concentration Calculations?                                                     ***** }
{ *****            c.  Perform CO2 Concentration Calculations?                                                    ***** }
{ *****       3.  The variables needed throughout the program are then initialized.                               ***** }
{ *****       4.  Additional information is then obtained from the user, including:                               ***** }
{ *****            a.  Data and output file names.                                                                ***** }
{ *****            b.  Instrument resolution.                                                                     ***** }
{ *****            c.  Initial temperature estimation.                                                            ***** }
{ *****            d.  CO, CO2 and N2 partial pressures (known values or estimates).                              ***** }
{ *****            e.  Total pressure.                                                                            ***** }
{ *****            f.  Level of calculation accuracy.                                                             ***** }
{ *****            g.  Calculate line strengths or partial pressures?                                             ***** }
{ *****            h.  Specific CO lines to be used.                                                              ***** }
{ *****            i.  Specific CO2 lines to be used.                                                             ***** }
{ *****       5.  The input and output files are then initialized.                                                ***** }
{ *****       6.  The CO and CO2 lines in the data file are identified and the corresponding                      ***** }
{ *****           spectroscopic data is initialized.                                                              ***** }
{ *****       7.  Photometric error corrections are performed.                                                    ***** }
{ *****       8.  Gas temperature calculations are performed.                                                     ***** }
{ *****       9.  CO/CO2 concentration or line strength calculations are performed.                               ***** }
{ *****       10. Temperature difference between calculated temperatures and estimated                            ***** }
{ *****           temperatures determined.                                                                        ***** }
{ *****       11. Additional temperature and concentration iterations performed.                                  ***** }
{ *****       12. If in single file mode, results plotted to screen and written to a output file.                 ***** }
{ *****       13. If in batch mode, results written to file; next file analyzed.                                  ***** }
{ *****                                                                                                            ***** }
{ ********************************************************************************************************************** }


{$N+}   { Setting for double precision }
{$I+}   { Disable I/O error trapping }
{$R+}   { Enable Range Checking }


Uses
    Dos, Crt, GDriver, GKernel, SpAnData, SpAnUser,
    GShell, GlobVar, COConc, CO2Conc, PeakCor, TempCalc, Output, OverLap;

{  The uses statement links this program with other Turbo Pascal units.  Some of these are standard Turbo  }
{  Pascal units (Dos, Crt, GDriver, GKernel, and GShell).  Others have been written specifically for this  }
{  work (SpAnData, SpAnUser, GlobVar, COConc, CO2Conc, PeakCor, TempCalc, and Output).                      }


begin       { Program Temp.pas }

    ClrScr;

{  User is asked if the program will be operated in single or multiple file mode and if CO and CO2 gas }
{  concentrations should be performed.                                                                  }
```

```
    Writeln('Do you wish to operate in Single File (S) or Multiple File (M) mode.');
    Readln(Mode);
    Mode := Upcase(mode);
    Writeln;
    Writeln('In addition to gas temperatures, do you also want...');
    Writeln('CO concentration calculations? (Yes = Y, No = N)');
    Readln(YesNoCOConcCalc);
    YesNoCOConcCalc := Upcase(YesNoCOConcCalc);
    Writeln('CO2 concentration calculations? (Yes = Y, No = N)');
    Readln(YesNoCO2ConcCalc);
    YesNoCO2ConcCalc := Upcase(YesNoCO2ConcCalc);

{  If operating in single file mode continue here.  }

    If Mode = 'S' Then
        begin

{  Initialize global variables, call to GlobVar unit.   }

        Initialize;

        InitialTemperatureGuess := 0;
        InstRes := 0;
        PathLength := 0;
        MValueRangeHigh := 0;
        MValueRangeLow := 0;
        MValueRangeHighCO2 := 0;
        MValueRangeLowCO2 := 0;
        TemperatureIterationTolerance := 0;
        NumResultsCO := 0;
        NumResultsCO2 := 0;
        AddOne := 1;
        repeat
            MExclude[AddOne] := 0;
            MExcludeCO2[AddOne] := 0;
            MExcludeII[AddOne] := 0;
            MExcludeIICO2[AddOne] := 0;
            AddOne := AddOne + 1;
        until AddOne = 31;

        ClrScr;

{  Get additional information from the user, call to SpAnUser unit.  }

        GetUserData;

{  Clear lines which should be excluded from the calculations.  }

        AddOne := 1;
        repeat
            MExclude[AddOne] := MExcludeII[AddOne];
            MExcludeCO2[AddOne] := MExcludeIICO2[AddOne];
            AddOne := AddOne + 1;
        until AddOne = 31;
{  Initialize input and output files.  }
        Assign(DataFile,DataFileName);
        Reset(DataFile);
        Assign(OutputFile,OutputFileName);
        Rewrite(OutputFile);

{  Find CO and CO2 lines from data file, assign spectroscopic information, call to SpAnData unit.  }

        GetLineInformation;

        TG := InitialTemperatureGuess;
        ResultsCount := 1;
        repeat
            Writeln('Begin iteration number ',ResultsCount);
            TemperatureDifference := 0;
```

```
{  Make photometric error corrections, call to PeakCor unit.  }
              CorrectOverlap;
              FindAtpeaks;

{  Make Temperature calculations, call to TempCalc.  }

              TemperatureCalculations;
              TemperatureDifference := Abs(TG-TemperatureResults[ResultsCount]);

{  Print results to screen.  }

              Writeln(OutputFile,'Iteration Number = ',ResultsCount);
              Writeln(OutputFile,'Temperature Guess = ',TG:7:2);
              Writeln(OutputFile,'Calculated Temperature = ',TemperatureResults[ResultsCount]:7:2);
              Writeln(OutputFile,'Standard Deviation = ',StandardDeviationResults[ResultsCount]:10:5);
              Writeln(OutputFile,'Variance = ',VarianceResults[ResultsCount]:10:5);
              Writeln(OutputFile,'Standard Error of Line = ',StandardErrorTemperature[ResultsCount]:8:4);
              Writeln(OutputFile,'PPCOGuess = ',PPCOGuess:7:3);
              Writeln(OutputFile,'PPCO2Guess = ',PPCO2Guess:7:3);
              Writeln(OutputFile,'PPN2 = ',PPN2:7:3);
              Writeln(OutputFile,' ');
              Writeln('Iteration Number = ',ResultsCount);
              Writeln('Temperature Guess = ',TG:7:2);
              Writeln('Calculated Temperature = ',TemperatureResults[ResultsCount]:7:2);
              Writeln('Standard Deviation = ',StandardDeviationResults[ResultsCount]:10:5);
              Writeln('Variance = ',VarianceResults[ResultsCount]:10:5);
              Writeln('Standard Error of Line = ',StandardErrorTemperature[ResultsCount]:8:4);
              Writeln('PPCOGuess = ',PPCOGuess:7:3);
              Writeln('PPCO2Guess = ',PPCO2Guess:7:3);
              Writeln('PPN2 = ',PPN2:7:3);

              If YesNoCOConcCalc = 'Y' Then
              Begin
                   If (CalculationChoice = 'S') Then

{  Perform CO concentration/line strength calculations, call to COCalc unit.  }

                   COConcentrationCalculations;
                   If (CalculationChoice = 'P') and (TG > 285) and (TG < 1260) Then
                   begin
                        COConcentrationCalculations;
                        PPCOGuess := AverageCOConcentration;
                   end;
              end;

              If YesNoCO2ConcCalc = 'Y' Then
              Begin
                   If (CalculationChoiceCO2 = 'S') Then

{  Perform CO2 concentration/line strength calculations, call to CO2Calc unit.  }

                   CO2ConcentrationCalculations;
                   If (CalculationChoiceCO2 = 'P') and (TG > 285) and (TG < 1260) Then
                   begin
                        CO2ConcentrationCalculations;
                        PPCO2Guess := AverageCO2Concentration;
                   end;
              end;

              PPN2 := TotPress - PPCOGuess - PPCO2Guess;
              TG := TemperatureResults[ResultsCount];
              ResultsCount := ResultsCount + 1;

         until TemperatureDifference < TemperatureIterationTolerance;

{  Plot results to screen.  }

         InitGraphic;
         ClearScreen;
         SetColorWhite;
         SetBackground(0);
```

```
          DefineHeader(1, 'Temperature Curve');
          SetHeaderOn;
          DefineWorld(1,0,-18,4000,-8);
          SelectWindow(1);
          SelectWorld(1);
          DrawBorder;
          DrawAxis(8,-7,0,0,0,0,0,0,false);
          DrawPolygon(TempPlot,1,40,4,1,0);
          repeat until KeyPressed;    { Wait until a key is pressed }
          LeaveGraphic;

{  Write results to output file.  }

          ResultsCount := 0;
          Writeln(OutputFile);
          Writeln(OutputFile,DataFileName);
          Writeln(OutputFile);

          OutputResults;

          Writeln('The temperature calculated from the absorption lines = ',TG:7:2);

          Close(DataFile);
          Close(OutputFile);

     End

{  If operating in batch mode continue here.  }

     Else
          begin

{  Initialize global variables.  }

          InitialTemperatureGuess := 0;
          InstRes := 0;
          PathLength := 0;
          MValueRangeHigh := 0;
          MValueRangeLow := 0;
          MValueRangeHighCO2 := 0;
          MValueRangeLowCO2 := 0;
          TemperatureIterationTolerance := 0;
          AddOne := 1;
          repeat
               MExclude[AddOne] := 0;
               MExcludeII[AddOne] := 0;
               MExcludeCO2[AddOne] := 0;
               MExcludeIICO2[AddOne] := 0;
               DataFileNameBatch[AddOne] := '00000000.000';
               OutputFileNameBatch[AddOne] := '00000000.000';
               PPCOBatch[AddOne] := 0;
               PPN2Batch[AddOne] :=0;
               TotalPressureBatch[AddOne] := 0;
               InitialTemperatureGuessBatch[AddOne] := 0;
               NumResultsCO := 0;
               NumResultsCO2 := 0;
               AddOne := AddOne + 1;
          until AddOne = 31;

          BatchIteration := 1;

          ClrScr;

{  Get additional information from the user, call to SpAnUser unit.  }

          GetUserDataBatch;

{  Clear lines which should be excluded from the calculations.  }

          AddOne := 1;
          repeat
```

```
            MExclude[AddOne] := MExcludeII[AddOne];
            MExcludeCO2[AddOne] := MExcludeIICO2[AddOne];
            AddOne := AddOne + 1;
        until AddOne = 31;

        repeat

{  Initialize global variables, call to GlobVar unit.  }

            Initialize;

{  Initialize input and output files.  }

            Assign(DataFile,DataFileNameBatch[BatchIteration]);
            Reset(DataFile);
            Assign(OutputFile,OutputFileNameBatch[BatchIteration]);
            Rewrite(OutputFile);

{  Initialize partial pressures and gas temperature for first iterations.  }

            PPCOGuess := PPCOBatch[BatchIteration];
            PPCO2Guess := PPCO2Batch[BatchIteration];
            PPN2 := PPN2Batch[BatchIteration];
            TotPress := TotalPressureBatch[BatchIteration];
            InitialTemperatureGuess := InitialTemperatureGuessBatch[BatchIteration];

            GetLineInformation;

            TG := InitialTemperatureGuess;
            ResultsCount := 1;
            repeat
                Writeln('Begin iteration number ',ResultsCount);
                TemperatureDifference := 0;

{  Make photometric error corrections, call to PeakCor unit.  }

                CorrectOverlap;
                FindAtpeaks;

{  Make temperature calculations, call to TempCalc.  }

                TemperatureCalculations;
                TemperatureDifference := Abs(TG-TemperatureResults[ResultsCount]);

{  Print results to screen.  }

                Writeln(OutputFile,'Iteration Number = ',ResultsCount);
                Writeln(OutputFile,'Temperature Guess = ',TG:7:2);
                Writeln(OutputFile,'Calculated Temperature = ',TemperatureResults[ResultsCount]:7:2);
                Writeln(OutputFile,'Standard Deviation = ',StandardDeviationResults[ResultsCount]:10:5);
                Writeln(OutputFile,'Variance = ',VarianceResults[ResultsCount]:10:5);
                Writeln(OutputFile,'Standard Error of Line =
',StandardErrorTemperature[ResultsCount]:8:4);
                Writeln(OutputFile,'PPCOGuess = ',PPCOGuess:7:3);
                Writeln(OutputFile,'PPCO2Guess = ',PPCO2Guess:7:3);
                Writeln(OutputFile,'PPN2 = ',PPN2:7:3);
                Writeln(OutputFile,' ');
                Writeln('File Number  ',BatchIteration,'  of  ',BatchSize);
                Writeln('Iteration Number = ',ResultsCount);
                Writeln('Temperature Guess = ',TG:7:2);
                Writeln('Calculated Temperature = ',TemperatureResults[ResultsCount]:7:2);
                Writeln('Standard Deviation = ',StandardDeviationResults[ResultsCount]:10:5);
                Writeln('Variance = ',VarianceResults[ResultsCount]:10:5);
                Writeln('Standard Error of Line = ',StandardErrorTemperature[ResultsCount]:8:4);
                Writeln('PPCOGuess = ',PPCOGuess:7:3);
                Writeln('PPCO2Guess = ',PPCO2Guess:7:3);
                Writeln('PPN2 = ',PPN2:7:3);

                If YesNoCOConcCalc = 'Y' Then
                Begin
                    If (CalculationChoice = 'S') Then
```

```
{  Perform CO concentration/line strength calculations, call to COCalc unit.  }

                        COConcentrationCalculations;
                        If (CalculationChoice = 'P') and (TG > 285) and (TG < 1260) Then
                        begin
                             COConcentrationCalculations;
                             PPCOGuess := AverageCOConcentration;
                        end;
                   end;

                   If YesNoCO2ConcCalc = 'Y' Then
                   Begin
                        If (CalculationChoiceCO2 = 'S') Then

{  Perform CO2 concentration/line strength calculations.  }

                        CO2ConcentrationCalculations;
                        If (CalculationChoiceCO2 = 'P') and (TG > 285) and (TG < 1260) Then
                        begin
                             CO2ConcentrationCalculations;
                             PPCO2Guess := AverageCO2Concentration;
                        end;
                   end;

                   PPN2 := TotPress - PPCOGuess - PPCO2Guess;
                   TG := TemperatureResults[ResultsCount];
                   ResultsCount := ResultsCount + 1;

              until TemperatureDifference < TemperatureIterationTolerance;

{  Write results to output file.  }

          ResultsCount := 0;
          Writeln(OutputFile);
          Writeln(OutputFile,DataFileNameBatch[BatchIteration]);
          Writeln(OutputFile);

          OutputResults;

          Close(DataFile);
          Close(OutputFile);

          BatchIteration := BatchIteration + 1;

          until BatchIteration = BatchSize + 1;

     End;

End.   { Program Temp.pas }
```

```
unit GlobVar;

{$I Float.inc }

Interface
    Uses      Dos, Crt, GDriver, GKernel, Integrat,
              Interp, LeastSqr, Common, GShell;

    {$IFOPT N+}
         type
              Float = Double;
    {$ELSE}
         type
              Float = Real;
    {$ENDIF}

    Type

{  Use Type statement to define various variable types.  }

         Batch = Array[1..30] of Float;
         BatchName = Array[1..30] of String[12];
         Exclude = Array[1..30] of Integer;
         ExcludeII = Array[1..30] of Integer;
         LineDataInteger = Array[-38..38] of Integer;
         LineDataFloat = Array[-38..38] of Float;
         LineDataIntegerCO2 = Array[1..100] of Integer;
         LineDataFloatCO2 = Array[1..100] of Float;
         Results = Array[1..100] of Float;
         StrLength12 = String[12];
         {Float = Double, variable precision established in the include file Float.inc }
         {TNVector = Array [0..50] of Float; defined in Interp.pas}
         {TNRowVector = Array [1..6] of Float; Defined in LeastSqr.pas}
         {TNColumnVector = Array [1..100] of Float; Defined in Least Sqr.pas}
         {FitType = text, (Expo,Fourier,Log,Poly,Power,User), defined in LeastSqr}

{  Define Variables.  }

    Var

         AddOne : Integer;
         Atpeak : LineDataFloat;
         AtpeakCO2 : LineDataFloatCO2;
         AtpeakGuess : Float;
         AverageCOConcentration : Float;
         AverageCO2Concentration : Float;
         AveragePercentCO : Float;
         AveragePercentCO2 : Float;
         BatchIteration : Integer;
         BatchSize : Integer;
         CalculationChoice : Char;
         CalculationChoiceCO2 : Char;
         COCOWidthLT : LineDataFloat;
         CON2WidthLT : LineDataFloat;
         CON2WidthHT : LineDataFloat;
         COCO2WidthHT : LineDataFloat;
         CO2CO2Width : LineDataFloatCO2;
         CO2N2Width : LineDataFloatCO2;
         CorLineHeightCO2 : LineDataFloatCO2;
         DataFile : Text;
         DataFileName : StrLength12;
         DataFileNameBatch : BatchName;
         Energy : LineDataFloat;
         E : LineDataFloat;
         HerWalCor : Float;
         Height : Float;
         InitialTemperatureGuess : Float;
         InitialTemperatureGuessBatch : Batch;
         InstRes : Float;
         LineHeight : LineDataFloat;
         LineHeightCO2 : LineDataFloatCO2;
```

```
        LineNumber : Integer;
        LinePosition : LineDataFloat;
        LinePositionCO2 : LineDataFloatCO2;
        LineStrength : LineDataFloat;
        LineStrengthCO2 : LineDataFloatCO2;
        LnPeak : LineDataFloat;
        MExclude : Exclude;
        MExcludeCO2 : Exclude;
        MExcludeII : ExcludeII;
        MExcludeIICO2 : ExcludeII;
        Mode : Char;
        MValue : LineDataInteger;
        MValueCO2 : LineDataIntegerCO2;
        MValueRangeHigh : Integer;
        MValueRangeHighCO2 : Integer;
        MValueRangeLow : Integer;
        MValueRangeLowCO2 : Integer;
        NCOCO2 : LineDataFloat;
        NCON2 : LineDataFloat;
        NCO2CO2 : LineDataFloatCO2;
        NCO2N2 : LineDataFloatCO2;
        NumResultsCO : Integer;
        NumResultsCO2 : Integer;
        OutputFile : Text;
        OutputFileName : StrLength12;
        OutputFileNameBatch : BatchName;
        PathLength : Float;
        PeakSep : Float;
        PPCOGuess : Float;
        PPCO2Guess : Float;
        PPCOBatch : Batch;
        PPCO2Batch : Batch;
        PPCOCalc : LineDataFloat;
        PPCO2Calc : LineDataFloatCO2;
        PeakSepLow : LineDataFloatCO2;
        PeakSepHigh : LineDataFloatCO2;
        PPN2 : Float;
        PPN2Batch : Batch;
        ResParameter : Float;
        ResultsCount : Integer;
        S297 : LineDataFloat;
        Slope : Float;
        StandardDeviationResults : Results;
        StandardDeviationCO : Float;
        StandardDeviationCO2 : Float;
        StandardErrorTemperature : Results;
        TG : Float;
        TemperatureIterationTolerance : Float;
        TemperatureDifference : Float;
        TemperatureResults : Results;
        TempPlot : PlotArray;
        TotPress : Float;
        TotalPressureBatch : Batch;
        TrueLinePosition : LineDataFloat;
        TrueLinePositionCO2 : LineDataFloatCO2;
        VarianceResults : Results;
        W : Float;
        YesNoCOConcCalc : Char;
        YesNoCO2ConcCalc : Char;
        YIntercept : Float;

    Procedure Initialize;

Implementation

    Procedure Initialize;   { Initialize global variables }

    Var
        LoopCount : Integer;

        begin
```

```
          AtpeakGuess := 0;
          AverageCOConcentration := 0;
          AverageCO2Concentration := 0;
          DataFileName := '00000000.000';
          HerWalCor := 0;
          LineNumber := 0;
          OutputFileName := '00000000.000';
          PPCOGuess := 0;
          PPCO2Guess := 0;
          PPN2 := 0;
          Slope := 0;
          ResParameter := 0;
          ResultsCount := 0;
          TemperatureDifference := 0;
          TG := 0;
          TotPress := 0;
          YIntercept := 0;
          LoopCount := -38;
               repeat
                    Atpeak[LoopCount] := 0;
                    COCOWidthLT[LoopCount] := 0;
                    CON2WidthLT[LoopCount] := 0;
                    CON2WidthHT[LoopCount] := 0;
                    COCO2WidthHT[LoopCount] := 0;
                    Energy[LoopCount] := 0;
                    LnPeak[LoopCount] := 0;
                    LineHeight[LoopCount] := 0;
                    LinePosition[LoopCount] := 0;
                    MValue[LoopCount] := 0;
                    NCOCO2[LoopCount] := 0;
                    NCON2[LoopCount] := 0;
                    TrueLinePosition[LoopCount] := 0;
                    LoopCount := LoopCount + 1;
               until LoopCount = 39;
          LoopCount := 1;
               repeat
                    StandardDeviationResults[LoopCount] := 0;
                    StandardErrorTemperature[LoopCount] := 0;
                    TemperatureResults[LoopCount] := 0;
                    VarianceResults[LoopCount] := 0;
                    MValueCO2[LoopCount] := 0;
                    CorLineHeightCO2[LoopCount] := 0;
                    PeakSepLow[LoopCount] := 0;
                    PeakSepHigh[LoopCount] := 0;
                    LineHeightCO2[LoopCount] := 0;
                    LinePositionCO2[LoopCount] := 0;
                    TrueLinePositionCO2[LoopCount] := 0;
                    CO2CO2Width[LoopCount] := 0;
                    CO2N2Width[LoopCount] := 0;
                    NCO2CO2[LoopCount] := 0;
                    NCO2N2[LoopCount] := 0;
                    AtpeakCO2[LoopCount] := 0;
                    LoopCount := LoopCount + 1;
               until LoopCount = 101;


     End;  {Procedure Initialize}

End.
```

```
unit SpAnUser;

{$I Float.inc}


Interface
        Uses  Dos, Crt, Common, GlobVar;


         {$IFOPT N+}
                 type
                    Float = Double;
         {$Else}
                type
                    Float = Real;
         {$ENDIF}

Procedure GetUserData;

Procedure GetUserDataBatch;

Implementation

Procedure GetUserData;

{ Procedure written to get information regarding the name of the data file containing the spectra   }
{ information, the name of the file to write the results, the partial pressure of CO in the gas     }
{ sample, the partial pressure of nitrogen in the gas sample, the total pressure of the gas sample, }
{ the nominal resolution of the FT-IR, the initial guess for the first iteration of the temperature }
{ calculations, the desired accuracy of the final temperature calculations, the range of m indexes  }
{ which should be included in the temperature and concentration calculations, and the indexes of    }
{ lines (if any) which should be excluded from temperature and concentration calculations.          }

    Var
         LoopCount : Integer;


    begin

{ Get name of file containing spectral data. }

         ClrScr;
         Writeln;
         Writeln('Data File Specifications' );
         Writeln;
              repeat
                   Writeln('Type the name of the Data File (include the .dat extention).' );
                   Readln(DataFileName);
                   IOCheck;          { Checks to make certain that inputed name of DataFileName   }
              until not IOerr;       { is of type StrLength.                                      }

{ Get name for the output file. }

         Writeln;
              repeat
                   Writeln('Type the desired name for the output file (include the .csv extension).' );
                   Readln(OutputFileName);
                   IOcheck;          { Checks to make certain that inputed name of OutputFileName }
              until not IOerr;       { is of type StrLength.                                      }

{ Get information regarding the experimental conditions. }

         ClrScr;
         Writeln('Experimental Conditions');
         Writeln;
              repeat
                   Writeln('Input the nominal instrument resolution.');
                   Readln(InstRes);
                   IOcheck;          { Checks to make certain that inputed resolution data is of  }
              until not IOerr;       { type Float.                                                }
```

```
{ Get the path length of the gas cell or reactor. }

        Writeln;
        Writeln;
             repeat
                  Writeln('Input the Path Length of the Gas Cell or Reactor (cm).');
                  Readln(PathLength);
                  IOcheck;         { Checks to make certain that inputed path length data is of  }
             until not IOerr;      { type Float.                                                 }

{ Get the partial pressure of CO recorded on the day of the experiment. }

        Writeln;
             repeat
                  Writeln('Input the partial pressure (TORR) of CO in the gas sample.');
                  Readln(PPCOGuess);
                  IOcheck;         { Checks to make certain that inputed partial pressure is }
             until not IOerr;      { of type Float.                                          }

{ Get the partial pressure of CO2 recorded on the day of the experiment. }

        Writeln;
             repeat
                  Writeln('Input the partial pressure (TORR) of CO2 in the gas sample.');
                  Readln(PPCO2Guess);
                  IOcheck;         { Checks to make certain that inputed partial pressure is }
             until not IOerr;      { of type Float.                                          }

{ Get the partial pressure of N2 recorded on the day of the experiment. }

        Writeln;
             repeat
                  Writeln('Input the partial pressure (TORR) of N2 in the gas sample.');
                  Readln(PPN2);
                  IOcheck;         { Checks to make certain that inputed partial pressure is }
             until not IOerr;      { of type Float.

{ Get the total pressure of the gas sample recorded on the day of the experiment. }

        Writeln;
             repeat
                  Writeln('Input the total pressure (TORR) of the gas sample.');
                  Readln(TotPress);
                  IOcheck;         { Checks to make certain that inputed pressure is }
             until not IOerr;      { of type Float.

{ Get information regarding the absorption lines which should be included in the temperature calculations. }

        ClrScr;
        Writeln('Specification of the CO lines (m indexes) to be included in');
        Writeln('the calculations to determine the gas phase temperature');
        Writeln('and CO gas concentration, (acceptable range -36 to -1).');
        Writeln;
        repeat

{ Specify the lower limit of the m index range to be searched. }
                  repeat
                       Writeln('Input lower m index (include negative sign)' );
                       Readln(MValueRangeLow);
                       IOcheck;     { Check to make certain that inputed value for }
                  until not IOerr;  { the lower m index is of type Integer.        }
                  Writeln;
{ Specify the upper limit of the m index range to be searched. }
                  repeat
                       Writeln('Input upper m index (include negative sign if appropriate)' );
                       Readln(MValueRangeHigh);
                       IOcheck;     { Check to make certain that inputed value for }
                  until not IOerr;  { the upper m index is of type Integer.        }

{ Check if the value for MValueRangeLow is smaller than the value inputed for MValueRangeHigh. }
                  if MValueRangeLow >= MValueRangeHigh Then
```

```
                    begin
                         Writeln;
                         Writeln('The lower m index must be less than the upper m index');
                         Writeln('and the two can also not be equal to each other.');
                         Writeln;
                    end;

          until MValueRangeLow < MValueRangeHigh;

{ Read any m indexes which should be excluded from the temperature calculations. }
          ClrScr;
          Writeln('Specify any lines (m indexes) within the range of indexes selected');
          Writeln('which should be excluded from temperature calculations.');
          Writeln;
          Writeln('Type in the m index of any line which should be excluded');
          Writeln('Type one index per line, followed by a <enter> (Maximum of 30 lines)');
          Writeln('When finished inputing indexes to be excluded, type "0" and <enter>');
          Writeln('If no lines are to be excluded simply type "0" and <enter> now');
          LoopCount := 0;
          repeat
               LoopCount := LoopCount + 1;
               repeat
                    Readln(MExcludeII[LoopCount]);
                    IOcheck;      { Checks to make certain that the inputed value for }
               until not IOerr;   { MExclude[LoopCount] is of type integer.           }
          until MExcludeII[LoopCount] = 0;


{ Get information regarding the initial temperature guess. }

               ClrScr;
               Writeln;
               Writeln('Input information regarding initial temperature');
               Writeln('guess and desired calculation accuracy.');
               Writeln;
               repeat
                    Writeln('Input initial temperature guess.' );
                    Readln(InitialTemperatureGuess);
                    IOcheck;     { Check to make certain that inputed value for the temperature }
               until not IOerr;  { guess is of type Float.                                       }
               Writeln;

{ Specify the desired accuracy of the temperature calculations. }

               repeat
                    Writeln('Input the tolerable difference between the calculated');
                    Writeln('temperature and the value of the temperature used to');
                    Writeln('make the calculations.');
                    Readln(TemperatureIterationTolerance);
                    IOcheck;    { Check to make certain that inputed value for the temperature }
               until not IOerr; { iteration tolerance is of type Float.                         }

{ Specify if you wish to calculate line strengths or partial pressures. }

               ClrScr;
               Writeln;
               repeat
                    Writeln('Do you want to calculate CO Partial Pressures (P) or Line Strengths (S).');
                    Readln(CalculationChoice);
                    CalculationChoice := Upcase(CalculationChoice);
                    IOcheck;    { Check to make certain that inputed values is of type Char. }
               until not IOerr;

    If YesNoCO2ConcCalc = 'Y' Then
    Begin

{ Get information regarding the absorption lines which should be included in the CO2 concentration calcula-
tions. }

          ClrScr;
          Writeln('Specification of the CO2 lines (m indexes)');
```

```
        Writeln('which are to be used for gas concentration');
        Writeln('calculations (acceptable range 51 to 91).');
        Writeln;
        repeat

{ Specify the lower limit of the m index range to be searched. }
                repeat
                    Writeln('Input lower m index' );
                    Readln(MValueRangeLowCO2);
                    IOcheck;     { Check to make certain that inputed value for }
                until not IOerr;  { the lower m index is of type Integer.        }
                Writeln;
{ Specify the upper limit of the m index range to be searched. }
                repeat
                    Writeln('Input upper m index' );
                    Readln(MValueRangeHighCO2);
                    IOcheck;     { Check to make certain that inputed value for }
                until not IOerr;  { the upper m index is of type Integer.        }

{ Check if the value for MValueRangeLow is smaller than the value inputed for MValueRangeHigh. }
                if MValueRangeLowCO2 >= MValueRangeHighCO2 Then
                    begin
                        Writeln;
                        Writeln('The lower m index must be less than the upper m index');
                        Writeln('and the two can also not be equal to each other.');
                        Writeln;
                    end;

        until MValueRangeLowCO2 < MValueRangeHighCO2;

{ Read any m indexes which should be excluded from the temperature calculations. }
        ClrScr;
        Writeln('Specify any lines (m indexes) within the range of indexes selected');
        Writeln('which should be excluded from CO2 concentration calculations.');
        Writeln;
        Writeln('Type in the m index of any line which should be excluded');
        Writeln('Type one index per line, followed by a <enter> (Maximum of 30 lines)');
        Writeln('When finished inputing indexes to be excluded, type "0" and <enter>');
        Writeln('If no lines are to be excluded simply type "0" and <enter> now');
        LoopCount := 0;
        repeat
            LoopCount := LoopCount + 1;
            repeat
                Readln(MExcludeIICO2[LoopCount]);
                IOcheck;      { Checks to make certain that the inputed value for }
            until not IOerr;   { MExclude[LoopCount] is of type integer.          }
        until MExcludeIICO2[LoopCount] = 0;

{ Specify if you wish to calculate line strengths or partial pressures. }

            ClrScr;
            Writeln;
            repeat
                Writeln('Do you want to calculate CO2 Partial Pressures (P) or Line Strengths (S).');
                Readln(CalculationChoiceCO2);
                CalculationChoiceCO2 := Upcase(CalculationChoiceCO2);
                IOcheck;    { Check to make certain that inputed values is of type Char. }
            until not IOerr;

        End;


    End; {Procedure GetUserData}



Procedure GetUserDataBatch;

{ Procedure written to get information regarding the name of the data file containing the spectra   }
{ information, the name of the file to write the results, the partial pressure of CO in the gas     }
```

```
{ sample, the partial pressure of nitrogen in the gas sample, the total pressure of the gas sample, }
{ the nominal resolution of the FT-IR, the initial guess for the first iteration of the temperature }
{ calculations, the desired accuracy of the final temperature calculations, the range of m indexes  }
{ which should be included in the temperature and concentration calculations, and the indexes of    }
{ lines (if any) which should be excluded from temperature and concentration calculations.  This    }
{ procedure is used by Temp.Pas when the temperature calculations are to be done in a batch mode    }
{ rather than a single file mode.                                                                   }

    Var
         LoopCount : Integer;
         BatchCount : Integer;

    begin

    BatchCount := 1;
    Writeln;
    Writeln('How many files will be analyzed in this batch?');
    Readln(BatchSize);

    repeat

{ Get name of file containing spectral data. }

         ClrScr;
         Writeln;
         Writeln('Data File Specifications for file number  ',BatchCount);
         Writeln;
              repeat
                   Writeln('Type the name of the Data File (include the .dat extention).' );
                   Readln(DataFileNameBatch[BatchCount]);
                   IOCheck;         { Checks to make certain that inputed name of DataFileName   }
              until not IOerr;      { is of type StrLength.                                      }

{ Get name for the output file. }

         Writeln;
              repeat
                   Writeln('Type the desired name for the output file (include the .csv extension).' );
                   Readln(OutputFileNameBatch[BatchCount]);
                   IOcheck;         { Checks to make certain that inputed name of OutputFileName }
              until not IOerr;      { is of type StrLength.                                      }

{ Get the partial pressure of CO recorded on the day of the experiment. }

         ClrScr;
         Writeln('Experimental Conditions for file number   ',BatchCount);
         Writeln;
              repeat
                   Writeln('Input the partial pressure (TORR) of CO in the gas sample.');
                   Readln(PPCOBatch[BatchCount]);
                   IOcheck;         { Checks to make certain that inputed partial pressure is }
              until not IOerr;      { of type Float.                                          }

{ Get the partial pressure of CO2 recorded on the day of the experiment. }

         Writeln;
              repeat
                   Writeln('Input the partial pressure (TORR) of CO2 in the gas sample.');
                   Readln(PPCO2Batch[BatchCount]);
                   IOcheck;         { Checks to make certain that inputed partial pressure is }
              until not IOerr;      { of type Float.                                          }

{ Get the partial pressure of N2 recorded on the day of the experiment. }

         Writeln;
              repeat
                   Writeln('Input the partial pressure (TORR) of N2 in the gas sample.');
                   Readln(PPN2Batch[BatchCount]);
                   IOcheck;         { Checks to make certain that inputed partial pressure is }
              until not IOerr;      { of type Float.
```

```
{ Get the total pressure of the gas sample recorded on the day of the experiment. }

        Writeln;
             repeat
                  Writeln('Input the total pressure (TORR) of the gas sample.');
                  Readln(TotalPressureBatch[BatchCount]);
                  IOcheck;        { Checks to make certain that inputed pressure is }
             until not IOerr;     { of type Float.

{ Get information regarding the initial temperature guess. }

             ClrScr;
             Writeln;
             Writeln('Input information regarding initial temperature guess for file number
',BatchCount);
             Writeln;
             repeat
                  Writeln('Input initial temperature guess.' );
                  Readln(InitialTemperatureGuessBatch[BatchCount]);
                  IOcheck;     { Check to make certain that inputed value for the temperature }
             until not IOerr;  { guess is of type Float.                                      }
             Writeln;

        BatchCount := BatchCount + 1;

    until BatchCount = BatchSize + 1;

{ Get information regarding the absorption lines which should be included in the temperature calculations. }

        ClrScr;
        Writeln('Specification of the CO lines (m indexes) to be included in');
        Writeln('the calculations to determine the gas phase temperature');
        Writeln('and CO gas concentration, (acceptable range -36 to -1).');
        Writeln;
        repeat
{ Specify the lower limit of the m index range to be searched. }
                  repeat
                       Writeln('Input lower m index, include negative sign.' );
                       Readln(MValueRangeLow);
                       IOcheck;     { Check to make certain that inputed value for }
                  until not IOerr;  { the lower m index is of type Integer.        }
                  Writeln;
{ Specify the upper limit of the m index range to be searched. }
                  repeat
                       Writeln('Input upper m index, include negative sign.' );
                       Readln(MValueRangeHigh);
                       IOcheck;     { Check to make certain that inputed value for }
                  until not IOerr;  { the upper m index is of type Integer.        }

{ Check if the value for MValueRangeLow is smaller than the value inputed for MValueRangeHigh. }
                  if MValueRangeLow >= MValueRangeHigh Then
                       begin
                            Writeln;
                            Writeln('The lower m index must be less than the upper m index');
                            Writeln('and the two can also not be equal to each other.');
                            Writeln;
                       end;

        until MValueRangeLow < MValueRangeHigh;

{ Read any m indexes which should be excluded from the temperature calculations. }
        ClrScr;
        Writeln('Specify any lines (m indexes) within the range of indexes selected');
        Writeln('which should be excluded from temperature calculations');
        Writeln('for all the files used in this batch.');
        Writeln;
        Writeln('Type in the m index of any line which should be excluded');
        Writeln('Type one index per line, followed by a <enter> (Maximum of 30 lines)');
        Writeln('When finished inputing indexes to be excluded, type "0" and <enter>');
        Writeln('If no lines are to be excluded simply type "0" and <enter> now');
        LoopCount := 0;
```

```
        repeat
             LoopCount := LoopCount + 1;
             repeat
                  Readln(MExcludeII[LoopCount]);
                  IOcheck;      { Checks to make certain that the inputed value for }
             until not IOerr;   { MExclude[LoopCount] is of type integer.          }
        until MExcludeII[LoopCount] = 0;


{ Specify the desired accuracy of the temperature calculations. }

             Clrscr;
             Writeln;
             repeat
                  Writeln('Input the tolerable difference between the calculated temperature');
                  Writeln('and the value of the temperature used to make the calculations');
                  Writeln('for all the files in this batch.');
                  Readln(TemperatureIterationTolerance);
                  IOcheck;    { Check to make certain that inputed value for the temperature }
             until not IOerr; { iteration tolerance is of type Float.                        }

{ Get information regarding the experimental conditions. }

        ClrScr;
        Writeln;
             repeat
                  Writeln('Input the nominal instrument resolution for all the files in this batch.');
                  Readln(InstRes);
                  IOcheck;         { Checks to make certain that inputed resolution data is of  }
             until not IOerr;      { type Float.                                                }

{ Get information regarding the path length of the gas cell or reactor. }

        Writeln;
        Writeln;
             repeat
                  Writeln('Input the Path Length of the Gas Cell or Reactor (cm).');
                  Readln(PathLength);
                  IOcheck;         { Checks to make certain that inputed path length is of      }
             until not IOerr;      { type Float.                                                }

{ Specify if you wish to calculate line strengths or partial pressures. }

       ClrScr;
       Writeln;
             repeat
                  Writeln('Do you want to calculate Partial Pressures (P) or Line Strengths (S).');
                  Readln(CalculationChoice);
                  CalculationChoice := Upcase(CalculationChoice);
                  IOcheck;    { Check to make certain that inputed values is of type Char. }
             until not IOerr;

   If YesNoCO2ConcCalc = 'Y' Then
   Begin

{ Get information regarding the absorption lines which should be included in the CO2 concentration calcula-
tions. }

        ClrScr;
        Writeln('Specification of the CO2 lines (m indexes)');
        Writeln('which are to be used for gas concentration');
        Writeln('calculations (acceptable range 51 to 91).');
        Writeln;
        repeat

{ Specify the lower limit of the m index range to be searched. }
             repeat
                  Writeln('Input lower m index' );
                  Readln(MValueRangeLowCO2);
                  IOcheck;     { Check to make certain that inputed value for }
             until not IOerr;  { the lower m index is of type Integer.        }
```

```
                    Writeln;
{ Specify the upper limit of the m index range to be searched. }
                    repeat
                         Writeln('Input upper m index' );
                         Readln(MValueRangeHighCO2);
                         IOcheck;     { Check to make certain that inputed value for }
                    until not IOerr;  { the upper m index is of type Integer.        }

{ Check if the value for MValueRangeLow is smaller than the value inputed for MValueRangeHigh. }
                    if MValueRangeLowCO2 >= MValueRangeHighCO2 Then
                         begin
                              Writeln;
                              Writeln('The lower m index must be less than the upper m index');
                              Writeln('and the two can also not be equal to each other.');
                              Writeln;
                         end;

          until MValueRangeLowCO2 < MValueRangeHighCO2;

{ Read any m indexes which should be excluded from the temperature calculations. }
          ClrScr;
          Writeln('Specify any lines (m indexes) within the range of indexes selected');
          Writeln('which should be excluded from CO2 concentration calculations.');
          Writeln;
          Writeln('Type in the m index of any line which should be excluded');
          Writeln('Type one index per line, followed by a <enter> (Maximum of 30 lines)');
          Writeln('When finished inputing indexes to be excluded, type "0" and <enter>');
          Writeln('If no lines are to be excluded simply type "0" and <enter> now');
          LoopCount := 0;
          repeat
               LoopCount := LoopCount + 1;
               repeat
                    Readln(MExcludeIICO2[LoopCount]);
                    IOcheck;      { Checks to make certain that the inputed value for }
               until not IOerr;   { MExclude[LoopCount] is of type integer.           }
          until MExcludeIICO2[LoopCount] = 0;

{ Specify if you wish to calculate line strengths or partial pressures. }

               ClrScr;
               Writeln;
               repeat
                    Writeln('Do you want to calculate CO2 Partial Pressures (P) or Line Strengths (S).');
                    Readln(CalculationChoiceCO2);
                    CalculationChoiceCO2 := Upcase(CalculationChoiceCO2);
                    IOcheck;    { Check to make certain that inputed values is of type Char. }
               until not IOerr;

          End;


     End; {Procedure GetUserDataBatch}


End.      { End Unit }
```

```
unit SpAnData;

{$I Float.inc}

Interface

    Uses Dos, Crt, GlobVar;

    {$IFOPT N+}
         type
              Float = Double;
    {$ELSE}
         type
              Float = Real;
    {$ENDIF}

    Procedure GetLineInformation;

Implementation

    Procedure GetLineInformation;

{ The objective of this segment of code is to convert the raw data read into the program during the }
{ "GetUserData" procedure into meaningful peak height information for specific lines.  This will be }
{ accomplished by reading each line of the data file and comparing the peak position to references  }
{ for carbon monoxide and carbon dioxide lines.  When the experimental line position is within some }
{ "tolerance" of the reference, m indexes, peak heights, standard line widths, and true peak        }
{ positions will all be assigned and stored into arrays.  This data will be later used throughout   }
{ the program.                                                                                      }


    Type
         StrLength40 = String[40];

    Var
         FileHeader1 : StrLength40;
         FileHeader2 : Float;
         FileHeader3 : Float;
         FileHeader4 : Float;
         FileHeader5 : Float;
         LineCenterTolerance : Float;
         LoopCount : Integer;
         LowLineWidth : Float;
         Marker : Integer;
         TempLineHeight : Float;
         TempLinePosition : Float;
         UpLineWidth : Float;


    begin

         LineCenterTolerance := 0.45;     { Allowed difference between true peak centers found in the AFGL }
                                          { data base and the experimental peak centers obtained with the  }
                                          { FT-IR.                                                         }

         ReadLn(DataFile,FileHeader1);
         ReadLn(DataFile,FileHeader2,FileHeader3,FileHeader4,FileHeader5);

{ These ReadLn's are only here to skip the first two lines of Laser    }
{ Precision Analytical's Peak program data files which includes        }
{ information (unwanted) about how the peak search was performed.      }

         repeat
              TempLinePosition := 0;
              TempLineHeight := 0;
              LowLineWidth := 0;
              UpLineWidth := 0;
              ReadLn(DataFile,TempLinePosition,TempLineHeight);

{ Peak information is read from the data file and temporarily stored into the }
{ positions TempLinePostion and TempLineHeight.                                }
```

```
            LowLineWidth := TempLinePosition - LineCenterTolerance;
            UpLineWidth := TempLinePosition + LineCenterTolerance;

{ A window of acceptable wavenumbers for each line is established by adding and  }
{ subtracting a constant, LineCenterTolerance, to the TempLinePosition.  This    }
{ window of values are then compared to all the first order transitions of       }
{ carbon monoxide with m indexes between -38 and +38.                            }

            If (1973.892 > LowLineWidth)  and  (1973.892 < UpLineWidth)  Then
                 begin
                      MValue[-38] := -38;
                      LineHeight[-38] := TempLineHeight;
                      LinePosition[-38] := TempLinePosition;
                      COCOWidthLT[-38] := 0.0389;
                      TrueLinePosition[-38] := 1973.892;
                      CON2WidthHT[-38] := 0.0344;
                      COCO2WidthHT[-38] := 0.0357;
                      NCON2[-38] := 0.40;
                      NCOCO2[-38] := 0.44;
                      S297[-38] := 0.0000926;
                      E[-38] := 2835.77;
                 end

{ When the values stored in LowLineWidth and UpLineWidth fall above and below a particular line, a match }
{ between an experimental line and a reference line is found.  The m index corresponding to this line is }
{ stored in the array MValue, the experimental line height is stored in the array LineHeight, the        }
{ experimental line position is stored in the array LinePosition, the line width at half height (HWHH)   }
{ is stored in the array StandardLineWidth, and finally the reference position for the line from the     }
{ AFGL standard indexes is stored in the array TrueLinePosition.                                         }

            Else If (1978.929 > LowLineWidth)  and  (1978.929 < UpLineWidth)  Then
                 begin
                      MValue[-37] := -37;
                      LineHeight[-37] := TempLineHeight;
                      LinePosition[-37] := TempLinePosition;
                      COCOWidthLT[-37] := 0.0395;
                      TrueLinePosition[-37] := 1978.929;
                      CON2WidthHT[-37] := 0.0348;
                      COCO2WidthHT[-37] := 0.0361;
                      NCON2[-37] := 0.40;
                      NCOCO2[-37] := 0.44;
                      S297[-37] := 0.000182;
                      E[-37] := 2690.99;
                 end

            Else If (1983.937 > LowLineWidth)  and  (1983.937 < UpLineWidth)  Then
                 begin
                      MValue[-36] := -36;
                      LineHeight[-36] := TempLineHeight;
                      LinePosition[-36] := TempLinePosition;
                      COCOWidthLT[-36] := 0.0402;
                      TrueLinePosition[-36] := 1983.937;
                      CON2WidthHT[-36] := 0.0358;
                      COCO2WidthHT[-36] := 0.0367;
                      NCON2[-36] := 0.41;
                      NCOCO2[-36] := 0.44;
                      S297[-36] := 0.000351;
                      E[-36] := 2549.96;
                 end

            Else If (1988.915 > LowLineWidth)  and  (1988.915 < UpLineWidth)  Then
                 begin
                      MValue[-35] := -35;
                      LineHeight[-35] := TempLineHeight;
                      LinePosition[-35] := TempLinePosition;
                      COCOWidthLT[-35] := 0.0409;
                      TrueLinePosition[-35] := 1988.915;
                      CON2WidthHT[-35] := 0.0368;
                      COCO2WidthHT[-35] := 0.0374;
```

```
          NCON2[-35] := 0.43;
          NCOCO2[-35] := 0.45;
          S297[-35] := 0.000665;
          E[-35] := 2412.68;
     end

Else If (1993.863 > LowLineWidth)  and  (1993.863 < UpLineWidth)  Then
     begin
          MValue[-34] := -34;
          LineHeight[-34] := TempLineHeight;
          LinePosition[-34] := TempLinePosition;
          COCOWidthLT[-34] := 0.0416;
          TrueLinePosition[-34] := 1993.863;
          CON2WidthHT[-34] := 0.0377;
          COCO2WidthHT[-34] := 0.038;
          NCON2[-34] := 0.44;
          NCOCO2[-34] := 0.45;
          S297[-34] := 0.00123;
          E[-34] := 2279.15;
     end

Else If (1998.781 > LowLineWidth)  and  (1998.781 < UpLineWidth)  Then
     begin
          MValue[-33] := -33;
          LineHeight[-33] := TempLineHeight;
          LinePosition[-33] := TempLinePosition;
          COCOWidthLT[-33] := 0.0424;
          TrueLinePosition[-33] := 1998.781;
          CON2WidthHT[-33] := 0.0387;
          COCO2WidthHT[-33] := 0.0387;
          NCON2[-33] := 0.45;
          NCOCO2[-33] := 0.46;
          S297[-33] := 0.00225;
          E[-33] := 2149.38;
     end

Else If (2003.668 > LowLineWidth)  and  (2003.668 < UpLineWidth)  Then
     begin
          MValue[-32] := -32;
          LineHeight[-32] := TempLineHeight;
          LinePosition[-32] := TempLinePosition;
          COCOWidthLT[-32] := 0.0431;
          TrueLinePosition[-32] := 2003.668;
          CON2WidthHT[-32] := 0.0398;
          COCO2WidthHT[-32] := 0.0394;
          NCON2[-32] := 0.46;
          NCOCO2[-32] := 0.46;
          S297[-32] := 0.00402;
          E[-32] := 2023.37;
     end

Else If (2008.526 > LowLineWidth)  and  (2008.526 < UpLineWidth)  Then
     begin
          MValue[-31] := -31;
          LineHeight[-31] := TempLineHeight;
          LinePosition[-31] := TempLinePosition;
          COCOWidthLT[-31] := 0.0440;
          TrueLinePosition[-31] := 2008.526;
          CON2WidthHT[-31] := 0.0409;
          COCO2WidthHT[-31] := 0.0402;
          NCON2[-31] := 0.47;
          NCOCO2[-31] := 0.47;
          S297[-31] := 0.00706;
          E[-31] := 1901.13;
     end

Else If (2013.353 > LowLineWidth)  and  (2013.353 < UpLineWidth)  Then
     begin
          MValue[-30] := -30;
          LineHeight[-30] := TempLineHeight;
          LinePosition[-30] := TempLinePosition;
```

```
        COCOWidthLT[-30] := 0.0448;
        TrueLinePosition[-30] := 2013.353;
        CON2WidthHT[-30] := 0.0420;
        COCO2WidthHT[-30] := 0.0409;
        NCON2[-30] := 0.48;
        NCOCO2[-30] := 0.47;
        S297[-30] := 0.0121;
        E[-30] := 1782.66;
    end

Else If (2018.149 > LowLineWidth) and (2018.149 < UpLineWidth) Then
    begin
        MValue[-29] := -29;
        LineHeight[-29] := TempLineHeight;
        LinePosition[-29] := TempLinePosition;
        COCOWidthLT[-29] := 0.0456;
        TrueLinePosition[-29] := 2018.149;
        CON2WidthHT[-29] := 0.0431;
        COCO2WidthHT[-29] := 0.0417;
        NCON2[-29] := 0.49;
        NCOCO2[-29] := 0.48;
        S297[-29] := 0.0205;
        E[-29] := 1667.97;
    end

Else If (2022.915 > LowLineWidth) and (2022.915 < UpLineWidth) Then
    begin
        MValue[-28] := -28;
        LineHeight[-28] := TempLineHeight;
        LinePosition[-28] := TempLinePosition;
        COCOWidthLT[-28] := 0.0465;
        TrueLinePosition[-28] := 2022.915;
        CON2WidthHT[-28] := 0.0442;
        COCO2WidthHT[-28] := 0.0425;
        NCON2[-28] := 0.5;
        NCOCO2[-28] := 0.48;
        S297[-28] := 0.0339;
        E[-28] := 1557.06;
    end

Else If (2027.649 > LowLineWidth) and (2027.659 < UpLineWidth) Then
    begin
        MValue[-27] := -27;
        LineHeight[-27] := TempLineHeight;
        LinePosition[-27] := TempLinePosition;
        COCOWidthLT[-27] := 0.0474;
        TrueLinePosition[-27] := 2027.649;
        CON2WidthHT[-27] := 0.0453;
        COCO2WidthHT[-27] := 0.0432;
        NCON2[-27] := 0.51;
        NCOCO2[-27] := 0.48;
        S297[-27] := 0.055;
        E[-27] := 1449.94;
    end

Else If (2032.353 > LowLineWidth) and (2032.353 < UpLineWidth) Then
    begin
        MValue[-26] := -26;
        LineHeight[-26] := TempLineHeight;
        LinePosition[-26] := TempLinePosition;
        COCOWidthLT[-26] := 0.0484;
        CON2WidthLT[-26] := 0.0520;
        TrueLinePosition[-26] := 2032.353;
        CON2WidthHT[-26] := 0.0463;
        COCO2WidthHT[-26] := 0.044;
        NCON2[-26] := 0.52;
        NCOCO2[-26] := 0.48;
        S297[-26] := 0.0875;
        E[-26] := 1346.6;
    end
```

```
Else If (2037.026 > LowLineWidth)  and  (2037.026 < UpLineWidth)  Then
     begin
          MValue[-25] := -25;
          LineHeight[-25] := TempLineHeight;
          LinePosition[-25] := TempLinePosition;
          COCOWidthLT[-25] := 0.0494;
          CON2WidthLT[-25] := 0.0526;
          TrueLinePosition[-25] := 2037.026;
          CON2WidthHT[-25] := 0.0474;
          COCO2WidthHT[-25] := 0.0448;
          NCON2[-25] := 0.53;
          NCOCO2[-25] := 0.48;
          S297[-25] := 0.1365;
          E[-25] := 1247.06;
     end

Else If (2041.667 > LowLineWidth)  and  (2041.667 < UpLineWidth)  Then
     begin
          MValue[-24] := -24;
          LineHeight[-24] := TempLineHeight;
          LinePosition[-24] := TempLinePosition;
          COCOWidthLT[-24] := 0.0504;
          CON2WidthLT[-24] := 0.0530;
          TrueLinePosition[-24] := 2041.667;
          CON2WidthHT[-24] := 0.0483;
          COCO2WidthHT[-24] := 0.0462;
          NCON2[-24] := 0.54;
          NCOCO2[-24] := 0.48;
          S297[-24] := 0.2087;
          E[-24] := 1151.32;
     end

Else If (2046.276 > LowLineWidth)  and  (2046.276 < UpLineWidth)  Then
     begin
          MValue[-23] := -23;
          LineHeight[-23] := TempLineHeight;
          LinePosition[-23] := TempLinePosition;
          COCOWidthLT[-23] := 0.0515;
          CON2WidthLT[-23] := 0.0533;
          TrueLinePosition[-23] := 2046.276;
          CON2WidthHT[-23] := 0.0491;
          COCO2WidthHT[-23] := 0.0476;
          NCON2[-23] := 0.55;
          NCOCO2[-23] := 0.49;
          S297[-23] := 0.313;
          E[-23] := 1059.37;
     end

Else If (2050.855 > LowLineWidth)  and  (2050.855 < UpLineWidth)  Then
     begin
          MValue[-22] := -22;
          LineHeight[-22] := TempLineHeight;
          LinePosition[-22] := TempLinePosition;
          COCOWidthLT[-22] := 0.0524;
          CON2WidthLT[-22] := 0.0535;
          TrueLinePosition[-22] := 2050.855;
          CON2WidthHT[-22] := 0.0500;
          COCO2WidthHT[-22] := 0.0491;
          NCON2[-22] := 0.55;
          NCOCO2[-22] := 0.49;
          S297[-22] := 0.459;
          E[-22] := 971.23;
     end

Else If (2055.401 > LowLineWidth)  and  (2055.401 < UpLineWidth)  Then
     begin
          MValue[-21] := -21;
          LineHeight[-21] := TempLineHeight;
          LinePosition[-21] := TempLinePosition;
          COCOWidthLT[-21] := 0.0535;
          CON2WidthLT[-21] := 0.0536;
```

```
        TrueLinePosition[-21] := 2055.401;
        CON2WidthHT[-21] := 0.0508;
        COCO2WidthHT[-21] := 0.0505;
        NCON2[-21] := 0.56;
        NCOCO2[-21] := 0.5;
        S297[-21] := 0.66;
        E[-21] := 886.9;
    end

Else If (2059.915 > LowLineWidth)  and  (2059.915 < UpLineWidth)  Then
    begin
        MValue[-20] := -20;
        LineHeight[-20] := TempLineHeight;
        LinePosition[-20] := TempLinePosition;
        COCOWidthLT[-20] := 0.0545;
        CON2WidthLT[-20] := 0.0537;
        TrueLinePosition[-20] := 2059.915;
        CON2WidthHT[-20] := 0.0522;
        COCO2WidthHT[-20] := 0.0518;
        NCON2[-20] := 0.57;
        NCOCO2[-20] := 0.5;
        S297[-20] := 0.931;
        E[-20] := 806.38;
    end

Else If (2064.397 > LowLineWidth)  and  (2064.397 < UpLineWidth)  Then
    begin
        MValue[-19] := -19;
        LineHeight[-19] := TempLineHeight;
        LinePosition[-19] := TempLinePosition;
        COCOWidthLT[-19] := 0.0556;
        CON2WidthLT[-19] := 0.0538;
        TrueLinePosition[-19] := 2064.397;
        CON2WidthHT[-19] := 0.0536;
        COCO2WidthHT[-19] := 0.0531;
        NCON2[-19] := 0.59;
        NCOCO2[-19] := 0.5;
        S297[-19] := 1.284;
        E[-19] := 729.68;
    end

Else If (2068.847 > LowLineWidth)  and  (2068.847 < UpLineWidth)  Then
    begin
        MValue[-18] := -18;
        LineHeight[-18] := TempLineHeight;
        LinePosition[-18] := TempLinePosition;
        COCOWidthLT[-18] := 0.0566;
        CON2WidthLT[-18] := 0.0539;
        TrueLinePosition[-18] := 2068.847;
        CON2WidthHT[-18] := 0.0550;
        COCO2WidthHT[-18] := 0.0544;
        NCON2[-18] := 0.60;
        NCOCO2[-18] := 0.50;
        S297[-18] := 1.734;
        E[-18] := 656.79;
    end

Else If (2073.265 > LowLineWidth)  and  (2073.265 < UpLineWidth)  Then
    begin
        MValue[-17] := -17;
        LineHeight[-17] := TempLineHeight;
        LinePosition[-17] := TempLinePosition;
        COCOWidthLT[-17] := 0.0577;
        CON2WidthLT[-17] := 0.0540;
        TrueLinePosition[-17] := 2073.265;
        CON2WidthHT[-17] := 0.0564;
        COCO2WidthHT[-17] := 0.0557;
        NCON2[-17] := 0.61;
        NCOCO2[-17] := 0.50;
        S297[-17] := 2.293;
        E[-17] := 587.72;
```

```
     end

Else If (2077.650 > LowLineWidth)  and  (2077.650 < UpLineWidth)  Then
     begin
          MValue[-16] := -16;
          LineHeight[-16] := TempLineHeight;
          LinePosition[-16] := TempLinePosition;
          COCOWidthLT[-16] := 0.0587;
          CON2WidthLT[-16] := 0.0542;
          TrueLinePosition[-16] := 2077.650;
          CON2WidthHT[-16] := 0.0577;
          COCO2WidthHT[-16] := 0.0582;
          NCON2[-16] := 0.62;
          NCOCO2[-16] := 0.51;
          S297[-16] := 2.965;
          E[-16] := 522.48;
     end

Else If (2082.003 > LowLineWidth)  and  (2082.003 < UpLineWidth)  Then
     begin
          MValue[-15] := -15;
          LineHeight[-15] := TempLineHeight;
          LinePosition[-15] := TempLinePosition;
          COCOWidthLT[-15] := 0.0597;
          CON2WidthLT[-15] := 0.0544;
          TrueLinePosition[-15] := 2082.003;
          CON2WidthHT[-15] := 0.0589;
          COCO2WidthHT[-15] := 0.0606;
          NCON2[-15] := 0.64;
          NCOCO2[-15] := 0.52;
          S297[-15] := 3.749;
          E[-15] := 461.05;
     end

Else If (2086.322 > LowLineWidth)  and  (2086.322 < UpLineWidth)  Then
     begin
          MValue[-14] := -14;
          LineHeight[-14] := TempLineHeight;
          LinePosition[-14] := TempLinePosition;
          COCOWidthLT[-14] := 0.0608;
          CON2WidthLT[-14] := 0.0548;
          TrueLinePosition[-14] := 2086.322;
          CON2WidthHT[-14] := 0.0602;
          COCO2WidthHT[-14] := 0.0631;
          NCON2[-14] := 0.65;
          NCOCO2[-14] := 0.53;
          S297[-14] := 4.633;
          E[-14] := 403.46;
     end

Else If (2090.609 > LowLineWidth)  and  (2090.609 < UpLineWidth)  Then
     begin
          MValue[-13] := -13;
          LineHeight[-13] := TempLineHeight;
          LinePosition[-13] := TempLinePosition;
          COCOWidthLT[-13] := 0.0618;
          CON2WidthLT[-13] := 0.0553;
          TrueLinePosition[-13] := 2090.609;
          CON2WidthHT[-13] := 0.0614;
          COCO2WidthHT[-13] := 0.0656;
          NCON2[-13] := 0.66;
          NCOCO2[-13] := 0.54;
          S297[-13] := 5.592;
          E[-13] := 349.7;
     end

Else If (2094.863 > LowLineWidth)  and  (2094.863 < UpLineWidth)  Then
     begin
          MValue[-12] := -12;
          LineHeight[-12] := TempLineHeight;
          LinePosition[-12] := TempLinePosition;
```

```
        COCOWidthLT[-12] := 0.0628;
        CON2WidthLT[-12] := 0.0559;
        TrueLinePosition[-12] := 2094.863;
        CON2WidthHT[-12] := 0.0622;
        COCO2WidthHT[-12] := 0.0699;
        NCON2[-12] := 0.66;
        NCOCO2[-12] := 0.56;
        S297[-12] := 6.586;
        E[-12] := 299.77;
    end

Else If (2099.083 > LowLineWidth) and (2099.083 < UpLineWidth) Then
    begin
        MValue[-11] := -11;
        LineHeight[-11] := TempLineHeight;
        LinePosition[-11] := TempLinePosition;
        COCOWidthLT[-11] := 0.0638;
        CON2WidthLT[-11] := 0.0567;
        TrueLinePosition[-11] := 2099.083;
        CON2WidthHT[-11] := 0.0629;
        COCO2WidthHT[-11] := 0.0742;
        NCON2[-11] := 0.67;
        NCOCO2[-11] := 0.58;
        S297[-11] := 7.561;
        E[-11] := 253.67;
    end

Else If (2103.270 > LowLineWidth) and (2103.270 < UpLineWidth) Then
    begin
        MValue[-10] := -10;
        LineHeight[-10] := TempLineHeight;
        LinePosition[-10] := TempLinePosition;
        COCOWidthLT[-10] := 0.0648;
        CON2WidthLT[-10] := 0.0578;
        TrueLinePosition[-10] := 2103.270;
        CON2WidthHT[-10] := 0.0637;
        COCO2WidthHT[-10] := 0.0785;
        NCON2[-10] := 0.67;
        NCOCO2[-10] := 0.61;
        S297[-10] := 8.45;
        E[-10] := 211.4;
    end

Else If (2107.424 > LowLineWidth) and (2107.424 < UpLineWidth) Then
    begin
        MValue[-9] := -9;
        LineHeight[-9] := TempLineHeight;
        LinePosition[-9] := TempLinePosition;
        COCOWidthLT[-9] := 0.0659;
        CON2WidthLT[-9] := 0.0590;
        TrueLinePosition[-9] := 2107.424;
        CON2WidthHT[-9] := 0.0644;
        COCO2WidthHT[-9] := 0.0828;
        NCON2[-9] := 0.68;
        NCOCO2[-9] := 0.63;
        S297[-9] := 9.178;
        E[-9] := 172.98;
    end

Else If (2111.543 > LowLineWidth) and (2111.543 < UpLineWidth) Then
    begin
        MValue[-8] := -8;
        LineHeight[-8] := TempLineHeight;
        LinePosition[-8] := TempLinePosition;
        COCOWidthLT[-8] := 0.0671;
        CON2WidthLT[-8] := 0.0606;
        TrueLinePosition[-8] := 2111.543;
        CON2WidthHT[-8] := 0.0654;
        COCO2WidthHT[-8] := 0.0866;
        NCON2[-8] := 0.69;
        NCOCO2[-8] := 0.65;
```

```
          S297[-8] := 9.664;
          E[-8] := 138.39;
     end

Else If (2115.629 > LowLineWidth)  and  (2115.629 < UpLineWidth)  Then
     begin
          MValue[-7] := -7;
          LineHeight[-7] := TempLineHeight;
          LinePosition[-7] := TempLinePosition;
          COCOWidthLT[-7] := 0.0684;
          CON2WidthLT[-7] := 0.0624;
          TrueLinePosition[-7] := 2115.629;
          CON2WidthHT[-7] := 0.0664;
          COCO2WidthHT[-7] := 0.0905;
          NCON2[-7] := 0.69;
          NCOCO2[-7] := 0.67;
          S297[-7] := 9.832;
          E[-7] := 107.64;
     end

Else If (2119.681 > LowLineWidth)  and  (2119.681 < UpLineWidth)  Then
     begin
          MValue[-6] := -6;
          LineHeight[-6] := TempLineHeight;
          LinePosition[-6] := TempLinePosition;
          COCOWidthLT[-6] := 0.0702;
          CON2WidthLT[-6] := 0.0645;
          TrueLinePosition[-6] := 2119.681;
          CON2WidthHT[-6] := 0.0673;
          COCO2WidthHT[-6] := 0.0943;
          NCON2[-6] := 0.70;
          NCOCO2[-6] := 0.69;
          S297[-6] := 9.618;
          E[-6] := 80.74;
     end

Else If (2123.699 > LowLineWidth)  and  (2123.699 < UpLineWidth)  Then
     begin
          MValue[-5] := -5;
          LineHeight[-5] := TempLineHeight;
          LinePosition[-5] := TempLinePosition;
          COCOWidthLT[-5] := 0.0722;
          CON2WidthLT[-5] := 0.0669;
          TrueLinePosition[-5] := 2123.699;
          CON2WidthHT[-5] := 0.0683;
          COCO2WidthHT[-5] := 0.0982;
          NCON2[-5] := 0.70;
          NCOCO2[-5] := 0.71;
          S297[-5] := 8.98;
          E[-5] := 57.67;
     end

Else If (2127.683 > LowLineWidth)  and  (2127.683 < UpLineWidth)  Then
     begin
          MValue[-4] := -4;
          LineHeight[-4] := TempLineHeight;
          LinePosition[-4] := TempLinePosition;
          COCOWidthLT[-4] := 0.0749;
          CON2WidthLT[-4] := 0.0697;
          TrueLinePosition[-4] := 2127.683;
          CON2WidthHT[-4] := 0.0703;
          COCO2WidthHT[-4] := 0.1016;
          NCON2[-4] := 0.72;
          NCOCO2[-4] := 0.72;
          S297[-4] := 7.9;
          E[-4] := 38.45;
     end

Else If (2131.632 > LowLineWidth)  and  (2131.632 < UpLineWidth)  Then
     begin
          MValue[-3] := -3;
```

```
                    LineHeight[-3] := TempLineHeight;
                    LinePosition[-3] := TempLinePosition;
                    COCOWidthLT[-3] := 0.0783;
                    CON2WidthLT[-3] := 0.0729;
                    TrueLinePosition[-3] := 2131.632;
                    CON2WidthHT[-3] := 0.0723;
                    COCO2WidthHT[-3] := 0.1051;
                    NCON2[-3] := 0.73;
                    NCOCO2[-3] := 0.73;
                    S297[-3] := 6.395;
                    E[-3] := 23.07;
               end

          Else If (2135.547 > LowLineWidth)  and  (2135.547 < UpLineWidth)  Then
               begin
                    MValue[-2] := -2;
                    LineHeight[-2] := TempLineHeight;
                    LinePosition[-2] := TempLinePosition;
                    COCOWidthLT[-2] := 0.0822;
                    CON2WidthLT[-2] := 0.0765;
                    TrueLinePosition[-2] := 2135.547;
                    CON2WidthHT[-2] := 0.0743;
                    COCO2WidthHT[-2] := 0.1085;
                    NCON2[-2] := 0.75;
                    NCOCO2[-2] := 0.75;
                    S297[-2] := 4.517;
                    E[-2] := 11.53;
               end

          Else If (2139.427 > LowLineWidth)  and  (2139.427 < UpLineWidth)  Then
               begin
                    MValue[-1] := -1;
                    LineHeight[-1] := TempLineHeight;
                    LinePosition[-1] := TempLinePosition;
                    COCOWidthLT[-1] := 0.0874;
                    CON2WidthLT[-1] := 0.0805;
                    TrueLinePosition[-1] := 2139.427;
                    CON2WidthHT[-1] := 0.0763;
                    COCO2WidthHT[-1] := 0.112;
                    NCON2[-1] := 0.76;
                    NCOCO2[-1] := 0.76;
                    S297[-1] := 2.348;
                    E[-1] := 3.85;
               end

{ CO2 Line Identification }

          Else If (2380.716 > LowLineWidth)  and  (2380.716 < UpLineWidth)  Then
               begin
                    MValueCO2[51] := 51;
                    LineHeightCO2[51] := TempLineHeight;
                    LinePositionCO2[51] := TempLinePosition;
                    TrueLinePositionCO2[51] := 2380.716;
                    CO2CO2Width[51] := 0.0757;
                    CO2N2Width[51] := 0.0716;
                    NCO2CO2[51] := 0.529;
                    NCO2N2[51] := 0.676;
               end

          Else If (2381.622 > LowLineWidth)  and  (2381.622 < UpLineWidth)  Then
               begin
                    MValueCO2[53] := 53;
                    LineHeightCO2[53] := TempLineHeight;
                    LinePositionCO2[53] := TempLinePosition;
                    TrueLinePositionCO2[53] := 2381.622;
                    CO2CO2Width[53] := 0.0742;
                    CO2N2Width[53] := 0.0713;
                    NCO2CO2[53] := 0.521;
                    NCO2N2[53] := 0.677;
               end
```

```
Else If (2382.503 > LowLineWidth)  and  (2382.503 < UpLineWidth)  Then
     begin
          MValueCO2[55] := 55;
          LineHeightCO2[55] := TempLineHeight;
          LinePositionCO2[55] := TempLinePosition;
          TrueLinePositionCO2[55] := 2382.503;
          CO2CO2Width[55] := 0.0728;
          CO2N2Width[55] := 0.0709;
          NCO2CO2[55] := 0.515;
          NCO2N2[55] := 0.672;
     end

Else If (2383.359 > LowLineWidth)  and  (2383.359 < UpLineWidth)  Then
     begin
          MValueCO2[57] := 57;
          LineHeightCO2[57] := TempLineHeight;
          LinePositionCO2[57] := TempLinePosition;
          TrueLinePositionCO2[57] := 2383.359;
          CO2CO2Width[57] := 0.0714;
          CO2N2Width[57] := 0.0704;
          NCO2CO2[57] := 0.508;
          NCO2N2[57] := 0.670;
     end

Else If (2384.189 > LowLineWidth)  and  (2384.189 < UpLineWidth)  Then
     begin
          MValueCO2[59] := 59;
          LineHeightCO2[59] := TempLineHeight;
          LinePositionCO2[59] := TempLinePosition;
          TrueLinePositionCO2[59] := 2384.189;
          CO2CO2Width[59] := 0.0702;
          CO2N2Width[59] := 0.0700;
          NCO2CO2[59] := 0.504;
          NCO2N2[59] := 0.666;
     end

Else If (2384.995 > LowLineWidth)  and  (2384.995 < UpLineWidth)  Then
     begin
          MValueCO2[61] := 61;
          LineHeightCO2[61] := TempLineHeight;
          LinePositionCO2[61] := TempLinePosition;
          TrueLinePositionCO2[61] := 2384.995;
          CO2CO2Width[61] := 0.0691;
          CO2N2Width[61] := 0.0695;
          NCO2CO2[61] := 0.500;
          NCO2N2[61] := 0.663;
     end

Else If (2385.775 > LowLineWidth)  and  (2385.775 < UpLineWidth)  Then
     begin
          MValueCO2[63] := 63;
          LineHeightCO2[63] := TempLineHeight;
          LinePositionCO2[63] := TempLinePosition;
          TrueLinePositionCO2[63] := 2385.775;
          CO2CO2Width[63] := 0.0680;
          CO2N2Width[63] := 0.0690;
          NCO2CO2[63] := 0.497;
          NCO2N2[63] := 0.659;
     end

Else If (2386.529 > LowLineWidth)  and  (2386.529 < UpLineWidth)  Then
     begin
          MValueCO2[65] := 65;
          LineHeightCO2[65] := TempLineHeight;
          LinePositionCO2[65] := TempLinePosition;
          TrueLinePositionCO2[65] := 2386.529;
          CO2CO2Width[65] := 0.0670;
          CO2N2Width[65] := 0.0685;
          NCO2CO2[65] := 0.493;
          NCO2N2[65] := 0.655;
     end
```

```
Else If (2387.258 > LowLineWidth)  and  (2387.258 < UpLineWidth)  Then
     begin
          MValueCO2[67] := 67;
          LineHeightCO2[67] := TempLineHeight;
          LinePositionCO2[67] := TempLinePosition;
          TrueLinePositionCO2[67] := 2387.258;
          CO2CO2Width[67] := 0.0660;
          CO2N2Width[67] := 0.0679;
          NCO2CO2[67] := 0.492;
          NCO2N2[67] := 0.650;
     end

Else If (2387.962 > LowLineWidth)  and  (2387.962 < UpLineWidth)  Then
     begin
          MValueCO2[69] := 69;
          LineHeightCO2[69] := TempLineHeight;
          LinePositionCO2[69] := TempLinePosition;
          TrueLinePositionCO2[69] := 2387.962;
          CO2CO2Width[69] := 0.0651;
          CO2N2Width[69] := 0.0673;
          NCO2CO2[69] := 0.488;
          NCO2N2[69] := 0.644;
     end

Else If (2388.640 > LowLineWidth)  and  (2388.640 < UpLineWidth)  Then
     begin
          MValueCO2[71] := 71;
          LineHeightCO2[71] := TempLineHeight;
          LinePositionCO2[71] := TempLinePosition;
          TrueLinePositionCO2[71] := 2388.640;
          CO2CO2Width[71] := 0.0643;
          CO2N2Width[71] := 0.0668;
          NCO2CO2[71] := 0.488;
          NCO2N2[71] := 0.639;
     end

Else If (2389.293 > LowLineWidth)  and  (2389.293 < UpLineWidth)  Then
     begin
          MValueCO2[73] := 73;
          LineHeightCO2[73] := TempLineHeight;
          LinePositionCO2[73] := TempLinePosition;
          TrueLinePositionCO2[73] := 2389.293;
          CO2CO2Width[73] := 0.0636;
          CO2N2Width[73] := 0.0661;
          NCO2CO2[73] := 0.487;
          NCO2N2[73] := 0.634;
     end

Else If (2389.921 > LowLineWidth)  and  (2389.921 < UpLineWidth)  Then
     begin
          MValueCO2[75] := 75;
          LineHeightCO2[75] := TempLineHeight;
          LinePositionCO2[75] := TempLinePosition;
          TrueLinePositionCO2[75] := 2389.921;
          CO2CO2Width[75] := 0.0629;
          CO2N2Width[75] := 0.0655;
          NCO2CO2[75] := 0.486;
          NCO2N2[75] := 0.628;
     end

Else If (2390.522 > LowLineWidth)  and  (2390.522 < UpLineWidth)  Then
     begin
          MValueCO2[77] := 77;
          LineHeightCO2[77] := TempLineHeight;
          LinePositionCO2[77] := TempLinePosition;
          TrueLinePositionCO2[77] := 2390.522;
          CO2CO2Width[77] := 0.0621;
          CO2N2Width[77] := 0.0649;
          NCO2CO2[77] := 0.485;
          NCO2N2[77] := 0.622;
```

```
     end

Else If (2391.099 > LowLineWidth)  and  (2391.099 < UpLineWidth)  Then
     begin
          MValueCO2[79] := 79;
          LineHeightCO2[79] := TempLineHeight;
          LinePositionCO2[79] := TempLinePosition;
          TrueLinePositionCO2[79] := 2391.099;
          CO2CO2Width[79] := 0.0615;
          CO2N2Width[79] := 0.0642;
          NCO2CO2[79] := 0.486;
          NCO2N2[79] := 0.616;
     end

Else If (2391.650 > LowLineWidth)  and  (2391.650 < UpLineWidth)  Then
     begin
          MValueCO2[81] := 81;
          LineHeightCO2[81] := TempLineHeight;
          LinePositionCO2[81] := TempLinePosition;
          TrueLinePositionCO2[81] := 2391.650;
          CO2CO2Width[81] := 0.0609;
          CO2N2Width[81] := 0.0636;
          NCO2CO2[81] := 0.485;
          NCO2N2[81] := 0.612;
     end

Else If (2392.175 > LowLineWidth)  and  (2392.175 < UpLineWidth)  Then
     begin
          MValueCO2[83] := 83;
          LineHeightCO2[83] := TempLineHeight;
          LinePositionCO2[83] := TempLinePosition;
          TrueLinePositionCO2[83] := 2392.175;
          CO2CO2Width[83] := 0.0603;
          CO2N2Width[83] := 0.0629;
          NCO2CO2[83] := 0.485;
          NCO2N2[83] := 0.606;
     end

Else If (2392.675 > LowLineWidth)  and  (2392.675 < UpLineWidth)  Then
     begin
          MValueCO2[85] := 85;
          LineHeightCO2[85] := TempLineHeight;
          LinePositionCO2[85] := TempLinePosition;
          TrueLinePositionCO2[85] := 2392.675;
          CO2CO2Width[85] := 0.0598;
          CO2N2Width[85] := 0.0623;
          NCO2CO2[85] := 0.485;
          NCO2N2[85] := 0.599;
     end

Else If (2393.149 > LowLineWidth)  and  (2393.149 < UpLineWidth)  Then
     begin
          MValueCO2[87] := 87;
          LineHeightCO2[87] := TempLineHeight;
          LinePositionCO2[87] := TempLinePosition;
          TrueLinePositionCO2[87] := 2393.149;
          CO2CO2Width[87] := 0.0593;
          CO2N2Width[87] := 0.0616;
          NCO2CO2[87] := 0.487;
          NCO2N2[87] := 0.593;
     end

Else If (2393.598 > LowLineWidth)  and  (2393.598 < UpLineWidth)  Then
     begin
          MValueCO2[89] := 89;
          LineHeightCO2[89] := TempLineHeight;
          LinePositionCO2[89] := TempLinePosition;
          TrueLinePositionCO2[89] := 2393.598;
          CO2CO2Width[89] := 0.0588;
          CO2N2Width[89] := 0.0609;
          NCO2CO2[89] := 0.487;
```

```
                    NCO2N2[89] := 0.588;
               end

          Else If (2394.021 > LowLineWidth)  and  (2394.021 < UpLineWidth)  Then
               begin
                    MValueCO2[91] := 91;
                    LineHeightCO2[91] := TempLineHeight;
                    LinePositionCO2[91] := TempLinePosition;
                    TrueLinePositionCO2[91] := 2394.021;
                    CO2CO2Width[91] := 0.0583;
                    CO2N2Width[91] := 0.0603;
                    NCO2CO2[91] := 0.487;
                    NCO2N2[91] := 0.581;
               end


     until TempLinePosition = 0;

{ Reset variables describing lines which should be excluded from temperature calculations to zero. }

     LoopCount := 1;
     repeat
          If MExclude[LoopCount] <> 0 Then
               Begin
                    Marker := MExclude[LoopCount];
                    MValue[Marker] := 0;
                    LineHeight[Marker] := 0;
                    LinePosition[Marker] := 0;
                    LoopCount := LoopCount + 1;
               End;
     until MExclude[LoopCount] = 0;

     LoopCount := 1;
     repeat
          If MExcludeCO2[LoopCount] <> 0 Then
               Begin
                    Marker := MExcludeCO2[LoopCount];
                    MValueCO2[Marker] := 0;
                    LineHeightCO2[Marker] := 0;
                    LinePositionCO2[Marker] := 0;
                    LoopCount := LoopCount + 1;
               End;
     until MExcludeCO2[LoopCount] = 0;


{ Reset variables describing lines which have m indexes lower than the lower limit, MValueRangeLow. }

     If MValueRangeLow > -38 Then
          Begin
               LoopCount := -38;
               repeat
                    MValue[LoopCount] := 0;
                    LineHeight[LoopCount] := 0;
                    LinePosition[LoopCount] := 0;
                    LoopCount := LoopCount + 1;
               until LoopCount = MValueRangeLow;
          End;

{ Reset variables describing lines which have m indexes greater than the upper limit, MValueRangeHigh. }

     If MValueRangeHigh < 38 Then
          Begin
               LoopCount := MValueRangeHigh + 1;
               repeat
                    MValue[LoopCount] := 0;
                    LineHeight[LoopCount] := 0;
                    LinePosition[LoopCount] := 0;
                    LoopCount := LoopCount + 1;
               until LoopCount = 39;
          End;
```

```
        If MValueRangeLowCO2 > 0 Then
             Begin
                  LoopCount := 0;
                  repeat
                       MValueCO2[LoopCount] := 0;
                       LineHeightCO2[LoopCount] := 0;
                       LinePositionCO2[LoopCount] := 0;
                       LoopCount := LoopCount + 1;
                  until LoopCount = MValueRangeLowCO2;
             End;

{ Reset variables describing lines which have m indexes greater than the upper limit, MValueRangeHigh. }

        If MValueRangeHighCO2 < 100 Then
             Begin
                  LoopCount := MValueRangeHighCO2 + 1;
                  repeat
                       MValueCO2[LoopCount] := 0;
                       LineHeightCO2[LoopCount] := 0;
                       LinePositionCO2[LoopCount] := 0;
                       LoopCount := LoopCount + 1;
                  until LoopCount = 101;
             End;


    End;  {GetLineInformation}


End.  { End Unit TempData }
```

```
unit OverLap;

{$I Float.inc}

Interface
    Uses  Dos, Crt, Common, GlobVar, Integrat;

    {$IFOPT N+}
         Type
              Float = Double;

    {$Else}
         Type
              Float = Real;

    {$ENDIF}


    Procedure CorrectOverlap;
    Function Cor1(X : Float) : Float;
    Function Cor2(Y : Float) : Float;

Implementation

    {$F+}

    Function Cor1(X: Float) : Float;

    begin
    Cor1 := (Sqr(sin(PI*InstRes*(X-PeakSep)))/Sqr(PI*InstRes*(X-PeakSep)))*exp(-
ln(10)*Height*Sqr(W)/(Sqr(X)+Sqr(W)));
    end;


    {$F-}

    {$F+}

    Function Cor2(Y: Float) : Float;

    begin
      Cor2 := Sqr(sin(PI*InstRes*(Y-PeakSep)))/Sqr(PI*InstRes*(Y-PeakSep));
    end;

    {$F-}


{  This procedure corrects CO2 absorption lines for errors in their apparent peak heights due to overlap  }
{  from neighboring absorption lines.  Since the peak's width is a result of both instrument broadening   }
{  and absorption by the gas, each of these factors has been taken into account in the correction         }
{  procedures.                                                                                            }

    Procedure CorrectOverlap;

    Var
         AaPeakLow : Float;
         AaPeakHigh : Float;
         Count : Integer;
         Count1 : Integer;
         Count2 : Integer;
         Count1Low : Integer;
         Count1High : Integer;
         Error : Byte;
         Integral : Float;
         Integral1 : Float;
         Integral2 : Float;
         LC : Integer;
         LCP : Integer;
         LCM : Integer;
         HW1 : Float;
         HW2 : Float;
```

```
        LowerLimit : Float;
        MaxIntervals : Integer;
        NumIntervals : Integer;
        TempHeight1 : Float;
        TempHeight2 : Float;
        Tolerance : Float;
        UpperLimit : Float;

    begin
        If YesNoCO2ConcCalc = 'Y' Then
        Begin

{ Initialize some of the local variables used in this procedure. }

        AaPeakLow := 0;
        AaPeakHigh := 0;
        Error := 0;
        LC := 0;
        Integral := 0;
        LowerLimit := 1E-10;
        MaxIntervals := 1000;
        NumIntervals := 500;
        Tolerance := 1E-8;
        UpperLimit := 75;

{  These peak separations are based upon the peak to peak separation found in the AFGL listings.  }

        PeakSepLow[53] := 0.906;
        PeakSepHigh[53] := 0.881;
        PeakSepLow[55] := 0.881;
        PeakSepHigh[55] := 0.856;
        PeakSepLow[57] := 0.856;
        PeakSepHigh[57] := 0.830;
        PeakSepLow[59] := 0.830;
        PeakSepHigh[59] := 0.806;
        PeakSepLow[61] := 0.806;
        PeakSepHigh[61] := 0.780;
        PeakSepLow[63] := 0.780;
        PeakSepHigh[63] := 0.754;
        PeakSepLow[65] := 0.754;
        PeakSepHigh[65] := 0.729;
        PeakSepLow[67] := 0.729;
        PeakSepHigh[67] := 0.704;
        PeakSepLow[69] := 0.704;
        PeakSepHigh[69] := 0.678;
        PeakSepLow[71] := 0.678;
        PeakSepHigh[71] := 0.653;
        PeakSepLow[73] := 0.653;
        PeakSepHigh[73] := 0.628;
        PeakSepLow[75] := 0.628;
        PeakSepHigh[75] := 0.601;
        PeakSepLow[77] := 0.601;
        PeakSepHigh[77] := 0.577;
        PeakSepLow[79] := 0.577;
        PeakSepHigh[79] := 0.551;
        PeakSepLow[81] := 0.551;
        PeakSepHigh[81] := 0.525;
        PeakSepLow[83] := 0.525;
        PeakSepHigh[83] := 0.500;
        PeakSepLow[85] := 0.500;
        PeakSepHigh[85] := 0.474;
        PeakSepLow[87] := 0.474;
        PeakSepHigh[87] := 0.449;
        PeakSepLow[89] := 0.449;
        PeakSepHigh[89] := 0.423;


        LC := MValueRangeLowCO2 - 1;
              repeat
                 LC := LC + 1;
                 LCM := LC - 2;
```

```
                LCP := LC + 2;

{  Peak height corrections are only made after the first iteration; when an estimate of the true peak }
{  height is known.                                                                                    }

                If (MValueCO2[LC] <> 0) and (AtPeakCO2[LCM] <> 0) and (AtPeakCO2[LCP] <> 0) and
(AtPeakCO2[LC] <> 0) Then

                begin
                   HW1 := CO2CO2Width[LC]*(PPCO2Guess/TotPress)*exp(NCO2CO2[LC]*ln(300/TG));
                   HW2 := CO2N2Width[LC]*(PPN2/TotPress)*exp(NCO2N2[LC]*ln(300/TG));
                   W := HW1 + HW2;

                   Height := AtPeakCO2[LCM];
                   Integral := 0;
                   Integral1 := 0;
                   Integral2 := 0;
                   PeakSep := PeakSepLow[LC];
                   AaPeakLow := 0;

                   Adaptive_Gauss_Quadrature(LowerLimit,UpperLimit,Tolerance,MaxIntervals,
                                             Integral,NumIntervals,Error,@Cor1);
                   Integral1 := Integral;
                   Integral := 0;
                   Adaptive_Gauss_Quadrature(LowerLimit,UpperLimit,Tolerance,MaxIntervals,
                                             Integral,NumIntervals,Error,@Cor2);
                   Integral2 := Integral;
                   AaPeakLow := -(ln(Integral1/Integral2)/ln(10));
                   Height := AtPeakCO2[LCP];
                   Integral := 0;
                   Integral1 := 0;
                   Integral2 := 0;
                   PeakSep := PeakSepHigh[LC];
                   AaPeakHigh := 0;

                   Adaptive_Gauss_Quadrature(LowerLimit,UpperLimit,Tolerance,MaxIntervals,
                                             Integral,NumIntervals,Error,@Cor1);
                   Integral1 := Integral;
                   Adaptive_Gauss_Quadrature(LowerLimit,UpperLimit,Tolerance,MaxIntervals,
                                             Integral,NumIntervals,Error,@Cor2);
                   Integral2 := Integral;
                   Integral := 0;
                   AaPeakHigh := -(ln(Integral1/Integral2)/ln(10));
                   CorLineHeightCO2[LC] := LineHeightCO2[LC] - AaPeakLow - AaPeakHigh;

                   end;

             until LC = MValueRangeHighCO2;
          End;

    End;    { Procedure CorrectOverLap }

End. { unit OverLap }
```

```
unit PeakCor;

{$I Float.inc}

Interface
    Uses  Dos, Crt, Integrat, Interp, Common, GlobVar;

    {$IFOPT N+}
        Type
            Float = Double;

    {$Else}
        Type
            Float = Real;

    {$ENDIF}

    Procedure FindAtpeaks;

    Function CalculateAapeak(X : Float) : Float;


Implementation

    {$F+}

    Function CalculateAapeak(X: Float) : Float;   { Triangular Apodization, sinc Squared ILS }

     begin
      CalculateAapeak := 2*(Sqr(sin(PI*X))/Sqr(PI*X))*exp(-
ln(10.0)*AtpeakGuess/(1.0+4.0*Sqr(ResParameter*X)));
     end;  { Function CalculateAapeak }

    {$F-}

    Procedure FindAtpeaks;

{ This procedure converts the data sorted in "GetLineInformation" into true peak height information.   }
{ The experimental peak heights, called apparent peak heights or Aapeaks, are biased by a photometric  }
{ error resulting from the instruments limited resolution.  This error is removed in this procedure    }
{ and true peak heights or Atpeaks are produced.  These true peak heights can then be used for temp-   }
{ erature calculations.  The photometric error is removed by fist plotting Atpeak's vs. Aapeaks's to   }
{ determine the functional nature of the error.  A spline interpolation is then performed to determine }
{ the specific true peak height for a particular apparent (experimental) peak.                         }

    Var
        Aapeak : Float;
        Coef0 : TNVector;
        Coef1 : TNVector;
        Coef2 : TNVector;
        Coef3 : TNVector;
        Count : Integer;
        Difference : Float;
        Error : Byte;
        XInter : TNVector;
        Integral : Float;
        LHCO2 : Float;
        LW : Float;
        LW1 : Float;
        LW2 : Float;
        LW3 : Float;
        LogAapeak : TNVector;
        LogAtpeak : TNVector;
        LogAtpeakGuess : Float;
        LogIntegral : Float;
        LC : Integer;
        LowerLimit : Float;
        MaxIntervals : Integer;
        NumInter : Integer;
        NumIntervals : Integer;
        NumPoints : Integer;
```

```
        TMinCO : Float;
        Tolerance : Float;
        UpperLimit : Float;
        YInter : TNVector;

    begin

{ Initialize some of the local variables used in this procedure. }

        Error := 0;
        Integral := 0;
        LC := 0;
        LowerLimit := 1E-10;
        MaxIntervals := 1000;
        NumInter := 1;
        NumIntervals := 500;
        NumPoints := 20;
        Tolerance := 1E-8;
        UpperLimit := 75;

{ Starting with the MValue of -38, this procedure first checks the value of MValue.  If Mvalue is    }
{ equal to 0, no peak height information is available for that line.  If peak height information is  }
{ available for a line, the program goes on to initialize the arrays LogAapeak and LogAtpeak.  These }
{ arrays will be used to store calculated values of the log Aapeak (LogAapeak), given known values   }
{ of log Atpeak (LogAtpeak).                                                                         }

        LC := MValueRangeLow - 1;
             repeat
                  LW := 0;
                  LW1 := 0;
                  LW2 := 0;
                  LW3 := 0;
                  TMinCO := 0;

                  LC := LC + 1;
                  If MValue[LC] <> 0 Then
                       begin
                            Count := 1;
                            repeat
                                 LogAapeak[Count] := 0;
                                 LogAtpeak[Count] := 0;
                                 Count := Count + 1;
                            until Count = 21;

{ A resolution parameter, ResParameter, is calculated.  This value is a function of the nominal instrument }
{ resolution, InstRes, and the line width of the absorption line, LineWidth.  The line width is a function }
{ of the standard line width, StandardLineWidth, the pressure within the gas cell, and the temperature of  }
{ the gas.  This resolution parameter, along with a value for the true line height (AtpeakGuess) are then  }
{ used by the function, CalculateAapeak, to calculate a value of Aapeak (apparent peak height).  Twenty of }
{ these calculations are done for different values of the true line height, so that Aapeak vs. Atpeak data }
{ can be plotted.                                                                                          }

                            Begin
                             LW1 := COCOWidthLT[LC]*(PPCOGuess/TotPress)*exp(0.75*ln(297/TG));
                             LW2 := CON2WidthHT[LC]*(PPN2/TotPress)*exp(NCON2[LC]*ln(300/TG));
                             LW3 := COCO2WidthHT[LC]*(PPCO2Guess/TotPress)*exp(NCOCO2[LC]*ln(300/TG));
                             LW := LW1+LW2+LW3;
                             TMinCO := 4*1.922529*ABS(MValue[LC])*1.5;
                             If TG < TMinCO Then
                               begin
                                 LW := 0;
                                 MValue[LC] := 0;
                               end
                            End;

                            If LW <> 0 Then
                            Begin
                            ResParameter := InstRes/(2.0*LW);
                            LogAtpeakGuess := -1.5;
                            AtpeakGuess := 0.0316;
                            Count := 1;
```

```
                        Writeln;
                        Writeln('Calculating Atpeak for line m = ',MValue[LC],' (Iteration = ',
                                ResultsCount,')');
                        repeat
                             Write('.');
                             Adaptive_Gauss_Quadrature(LowerLimit,UpperLimit, Tolerance,MaxIntervals,
                                                       Integral,NumIntervals,Error,@CalculateAapeak);
    { Store Log(AtpeakGuess) }    LogAtpeak[Count] := LogAtpeakGuess;
    { Convert from %T to Abs }    LogIntegral := -(ln(Integral)/ln(10));
    { Store Log(Aapeak) }         LogAapeak[Count] := ln(LogIntegral)/ln(10);
    { Get new LogAtpeakGuess }    LogAtpeakGuess := LogAtpeakGuess + 0.175;
    { Antilog of LogAtpeakGuess } AtpeakGuess := exp(LogAtpeakGuess*ln(10.0));
                             Count := Count + 1;
                        until Count = 21;
                        Writeln;

{ Once the functional relationship between Aapeak and Atpeak (Log Aapeak vs. Log Atpeak) is known, the     }
{ data is plotted and a cubic spline interpolation is performed to determine the value of Atpeak given an  }
{ experimental value of Aapeak.  This procedure then yields the correction for the photometric error for a }
{ given experimental line of interest.                                                                      }

                        YInter[1] := 0;
                        XInter[1] := ln(LineHeight[LC])/ln(10);
                        Error := 0;
                        CubicSplineFree(NumPoints, LogAapeak, LogAtpeak, NumInter, XInter,
                                        Coef0, Coef1, Coef2, Coef3, YInter, Error);
                        Atpeak[LC] := exp(YInter[1]*ln(10));

{ Before completing this procedure, a check is made of the difference between the interpolated value of }
{ Aapeak, and a value of Aapeak which would have been calculated given the knowledge of the value of    }
{ Atpeak.  The interpolated value of Atpeak found above is put into the function CalculateAapeak and a  }
{ calculated value of Aapeak is obtained.  This value is then compared with the experimentally obtained }
{ value of the line height, LineHeight, and the difference between the two is calculated.                }

                        Difference := 0;
                        Aapeak := 0;
                        AtpeakGuess := Atpeak[LC];
                        Adaptive_Gauss_Quadrature(LowerLimit,UpperLimit,Tolerance,MaxIntervals,
                                                  Integral,NumIntervals,Error,@CalculateAapeak);
                        Aapeak := -(ln(Integral)/ln(10));
                        Difference := Abs(Aapeak - LineHeight[LC]);
                        If Difference > 0.005 Then
                             begin
                                  Writeln('Couldn"t find good Atpeak for m =',MValue[LC]);
                                  MValue[LC] := 0;
                                  Atpeak[LC] := 0;
                             end;
                        end;
                   end;

              until LC = MValueRangeHigh;


{ Perform peak height corrections for CO2 peaks. }

              If YesNoCO2ConcCalc = 'Y' Then
              Begin

{ Initialize some of the local variables used in this procedure. }

              Error := 0;
              Integral := 0;
              LC := 0;
              LowerLimit := 1E-10;
              LW := 0;
              LW1 := 0;
              LW2 := 0;

{ Starting with the MValueCO2 of 1, this procedure first checks the value of MValue.  If Mvalue is    }
{ equal to 0, no peak height information is available for that line.  If peak height information is  }
{ available for a line, the program goes on to initialize the arrays LogAapeak and LogAtpeak.  These }
```

```
{ arrays will be used to store calculated values of the log Aapeak (LogAapeak), given known values   }
{ of log Atpeak (LogAtpeak).                                                                        }

              LC := MValueRangeLowCO2 - 1;
                   repeat
                        LC := LC + 1;
                        If MValueCO2[LC] <> 0 Then
                             begin
                                  Count := 1;
                                  repeat
                                       LogAapeak[Count] := 0;
                                       LogAtpeak[Count] := 0;
                                       Count := Count + 1;
                                  until Count = 21;

{ A resolution parameter, ResParameter, is calculated. }

                                  LHCO2 := 0;
                                  LHCO2 := LineHeightCO2[LC];
                                  If CorLineHeightCO2[LC] <> 0 Then
                                    LHCO2 := CorLineHeightCO2[LC];

                                  LW1 := CO2CO2Width[LC]*(PPCO2Guess/TotPress)*exp(NCO2CO2[LC]*ln(300/TG));
                                  LW2 := CO2N2Width[LC]*(PPN2/TotPress)*exp(NCO2N2[LC]*ln(300/TG));
                                  LW := LW1+LW2;

                                  ResParameter := InstRes/(2.0*LW);

                                  LogAtpeakGuess := -1.5;
                                  AtpeakGuess := 0.0316;
                                  Count := 1;
                                  Writeln;
                                  Writeln('Calculating Atpeak for line m = ',MValueCO2[LC],' (Iteration = ',
                                          ResultsCount,')');
                                  repeat
                                       Write('.');
                                       Adaptive_Gauss_Quadrature(LowerLimit,UpperLimit, Toler-
ance,MaxIntervals,
                                                                                  Inte-
gral,NumIntervals,Error,@CalculateAapeak);
    { Store Log(AtpeakGuess) }         LogAtpeak[Count] := LogAtpeakGuess;
    { Convert from %T to Abs }         LogIntegral := -(ln(Integral)/ln(10));
    { Store Log(Aapeak) }              LogAapeak[Count] := ln(LogIntegral)/ln(10);
    { Get new LogAtpeakGuess }         LogAtpeakGuess := LogAtpeakGuess + 0.175;
    { Antilog of LogAtpeakGuess }      AtpeakGuess := exp(LogAtpeakGuess*ln(10.0));
                                       Count := Count + 1;
                                  until Count = 21;
                                  Writeln;

{ Once the functional relationship between Aapeak and Atpeak (Log Aapeak vs. Log Atpeak) is known, the     }
{ data is plotted and a cubic spline interpolation is performed to determine the value of Atpeak given an  }
{ experimental value of Aapeak.  This procedure then yields the correction for the photometric error for a }
{ given experimental line of interest.                                                                      }

                                  YInter[1] := 0;
                                  XInter[1] := ln(LHCO2)/ln(10);
                                  Error := 0;
                                  CubicSplineFree(NumPoints, LogAapeak, LogAtpeak, NumInter, XInter,
                                                  Coef0, Coef1, Coef2, Coef3, YInter, Error);
                                  AtpeakCO2[LC] := exp(YInter[1]*ln(10));

{ Before completing this procedure, a check is made of the difference between the interpolated value of }
{ Aapeak, and a value of Aapeak which would have been calculated given the knowledge of the value of    }
{ Atpeak.  The interpolated value of Atpeak found above is put into the function CalculateAapeak and a  }
{ calculated value of Aapeak is obtained.  This value is then compared with the experimentally obtained }
{ value of the line height, LineHeight, and the difference between the two is calculated.                }

                                  Difference := 0;
                                  Aapeak := 0;
                                  AtpeakGuess := AtpeakCO2[LC];
                                  Adaptive_Gauss_Quadrature(LowerLimit,UpperLimit,Tolerance,MaxIntervals,
```

```
                                        Integral,NumIntervals,Error,@CalculateAapeak);
                                Aapeak := -(ln(Integral)/ln(10));
                                Difference := Abs(Aapeak - LHCO2);
                                If Difference > 0.005 Then
                                     begin
                                          Writeln('Couldn"t find good Atpeak for m =',MValueCO2[LC]);
                                          MValueCO2[LC] := 0;
                                          AtpeakCO2[LC] := 0;
                                     end;
                           end;

                      until LC = MValueRangeHighCO2;

                End;

        End;    { Procedure FindAtpeaks }

End. { unit PeakCor }
```

```
unit TempCalc;

{$I Float.inc}

Interface
    Uses   Dos, Crt, LeastSqr, Common, GlobVar;

    {$IFOPT N+}
         Type
              Float = Double;
    {$Else}
         Type
              Float = Real;
    {$ENDIF}

    Procedure TemperatureCalculations;

Implementation

    Procedure TemperatureCalculations;

{ This procedure uses the corrected peak heights of carbon monoxide to calculate the rotaional   }
{ temperature of the gas.  This is accomplished by first initializing the local variables used   }
{ in this procedure.  A large repeat..until loop is then begun with the value of MValue the key  }
{ directive.  If it is zero, no peak height information is available for that particular         }
{ absorption line.  If this is the case, then the value of LoopCount is increased by one and     }
{ and the next absorption line is examined.  If MValue at element LoopCount is not equal to      }
{ zero then it must be determined if the absorption line is from the R or the P absorption       }
{ branch.  If MValue is positive, the line is from the R branch.  If MValue is negative, the     }
{ absorption line is from the P branch.  The rotational energy of the initial state of the       }
{ transition is then calculated, Energy, as well as a modified peak height, LnPeak.  This        }
{ procedure is repeated for each line and the results are stored in the arrays Energy and LnPeak. }
{ These arrays are then plotted and a linear least squares fit of the data is performed.  The    }
{ linear regression yields a value for the slope of the fitted line, and the the temperature is  }
{ calculated from the slope.                                                                     }

    Var
         Add : Integer;
         AverageEnergy : Float;
         Count : Integer;
         EnergyPart1 : Float;
         EnergyPart2 : Float;
         EnergyRegression : TNColumnVector;
         Error : Byte;
         Fit : FitType;
         LW : Float;
         LW1 : Float;
         LW2 : Float;
         LW3 : Float;
         J : Integer;
         LnPeakPart1 : Float;
         LnPeakPart2 : Float;
         LnPeakPart3 : Float;
         LnPeakRegression : TNColumnVector;
         LC : Integer;
         NumPoints : Integer;
         NumTerms : Integer;
         Residual : TNColumnVector;
         StandardErrorSlope : Float;
         Solution : TNRowVector;
         StandardDeviation : Float;
         Sum : Float;
         SumEnergySquared : Float;
         Temperature : Float;
         TMinCO : Float;
         Variance : Float;
         YFit : TNColumnVector;


    begin
```

```
{ Initialize some of the local variables used in this procedure. }

        LC := 0;
        Count := -38;
             repeat
                  Energy[Count] := 0;
                  LnPeak[Count] := 0;
                  Count := Count + 1;
             until Count = 39;


        Count := 1;
        repeat
             TempPlot[Count,1] := 0;
             TempPlot[Count,2] := 0;
             Count := Count + 1;
        until Count = 101;


{ Starting with the MValue of -38 or MValueRangeLow, this procedure first checks the value stored in  }
{ MValue.  If MValue is equal to 0, no peak height information is available for that line.  If peak   }
{ height information is available for that line, the program goes on to calculate the energy term     }
{ corresponding to that line.  It also calculates a term containing peak height information which in  }
{ part uses the values of Atpeak calculated in the previous procedure.                               }


             LC := MValueRangeLow -1;
             Count := 1;

             repeat
                  J := 1;
                  EnergyPart1 := 0;
                  EnergyPart2 := 0;
                  HerWalCor := 0;
                  LnPeakPart1 := 0;
                  LnPeakPart2 := 0;
                  LnPeakPart3 := 0;
                  LC := LC + 1;

                  If MValue[LC] <> 0 Then
                  begin
                       If MValue[LC] < 0 Then
                       Begin
                            LW := 0;
                            LW1 := 0;
                            LW2 := 0;
                            LW3 := 0;
                            TMinCO := 0;
                            J := Abs(MValue[LC]);

{ Rotational Energy}        EnergyPart1 := 1.922529*J*(J+1)*2.998E+10*6.62618E-34/1.38066E-23;
                            EnergyPart2 := 6.1193E-6*J*J*Sqr(J+1)*2.998E+10*6.62618E-34/1.38066E-23;
                            Energy[LC] := EnergyPart1-EnergyPart2;

{ Herman-Wallis Corrections} HerWalCor := 1+1.77E-4*MValue[LC]+6.67E-6*Sqr(MValue[LC]);

                            Begin
                                 LW1 := COCOWidthLT[LC]*(PPCOGuess/TotPress)*exp(0.75*ln(297/TG));
                                 LW2 := CON2WidthHT[LC]*(PPN2/TotPress)*exp(NCON2[LC]*ln(300/TG));
                                 LW3 := COCO2WidthHT[LC]*(PPCO2Guess/TotPress)*exp(NCOCO2[LC]*ln(300/TG));
                                 LW := LW1+LW2+LW3;
                                 TMinCO := 4*1.922529*ABS(MValue[LC])*1.5;
                                 If TG < TMinCO Then
                                   LW := 0;
                            End;

                            If LW <> 0 Then
                            Begin
                                 LnPeakPart1 := Atpeak[LC]*LW/TrueLinePosition[LC];
                                 LnPeakPart2 := Abs(MValue[LC])*HerWalCor;
                                 LnPeakPart3 := 1-exp(-2.998E+10*6.62618E-
```

```
34*TrueLinePosition[LC]/(1.38066E-23*TG));
                              LnPeak[LC] := ln(LnPeakPart1/(LnPeakPart2*LnPeakPart3));
                         End;
                    End
               Else
                    Begin
                         LW := 0;
                         LW1 := 0;
                         LW2 := 0;
                         LW3 := 0;
                         TMinCO := 0;
                         J :=  MValue[LC] - 1;

                         EnergyPart1 := 1.922529*J*(J+1)*2.998E+10*6.62618E-34/1.38066E-23;
                         EnergyPart2 := 6.1193E-6*J*J*Sqr(J+1)*2.998E+10*6.62618E-34/1.38066E-23;
                         Energy[LC] := (EnergyPart1-EnergyPart2);

                         HerWalCor := 1+1.77E-4*MValue[LC]+6.67E-6*Sqr(MValue[LC]);

                         Begin
                              LW1 := COCOWidthLT[LC]*(PPCOGuess/TotPress)*exp(0.75*ln(297/TG));
                              LW2 := CON2WidthHT[LC]*(PPN2/TotPress)*exp(NCON2[LC]*ln(300/TG));
                              LW3 := COCO2WidthHT[LC]*(PPCO2Guess/TotPress)*exp(NCOCO2[LC]*ln(300/TG));
                              LW := LW1+LW2+LW3;
                              TMinCO := 4*1.922529*ABS(MValue[LC])*1.5;
                              If TG < TMinCO Then
                                LW := 0;
                         End;

                         If LW <> 0 Then
                         Begin
                              LnPeakPart1 := Atpeak[LC]*LW/TrueLinePosition[LC];
                              LnPeakPart2 := Abs(MValue[LC])*HerWalCor;
                              LnPeakPart3 := 1-exp(-2.998E+10*6.62618E-
34*TrueLinePosition[LC]/(1.38066E-23*TG));
                              LnPeak[LC] := ln(LnPeakPart1/(LnPeakPart2*LnPeakPart3));
                         End;
                    end;

               If LW <> 0 Then
               Begin
                    TempPlot[Count,1] := Energy[LC];
                    TempPlot[Count,2] := LnPeak[LC];
                    Count := Count + 1;
               End;

               end;

          until LC = MValueRangeHigh;


{ The values calculated for LnPeak and Energy are put into two new arrays, LnPeakRegression and   }
{ EnergyRegression respectively.                                                                   }

     LC := MValueRangeLow - 1;
     NumPoints := 0;
     repeat
          LC := LC +1;
          If LnPeak[LC] <> 0 Then
          begin
               NumPoints := NumPoints + 1;
               LnPeakRegression[NumPoints] := LnPeak[LC];
               EnergyRegression[NumPoints] := Energy[LC];
          end;

     until MValueRangeHigh = LC;

{ The arrays EnergyRegression and LnPeakRegression are sent to the procedure LeastSquares in order to     }
{ calculate the equation of the line (linear function) to the data.  From this equation, the slope of the }
{ line is also calculated which, when the negative reciprocal is taken, yields the value of the           }
{ temperature of the gas.                                                                                  }
```

```
        Solution[1] := 0;
        Solution[2] := 0;
        StandardDeviation := 0;
        Variance := 0;
        Error := 0;
        NumTerms := 2;
        Fit := Poly;
        StandardErrorSlope := 0;
        SumEnergySquared := 0;
        AverageEnergy := 0;
        Sum := 0;
        LeastSquares(NumPoints,EnergyRegression,LnPeakRegression,NumTerms,Solution,
                     YFit,Residual,StandardDeviation,Variance,Error,Fit);
        Temperature := -1/Solution[2];
        TemperatureResults[ResultsCount] := Temperature;
        VarianceResults[ResultsCount] := Variance;
        StandardDeviationResults[ResultsCount] := StandardDeviation;

{ Calculate the Standard Error (Standard Deviation) of least squares line.  }

        Add := 0;
        repeat
             Add := Add + 1;
             Sum := Sum + TempPlot[Add,1];
        until Add = NumPoints;

        AverageEnergy := Sum/NumPoints;
        Add := 0;

        repeat
             Add := Add + 1;
             SumEnergySquared := SumEnergySquared + SQR(EnergyRegression[Add] - AverageEnergy);
        until Add = NumPoints;

        StandardErrorSlope := StandardDeviation/SQRT(SumEnergySquared);
        StandardErrorSlope := -1*StandardErrorSlope/Solution[2];
        StandardErrorTemperature[ResultsCount] := StandardErrorSlope*Temperature;

    end;   { Procedure TemperatureCalculations }

End.   { unit TempCalc.pas }
```

```
unit COConc;

{$I Float.inc}

Interface

Uses    Dos, Crt, Interp, LeastSqr, Common, GlobVar;

{$IFOPT N+}
    Type
        Float = Double;
{$Else}
    Type
        Float = Real;
{$ENDIF}

Procedure COConcentrationCalculations;


Implementation

Procedure COConcentrationCalculations;

{  Define local variables.  }

    Var
        Coef0 : TNVector;
        Coef1 : TNVector;
        Coef2 : TNVector;
        Coef3 : TNVector;
        COConcCount : Integer;
        Count : Integer;
        Error : Byte;
        LW : Float;
        LW1 : Float;
        LW2 : Float;
        LW3 : Float;
        LC : Integer;
        NumInter : Integer;
        NumPointsSpline : Integer;
        S : Float;
        SSXDifference : Float;
        TempTooLow : LineDataFloat;
        TempTooHigh : LineDataFloat;
        TMinCO : Float;
        XData : TNVector;
        YData : TNVector;
        XInter : TNVector;
        YInter : TNVector;

Begin

{  Initialize variables.  }

    Error := 0;
    NumInter := 1;
    XInter[1] := TG;
    LC := 0;
    Count := -38;
    repeat
        PPCOCalc[Count] := 0;
        LineStrength[Count] := 0;
        TempTooLow[Count] := 0;
        TempTooHigh[Count] := 0;
        Count := Count + 1;
    until Count = 39;

    TempTooLow[-5] := 10.522;
    TempTooLow[-6] := 11.013;
    TempTooLow[-7] := 11.367;
    TempTooLow[-8] := 11.241;
```

```
    TempTooLow[-9] := 10.364;
    TempTooLow[-11] := 8.472;
    TempTooLow[-12] := 7.347;
    TempTooLow[-13] := 6.196;
    TempTooLow[-14] := 5.031;
    TempTooLow[-15] := 4.113;
    TempTooLow[-21] := 0.704;
    TempTooLow[-22] := 0.493;
    TempTooLow[-23] := 0.346;
    TempTooLow[-25] := 0.154;
    TempTooHigh[-5] := 0.546;
    TempTooHigh[-6] := 0.653;
    TempTooHigh[-7] := 0.724;
    TempTooHigh[-8] := 0.771;
    TempTooHigh[-9] := 0.834;
    TempTooHigh[-11] := 0.926;
    TempTooHigh[-12] := 0.966;
    TempTooHigh[-13] := 0.982;
    TempTooHigh[-14] := 0.994;
    TempTooHigh[-15] := 1.003;
    TempTooHigh[-21] := 0.860;
    TempTooHigh[-22] := 0.759;
    TempTooHigh[-23] := 0.752;
    TempTooHigh[-25] := 0.673;
    TempTooHigh[-26] := 0.582;
    TempTooHigh[-27] := 0.541;
    TempTooHigh[-28] := 0.522;
    TempTooHigh[-29] := 0.468;
    TempTooHigh[-30] := 0.376;
    TempTooHigh[-31] := 0.372;
    TempTooHigh[-34] := 0.225;
    TempTooHigh[-35] := 0.236;

        LC := MValueRangeLow - 1;
        repeat
            LC := LC + 1;
            S := 0;
            LW := 0;
            LW1 := 0;
            LW2 := 0;
            LW3 := 0;
            TMinCO := 0;
            If MValue[LC] <> 0 Then
            begin

{  Calculate halfwidths of the CO lines.  }

                Begin
                    LW1 := COCOWidthLT[LC]*(PPCOGuess/TotPress)*exp(0.75*ln(297/TG));
                    LW2 := CON2WidthHT[LC]*(PPN2/TotPress)*exp(NCON2[LC]*ln(300/TG));
                    LW3 := COCO2WidthHT[LC]*(PPCO2Guess/TotPress)*exp(NCOCO2[LC]*ln(300/TG));
                    LW := LW1+LW2+LW3;
                    TMinCO := 4*1.922529*ABS(MValue[LC])*1.5;
                    If TG < TMinCO Then
                      LW := 0;
                End;

{  Assign temperature and line strength data to variables.  }

                If (CalculationChoice = 'P') and (TG > 285) and (TG < 1260) and (LC < -4) and (LC > -36)
Then
                begin
                    If LC > -25.5 Then
                    begin
                        NumPointsSpline := 8;
                        XData[1] := 294.2;
                        XData[2] := 353.1;
                        XData[3] := 535.1;
                        XData[4] := 719.7;
                        XData[5] := 936.2;
                        XData[6] := 1033.8;
```

```
     XData[7] := 1143.9;
     XData[8] := 1226.5;
end
Else If (LC > -27.5) and (LC < -25.5) and (TG > 353.1) Then
begin
     NumPointsSpline := 7;
     XData[1] := 353.1;
     XData[2] := 535.1;
     XData[3] := 719.7;
     XData[4] := 936.2;
     XData[5] := 1033.8;
     XData[6] := 1143.9;
     XData[7] := 1226.5;
End
Else If (LC > -31.5) and (LC < -27.5) and (TG > 535.1) Then
begin
     NumPointsSpline := 6;
     XData[1] := 535.1;
     XData[2] := 719.7;
     XData[3] := 936.2;
     XData[4] := 1033.8;
     XData[5] := 1143.9;
     XData[6] := 1226.5;
End

Else If (LC > -36) and (LC < -31.5) and (TG > 719.7) Then
begin
     NumPointsSpline := 5;
     XData[1] := 719.7;
     XData[2] := 936.2;
     XData[3] := 1033.8;
     XData[4] := 1143.9;
     XData[5] := 1226.5;
End;

If LC = -5 Then
begin
     YData[1] := 10.522;
     YData[2] := 7.538;
     YData[3] := 3.425;
     YData[4] := 2.021;
     YData[5] := 1.096;
     YData[6] := 0.875;
     YData[7] := 0.661;
     YData[8] := 0.546;
end

Else If LC = -6 Then
begin
     YData[1] := 11.013;
     YData[2] := 8.198;
     YData[3] := 3.787;
     YData[4] := 2.306;
     YData[5] := 1.271;
     YData[6] := 1.001;
     YData[7] := 0.780;
     YData[8] := 0.653;
end

Else If LC = -7 Then
begin
     YData[1] := 11.367;
     YData[2] := 8.378;
     YData[3] := 4.088;
     YData[4] := 2.510;
     YData[5] := 1.391;
     YData[6] := 1.106;
     YData[7] := 0.878;
     YData[8] := 0.724;
end
```

```
Else If LC = -8 Then
begin
     YData[1] := 11.241;
     YData[2] := 8.567;
     YData[3] := 4.267;
     YData[4] := 2.626;
     YData[5] := 1.511;
     YData[6] := 1.207;
     YData[7] := 0.928;
     YData[8] := 0.771;
end

Else If LC = -9 Then
begin
     YData[1] := 10.364;
     YData[2] := 8.500;
     YData[3] := 4.373;
     YData[4] := 2.814;
     YData[5] := 1.581;
     YData[6] := 1.283;
     YData[7] := 1.025;
     YData[8] := 0.834;
end

Else If LC = -11 Then
begin
     YData[1] := 8.472;
     YData[2] := 7.155;
     YData[3] := 4.275;
     YData[4] := 2.854;
     YData[5] := 1.712;
     YData[6] := 1.387;
     YData[7] := 1.109;
     YData[8] := 0.926;
end

Else If LC = -12 Then
begin
     YData[1] := 7.347;
     YData[2] := 6.552;
     YData[3] := 4.085;
     YData[4] := 2.864;
     YData[5] := 1.741;
     YData[6] := 1.427;
     YData[7] := 1.155;
     YData[8] := 0.966;
end

Else If LC = -13 Then
begin
     YData[1] := 6.196;
     YData[2] := 5.794;
     YData[3] := 3.874;
     YData[4] := 2.800;
     YData[5] := 1.728;
     YData[6] := 1.437;
     YData[7] := 1.176;
     YData[8] := 0.982;
end

Else If LC = -14 Then
begin
     YData[1] := 5.031;
     YData[2] := 4.856;
     YData[3] := 3.629;
     YData[4] := 2.719;
     YData[5] := 1.728;
     YData[6] := 1.442;
     YData[7] := 1.202;
     YData[8] := 0.994;
end
```

```
Else If LC = -15 Then
begin
     YData[1] := 4.113;
     YData[2] := 4.069;
     YData[3] := 3.301;
     YData[4] := 2.598;
     YData[5] := 1.680;
     YData[6] := 1.413;
     YData[7] := 1.179;
     YData[8] := 1.003;
end

Else If LC = -21 Then
begin
     YData[1] := 0.704;
     YData[2] := 1.010;
     YData[3] := 1.420;
     YData[4] := 1.503;
     YData[5] := 1.216;
     YData[6] := 1.094;
     YData[7] := 0.947;
     YData[8] := 0.860;
end

Else If LC = -22 Then
begin
     YData[1] := 0.493;
     YData[2] := 0.779;
     YData[3] := 1.197;
     YData[4] := 1.312;
     YData[5] := 1.119;
     YData[6] := 1.014;
     YData[7] := 0.875;
     YData[8] := 0.759;
end

Else If LC = -23 Then
begin
     YData[1] := 0.346;
     YData[2] := 0.539;
     YData[3] := 0.986;
     YData[4] := 1.182;
     YData[5] := 1.022;
     YData[6] := 0.916;
     YData[7] := 0.829;
     YData[8] := 0.752;
end

Else If LC = -25 Then
begin
     YData[1] := 0.154;
     YData[2] := 0.303;
     YData[3] := 0.656;
     YData[4] := 0.905;
     YData[5] := 0.826;
     YData[6] := 0.773;
     YData[7] := 0.705;
     YData[8] := 0.673;
end

Else If (LC = -26) and (TG > 353.1) Then
begin
     YData[1] := 0.185;
     YData[2] := 0.491;
     YData[3] := 0.735;
     YData[4] := 0.731;
     YData[5] := 0.679;
     YData[6] := 0.640;
     YData[7] := 0.582;
end
```

```
Else If (LC = -27) and (TG > 353.1) Then
begin
     YData[1] := 0.130;
     YData[2] := 0.402;
     YData[3] := 0.635;
     YData[4] := 0.647;
     YData[5] := 0.629;
     YData[6] := 0.594;
     YData[7] := 0.541;
end

Else If (LC = -28) and (TG > 535.1) Then
begin
     YData[1] := 0.306;
     YData[2] := 0.520;
     YData[3] := 0.571;
     YData[4] := 0.556;
     YData[5] := 0.533;
     YData[6] := 0.522;
end

Else If (LC = -29) and (TG > 535.1) Then
begin
     YData[1] := 0.248;
     YData[2] := 0.431;
     YData[3] := 0.496;
     YData[4] := 0.488;
     YData[5] := 0.482;
     YData[6] := 0.468;
end

Else If (LC = -30) and (TG > 535.1) Then
begin
     YData[1] := 0.178;
     YData[2] := 0.333;
     YData[3] := 0.428;
     YData[4] := 0.432;
     YData[5] := 0.437;
     YData[6] := 0.376;
end

Else If (LC = -31) and (TG > 535.1) Then
begin
     YData[1] := 0.140;
     YData[2] := 0.307;
     YData[3] := 0.378;
     YData[4] := 0.397;
     YData[5] := 0.374;
     YData[6] := 0.372;
end

Else If (LC = -34) and (TG > 719.7) Then
begin
     YData[1] := 0.154;
     YData[2] := 0.215;
     YData[3] := 0.235;
     YData[4] := 0.266;
     YData[5] := 0.225;
end

Else If (LC = -35) and (TG > 719.7) Then
begin
     YData[1] := 0.111;
     YData[2] := 0.183;
     YData[3] := 0.210;
     YData[4] := 0.209;
     YData[5] := 0.236;
end

Else
```

```
                    begin
                         LW := 0
                    end;

{  Perform interpolation to get line strength at a specific temperature.  }

                   If (TG > 294.2) and (TG < 1226.6) and (LW <> 0) Then
                    begin
                         CubicSplineFree(NumPointsSpline,XData,YData,NumInter,XInter,
                                         Coef0,Coef1,Coef2,Coef3,YInter,Error);
                         S := YInter[1];
                    end;

                    If (TG <= 294.2) and (TG > 285) and (LC > -25.5) Then
                      begin
                        S := TempTooLow[LC];
                      end;
                    If (TG >= 1226.5) and (TG < 1260) Then
                      begin
                        S := TempTooHigh[LC];
                      end;

{  Calculate the partial pressure.  }

                    If (S <> 0) Then
                      PPCOCalc[LC] := Atpeak[LC]*PI*ln(10)*LW/(PathLength*S/760);

               end
               Else If (CalculationChoice = 'S') Then
               begin

{  Calculate the line strength.  }

                    LineStrength[LC] := Atpeak[LC]*PI*ln(10)*LW/(PathLength*PPCOGuess/760);
               end;
          end;

     until LC = MValueRangeHigh;

  LC := MValueRangeLow - 1;
  COConcCount := 0;
  AverageCOConcentration := 0;

{  Sum all the calculated concentrations.  }

  repeat
       LC := LC +1;
       If (MValue[LC] <> 0) and (PPCOCalc[LC] <> 0) Then
       begin
            COConcCount := COConcCount + 1;
            AverageCOConcentration := AverageCOConcentration + PPCOCalc[LC];
        end;
  until MValueRangeHigh = LC;

{  Calculate average CO concentration.  }

  If COConcCount <> 0 Then
  begin
       AverageCOConcentration := AverageCOConcentration/COConcCount;
       AveragePercentCO := 100*(AverageCOConcentration/TotPress);
  end;

{  Calculate standard deviation of the average CO gas concentration.  }

  StandardDeviationCO := 0;
  SSXDifference := 0;
  LC := MValueRangeLow - 1;
  repeat
       LC := LC + 1;
       If PPCOCalc[LC] <> 0 Then
         SSXDifference := SSXDifference + SQR(PPCOCalc[LC] - AverageCOConcentration);
```

```
    until MValueRangeHigh = LC;

    If (AverageCOConcentration <> 0) and (COConcCount > 1) Then
    Begin
       StandardDeviationCO := SQRT(SSXDifference/(COConcCount - 1));
       StandardDeviationCO := StandardDeviationCO*AveragePercentCO/AverageCOConcentration;
    end;

end; {Procedure COConcentrationCalculation }

End.   { unit COConc }
```

```
unit CO2Conc;

{$I Float.inc}


Interface

Uses  GlobVar, Dos, Crt, Interp, LeastSqr, Common;

{$IFOPT N+}
    Type
         Float = Double;
{$Else}
    Type
         Float = Real;
{$ENDIF}

Procedure CO2ConcentrationCalculations;


Implementation

Procedure CO2ConcentrationCalculations;

{  Define local variables.  }

    Var
         Coef0 : TNVector;
         Coef1 : TNVector;
         Coef2 : TNVector;
         Coef3 : TNVector;
         Count : Integer;
         CO2ConcCount : Integer;
         Error : Byte;
         LW : Float;
         LW1 : Float;
         LW2 : Float;
         LC : Integer;
         LCL : Integer;
         LCH : Integer;
         NumInter : Integer;
         NumPointsSpline : Integer;
         S : Float;
         SSXDifference : Float;
         TempTooLow : LineDataFloatCO2;
         TempTooHigh : LineDataFloatCo2;
         XData : TNVector;
         YData : TNVector;
         XInter : TNVector;
         YInter : TNVector;

    Begin

{  Initialize variables.  }

    Error := 0;
    NumInter := 1;
    XInter[1] := TG;
    Count := 1;
    repeat
         PPCO2Calc[Count] := 0;
         LineStrengthCO2[Count] := 0;
         TempTooLow[Count] := 0;
         TempTooHigh[Count] := 0;
         Count := Count + 1;
    until Count = 101;

    LW := 0;
    LW1 := 0;
    LW2 := 0;
    S := 0;
```

```
    TempTooLow[53] := 2.776;
    TempTooLow[55] := 1.919;
    TempTooLow[57] := 1.284;
    TempTooLow[59] := 0.854;
    TempTooLow[61] := 0.560;
    TempTooLow[63] := 0.367;
    TempTooLow[65] := 0.228;
    TempTooLow[67] := 0.145;
    TempTooHigh[53] := 2.462;
    TempTooHigh[55] := 2.444;
    TempTooHigh[57] := 2.281;
    TempTooHigh[59] := 2.111;
    TempTooHigh[61] := 1.812;
    TempTooHigh[63] := 1.303;
    TempTooHigh[65] := 1.194;
    TempTooHigh[67] := 1.092;
    TempTooHigh[69] := 0.999;
    TempTooHigh[71] := 0.915;
    TempTooHigh[73] := 0.838;
    TempTooHigh[75] := 0.752;
    TempTooHigh[77] := 0.593;
    TempTooHigh[79] := 0.530;
    TempTooHigh[81] := 0.477;
    TempTooHigh[83] := 0.411;
    TempTooHigh[85] := 0.367;
    TempTooHigh[87] := 0.329;
    TempTooHigh[89] := 0.287;

        LC := MValueRangeLowCO2 - 1;
        repeat
            LC := LC + 1;
            LCL := LC - 2;
            LCH := LC + 2;
            If (MValueCO2[LC] <> 0) and (MValueCO2[LCL] <> 0) and (MValueCO2[LCH] <> 0) Then
            begin

{  Calculate halfwidths of CO2 lines.  }

                LW1 := CO2CO2Width[LC]*(PPCO2Guess/TotPress)*exp(NCO2CO2[LC]*ln(300/TG));
                LW2 := CO2N2Width[LC]*(PPN2/TotPress)*exp(NCO2N2[LC]*ln(300/TG));
                LW := LW1+LW2;

                If (CalculationChoiceCO2 = 'P') and (TG > 285) and (TG < 1260) and (LC > 52) and (LC <
90) Then
                begin

                    If LC < 68 Then
                    Begin
                        NumPointsSpline := 8;
                        XData[1] := 294.2;
                        XData[2] := 353.1;
                        XData[3] := 535.1;
                        XData[4] := 719.7;
                        XData[5] := 936.2;
                        XData[6] := 1033.8;
                        XData[7] := 1143.9;
                        XData[8] := 1226.5;
                    end
                    Else If (LC > 68) and (LC < 72) and (TG > 353.1) Then
                    begin
                        NumPointsSpline := 7;
                        XData[1] := 353.1;
                        XData[2] := 535.1;
                        XData[3] := 719.7;
                        XData[4] := 936.2;
                        XData[5] := 1033.8;
                        XData[6] := 1143.9;
                        XData[7] := 1226.5;
                    end

                    Else If (LC > 72) and (LC < 84) and (TG > 535.1) Then
```

```
begin
     NumPointsSpline := 6;
     XData[1] := 535.1;
     XData[2] := 719.7;
     XData[3] := 936.2;
     XData[4] := 1033.8;
     XData[5] := 1143.9;
     XData[6] := 1226.5;
end

Else If (LC > 84) and (LC < 90) and (TG > 719.7) Then
begin
     NumPointsSpline := 5;
     XData[1] := 719.7;
     XData[2] := 936.2;
     XData[3] := 1033.8;
     XData[4] := 1143.9;
     XData[5] := 1226.5;
end;

If LC = 53 Then
begin
     YData[1] := 2.776;
     YData[2] := 4.426;
     YData[3] := 6.695;
     YData[4] := 5.939;
     YData[5] := 4.056;
     YData[6] := 3.513;
     YData[7] := 2.996;
     YData[8] := 2.462;
end

Else If LC = 55 Then
begin
     YData[1] := 1.919;
     YData[2] := 3.246;
     YData[3] := 5.692;
     YData[4] := 5.505;
     YData[5] := 3.694;
     YData[6] := 3.293;
     YData[7] := 2.900;
     YData[8] := 2.444;
end

Else If LC = 57 Then
begin
     YData[1] := 1.284;
     YData[2] := 2.321;
     YData[3] := 4.497;
     YData[4] := 4.515;
     YData[5] := 3.356;
     YData[6] := 3.047;
     YData[7] := 2.723;
     YData[8] := 2.281;
end

Else If LC = 59 Then
begin
     YData[1] := 0.854;
     YData[2] := 1.678;
     YData[3] := 3.555;
     YData[4] := 3.845;
     YData[5] := 2.979;
     YData[6] := 2.734;
     YData[7] := 2.478;
     YData[8] := 2.111;
end

Else If LC = 61 Then
begin
     YData[1] := 0.560;
```

```
     YData[2] := 1.187;
     YData[3] := 2.835;
     YData[4] := 3.176;
     YData[5] := 2.496;
     YData[6] := 2.287;
     YData[7] := 2.098;
     YData[8] := 1.812;
end

Else If LC = 63 Then
begin
     YData[1] := 0.367;
     YData[2] := 0.832;
     YData[3] := 2.251;
     YData[4] := 2.679;
     YData[5] := 2.119;
     YData[6] := 1.865;
     YData[7] := 1.604;
     YData[8] := 1.303;
end

Else If LC = 65 Then
begin
     YData[1] := 0.228;
     YData[2] := 0.576;
     YData[3] := 1.734;
     YData[4] := 2.290;
     YData[5] := 1.882;
     YData[6] := 1.696;
     YData[7] := 1.464;
     YData[8] := 1.194;
end

Else If LC = 67 Then
begin
     YData[1] := 0.145;
     YData[2] := 0.395;
     YData[3] := 1.363;
     YData[4] := 1.856;
     YData[5] := 1.655;
     YData[6] := 1.504;
     YData[7] := 1.333;
     YData[8] := 1.092;
end

Else If (LC = 69) and (TG > 353.1) Then
begin
     YData[1] := 0.246;
     YData[2] := 1.072;
     YData[3] := 1.568;
     YData[4] := 1.463;
     YData[5] := 1.346;
     YData[6] := 1.198;
     YData[7] := 0.999;
end

Else If (LC = 71) and (TG > 353.1) Then
begin
     YData[1] := 0.175;
     YData[2] := 0.832;
     YData[3] := 1.314;
     YData[4] := 1.278;
     YData[5] := 1.208;
     YData[6] := 1.095;
     YData[7] := 0.915;
end

Else If (LC = 73) and (TG > 535.1) Then
begin
     YData[1] := 0.623;
     YData[2] := 1.085;
```

```
     YData[3] := 1.106;
     YData[4] := 1.063;
     YData[5] := 0.987;
     YData[6] := 0.838;
end

Else If (LC = 75) and (TG > 535.1) Then
begin
     YData[1] := 0.476;
     YData[2] := 0.892;
     YData[3] := 0.969;
     YData[4] := 0.951;
     YData[5] := 0.882;
     YData[6] := 0.752;
end

Else If (LC = 77) and (TG > 535.1) Then
begin
     YData[1] := 0.326;
     YData[2] := 0.707;
     YData[3] := 0.692;
     YData[4] := 0.702;
     YData[5] := 0.684;
     YData[6] := 0.593;
end

Else If (LC = 79) and (TG > 535.1) Then
begin
     YData[1] := 0.196;
     YData[2] := 0.465;
     YData[3] := 0.596;
     YData[4] := 0.612;
     YData[5] := 0.598;
     YData[6] := 0.530;
end

Else If (LC = 81) and (TG > 535.1) Then
begin
     YData[1] := 0.142;
     YData[2] := 0.372;
     YData[3] := 0.494;
     YData[4] := 0.515;
     YData[5] := 0.522;
     YData[6] := 0.477;
end

Else If (LC = 83) and (TG > 535.1) Then
begin
     YData[1] := 0.101;
     YData[2] := 0.293;
     YData[3] := 0.419;
     YData[4] := 0.455;
     YData[5] := 0.452;
     YData[6] := 0.411;
end

Else If (LC = 85) and (TG > 719.7) Then
begin
     YData[1] := 0.231;
     YData[2] := 0.348;
     YData[3] := 0.381;
     YData[4] := 0.399;
     YData[5] := 0.367;
end

Else If (LC = 87) and (TG > 719.7) Then
begin
     YData[1] := 0.183;
     YData[2] := 0.303;
     YData[3] := 0.336;
     YData[4] := 0.350;
```

```
                    YData[5] := 0.329;
               end

               Else If (LC = 89) and (TG > 719.7) Then
               begin
                    YData[1] := 0.142;
                    YData[2] := 0.243;
                    YData[3] := 0.280;
                    YData[4] := 0.303;
                    YData[5] := 0.287;
               end

               Else
               Begin
                    LW := 0;
               End;

{  Perform interpolation to get line strength at a specific temperature.  }

               If (TG > 294.2) and (TG < 1226.6) and (LW <> 0) Then
               begin
                    CubicSplineFree(NumPointsSpline,XData,YData,NumInter,XInter,
                                    Coef0,Coef1,Coef2,Coef3,YInter,Error);
                    S := YInter[1];
               end;

               If (TG <= 294.2) and (TG > 285) and (LC < 68) Then
               begin
                    S := TempTooLow[LC];
               end;
               If (TG >= 1226.5) and (TG < 1260) Then
               begin
                    S := TempTooHigh[LC];
               end;

{  Calculate the partial pressure.  }

               If (S <> 0) Then
                 PPCO2Calc[LC] := AtpeakCO2[LC]*PI*ln(10)*LW/(PathLength*S/760);

          end
          Else If (CalculationChoiceCO2 = 'S') Then
          begin

{  Calculate the line strength.  }

               LineStrengthCO2[LC] := AtpeakCO2[LC]*PI*ln(10)*LW/(PathLength*PPCO2Guess/760);
          end;
     end;
until LC = MValueRangeHighCO2;

LC := MValueRangeLowCO2 - 1;
CO2ConcCount := 0;
AverageCO2Concentration := 0;

{  Sum all the calculated concentrations.  }

repeat
     LC := LC + 1;
     If (MValueCO2[LC] <> 0) and (PPCO2Calc[LC] <> 0) Then
     begin
          CO2ConcCount := CO2ConcCount + 1;
          AverageCO2Concentration := AverageCO2Concentration + PPCO2Calc[LC];
     end;
until MValueRangeHighCO2 = LC;

{  Calculate average CO2 concentration.  }

NumResultsCO2 := CO2ConcCount;
If CO2ConcCount <> 0 Then
Begin
```

```
        AverageCO2Concentration := AverageCO2Concentration/CO2ConcCount;
        AveragePercentCO2 := 100*(AverageCO2Concentration/TotPress);
    end;

{  Calculate Standard Deviation of the average CO2 gas concentration.  }

    StandardDeviationCO2 := 0;
    SSXDifference := 0;
    LC := MValueRangeLowCO2 - 1;
    repeat
        LC := LC + 1;
        If PPCO2Calc[LC] <> 0 Then
          SSXDifference := SSXDifference + SQR(PPCO2Calc[LC] - AverageCO2Concentration);
   until MValueRangeHighCO2 = LC;

   If (AverageCO2Concentration <> 0) and (CO2ConcCount > 1) Then
   begin
      StandardDeviationCO2 := SQRT(SSXDifference/(CO2ConcCount - 1));
      StandardDeviationCO2 := StandardDeviationCO2*AveragePercentCO2/AverageCO2Concentration;
   end;

   end; {Procedure CO2ConcentrationCalculation }

End.   { unit CO2Conc }
```

```
unit Output;

{$I Float.inc}

Interface

Uses    Dos, Crt, Common, GlobVar;

{$IFOPT N+}
    Type
        Float = Double;
{$Else}
    Type
        Float = Real;
{$ENDIF}

Procedure OutputResults;


Implementation

Procedure OutputResults;

Var
     LC : Integer;

Begin

{  If CO line strengths or concentrations have been calculated, the results are written to the screen }
{  and to the output file.                                                                              }

         If YesNoCOConcCalc = 'Y' Then
         begin
              If CalculationChoice = 'P' Then
                   begin
                   Writeln(OutputFile,'Energy',',',' Intensity',',',' Corrected Peak Height',
                                      ',',' Partial Pressure CO (Torr)',',');
                   Writeln(OutputFile,'M Value',',',' True Line Position');
                   end
              Else
                   begin
                   Writeln(OutputFile,'Energy',',',' Intensity',',',' Corrected Peak Height',
                                       ',',' Absorptivity (1/(cm cm atm))',',');
                   Writeln(OutputFile,'M Value',',',' True Line Position');
                   end;
              Writeln(OutputFile);

              If (CalculationChoice = 'P') and (TG > 285) and (TG < 1260) Then
              begin
                   LC := MValueRangeLow - 1;
                   repeat
                        LC := LC + 1;
                        If MValue[LC] <> 0 Then
                        Writeln(OutputFile,Energy[LC]:8:3,',',LnPeak[LC]:8:3,',',Atpeak[LC]:6:3,',',
                                PPCOCalc[LC]:8:3,',',MValue[LC]:4,',',TrueLinePosition[LC]:6:3);
                   until LC = MValueRangeHigh;
                   Writeln(OutputFile);
                   Writeln(OutputFile,'Average CO Partial Pressure (Torr) = ',AverageCOConcentration:6:2);
                   Writeln(OutputFile,'Average CO Concentration (Percent) = ',AveragePercentCO:5:2);
                   Writeln(OutputFile,'Standard Deviation of Concentration Calculations (%) =
',StandardDeviationCO:8:4);
              end;

              If (CalculationChoice = 'P') and (TG < 285) Then
              begin
                   LC := MValueRangeLow - 1;
                   repeat
                        LC := LC + 1;
                        If MValue[LC] <> 0 Then
                        Writeln(OutputFile,Energy[LC]:8:3,',',LnPeak[LC]:8:3,',',Atpeak[LC]:6:3,',',
                                '...',',',MValue[LC]:4,',',TrueLinePosition[LC]:6:3);
```

```
                    until LC = MValueRangeHigh;
               Writeln(OutputFile);
               Writeln(OutputFile,'Concentration Results Not Available');
               Writeln(OutputFile,'Final guessed temperature less than 285 K');
               end;

               If (CalculationChoice = 'P') and (TG > 1260) Then
               begin
                    LC := MValueRangeLow - 1;
                    repeat
                         LC := LC + 1;
                         If MValue[LC] <> 0 Then
                         Writeln(OutputFile,Energy[LC]:8:3,',',LnPeak[LC]:8:3,',',Atpeak[LC]:6:3,',',
                                   '...',',',MValue[LC]:4,',',TrueLinePosition[LC]:6:3);
                    until LC = MValueRangeHigh;
               Writeln(OutputFile);
               Writeln(OutputFile,'Concentration Results Not Available');
               Writeln(OutputFile,'Final guessed temperature greater than 1260');
               end;

               If (CalculationChoice = 'S') Then
               begin
                    LC := MValueRangeLow - 1;
                    repeat
                         LC := LC + 1;
                         If MValue[LC] <> 0 Then
                         Writeln(OutputFile,Energy[LC]:8:3,',',LnPeak[LC]:8:3,',',Atpeak[LC]:6:3,',',
                                   LineStrength[LC]:6:3,',',MValue[LC]:4,',',TrueLinePosition[LC]:6:3);
                    until LC = MValueRangeHigh;
               end;
          end;

          Writeln(OutputFile);
          Writeln(OutputFile);
          ResultsCount := 0;

          If YesNoCO2ConcCalc = 'Y' Then
               begin
               If CalculationChoiceCO2 = 'P' Then
                    begin
                    Writeln(OutputFile,'Corrected Peak Height',',',' True Line Position',
                            ',',' CO2 M Value',',');
                    Writeln(OutputFile,'CO2 Partial Pressure (torr)');
                    end
               Else
                    begin
                    Writeln(OutputFile,' Corrected Peak Height',',',' True Line Position',
                            ',','CO2 M Value',',',' CO2 Absorptivity');
                    end;
               Writeln(OutputFile);
               If (CalculationChoiceCO2 = 'P') and (TG > 285) and (TG < 1260) and (NumResultsCO2 > 0) Then
               begin
                    LC := MValueRangeLowCO2 - 1;
                    repeat
                         LC := LC + 1;
                         If MValueCO2[LC] <> 0 Then
                         Writeln(OutputFile,AtpeakCO2[LC]:6:3,',',TrueLinePositionCO2[LC]:10:3,',',
                                   MValueCO2[LC]:4,',',PPCO2Calc[LC]:8:3);
                    until LC = MValueRangeHighCO2;
               Writeln(OutputFile);
               Writeln(OutputFile,'Average CO2 Partial Pressure (Torr) = ',AverageCO2Concentration:6:2);
               Writeln(OutputFile,'Average CO2 Concentration (Percent) = ',AveragePercentCO2:5:2);
               Writeln(OutputFile,'Standard Deviation of Concentration Calculations (%) =
',StandardDeviationCO2:8:4);
               end;

{  If CO2 line strengths or concentrations have been calculated, the results are written to the screen }
{  and to the output file.                                                                              }

               If (CalculationChoiceCO2 = 'P') and (TG < 285) Then
               begin
```

```
                LC := MValueRangeLowCO2 - 1;
                repeat
                     LC := LC + 1;
                     If MValueCO2[LC] <> 0 Then
                     Writeln(OutputFile,AtpeakCO2[LC]:6:3,',',TrueLinePositionCO2[LC]:10:3,',',
                             MValueCO2[LC]:4,',','...');
                until LC = MValueRangeHighCO2;
           Writeln(OutputFile);
           Writeln(OutputFile,'Concentration Results Not Available');
           Writeln(OutputFile,'Final guessed temperature less than 285 K');
           end;

           If (CalculationChoiceCO2 = 'P') and (TG > 1260) Then
           begin
                LC := MValueRangeLowCO2 - 1;
                repeat
                     LC := LC + 1;
                     If MValueCO2[LC] <> 0 Then
                     Writeln(OutputFile,AtpeakCO2[LC]:6:3,',',TrueLinePositionCO2[LC]:10:3,',',
                             MValueCO2[LC]:4,',','...');
                until LC = MValueRangeHighCO2;
           Writeln(OutputFile);
           Writeln(OutputFile,'Concentration Results Not Available');
           Writeln(OutputFile,'Final guessed temperature greater than 1260');
           end;

           If (CalculationChoiceCO2 = 'S') Then
           begin
                LC := MValueRangeLowCO2 - 1;
                repeat
                     LC := LC + 1;
                     If MValueCO2[LC] <> 0 Then
                     Writeln(OutputFile,AtpeakCO2[LC]:6:3,',',TrueLinePositionCO2[LC]:10:3,',',
                             MValueCO2[LC]:4,',',LineStrengthCO2[LC]:8:3);
                until LC = MValueRangeHighCO2;
           end;
      end;

  End;  { Procedure OutputResults }

End.   { Unit Output }
```

APPENDIX VII

CO AND CO_2 LINES USED FOR TEMPERATURE AND CONCENTRATION DETERMINATIONS

The lines designated in the Table A7-1, have been used for the determination of gas temperatures and concentrations is this work. Included in this table is a listing of the line identification as well as the peak position.[78]

Table A7-1. CO and CO_2 lines used for temperature and concentration calculations in this work. Also included are the peak positions which have been reported in the literature.

CO LINES		CO_2 LINES	
Absorption Line (J")	Peak Position (cm^{-1})	Absorption Line (J")	Peak Position (cm^{-1})
P (5)	2123.699	R (50)	2380.716
P (6)	2119.681	R (52)	2381.622
P (7)	2115.629	R (54)	2382.503
P (8)	2111.543	R (56)	2383.359
P (9)	2107.424	R (58)	2384.189
P (11)	2099.083	R (60)	2384.995
P (12)	2094.863	R (62)	2385.775
P (13)	2090.609	R (64)	2386.529
P (14)	2086.322	R (66)	2387.258
P (15)	2082.003	R (68)	2387.962
P (21)	2055.401	R (70)	2388.640
P (22)	2050.855	R (72)	2389.293
P (23)	2146.276	R (74)	2389.921
P (25)	2037.026	R (76)	2390.522
P (26)	2032.353	R (78)	2391.099
P (27)	2027.649	R (80)	2391.650
P (28)	2022.915	R (82)	2392.175
P (29)	2018.149	R (84)	2392.675
P (30)	2013.353	R (86)	2393.149
P (31)	2008.527	R (88)	2393.598
P (34)	1993.863	R (90)	2394.021
P (35)	1988.915	R (92)	2394.418

APPENDIX VIII

CO AND CO_2 ABSORPTION SPECTRA

CO and CO_2 absorption spectra recorded in the high temperature gas are presented in the following figures. The spectra were recorded at furnace temperatures of 295, 361, 547, 746, 948, 1048, 1149, and 1247 K. Absorption spectra of the P branch of the CO fundamental band and the R branch of the CO_2 ν_3 vibrational band are presented in these spectra.

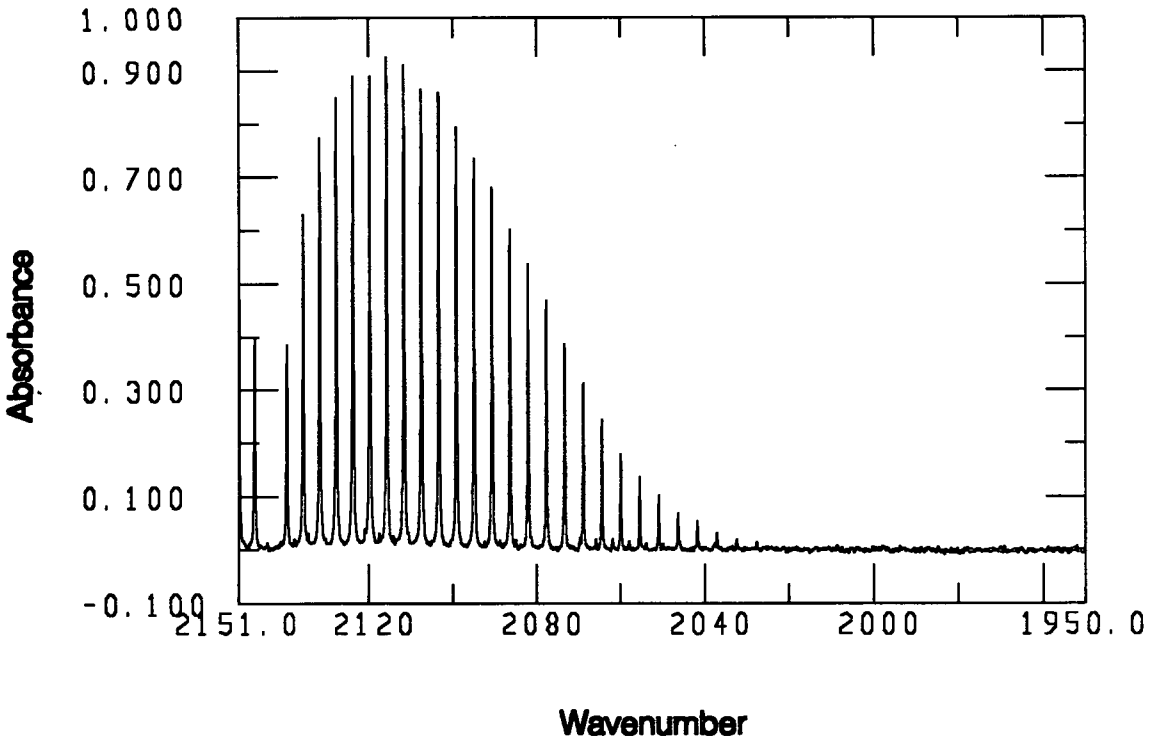

Figure A8-1. CO absorption spectrum at 295 K.

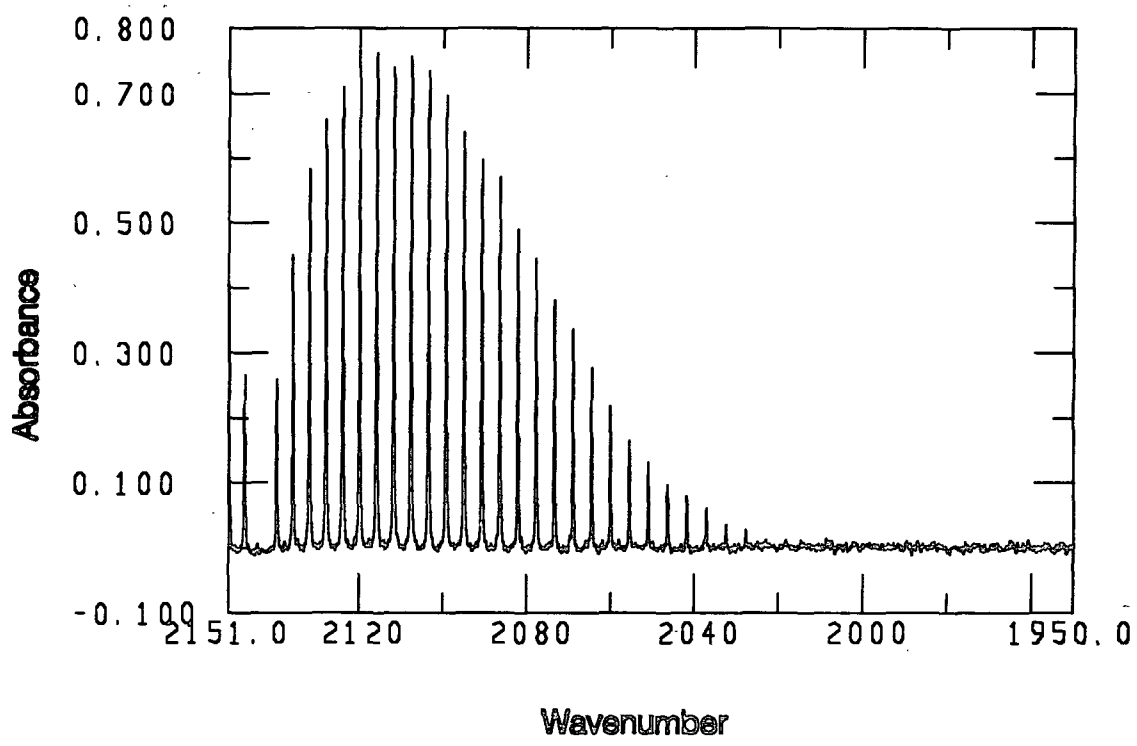

Figure A8-2. CO absorption spectrum at 361 K.

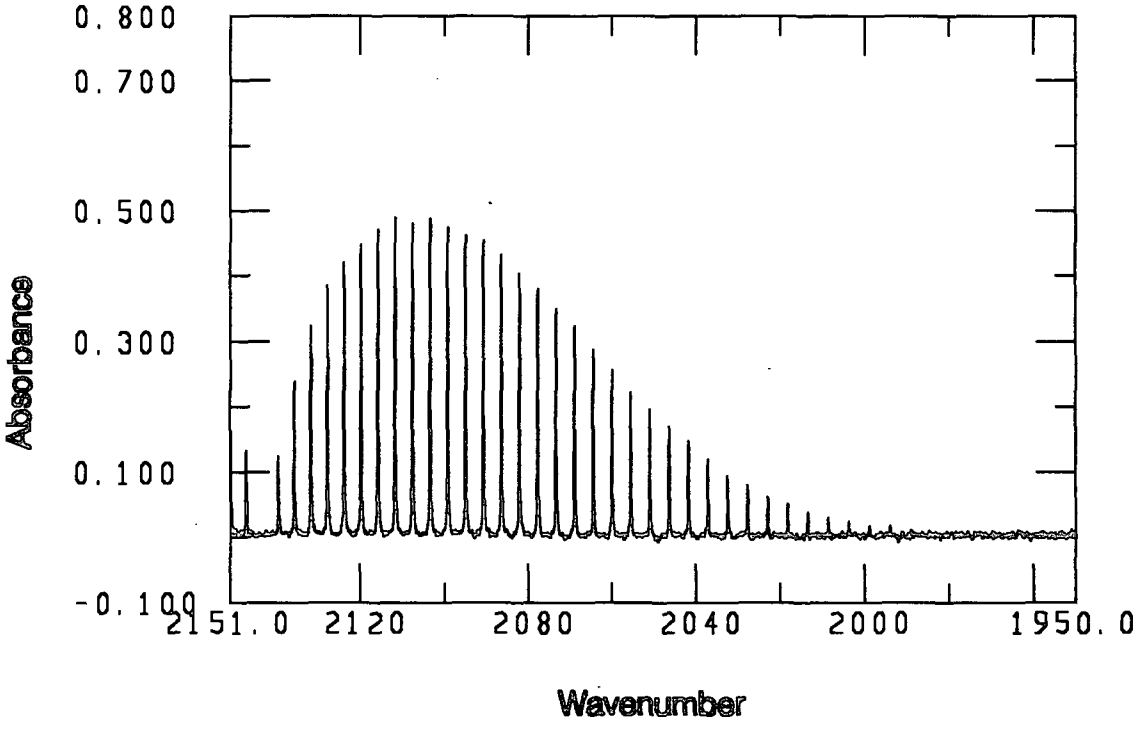

Figure A8-3. CO absorption spectrum at 547 K.

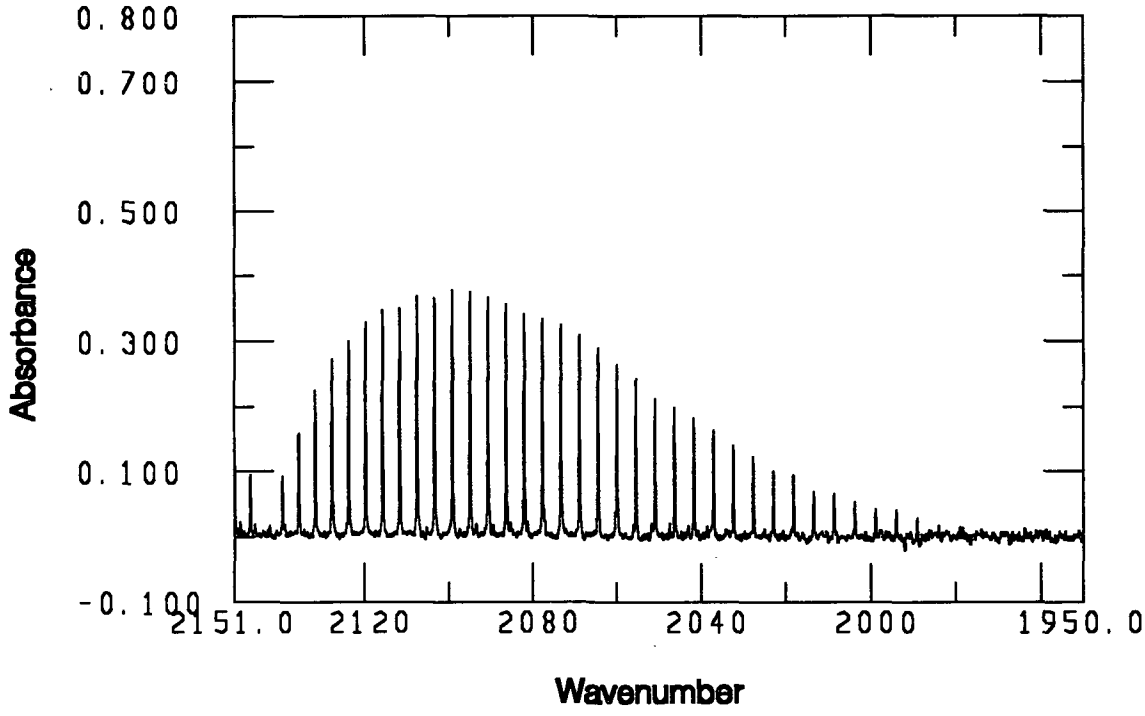

Figure A8-4. CO absorption spectrum at 746 K.

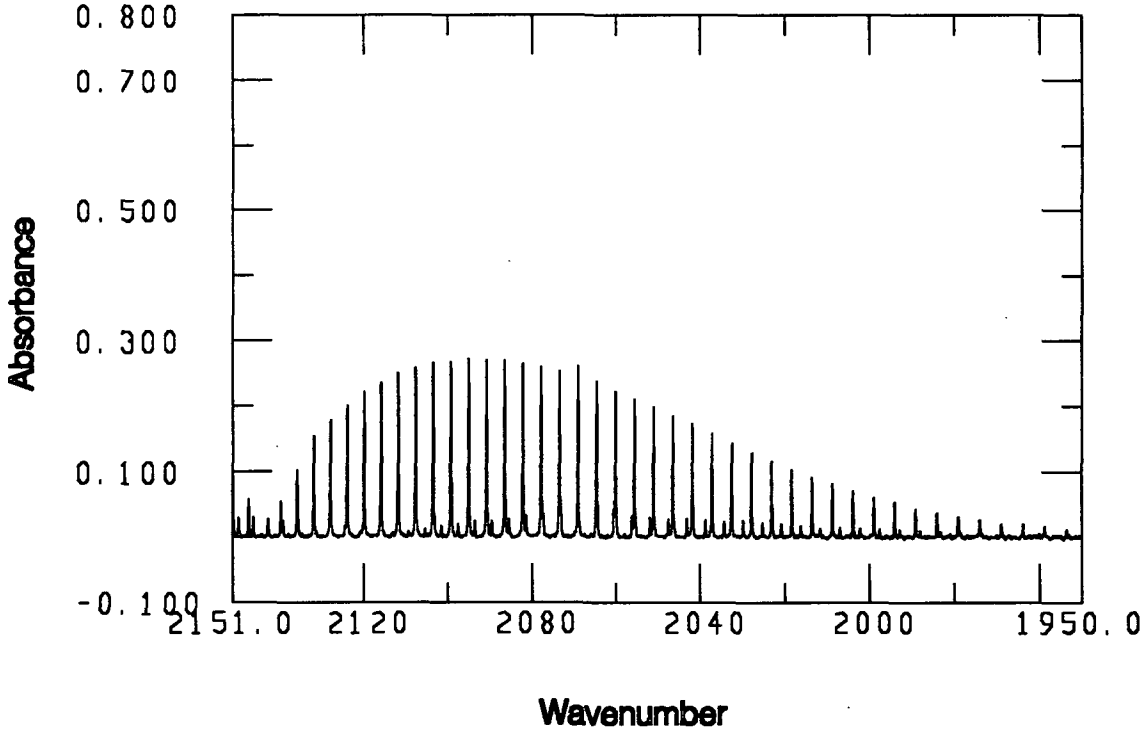

Figure A8-5. CO absorption spectrum at 948 K.

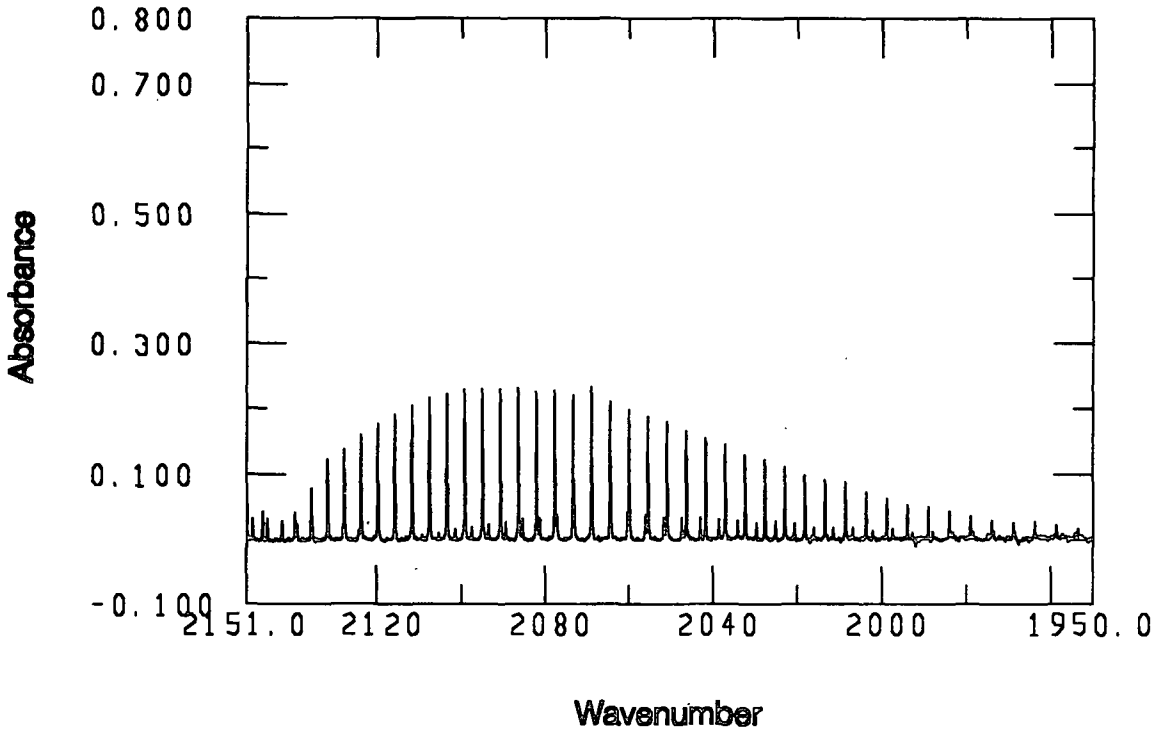

Figure A8-6. CO absorption spectrum at 1048 K.

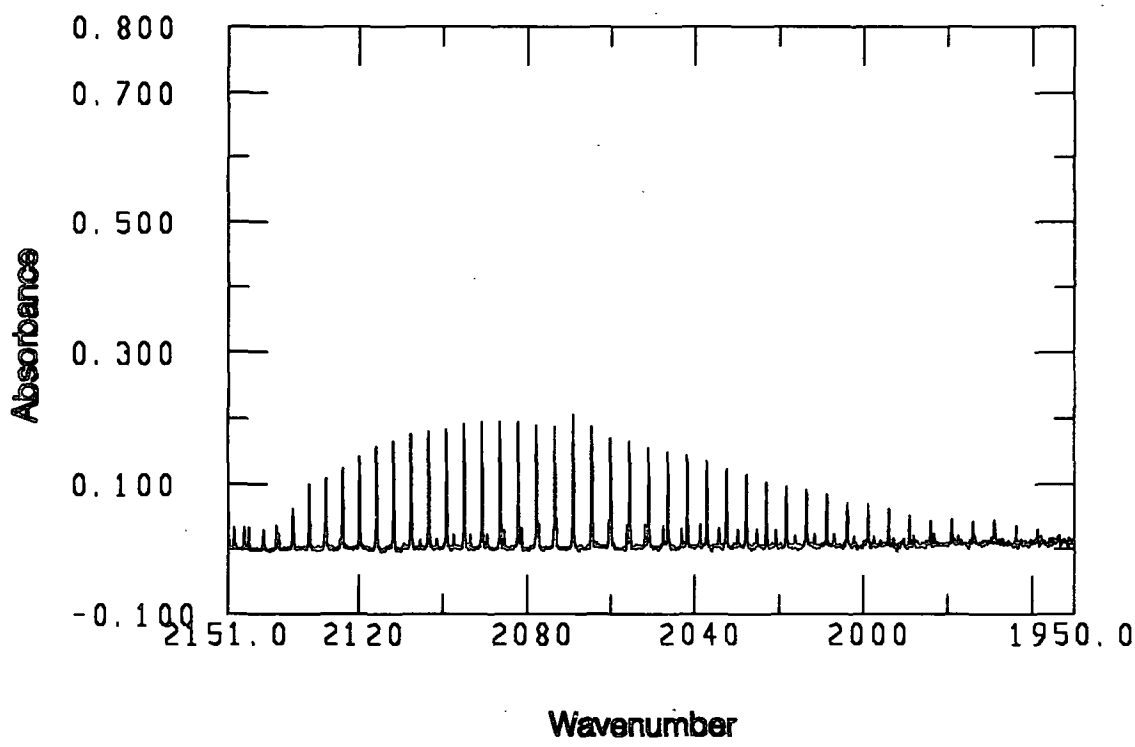

Figure A8-7. CO absorption spectrum at 1149 K.

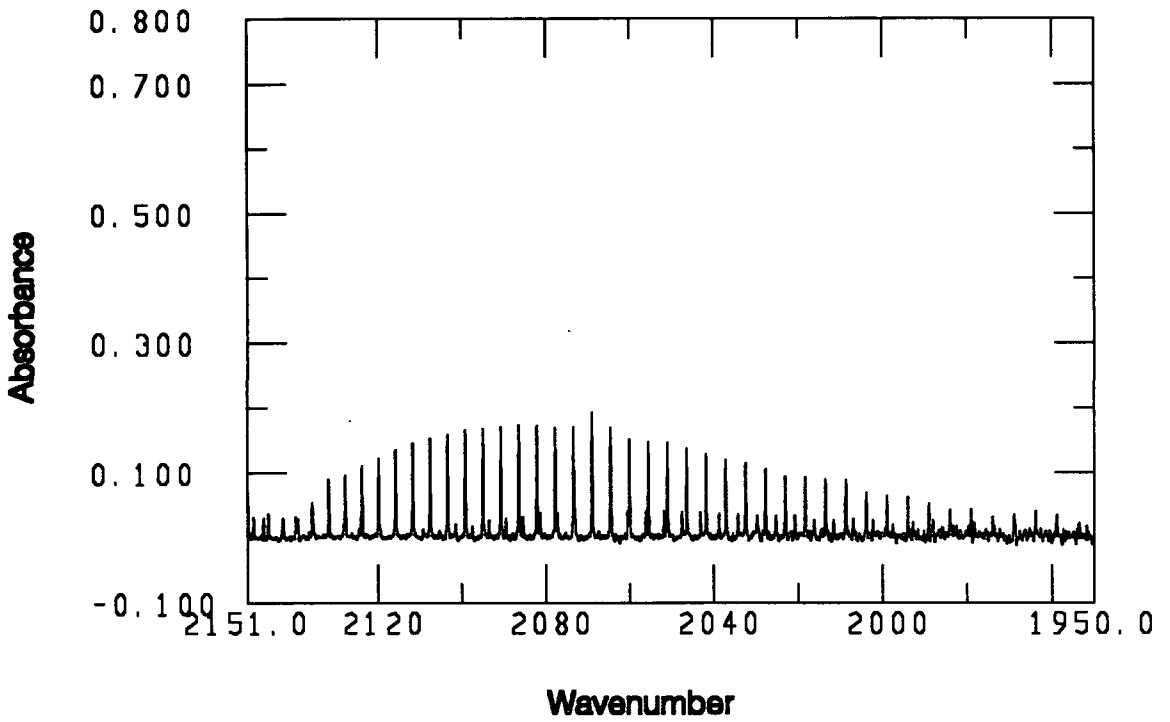

Figure A8-8. CO absorption spectrum at 1247 K.

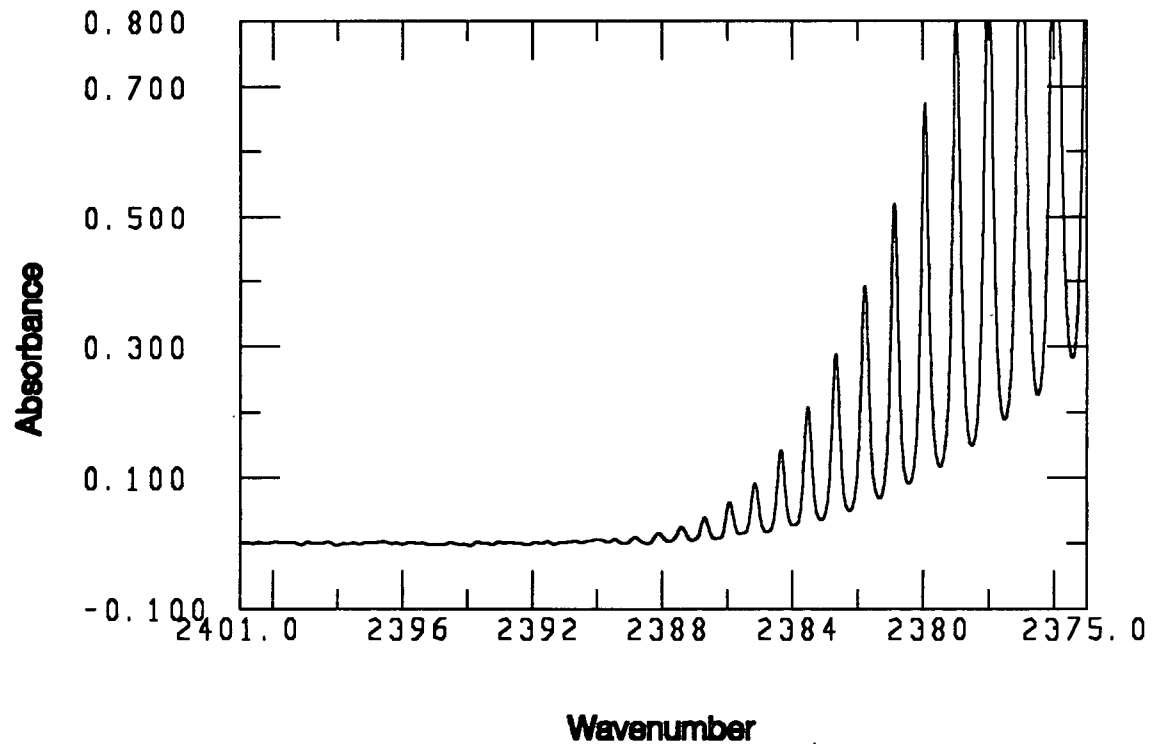

Figure A8-9. CO_2 absorption spectrum at 295 K.

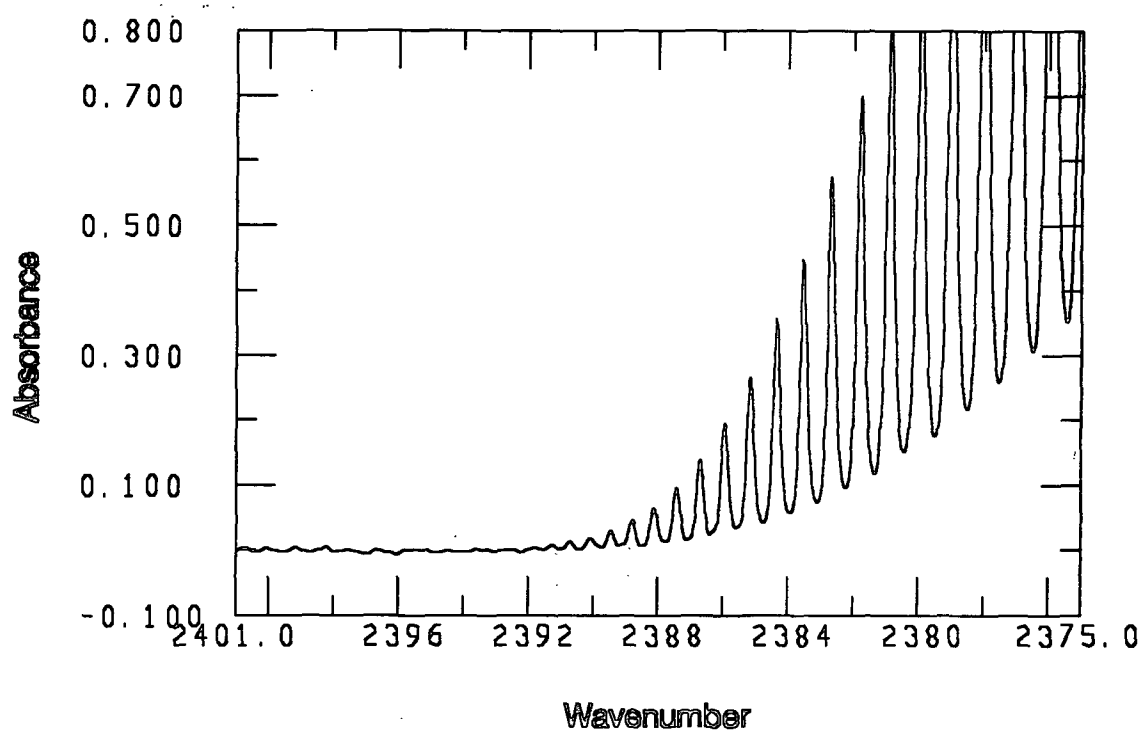

Figure A8-10. CO_2 absorption spectrum at 361 K.

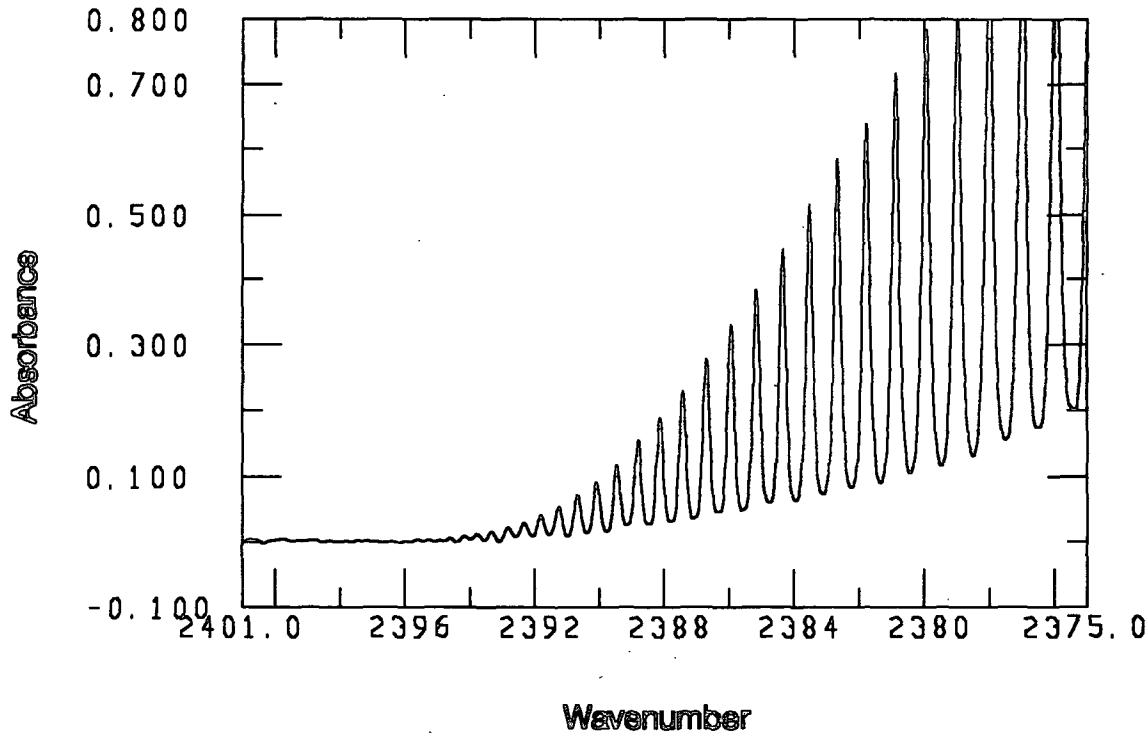

Figure A8-11. CO_2 absorption spectrum at 547 K.

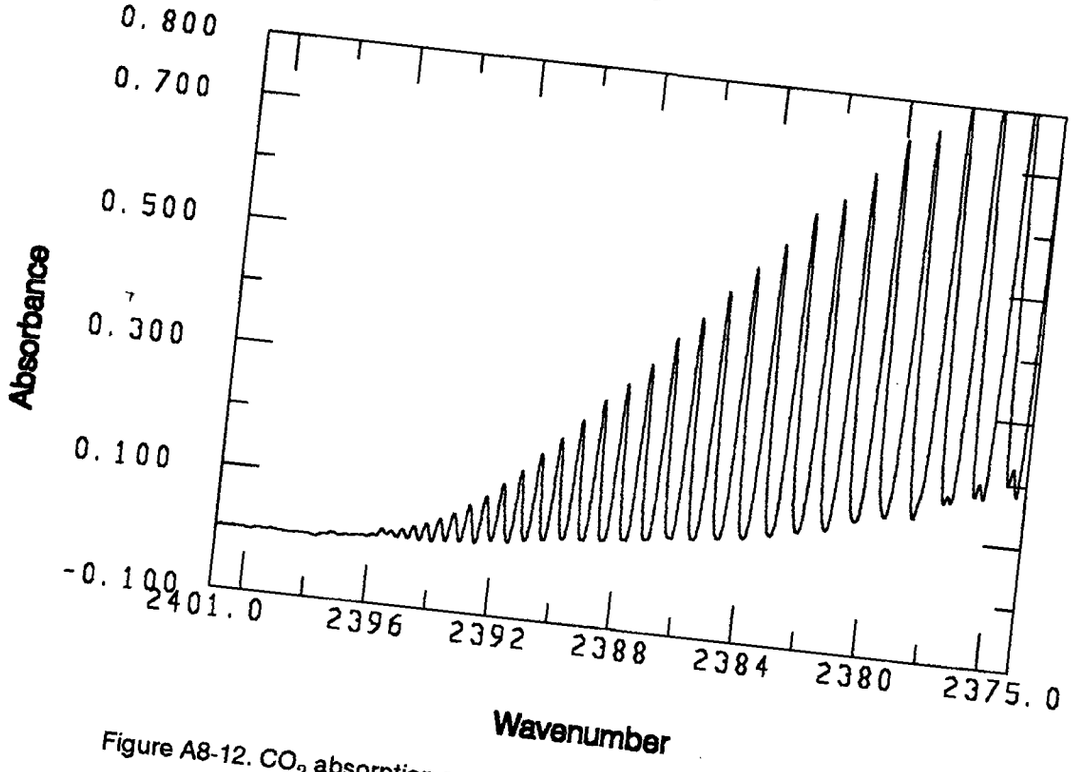

Figure A8-12. CO_2 absorption spectrum at 746 K.

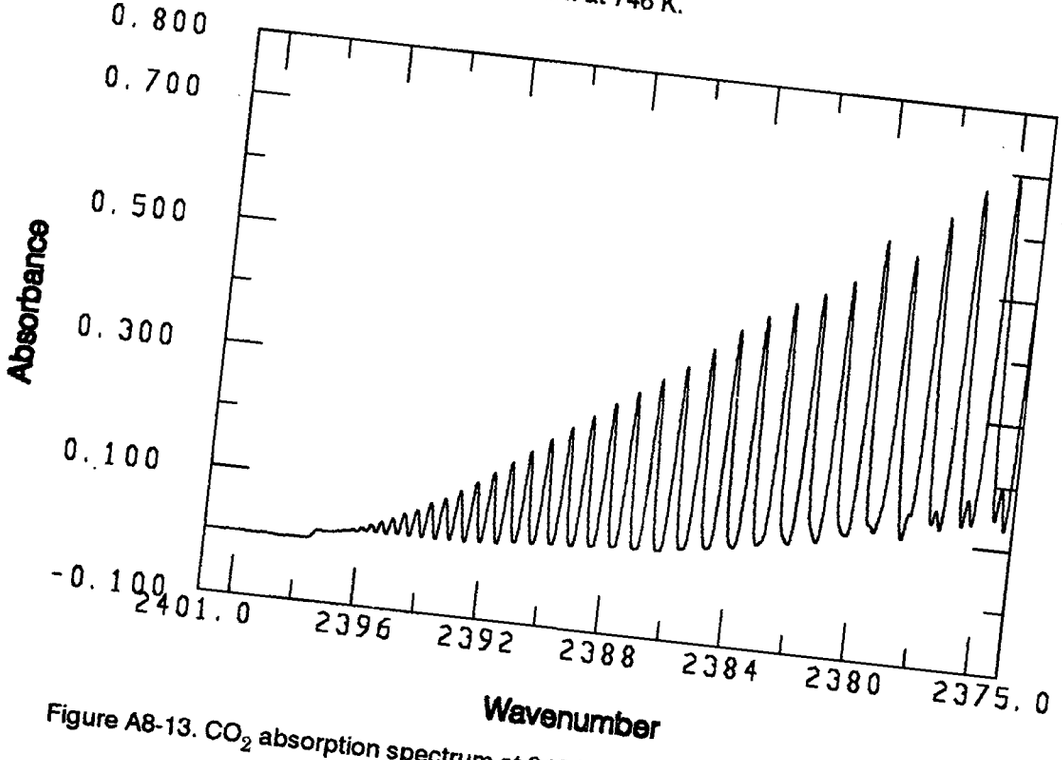

Figure A8-13. CO_2 absorption spectrum at 948 K.

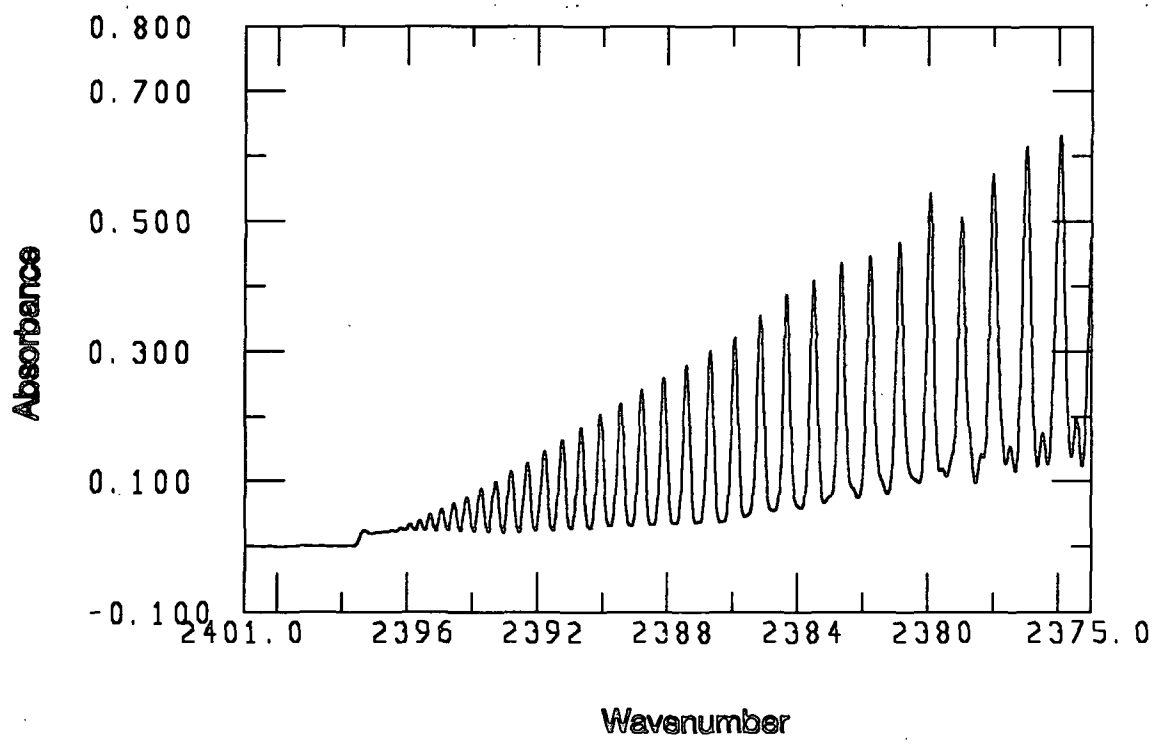

Figure A8-14. CO_2 absorption spectrum at 1048 K.

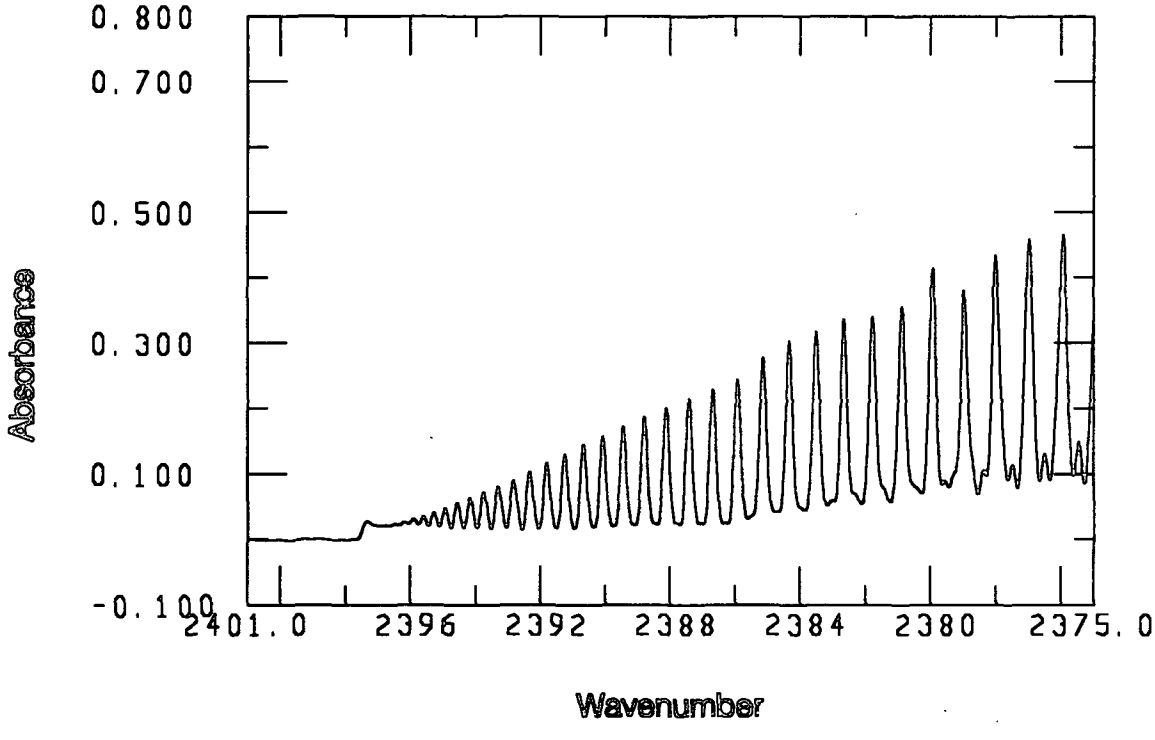

Figure A8-15. CO_2 absorption spectrum at 1149 K.

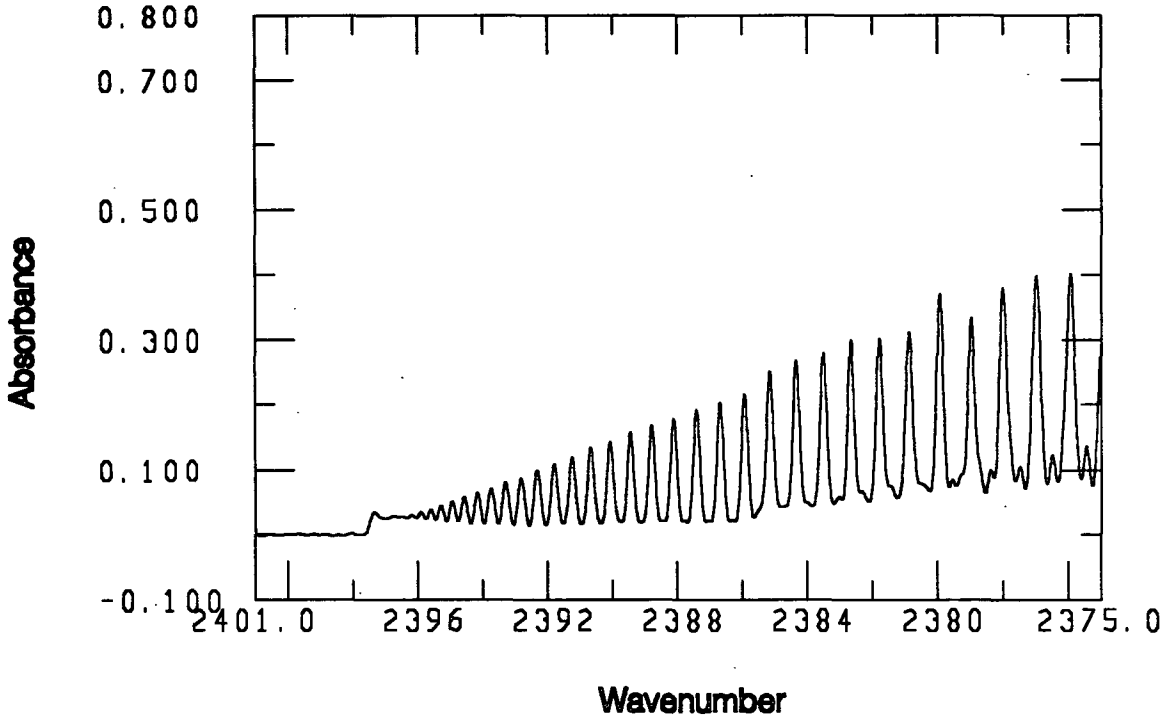

Figure A8-16. CO_2 absorption spectrum at 1247 K.

APPENDIX IX

CALCULATION RESULTS FROM TEMPERATURE DETERMINATIONS

The raw data resulting from the calculations for the determination of gas temperatures from CO absorption spectra are included in the Table below. Included in this table is the spectrum name, pressure in the gas cell, measured temperature (thermocouple), the calculated CO and CO_2 concentrations, the calculated gas temperature, the percent difference between the calculated and measured gas temperatures, and the standard error associated with the least squares fit (LSF) to the data.

Table A9-1 Raw data for temperature calculations from CO absorption spectra.

Spectrum Name	Pressure (Torr)	Thermocouple Temp. K	Calculated % CO	Calculated % CO_2	Calculated Temp. (K)	% Temp. Difference	Standard Error of LSF
C9825A	765	295	0.43	0	300.2	1.76	0.7
C9825B	765	295	0.75	0	295.0	0.00	0.5
C9825C	765	295	0.80	0	295.4	0.14	0.7
C0325A	765	296	1.07	0	297.3	0.44	0.6
C0325B	765	296	0.93	0	297.5	0.51	0.6
C0325C	765	296	0.91	0	296.4	0.14	0.6
C0625A	765	297	0.89	0	296.9	-0.03	0.6
C0625B	765	297	1.03	0	296.2	-0.27	0.4
C0625C	765	297	1.04	0	294.8	-0.74	0.6
C0625D	765	297	1.06	0	296.0	-0.34	0.5
C0625E	765	297	1.10	0	297.6	-0.20	0.6
C0625F	765	297	1.07	0	293.9	-1.04	0.6
C98100A	765	361	2.49	0	353.4	-2.11	0.7
C98100B	765	361	2.45	0	354.6	-1.77	0.7
C98100C	765	361	2.43	0	357.0	-1.11	0.8
C04100A	765	361	2.64	0	348.3	-3.52	1.0
C04100B	765	361	2.65	0	353.1	-2.19	1.0
C04100C	765	361	2.74	0	354.2	-1.88	1.0
C98300A	765	547	2.00	0.29	529.4	-3.22	1.1
C98300B	765	547	1.98	0.27	532.9	-2.58	0.9
C98300C	765	547	2.02	0.28	532.1	-2.72	1.3
C04300A	765	547	2.24	0.44	532.2	-2.71	1.0
C04300B	765	547	2.25	0.42	532.6	-2.63	1.1
C04300C	765	547	2.26	0.42	533.8	-2.41	0.9

Spectrum Name	Pressure (Torr)	Thermocouple Temp. K	Calculated % CO	Calculated % CO_2	Calculated Temp. (K)	% Temp. Difference	Standard Error of LSF
C99500A	765	746	1.28	1.05	726.2	-2.65	1.8
C99500B	765	746	1.32	1.00	719.7	-3.53	2.1
C99500C	765	746	1.36	0.99	723.0	-3.08	1.3
C04500A	765	746	1.16	1.30	725.1	-2.80	1.5
C04500B	765	746	1.27	1.22	721.7	-3.26	2.2
C04500C	765	746	1.33	1.12	726.7	-2.59	2.7
C99700A	765	948	1.85	2.30	922.2	-2.72	2.6
C99700B	765	948	2.03	2.17	919.6	-3.00	4.6
C99700C	765	948	2.17	2.15	926.6	-2.26	4.0
C05700A	765	948	1.74	2.75	932.7	-1.61	3.1
C05700B	765	948	2.08	2.35	924.6	-2.47	3.4
C05700C	765	948	2.24	2.25	925.4	-2.38	3.4
C00800A	765	1048	1.63	6.20	1032.8	-1.45	5.8
C00800B	765	1048	1.98	5.89	1041.7	-0.60	4.0
C00800C	765	1048	2.02	5.61	1032.8	-1.45	4.2
C05800A	765	1048	1.29	3.07	1026.4	-2.06	6.9
C05800B	765	1048	1.43	2.78	1021.2	-2.56	3.8
C05800C	765	1048	1.59	2.76	1037.9	-0.96	3.9
C00900A	765	1149	1.89	5.82	1160.7	1.02	7.4
C00900B	765	1149	2.09	5.80	1174.8	2.25	6.7
C00900C	765	1149	2.22	5.51	1160.3	0.98	7.0
C05900A	765	1149	1.26	2.80	1144.2	-0.42	6.6
C05900B	765	1149	1.29	2.75	1130.1	-1.64	7.1
C05900C	765	1149	1.36	2.80	1143.3	-0.50	6.2
C00999A	765	1247	1.47	5.90	1228.9	-1.45	16.8
C00999B	765	1247	1.73	5.93	1254.5	0.60	13.9
C00999C	765	1247	2.11	5.69	1257.5	0.84	12.0
C06999A	765	1247	1.05	2.91	1244.9	-0.17	21.9
C06999B	765	1247	-	-	1309.8	5.04	21.3
C06999C	765	1247	-	-	1385.8	11.13	23.2
C07999A	765	1247	-	-	1292.2	3.62	21.5
C07999B	765	1247	2.13	2.86	1251.4	0.35	23.9
C07999C	765	1247	-	-	1328.3	6.52	25.7
C07999D	765	1247	2.33	2.65	1236.7	-0.83	14.9
C07999E	765	1247	2.53	2.50	1225.5	-1.72	19.2
C07999F	765	1247	2.86	2.47	1246.9	-0.01	11.7

APPENDIX X

CO/CO_2 CONVERSION REACTIONS IN THE GAS CELL

The concentration of the CO and CO_2 which is metered into the gas cell is significantly different than the concentration which exits the cell. The composition of the $CO/CO_2/N_2$ gas mixture changes because of gaseous reactions which occur within the cell at temperatures between 750-1250 K. One reaction of primary importance is the equilibrium reaction,[81,82]

$$2CO \leftrightarrow C_{gr} + CO_2 \ . \qquad \text{A10-1}$$

Regardless of the material of the reactor, an equilibrium will be established between CO, CO_2, and graphite (C_{gr}) which is dependent upon the gas temperature. The conversion between CO and CO_2 can be very substantial. For example, for a pure CO/N_2 mixture at 950 K, the composition will shift to approximately a 50/50 mixture of CO and CO_2.[82] Changes of this magnitude were observed in the temperature determination work which involved initially pure CO/N_2 gas mixtures.

The intermediate steps in this equilibration reaction, involve the formation of O_2. In addition to oxidizing the carbon monoxide, the O_2 can oxidize metals within the stainless steel to form oxides of Ni, Cr, Fe, and Mn.[79] It is likely that these reactions also occur in the gas cell since these metals have been found inside the cell in the form of a scale. The metals were identified by ICP (inductively coupled plasma) analysis.

For this work, it is important to know the composition of the gas phase inside the cell at the time that the absorption spectra are recorded. It has been assumed that the CO and CO_2 gas compositions could be approximated by the measured quantities determined with

the NDIR gas analyzer attached to the exit of the gas cell. It is expected that the gaseous reactions occurring within the cell should be quickly quenched as the gas leaves the cell by the relatively cooler temperatures of the exit tube. This assumption has been evaluated in several ways.

First, the flow rate of the gas through the cell was varied by a factor of three and the gas composition was measured by the analyzer. Between the two extreme flow rates, the gas composition exiting the cell varied by 11% for CO and by 6% for the CO_2 (single experiments without duplication). At higher flow rates the concentration of CO increased and the concentration of CO_2 decreased. The data from this experiment are show in the table below.

Table A10-1. CO and CO_2 concentrations exiting the gas cell at various flow rates. Gas temperature was approximately 1050 K and the inital CO and CO_2 concentration was the same at each flow rate.

Flow Rate (L/Min.)	CO Conc. (%)	CO_2 Conc. (%)
1	1.20	1.49
2	1.32	1.44
3	1.35	1.40

These results suggest that the conversion of CO to CO_2 is only slightly dependent upon the residence time in the gas cell, *i.e.* there is a ten percent or less change in the conversion with a 300% increase in residence time. If there is a linear relationship between the percent conversion and the residence time in the gas cell, then the concentration gradient along the path of the infared beam would be less than 5%. Relative to the accuracy of the NDIR instrument, this error is not significant.

The temperature calculation results would also suggest that the concentration gradient is relatively small, since the energy versus intensity plots were highly linear. This high degree of linearity is not expected with significant concentration or temperature gradients

along the path of the infrared beam. Similarly, the plots of peak height versus concentration were also very linear, which suggests that the gas composition and peak heights are accurately known. Finally, the high degree of accuracy between theoretical and spectroscopic CO line strength measurements further suggest that the concentrations have been accurately measured.

APPENDIX XI

CALCULATION RESULTS FROM LINE STRENGTH MEASUREMENTS

Presented in this Appendix is first a sample of a results file produced from the Pascal program *SpecAnal* which has been run here to calculated gas temperatures and CO and CO2 line strengths. Following this output file, is the original data for the calculated line strengths from 52 absorption spectra. In the tables of line strength data, is included the spectral file names, line numbers (m), average line strengths, the standard deviation of the 6 (or ten) replicates, and the percentage of the standard deviation divided by the average.

Sample Output File for Line Strength Calculations

Iteration Number = 1
Temperature Guess = 360.00
Calculated Temperature = 352.80
Standard Deviation = 0.04295
Variance = 0.02583
Standard Error of Line = 1.9434
PPCOGuess = 18.210
PPCO2Guess = 17.620
PPN2 = 731.170

Iteration Number = 2
Temperature Guess = 352.80
Calculated Temperature = 353.66
Standard Deviation = 0.04298
Variance = 0.02586
Standard Error of Line = 1.9539
PPCOGuess = 18.210
PPCO2Guess = 17.620
PPN2 = 731.170

Iteration Number = 3
Temperature Guess = 353.66
Calculated Temperature = 353.55
Standard Deviation = 0.04297
Variance = 0.02585
Standard Error of Line = 1.9526
PPCOGuess = 18.210
PPCO2Guess = 17.620
PPN2 = 731.170

Iteration Number = 4
Temperature Guess = 353.55
Calculated Temperature = 353.57
Standard Deviation = 0.04297
Variance = 0.02585
Standard Error of Line = 1.9527
PPCOGuess = 18.210
PPCO2Guess = 17.620
PPN2 = 731.170

c66100e.dat

Energy, Intensity, Corrected Peak Height, Absorptivity (1/(cm cm atm)),M Value, True Line Position

2086.203, -16.326, 0.107, 0.122, -27,2027.649
1937.522, -15.847, 0.163, 0.190, -26,2032.353
1794.299, -15.385, 0.244, 0.291, -25,2037.026
1524.251, -14.720, 0.425, 0.523, -23,2046.276
1397.435, -14.326, 0.593, 0.743, -22,2050.855
1276.098, -13.987, 0.783, 0.997, -21,2055.401
663.377, -12.282, 2.723, 3.966, -15,2082.003
580.510, -12.017, 3.252, 4.836, -14,2086.322
503.154, -11.796, 3.706, 5.614, -13,2090.609
431.310, -11.594, 4.135, 6.352, -12,2094.863
364.983, -11.493, 4.155, 6.454, -11,2099.083
248.885, -10.993, 5.493, 8.743, -9,2107.424
199.120, -10.977, 4.900, 7.914, -8,2111.543
154.879, -10.835, 4.871, 7.996, -7,2115.629
116.164, -10.681, 4.818, 8.011, -6,2119.681
82.978, -10.607, 4.264, 7.203, -5,2123.699

Corrected Peak Height, True Line Position,CO2 M Value, CO2 Absorptivity

5.005, 2380.716, 51, 8.898
2.609, 2381.622, 53, 4.616
1.880, 2382.503, 55, 3.310
1.343, 2383.359, 57, 2.347
0.976, 2384.189, 59, 1.698
0.698, 2384.995, 61, 1.206
0.487, 2385.775, 63, 0.835
0.340, 2386.529, 65, 0.580
0.231, 2387.258, 67, 0.391
0.156, 2387.962, 69, 0.261
0.107, 2388.640, 71, 0.179
0.069, 2389.293, 73, 0.114
0.055, 2389.921, 75, 0.090

Line Strength Data at a Furnace Set Point Temperature of 295 K

CO LINE STRENGTHS

	C65E	C65F	C65G	C65H	C66A	C66B	C66C	C66D	C66E	C66F	AVG.	SD.	Rel. %SD
-26													
-25			0.158	0.164			0.165	0.144	0.144	0.147	0.154	0.010	6.41
-23	0.328	0.347	0.369	0.359	0.386	0.323	0.367	0.331	0.323	0.324	0.346	0.023	6.70
-22	0.478	0.514	0.498	0.507	0.504	0.479	0.513	0.482	0.484	0.475	0.493	0.015	3.12
-21	0.654	0.683	0.736	0.694	0.779	0.676	0.759	0.709	0.679	0.674	0.704	0.041	0.81
-15	4.106	4.180	4.258	4.310	4.463	3.820	4.231	4.004	3.972	3.787	4.113	0.217	5.28
-14	5.016	4.966	5.132	5.195	5.482	4.715	5.175	5.014	4.887	4.727	5.031	0.231	4.59
-13	6.104	6.210	6.361	7.129	6.462	5.651	6.229	5.811	6.076	5.926	6.196	0.410	6.61
-12	7.223	7.295	7.834	8.107	7.761	6.779	7.420	7.007	7.076	6.963	7.347	0.431	5.86
-11	8.440	8.505	9.186	8.703	9.023	7.807	8.787	8.115	7.732	8.426	8.472	0.482	5.68
-9	10.047	10.192	11.372	11.178	10.838	9.450	10.269	9.528	9.994	10.770	10.364	0.656	6.33
-8	10.622	11.297	11.977	12.373	11.650	10.288	11.449	10.759	10.443	11.551	11.241	0.691	6.14
-7	10.710	11.137	12.104	12.519	11.831	10.308	11.435	10.695	10.735	12.192	11.367	0.762	6.71
-6	10.964	11.078	11.689	11.385	11.427	10.080	10.889	10.278	11.115	11.222	11.013	0.500	4.54
-5	10.174	10.044	10.863	12.016	10.787	9.632	10.466	10.110	10.268	10.859	10.522	0.659	6.27

CO_2 LINE STRENGTHS

	C65E	C65F	C65G	C65H	C66A	C66B	C66C	C66D	C66E	C66F	AVG	SD	Rel. % SD
51													
53	2.785	2.640	2.868	2.853	2.695	2.772	2.720	2.805	2.815	2.802	2.776	0.071	2.57
55	1.955	1.809	1.988	1.963	1.887	1.924	1.881	1.958	1.899	1.926	1.919	0.052	2.72
57	1.299	1.210	1.314	1.290	1.275	1.278	1.295	1.301	1.279	1.302	1.284	0.029	2.25
59	0.890	0.798	0.888	0.865	0.832	0.851	0.849	0.861	0.845	0.857	0.854	0.027	3.12
61	0.587	0.530	0.581	0.564	0.535	0.573	0.529	0.572	0.563	0.564	0.560	0.021	3.77
63	0.402	0.328	0.386	0.372		0.356	0.359	0.362	0.364	0.373	0.367	0.021	5.61
65			0.237	0.230			0.219	0.226	0.225	0.228	0.228	0.006	2.62
67				0.151					0.141	0.143	0.145	0.005	3.65
69													
71													

Line Strength Data at a Furnace Set Point Temperature of 373 K

CO LINE STRENGTHS

	C66A	C66B	C66C	C66D	C66E	C66F	AVERAGE	STD.DEV.	RELATIVE % STD.DEV.
-28						0.069	0.069		
-27			0.126	0.143	0.122	0.128	0.130	0.009	7.07
-26		0.162	0.189	0.195	0.190	0.189	0.185	0.013	7.08
-25	0.323	0.301	0.315	0.306	0.291	0.283	0.303	0.015	4.89
-23	0.586	0.528	0.560	0.523	0.523	0.516	0.539	0.028	5.12
-22	0.858	0.766	0.809	0.743	0.743	0.754	0.779	0.046	5.89
-21	1.092	0.978	1.064	0.978	0.997	0.952	1.010	0.055	5.46
-15	4.306	4.044	4.355	3.895	3.966	3.849	4.069	0.213	5.25
-14	5.000	4.759	5.005	4.594	4.836	4.942	4.856	0.160	3.30
-13	6.151	5.480	6.081	5.634	5.614	5.803	5.794	0.271	4.67
-12	6.623	6.193	7.011	6.366	6.352	6.764	6.552	0.305	4.65
-11	7.273	6.934	7.845	6.860	6.454	7.562	7.155	0.507	7.08
-9	8.403	7.510	9.335	8.426	8.743	8.582	8.500	0.593	6.98
-8	9.175	8.017	8.878	8.834	7.914	8.583	8.567	0.503	5.88
-7	8.362	7.795	8.816	8.235	7.996	9.066	8.378	0.484	5.78
-6	8.179	7.581	8.824	8.159	8.011	8.433	8.198	0.416	5.07
-5	7.538	7.097	8.254	7.237	7.203	7.896	7.538	0.456	6.05

CO_2 LINE STRENGTHS

	C66A	C66B	C66C	C66D	C66E	C66F	AVERAGE	STD.DEV.	RELATIVE % STD.DEV.
53	4.266	4.205	4.203	4.614	4.616	4.652	4.426	0.222	5.02
55	3.132	3.177	3.166	3.349	3.310	3.341	3.246	0.098	3.02
57	2.282	2.258	2.274	2.439	2.347	2.328	2.321	0.067	2.88
59	1.641	1.656	1.665	1.743	1.698	1.666	1.678	0.037	2.20
61	1.172	1.160	1.142	1.235	1.206	1.205	1.187	0.035	2.91
63	0.845	0.813	0.815	0.865	0.835	0.817	0.832	0.021	2.49
65	0.563	0.574	0.557	0.595	0.580	0.585	0.576	0.014	2.45
67	0.403	0.395	0.377	0.420	0.391	0.385	0.395	0.015	3.80
69		0.237	0.226	0.256	0.261	0.249	0.246	0.014	5.81
71				0.174	0.179	0.173	0.175	0.003	1.83
73					0.114	0.114	0.114	0.000	0.00
75									
77									

Line Strength Data at a Furnace Set Point Temperature of 573 K

CO LINE STRENGTHS

	C66A	C66B	C66C	C66D	C66E	C66F	AVERAGE	STD.DEV.	RELATIVE % STD.DEV.
-34					0.069	0.059	0.064	0.007	11.05
-31		0.142	0.145	0.135	0.144	0.135	0.140	0.005	3.47
-30		0.183	0.176	0.173	0.183	0.174	0.178	0.005	2.74
-29	0.285	0.253	0.245	0.234	0.237	0.232	0.248	0.020	8.03
-28	0.306	0.310	0.308	0.305	0.300	0.305	0.306	0.003	1.11
-27	0.397	0.413	0.401	0.393	0.406	0.401	0.402	0.007	1.74
-26	0.450	0.504	0.493	0.498	0.491	0.507	0.491	0.021	4.23
-25	0.641	0.658	0.663	0.665	0.658	0.648	0.656	0.009	1.41
-23	0.948	0.998	1.011	0.992	0.982	0.984	0.986	0.021	2.16
-22	1.164	1.190	1.211	1.192	1.184	1.243	1.197	0.027	2.25
-21	1.390	1.400	1.431	1.444	1.447	1.407	1.420	0.024	1.69
-15	3.267	3.257	3.378	3.192	3.319	3.395	3.301	0.078	2.35
-14	3.509	3.615	3.576	3.509	3.721	3.841	3.629	0.131	3.60
-13	3.706	3.902	3.710	3.807	4.056	4.064	3.874	0.161	4.16
-12	3.746	4.000	4.023	4.057	4.044	4.637	4.085	0.294	7.21
-11	4.019	4.171	4.376	4.298	4.478	4.309	4.275	0.161	3.76
-9	4.204	4.230	4.303	4.252	4.381	4.867	4.373	0.250	5.72
-8	4.068	4.337	4.106	4.214	4.470	4.408	4.267	0.164	3.84
-7	3.886	4.048	4.099	4.130	4.151	4.214	4.088	0.113	2.77
-6	3.637	3.708	3.880	3.746	3.869	3.883	3.787	0.105	2.77
-5	3.226	3.348	3.389	3.444	3.470	3.675	3.425	0.149	4.36

CO_2 LINE STRENGTHS

	C66A	C66B	C66C	C66D	C66E	C66F	AVERAGE	STD.DEV.	RELATIVE % STD.DEV.
53	5.860	6.130	6.506	6.772	7.391	7.513	6.695	0.665	9.93
55	5.125	5.266	5.255	5.457	6.169	6.882	5.692	0.692	12.15
57	4.124	4.256	4.426	4.327	4.614	5.232	4.497	0.396	8.81
59	3.353	3.372	3.365	3.570	3.708	3.960	3.555	0.244	6.87
61	2.747	2.700	2.722	2.747	2.975	3.118	2.835	0.171	6.03
63	2.222	2.194	2.207	2.197	2.348	2.339	2.251	0.072	3.21
65	1.702	1.743	1.710	1.698	1.774	1.776	1.734	0.036	2.05
67	1.352	1.366	1.358	1.329	1.402	1.372	1.363	0.024	1.77
69	1.075	1.079	1.062	1.060	1.074	1.081	1.072	0.009	0.82
71	0.841	0.857	0.809	0.825	0.815	0.844	0.832	0.019	2.23
73	0.602	0.623	0.621	0.628	0.640	0.625	0.623	0.012	1.98
75	0.501	0.482	0.478	0.461	0.467	0.467	0.476	0.015	3.05
77	0.233	0.265	0.358	0.369	0.368	0.364	0.326	0.061	18.62
79		0.198	0.206	0.190	0.195	0.190	0.196	0.007	3.40
81			0.139	0.142	0.146	0.139	0.142	0.003	2.34
83				0.100	0.105	0.099	0.101	0.003	3.17
85					0.074	0.073	0.074	0.001	0.96

Line Strength Data at a Furnace Set Point Temperature of 773 K

CO LINE STRENGTHS

	C66A	C66B	C66C	C66D	C66E	C66F	AVERAGE	STD.DEV.	RELATIVE % STD.DEV.
-35		0.127	0.097	0.107	0.112	0.112	0.111	0.011	9.77
-34		0.182	0.154	0.143	0.155	0.137	0.154	0.017	11.21
-31	0.334	0.309	0.302	0.296	0.304	0.299	0.307	0.014	4.49
-30	0.365	0.323	0.313	0.330	0.327	0.337	0.333	0.018	5.35
-29	0.457	0.457	0.431	0.412	0.421	0.408	0.431	0.022	5.02
-28	0.554	0.491	0.529	0.510	0.523	0.510	0.520	0.021	4.12
-27	0.746	0.625	0.620	0.619	0.612	0.590	0.635	0.056	8.75
-26	0.769	0.738	0.729	0.723	0.724	0.728	0.735	0.017	2.37
-25	0.973	0.894	0.900	0.871	0.917	0.875	0.905	0.037	4.13
-23	1.339	1.150	1.122	1.130	1.143	1.208	1.182	0.083	6.99
-22	1.456	1.258	1.265	1.292	1.307	1.294	1.312	0.073	5.56
-21	1.670	1.516	1.392	1.446	1.496	1.496	1.503	0.094	6.22
-15	2.784	2.481	2.565	2.550	2.563	2.644	2.598	0.105	4.04
-14	2.872	2.652	2.599	2.824	2.613	2.756	2.719	0.115	4.22
-13	3.101	2.769	2.799	2.619	2.809	2.702	2.800	0.164	5.85
-12	3.203	2.866	2.805	2.742	2.780	2.787	2.864	0.171	5.97
-11	2.997	2.897	2.725	2.789	2.809	2.905	2.854	0.098	3.43
-9	2.942	2.762	2.590	2.709	2.793	3.088	2.814	0.177	6.27
-8	2.882	2.533	2.506	2.558	2.644	2.634	2.626	0.137	5.21
-7	2.685	2.486	2.418	2.499	2.478	2.492	2.510	0.091	3.61
-6	2.459	2.260	2.150	2.285	2.274	2.407	2.306	0.111	4.81
-5	2.188	1.969	1.926	1.930	2.003	2.109	2.021	0.106	5.24

CO_2 LINE STRENGTHS

	C66A	C66B	C66C	C66D	C66E	C66F	AVERAGE	STD.DEV.	RELATIVE % STD.DEV.
53	4.788	5.499	5.626	6.105	6.560	7.055	5.939	0.809	13.63
55	4.408	5.128	4.878	5.695	6.098	6.823	5.505	0.879	15.97
57	3.766	4.253	4.231	4.508	4.859	5.471	4.515	0.590	13.08
59	3.357	3.686	3.597	3.989	4.032	4.407	3.845	0.373	9.71
61	2.782	3.157	3.046	3.293	3.228	3.550	3.176	0.256	8.07
63	2.452	2.638	2.548	2.625	2.772	3.040	2.679	0.206	7.69
65	2.119	2.287	2.161	2.304	2.351	2.516	2.290	0.142	6.20
67	1.728	1.872	1.752	1.840	1.876	2.067	1.856	0.121	6.49
69	1.464	1.568	1.512	1.580	1.593	1.689	1.568	0.077	4.89
71	1.251	1.362	1.275	1.297	1.297	1.404	1.314	0.057	4.37
73	1.029	1.128	1.039	1.084	1.081	1.151	1.085	0.048	4.41
75	0.860	0.925	0.862	0.885	0.889	0.931	0.892	0.030	3.40
77	0.554	0.767	0.701	0.718	0.720	0.783	0.707	0.081	11.51
79	0.465	0.471	0.463	0.448	0.457	0.485	0.465	0.013	2.71
81	0.364	0.375	0.371	0.370	0.366	0.387	0.372	0.008	2.21
83	0.282	0.301	0.279	0.293	0.293	0.307	0.293	0.011	3.67
85	0.218	0.234	0.231	0.230	0.226	0.248	0.231	0.010	4.29
87		0.181	0.183	0.179	0.179	0.195	0.183	0.007	3.65
89		0.141	0.136	0.143	0.138	0.152	0.142	0.006	4.37
91									

Line Strength Data at a Furnace Set Point Temperature of 973 K

CO LINE STRENGTHS

	C66A	C66B	C66C	C66D	C66E	C66F	AVERAGE	STD.DEV.	% STD.DEV.
-35		0.182	0.192	0.185	0.179	0.177	0.183	0.006	3.21
-34		0.221	0.220	0.212	0.214	0.208	0.215	0.005	2.55
-31	0.425	0.374	0.384	0.364	0.363	0.359	0.378	0.025	6.52
-30	0.479	0.429	0.431	0.411	0.409	0.407	0.428	0.027	6.36
-29	0.558	0.505	0.496	0.477	0.477	0.462	0.496	0.034	6.87
-28	0.642	0.573	0.580	0.551	0.545	0.536	0.571	0.039	6.75
-27	0.706	0.652	0.667	0.625	0.624	0.609	0.647	0.036	5.51
-26	0.805	0.731	0.739	0.705	0.710	0.698	0.731	0.039	5.38
-25	0.903	0.841	0.840	0.792	0.792	0.790	0.826	0.045	5.40
-23	1.123	1.039	1.033	0.987	0.972	0.979	1.022	0.057	5.57
-22	1.230	1.118	1.132	1.075	1.081	1.077	1.119	0.059	5.31
-21	1.322	1.220	1.234	1.184	1.163	1.172	1.216	0.059	4.84
-15	1.816	1.714	1.715	1.613	1.612	1.607	1.680	0.084	5.00
-14	1.885	1.736	1.745	1.687	1.667	1.645	1.728	0.086	5.00
-13	1.883	1.747	1.767	1.659	1.672	1.642	1.728	0.091	5.25
-12	1.893	1.770	1.747	1.670	1.681	1.683	1.741	0.085	4.87
-11	1.832	1.721	1.730	1.666	1.660	1.662	1.712	0.067	3.89
-9	1.707	1.593	1.598	1.536	1.533	1.521	1.581	0.070	4.40
-8	1.617	1.516	1.521	1.485	1.462	1.464	1.511	0.058	3.82
-7	1.496	1.399	1.410	1.353	1.349	1.337	1.391	0.059	4.26
-6	1.364	1.271	1.279	1.242	1.235	1.236	1.271	0.049	3.87
-5	1.153	1.091	1.117	1.078	1.068	1.068	1.096	0.033	3.06

CO_2 LINE STRENGTHS

	C66A	C66B	C66C	C66D	C66E	C66F	AVERAGE	STD.DEV.	RELATIVE % STD.DEV.
53	3.544	3.767	3.631	4.095	4.512	4.785	4.056	0.503	12.41
55	3.279	3.515	3.395	3.694	4.031	4.248	3.694	0.378	10.23
57	2.938	3.169	3.051	3.357	3.686	3.936	3.356	0.387	11.52
59	2.633	2.832	2.701	3.006	3.250	3.451	2.979	0.321	10.78
61	2.306	2.426	2.306	2.495	2.679	2.763	2.496	0.191	7.64
63	2.016	2.091	1.974	2.110	2.230	2.293	2.119	0.123	5.78
65	1.796	1.864	1.750	1.884	1.978	2.021	1.882	0.104	5.51
67	1.575	1.647	1.540	1.657	1.737	1.775	1.655	0.090	5.46
69	1.397	1.464	1.357	1.467	1.526	1.564	1.463	0.077	5.28
71	1.230	1.279	1.193	1.278	1.336	1.352	1.278	0.061	4.74
73	1.055	1.110	1.033	1.106	1.155	1.178	1.106	0.056	5.04
75	0.931	0.978	0.910	0.972	1.008	1.016	0.969	0.042	4.32
77	0.661	0.701	0.651	0.689	0.720	0.727	0.692	0.031	4.45
79	0.582	0.605	0.561	0.598	0.615	0.617	0.596	0.021	3.60
81	0.472	0.506	0.464	0.498	0.511	0.515	0.494	0.021	4.31
83	0.405	0.423	0.397	0.421	0.433	0.436	0.419	0.015	3.67
85	0.326	0.352	0.331	0.353	0.363	0.364	0.348	0.016	4.62
87	0.297	0.312	0.284	0.305	0.313	0.309	0.303	0.011	3.66
89	0.225	0.245	0.230	0.248	0.257	0.255	0.243	0.013	5.39

Line Strength Data at a Furnace Set Point Temperature of 1073 K

CO LINE STRENGTHS

	C66A	C66B	C66C	C66D	C66E	C66F	AVERAGE	STD.DEV.	RELATIVE % STD.DEV.
-35		0.208	0.220	0.207	0.206	0.209	0.210	0.006	2.71
-34		0.243	0.233	0.229	0.239	0.231	0.235	0.006	2.48
-31	0.400	0.373	0.420	0.403	0.398	0.389	0.397	0.016	3.92
-30	0.428	0.406	0.444	0.433	0.446	0.433	0.432	0.014	3.33
-29	0.509	0.465	0.483	0.497	0.486	0.488	0.488	0.015	3.01
-28	0.548	0.518	0.562	0.578	0.570	0.559	0.556	0.021	3.80
-27	0.614	0.609	0.631	0.645	0.640	0.633	0.629	0.014	2.27
-26	0.652	0.630	0.686	0.702	0.702	0.702	0.679	0.031	4.55
-25	0.777	0.728	0.788	0.772	0.794	0.779	0.773	0.023	3.03
-23	0.871	0.870	0.937	0.947	0.946	0.927	0.916	0.036	3.95
-22	0.974	0.958	1.043	1.045	1.022	1.044	1.014	0.039	3.82
-21	1.067	1.030	1.109	1.125	1.109	1.122	1.094	0.037	3.43
-15	1.391	1.339	1.413	1.446	1.447	1.443	1.413	0.043	3.02
-14	1.363	1.348	1.467	1.509	1.501	1.461	1.442	0.069	4.81
-13	1.384	1.352	1.448	1.499	1.455	1.486	1.437	0.058	4.02
-12	1.362	1.346	1.435	1.462	1.470	1.488	1.427	0.059	4.16
-11	1.312	1.302	1.422	1.429	1.414	1.441	1.387	0.062	4.50
-9	1.216	1.200	1.303	1.320	1.321	1.337	1.283	0.059	4.61
-8	1.143	1.136	1.217	1.242	1.250	1.256	1.207	0.054	4.49
-7	1.067	1.035	1.101	1.150	1.136	1.149	1.106	0.047	4.29
-6	0.923	0.924	0.988	1.017	1.025	1.049	1.001	0.048	4.80
-5	0.805	0.805	0.869	0.905	0.897	0.897	0.875	0.041	4.72

CO_2 LINE STRENGTHS

	C66A	C66B	C66C	C66D	C66E	C66F	AVERAGE	STD.DEV.	RELATIVE % STD.DEV.
53	3.120	3.355	3.309	3.511	3.738	4.043	3.513	0.332	9.46
55	2.993	3.226	3.152	3.290	3.448	3.646	3.293	0.229	6.97
57	2.662	2.884	2.882	3.036	3.285	3.532	3.047	0.314	10.32
59	2.432	2.624	2.604	2.734	2.910	3.098	2.734	0.238	8.71
61	2.141	2.270	2.190	2.264	2.363	2.495	2.287	0.127	5.55
63	1.818	1.902	1.787	1.829	1.898	1.957	1.865	0.064	3.43
65	1.670	1.732	1.624	1.691	1.709	1.748	1.696	0.045	2.64
67	1.479	1.534	1.449	1.487	1.515	1.562	1.504	0.041	2.71
69	1.328	1.383	1.288	1.323	1.359	1.397	1.346	0.041	3.04
71	1.198	1.243	1.162	1.187	1.222	1.234	1.208	0.031	2.55
73	1.060	1.095	1.021	1.044	1.073	1.086	1.063	0.028	2.59
75	0.946	0.988	0.920	0.935	0.954	0.962	0.951	0.023	2.46
77	0.695	0.731	0.682	0.689	0.706	0.710	0.702	0.018	2.50
79	0.612	0.639	0.594	0.600	0.609	0.616	0.612	0.016	2.56
81	0.509	0.537	0.499	0.512	0.515	0.520	0.515	0.013	2.47
83	0.453	0.478	0.439	0.448	0.455	0.454	0.455	0.013	2.85
85	0.374	0.399	0.371	0.376	0.383	0.385	0.381	0.010	2.67
87	0.337	0.354	0.326	0.332	0.335	0.333	0.336	0.009	2.82
89	0.272	0.295	0.270	0.276	0.282	0.284	0.280	0.009	3.29

Line Strength Data at a Furnace Set Point Temperature of 1173 K

CO LINE STRENGTHS

	C66A	C66B	C66C	C66D	C66E	C66F	AVERAGE	STD.DEV.	RELATIVE % STD.DEV.
-35		0.177	0.241	0.203	0.211	0.215	0.209	0.023	11.00
-34	0.286	0.227	0.291	0.245	0.266	0.282	0.266	0.025	9.57
-31	0.355	0.323	0.419	0.379	0.385	0.382	0.374	0.032	8.62
-30	0.469	0.397	0.457	0.423	0.428	0.445	0.437	0.026	5.94
-29	0.496	0.462	0.496	0.475	0.495	0.470	0.482	0.015	3.15
-28	0.521	0.524	0.531	0.532	0.533	0.554	0.533	0.012	2.17
-27	0.574	0.582	0.607	0.582	0.599	0.622	0.594	0.018	3.07
-26	0.608	0.624	0.662	0.627	0.649	0.667	0.640	0.023	3.66
-25	0.711	0.650	0.749	0.690	0.731	0.701	0.705	0.034	4.88
-23	0.798	0.775	0.853	0.840	0.856	0.850	0.829	0.034	4.09
-22	0.808	0.851	0.895	0.890	0.896	0.912	0.875	0.039	4.42
-21	0.902	0.899	0.978	0.955	0.988	0.958	0.947	0.038	4.00
-15	1.135	1.122	1.218	1.167	1.212	1.221	1.179	0.044	3.74
-14	1.142	1.141	1.222	1.203	1.236	1.269	1.202	0.052	4.30
-13	1.101	1.108	1.211	1.189	1.217	1.227	1.176	0.056	4.80
-12	1.109	1.083	1.182	1.145	1.199	1.214	1.155	0.052	4.51
-11	1.037	1.059	1.107	1.142	1.145	1.166	1.109	0.052	4.65
-9	0.953	0.978	1.048	1.028	1.048	1.093	1.025	0.051	4.99
-8	0.834	0.878	0.962	0.947	0.975	0.974	0.928	0.059	6.31
-7	0.807	0.845	0.894	0.909	0.897	0.914	0.878	0.042	4.83
-6	0.728	0.752	0.783	0.796	0.806	0.816	0.780	0.034	4.34
-5	0.601	0.601	0.667	0.691	0.698	0.708	0.661	0.048	7.32

CO_2 LINE STRENGTHS

	C66A	C66B	C66C	C66D	C66E	C66F	AVERAGE	STD.DEV.	RELATIVE % STD.DEV.
53	2.721	2.750	2.843	3.009	3.171	3.480	2.996	0.291	9.73
55	2.703	2.719	2.783	2.907	3.005	3.280	2.900	0.219	7.57
57	2.452	2.484	2.557	2.731	2.915	3.199	2.723	0.290	10.66
59	2.264	2.268	2.366	2.500	2.587	2.885	2.478	0.237	9.56
61	1.978	1.966	1.996	2.081	2.181	2.387	2.098	0.163	7.77
63	1.610	1.597	1.564	1.589	1.594	1.671	1.604	0.036	2.25
65	1.472	1.441	1.435	1.427	1.453	1.555	1.464	0.047	3.23
67	1.341	1.312	1.307	1.319	1.316	1.402	1.333	0.036	2.69
69	1.222	1.185	1.169	1.183	1.176	1.255	1.198	0.033	2.78
71	1.104	1.089	1.072	1.077	1.081	1.149	1.095	0.029	2.61
73	0.994	0.970	0.968	0.984	0.975	1.030	0.987	0.023	2.36
75	0.885	0.886	0.870	0.865	0.875	0.911	0.882	0.016	1.86
77	0.688	0.685	0.672	0.675	0.679	0.707	0.684	0.013	1.84
79	0.608	0.601	0.586	0.585	0.592	0.618	0.598	0.013	2.19
81	0.527	0.528	0.510	0.516	0.516	0.534	0.522	0.009	1.76
83	0.448	0.457	0.445	0.453	0.441	0.468	0.452	0.010	2.14
85	0.399	0.396	0.395	0.396	0.397	0.412	0.399	0.006	1.61
87	0.354	0.350	0.341	0.346	0.345	0.363	0.350	0.008	2.24
89	0.300	0.300	0.295	0.302	0.301	0.317	0.303	0.008	2.48

Line Strength Data at a Furnace Set Point Temperature of 1273 K

CO LINE STRENGTHS

	C66A	C66B	C66C	C66D	C66E	C66F	AVERAGE	STD.DEV.	RELATIVE % STD.DEV.
-35	0.324	0.215	0.208	0.230	0.226	0.215	0.236	0.044	18.49
-34		0.231	0.236	0.208	0.226	0.224	0.225	0.011	4.70
-31	0.389	0.339	0.364	0.360	0.398	0.384	0.372	0.022	5.89
-30	0.410	0.348	0.370	0.365	0.385	0.380	0.376	0.021	5.57
-29	0.527	0.479	0.463	0.452	0.433	0.451	0.468	0.033	7.03
-28	0.615	0.524	0.533	0.482	0.479	0.496	0.522	0.051	9.74
-27	0.612	0.555	0.539	0.522	0.497	0.519	0.541	0.040	7.41
-26	0.584	0.583	0.618	0.588	0.575	0.542	0.582	0.024	4.20
-25	0.748	0.682	0.689	0.655	0.615	0.649	0.673	0.045	6.72
-23	0.824	0.758	0.768	0.709	0.713	0.741	0.752	0.042	5.63
-22	0.794	0.739	0.799	0.717	0.762	0.745	0.759	0.032	4.24
-21	0.930	0.885	0.860	0.812	0.862	0.808	0.860	0.046	5.34
-15	1.077	1.037	1.053	0.941	0.948	0.963	1.003	0.059	5.91
-14	1.023	1.020	1.015	0.959	0.970	0.976	0.994	0.029	2.88
-13	1.044	0.990	1.014	0.934	0.978	0.931	0.982	0.044	4.52
-12	1.011	0.971	0.983	0.921	0.962	0.945	0.966	0.031	3.22
-11	0.991	0.961	0.943	0.872	0.883	0.906	0.926	0.047	5.04
-9	0.906	0.846	0.846	0.777	0.796	0.831	0.834	0.045	5.41
-8	0.813	0.787	0.784	0.743	0.755	0.744	0.771	0.028	3.65
-7	0.769	0.723	0.743	0.708	0.699	0.704	0.724	0.027	3.74
-6	0.724	0.665	0.646	0.614	0.640	0.631	0.653	0.038	5.89
-5	0.588	0.578	0.579	0.523	0.514	0.537	0.546	0.031	5.60

CO_2 LINE STRENGTHS

	C66A	C66B	C66C	C66D	C66E	C66F	AVERAGE	STD.DEV.	RELATIVE % STD.DEV.
51									
53	2.120	2.018	2.264	2.571	2.864	2.934	2.462	0.387	15.73
55	2.115	2.074	2.270	2.559	2.777	2.869	2.444	0.341	13.94
57	1.882	1.909	2.087	2.410	2.600	2.800	2.281	0.380	16.67
59	1.774	1.769	1.939	2.198	2.400	2.583	2.111	0.339	16.05
61	1.601	1.571	1.680	1.886	2.016	2.117	1.812	0.228	12.59
63	1.267	1.172	1.246	1.328	1.390	1.414	1.303	0.092	7.05
65	1.160	1.096	1.142	1.227	1.259	1.281	1.194	0.073	6.08
67	1.073	0.994	1.048	1.135	1.139	1.160	1.092	0.064	5.88
69	0.974	0.909	0.970	1.012	1.061	1.070	0.999	0.061	6.11
71	0.902	0.848	0.883	0.937	0.959	0.960	0.915	0.045	4.92
73	0.825	0.777	0.806	0.859	0.876	0.886	0.838	0.043	5.09
75	0.731	0.697	0.727	0.773	0.799	0.784	0.752	0.039	5.24
77	0.582	0.550	0.583	0.598	0.616	0.626	0.593	0.027	4.60
79	0.522	0.488	0.516	0.541	0.556	0.557	0.530	0.027	5.03
81	0.468	0.442	0.470	0.489	0.494	0.496	0.477	0.021	4.35
83	0.396	0.386	0.403	0.418	0.429	0.431	0.411	0.018	4.47
85	0.362	0.343	0.355	0.378	0.378	0.384	0.367	0.016	4.36
87	0.311	0.312	0.322	0.332	0.344	0.351	0.329	0.017	5.05
89	0.280	0.269	0.278	0.295	0.298	0.304	0.287	0.014	4.74

APPENDIX XII

CALCULATION RESULTS FROM GAS CONCENTRATION MEASUREMENTS

The results from the gas concentration calculations are presented in the tables provided in this appendix. The data are divided into three sets; 66, 68 and 70. Gas temperatures and concentrations are calculated from 52 spectra in set 66, 48 spectra in set 68 and 28 spectra in set 70. Each table contains a listing of the spectrum name, pressure, measured gas concentrations and temperature, calculated gas concentrations and temperatures, and percent differences between the measured and calculated concentrations and temperatures. Presented in this Appendix is first a sample of a results file produced from the Pascal program *SpecAnal* which has been run here to calculated gas temperatures and CO and CO_2 concentrations.

Sample Output File for Line Strength Calculations

Iteration Number = 1
Temperature Guess = 950.00
Calculated Temperature = 930.97
Standard Deviation = 0.01203
Variance = 0.00290
Standard Error of Line = 2.0724
PPCOGuess = 10.000
PPCO2Guess = 10.000
PPN2 = 740.000

Iteration Number = 2
Temperature Guess = 930.97
Calculated Temperature = 932.54
Standard Deviation = 0.01234
Variance = 0.00305
Standard Error of Line = 2.1327
PPCOGuess = 8.494
PPCO2Guess = 13.677
PPN2 = 744.829

Iteration Number = 3
Temperature Guess = 932.54
Calculated Temperature = 932.43

Standard Deviation = 0.01230
Variance = 0.00302
Standard Error of Line = 2.1249
PPCOGuess = 8.294
PPCO2Guess = 11.589
PPN2 = 747.118

Iteration Number = 4
Temperature Guess = 932.43
Calculated Temperature = 932.44
Standard Deviation = 0.01230
Variance = 0.00303
Standard Error of Line = 2.1256
PPCOGuess = 8.310
PPCO2Guess = 11.811
PPN2 = 746.880

c66700b.dat

Energy, Intensity, Corrected Peak Height, Partial Pressure CO (Torr),
M Value, True Line Position

3471.413, -16.911, 0.134, 8.285, -35,1988.915
3279.290, -16.687, 0.161, 8.554, -34,1993.863
2735.390, -16.077, 0.259, 8.222, -31,2008.526
2564.936, -15.910, 0.293, 8.313, -30,2013.353
2399.916, -15.715, 0.339, 8.431, -29,2018.149
2240.336, -15.556, 0.380, 8.312, -28,2022.915
2086.203, -15.393, 0.427, 8.344, -27,2027.649
1937.522, -15.243, 0.474, 8.270, -26,2032.353
1794.299, -15.066, 0.538, 8.414, -25,2037.026
1524.251, -14.776, 0.656, 8.392, -23,2046.276
1397.435, -14.661, 0.693, 8.251, -22,2050.855
1276.098, -14.530, 0.752, 8.278, -21,2055.401
663.377, -13.867, 0.996, 8.392, -15,2082.003
580.510, -13.788, 0.998, 8.263, -14,2086.322
503.154, -13.710, 0.995, 8.311, -13,2090.609
431.310, -13.619, 0.995, 8.353, -12,2094.863
364.983, -13.562, 0.966, 8.260, -11,2099.083
248.885, -13.444, 0.883, 8.271, -9,2107.424
199.120, -13.377, 0.836, 8.242, -8,2111.543
154.879, -13.327, 0.760, 8.256, -7,2115.629
116.164, -13.271, 0.689, 8.207, -6,2119.681
82.978, -13.243, 0.582, 8.175, -5,2123.699

Average CO Partial Pressure (Torr) = 8.31
Average CO Concentration (Percent) = 1.08
Standard Deviation of Concentration Calculations (%) = 0.0113

Corrected Peak Height, True Line Position, CO2 M Value,
CO2 Partial Pressure (torr)

3.518, 2380.716, 51, 0.000
2.733, 2381.622, 53, 10.990
2.549, 2382.503, 55, 11.258
2.309, 2383.359, 57, 11.183
2.066, 2384.189, 59, 11.265
1.777, 2384.995, 61, 11.516
1.536, 2385.775, 63, 11.682
1.373, 2386.529, 65, 11.732
1.217, 2387.258, 67, 11.799
1.084, 2387.962, 69, 11.872
0.949, 2388.640, 71, 11.881
0.828, 2389.293, 73, 11.926
0.732, 2389.921, 75, 12.011
0.525, 2390.522, 77, 12.042
0.455, 2391.099, 79, 12.089
0.382, 2391.650, 81, 12.202
0.321, 2392.175, 83, 12.047
0.268, 2392.675, 85, 12.100
0.238, 2393.149, 87, 12.299
0.188, 2393.598, 89, 12.072
0.188, 2394.021, 91, 0.000

Average CO2 Partial Pressure (Torr) = 11.79
Average CO2 Concentration (Percent) = 1.54
Standard Deviation of Concentration Calculations (%) = 0.0492

Concentration Data from Set 66

File	Press.	Meas CO	Meas. CO2	Meas. Temp.	Calc. CO	Calc. CO2	Calc. Temp.	CO % Diff.	CO2 % Diff.	Temp. % Diff.
C6525E	763	0.68	0.77	297	0.66	0.80	291.9	-2.94	3.90	-1.71
C6525F	764	1.24	1.33	297	1.24	1.25	294.6	0.00	-6.02	-0.81
C6525G	764	1.72	1.89	297	1.80	1.96	293.2	4.65	3.70	-1.28
C6525H	764	2.19	2.46	297	2.34	2.50	291.5	6.85	1.63	-1.85
C6625A	764	0.59	0.72	297	0.62	0.69	296.0	5.08	-4.17	-0.34
C6625B	764	0.97	1.00	297	0.90	0.96	296.3	-7.22	-4.00	-0.24
C6625C	765	1.25	1.34	297	1.27	1.20	298.4	1.60	-10.45	0.47
C6625D	765	1.61	1.82	297	1.54	1.78	295.9	-4.35	-2.20	-0.37
C6625E	765	2.00	2.24	297	1.92	2.22	293.9	-4.00	-0.89	-1.04
C6625F	765	2.38	2.87	297	2.34	2.87	290.3	-1.68	0.00	-2.26
C66100A	767	0.78	0.85	361	0.81	0.80	360.8	3.85	-5.88	-0.06
C66100B	768	1.16	1.20	361	1.10	1.16	354.4	-5.17	-3.33	-1.83
C66100C	767	1.51	1.53	361	1.60	1.54	348.8	5.96	0.65	-3.38
C66100D	767	1.97	1.86	361	1.94	1.86	356.3	-1.52	0.00	-1.30
C66100E	767	2.37	2.30	361	2.30	2.33	353.6	-2.95	1.30	-2.05
C66100F	767	2.94	2.78	361	2.93	3.02	344.9	-0.34	8.63	-4.46
C66300A	767	0.79	0.81	547	0.77	0.75	541.6	-2.53	-7.41	-0.99
C66300B	767	1.41	1.32	547	1.41	1.26	537.6	0.00	-4.55	-1.72
C66300C	767	1.86	2.00	547	1.86	1.95	534.9	0.00	-2.50	-2.21
C66300D	767	2.41	2.29	547	2.39	2.26	531.6	-0.83	-1.31	-2.82
C66300E	767	3.19	3.10	547	3.22	3.18	537.8	0.94	2.58	-1.68
C66300F	767	3.83	3.91	547	3.95	4.31	527.3	3.13	10.23	-3.60
C66500A	768	0.60	1.01	746	0.65	0.92	721.9	8.33	-8.91	-3.23
C66500B	768	1.51	1.60	746	1.52	1.58	734.0	0.66	-1.25	-1.61
C66500C	768	2.24	2.38	746	2.16	2.28	719.7	-3.57	-4.20	-3.53
C66500D	768	2.90	3.05	746	2.81	3.07	715.5	-3.10	0.66	-4.09
C66500E	768	3.40	3.53	746	3.36	3.59	719.9	-1.18	1.70	-3.50
C66500F	768	4.06	4.20	746	4.03	4.69	707.1	-0.74	11.67	-5.21
C66700A	767	0.55	1.00	948	0.61	0.96	953.6	10.91	-4.00	0.59
C66700B	767	1.08	1.55	948	1.08	1.54	932.4	0.00	-0.65	-1.65
C66700C	767	1.73	2.38	948	1.76	2.21	936.0	1.73	-7.14	-1.27
C66700D	767	2.53	2.86	948	2.45	2.87	933.7	-3.16	0.35	-1.51
C66700E	768	3.39	3.62	948	3.26	3.82	933.0	-3.83	5.52	-1.58
C66700F	768	4.27	4.29	948	4.06	4.62	928.7	-4.92	7.69	-2.04
C66800A	769	0.55	1.02	1048	0.55	1.00	1060.9	0.00	-1.96	1.23
C66800B	769	0.99	1.58	1048	0.95	1.64	1046.8	-4.04	3.80	-0.11
C66800C	769	1.51	2.57	1048	1.54	2.47	1037.8	1.99	-3.89	-0.97
C66800D	769	2.29	3.15	1048	2.30	3.10	1019.3	0.44	-1.59	-2.74
C66800E	769	3.25	3.91	1048	3.29	3.97	1023.7	1.23	1.53	-2.32
C66800F	769	4.17	4.86	1048	4.16	5.07	1014.7	-0.24	4.32	-3.18
C66900A	771	0.58	1.29	1149	0.61	1.39	1201.5	5.17	7.75	4.57
C66900B	771	0.99	1.79	1149	0.89	1.70	1114.3	-10.10	-5.03	-3.02
C66900C	771	1.44	2.57	1149	1.55	2.61	1172.7	7.64	1.56	2.06
C66900D	771	2.22	3.34	1149	2.15	3.22	1117.7	-3.15	-3.59	-2.72
C66900E	771	2.93	4.01	1149	2.94	3.96	1127.9	0.34	-1.25	-1.84
C66900F	771	3.94	4.77	1149	4.01	5.03	1129.6	1.78	5.45	-1.69
C66999A	768	0.54	1.40	1247	-	-	1293.5	-	-	3.73
C66999B	768	1.21	2.38	1247	1.15	2.00	1190.8	-4.96	-15.97	-4.51
C66999C	768	1.68	2.77	1247	1.63	2.49	1198.7	-2.98	-10.11	-3.87
C66999D	768	2.78	3.05	1247	2.66	3.14	1227.0	-4.32	2.95	-1.60
C66999E	768	3.55	3.81	1247	3.44	4.08	1229.1	-3.10	7.09	-1.44
C66999F	768	4.32	4.96	1247	4.15	5.35	1220.5	-3.94	7.86	-2.13

Concentration Data from Set 68

File	Press.	Meas CO	Meas. CO2	Meas. Temp.	Calc. CO	Calc. CO2	Calc. Temp.	CO % Diff.	CO2 % Diff.	Temp. % Diff.
C6825A	766	0.73	0.86	297	0.77	0.78	297.4	5.48	-9.30	0.13
C6825B	766	1.07	1.14	297	1.03	1.03	297.9	-3.74	-9.65	0.30
C6825C	766	1.53	1.54	297	1.57	1.49	294.6	2.61	-3.25	-0.81
C6825D	766	1.91	2.10	297	1.87	2.01	292.9	-2.09	-4.29	-1.38
C6825E	766	2.18	2.71	297	2.14	2.72	293.2	-1.83	0.37	-1.28
C6825F	766	2.44	3.24	297	2.41	3.24	293.0	-1.23	0.00	-1.35
C68100A	767	0.96	1.05	361	0.92	0.95	361.2	-4.17	-9.52	0.06
C68100B	767	1.41	1.45	361	1.43	1.36	354.7	1.42	-6.21	-1.75
C68100C	767	1.86	1.91	361	1.83	1.83	354.3	-1.61	-4.19	-1.86
C68100D	767	2.20	2:21	361	2.24	2.21	349.8	1.82	0.00	-3.10
C68100E	767	2.57	2.55	361	2.52	2.66	345.3	-1.95	4.31	-4.35
C68100F	767	2.91	3.06	361	2.96	3.26	347.7	1.72	6.54	-3.68
C68300A	767	0.99	1.10	547	0.94	1.05	534.1	-5.05	-4.55	-2.36
C68300B	767	1.82	1.65	547	1.82	1.70	536.1	0.00	3.03	-1.99
C68300C	767	2.27	2.19	547	2.30	2.20	533.5	1.32	0.46	-2.47
C68300D	767	2.89	2.96	547	2.94	3.02	534.0	1.73	2.03	-2.38
C68300E	767	3.35	3.43	547	3.45	3.61	529.3	2.99	5.25	-3.24
C68300F	768	3.96	4.10	547	4.16	4.67	527.4	5.05	13.90	-3.58
C68500A	768	0.87	1.12	746	0.85	1.08	734.6	-2.30	-3.57	-1.53
C68500B	768	1.72	1.91	746	1.79	1.82	745.6	4.07	-4.71	-0.05
C68500C	768	2.36	2.53	746	2.39	2.46	722.8	1.27	-2.77	-3.11
C68500D	768	2.99	3.24	746	2.96	3.28	709.5	-1.00	1.23	-4.89
C68500E	768	3.71	3.81	746	3.79	4.08	717.5	2.16	7.09	-3.82
C68500F	767	4.58	4.58	746	4.58	5.08	710.3	0.00	10.92	-4.79
C68700A	768	0.81	1.12	948	0.80	1.12	940.3	-1.23	0.00	-0.81
C68700B	768	1.62	1.86	948	1.57	1.87	930.9	-3.09	0.54	-1.80
C68700C	768	2.28	2.57	948	2.17	2.54	931.9	-4.82	-1.17	-1.70
C68700D	768	2.80	3.05	948	2.75	3.11	926.3	-1.79	1.97	-2.29
C68700E	767	3.55	4.01	948	3.45	4.17	925.6	-2.82	3.99	-2.36
C68700F	767	4.49	4.48	948	4.38	4.81	924.2	-2.45	7.37	-2.51
C68800A	768	0.78	1.18	1048	0.75	1.20	1048.3	-3.85	1.69	0.03
C68800B	768	1.42	1.62	1048	1.34	1.70	1035.2	-5.63	4.94	-1.22
C68800C	768	2.08	2.48	1048	2.03	2.40	1036.2	-2.40	-3.23	-1.13
C68800D	768	2.81	3.24	1048	2.68	3.26	1020.8	-4.63	0.62	-2.60
C68800E	768	3.42	4.01	1048	3.36	4.15	1028.3	-1.75	3.49	-1.88
C68800F	768	4.20	4.86	1048	4.20	5.26	1031.1	0.00	8.23	-1.61
C68900A	770	0.89	1.21	1149	0.87	1.19	1145.3	-2.25	-1.65	-0.32
C68900B	770	1.62	2.10	1149	1.56	1.98	1135.8	-3.70	-5.71	-1.15
C68900C	770	2.24	2.77	1149	2.26	2.67	1148.6	0.89	-3.61	-0.03
C68900D	770	2.71	3.24	1149	2.54	3.01	1108.6	-6.27	-7.10	-3.52
C68900E	770	3.30	3.91	1149	3.25	3.90	1127.0	-1.52	-0.26	-1.91
C68900F	770	4.28	4.53	1149	4.18	4.61	1114.4	-2.34	1.77	-3.01
C68999A	769	0.99	1.28	1247	-	-	1273.5	-	-	2.13
C68999B	769	1.62	1.91	1247	-	-	1261.9	-	-	1.19
C68999C	769	2.31	2.57	1247	2.22	2.59	1237.7	-3.90	0.78	-0.75
C68999D	769	2.89	3.24	1247	2.73	3.27	1225.3	-5.54	0.93	-1.74
C68999E	769	3.61	3.91	1247	3.46	4.16	1235.6	-4.16	6.39	-0.91
C68999F	769	4.49	4.86	1247	4.38	5.29	1252.4	-2.45	8.85	0.43

Concentration Data from Set 70

File	Press.	Meas CO	Meas. CO2	Meas. Temp.	Calc. CO	Calc. CO2	Calc. Temp.	CO % Diff.	CO2 % Diff.	Temp. % Diff.
C7065A	764	0.99	1.09	338	0.91	0.91	332.2	-8.23	-16.89	-1.72
C7065B	764	1.52	1.52	338	1.46	1.37	329.0	-4.08	-9.75	-2.66
C7065C	764	2.13	2.07	338	1.90	1.81	329.8	-10.98	-12.60	-2.43
C7065D	764	2.68	2.68	338	2.48	2.38	329.6	-7.59	-11.23	-2.49
C70200A	768	0.99	0.99	450	0.90	0.93	446.4	-8.77	-6.17	-0.80
C70200B	768	1.94	1.91	450	1.84	1.81	443.0	-5.22	-5.08	-1.56
C70200C	768	2.89	2.86	450	2.84	2.78	439.0	-1.59	-2.82	-2.44
C70200D	768	3.83	3.72	450	3.78	3.66	436.8	-1.31	-1.59	-2.93
C70400A	762	0.58	1.35	650	0.66	1.20	645.3	14.33	-11.35	-0.72
C70400B	763	1.85	2.00	650	1.74	1.84	626.0	-5.79	-8.10	-3.69
C70400C	763	2.76	2.96	650	2.59	2.73	634.0	-6.16	-7.65	-2.46
C70400D	763	3.61	3.72	650	3.38	3.62	632.3	-6.37	-2.67	-2.72
C70600A	766	0.45	1.36	850	0.61	1.29	898.7	35.14	-5.37	5.73
C70600B	766	1.34	2.38	850	1.50	2.17	852.2	11.66	-8.97	0.26
C70600C	766	2.55	3.00	850	2.52	2.93	832.8	-1.18	-2.46	-2.02
C70600D	766	3.62	4.10	850	3.54	4.39	833.0	-2.22	7.05	-2.00
C70750A	768	0.52	1.33	1000	0.58	1.27	982.7	10.51	-4.84	-1.73
C70750B	768	1.27	2.48	1000	1.34	2.28	983.0	5.52	-8.03	-1.70
C70750C	768	2.15	3.34	1000	2.11	3.16	971.9	-1.92	-5.32	-2.81
C70750D	768	3.11	3.81	1000	3.05	3.92	975.6	-1.81	2.76	-2.44
C70850A	766	0.58	1.29	1100	0.55	1.26	1102.5	-4.73	-2.09	0.23
C70850B	766	1.30	2.48	1100	1.21	2.32	1078.1	-7.02	-6.42	-1.99
C70850C	766	1.95	3.43	1100	1.95	3.24	1072.0	-0.10	-5.62	-2.55
C70850D	766	2.83	4.20	1100	2.78	4.06	1070.5	-1.88	-3.24	-2.68
C70950A	768	0.70	1.28	1200	0.69	1.39	1244.4	-1.88	8.82	3.70
C70950B	768	1.53	2.29	1200	1.55	2.26	1200.1	1.16	-1.24	0.01
C70950C	769	2.50	3.05	1200	2.60	3.15	1205.5	4.10	3.23	0.46
C70950D	769	3.50	3.81	1200	3.68	4.01	1200.8	4.99	5.12	0.06